AD-A138 530 LEADING EDGE DEVICES SLATS ON SWEPT-BACK SLENDER WINGS 1/2
WITH FLOW SEPARATI..(U) BRISTOL UNIV (ENGLAND) DEPT OF
AERONAUTICAL ENGINEERING R K NANGIA JUN 80 RKN/8001

UNCLASSIFIED F49620-79-C-0075 F/G 20/4 NL

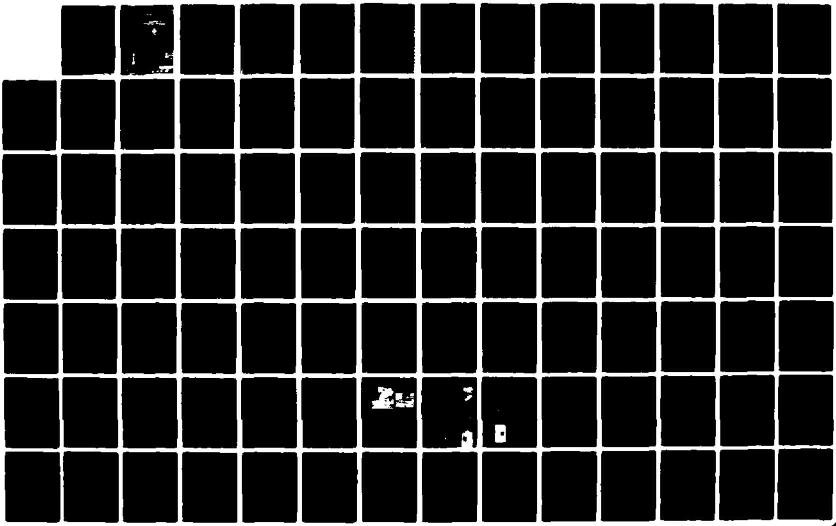

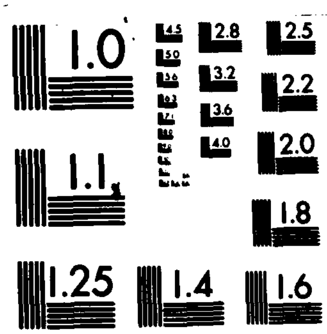

MICROCOPY RESOLUTION TEST CHART
NATIONAL BUREAU OF STANDARDS-1963-A

REPORT DOCUMENTATION PAGE		READ INSTRUCTIONS BEFORE COMPLETING FORM
1. Report Number	2. Govt Accession No. AD-A138530	3. Recipient's Catalog Number
4. Title (and Subtitle) LEADING EDGE DEVICES, SLATS ON SWEPT-BACK SLENDER WINGS WITH FLOW SEPARATION.		5. Type of Report & Period Covered Final Report May 1st, 1979 to June 30th 1980
		6. Performing Org. Report Number Dept. of Aeronautical Engineering University of Bristol RKN/8001
7. Author(s) Dr. R. K. NANGIA		8. Contract or Grant Number F 496-20-79-C-0075
9. Performing Organization Name and Address Dept. of Aeronautical Engineering University of Bristol, Queens's Building, Bristol, BS8 1TR U.K.		10. Program Element, Project, Task Area & Work Unit Numbers
11. Controlling Office Name and Address Air Force Wright Aeronautical Laboratories (AFSC) Wright-Patterson A.F.B. Ohio 45433 U.S.A.		12. Report Date June 1980
		13. Number of Pages
14. Monitoring Agency Name and Address EOARD/LNV Box 14 F.P.O. New York 09510		15.

16. & 17. Distribution Statement

Approved for public release; distribution unlimited.

18. Supplementary Notes

19. Key Words

Slender Wings, Delta Wings, Leading Edge Devices, Slats, Conical Flow, Vortices, Flow Separation, High Lift.

20. Abstract

Leading edge devices and slats are applicable to high speed wing planforms with high sweepback or strakes. This includes aircraft with transonic manoeuvrability capability and supersonic cruise vehicles.

A theoretical approach within the framework of conical slender wing theory has been presented that deals with thin delta wings with leading edge slats including flow separations.

Specimen calculations suggest that benefits in performance (lift/drag) are strongly dependent on the flow conditions prevailing at the edges of the configuration (i.e. whether the flow is attached or separated).

In general lift-drag benefits of 10% -40% are obtainable with suitable configurations. These benefits are of the same order as those indicated by experiments.

Further work, both theoretical and experimental leading to practical applications has been recommended.

FORM 1473

CONTRACT NUMBER F 496-20-79-C-0075

LEADING EDGE DEVICES, SLATS ON SWEPT-BACK SLENDER WINGS WITH FLOW SEPARATION

R. K. Nangia

Department of Aeronautical Engineering,

University of Bristol, U.K.

June 1980

Final Report 1st May, 1979 - 30th June, 1980.

Approved for public release;

Distribution unlimited

Prepared for:

Air Force Wright Aeronautical Laboratories (AFSC)
Wright-Patterson AFB, Ohio 45433, U.S.A.

and

European Office of Aerospace Research and Development,
London, U.K.

ACKNOWLEDGEMENTS

The author wishes to acknowledge the support provided by USAF - Wright Aeronautical Laboratories (AFSC) under Contract F 496-20-79-C-0075 for the programme of work mentioned in this report. The author also wishes to acknowledge helpful discussions with Mr. J.H.B. Smith (Royal Aircraft Establishment, U.K.) and Professor L.F. Crabtree (University of Bristol, U.K.). Thanks are due to Mrs. P. Packham and Mrs. J. Dick for typing the script.

SUMMARY

Leading edge devices and slats are applicable to high speed wing planforms with high sweepback or strakes. This includes aircraft with transonic manoeuvrability capability and supersonic cruise vehicles.

A theoretical approach within the framework of conical slender wing theory has been presented that deals with thin delta wings with leading edge slats including flow separations.

Specimen calculations suggest that benefits in performance (lift/drag) are strongly dependent on the flow conditions prevailing at the edges of the configuration (i.e. whether the flow is attached or separated).

In general lift-drag benefits of 10% - 40% are obtainable with suitable configurations. These benefits are of the same order as those indicated by experiments.

Further work, both theoretical and experimental leading to practical applications has been recommended.

LIST OF SYMBOLS

A	Wing
a_p (p=1 ... M)	Unknowns in series for δ_A Equation (11)
av_{δ_A} (p, y, z), aw_{δ_A} (p, y, z) or aw_{δ_A} (p, θ_A)	Sidewash and upwash velocity influence coefficients due to the p^{th} term of δ_A series in v, w system
B	Starboard slat
b_q (q=1 ... N)	Unknowns in series for δ_B Equation (15)
bv_{δ_B} (q, y_B, z_B), bw_{δ_B} (q, y_B, z_B) or bw_{δ_B} (q, θ_B)	Sidewash and upwash velocity coefficients due to the q^{th} term of δ_B series in v_B, w_B system
C	Port slat
C_L	Lift coefficient
C_D, C_{D_i}	Induced drag coefficient
C_{D_o}	Profile drag coefficient
C_N	Normal force coefficient
C_{L_w}, C_{D_w}, C_{N_w}	Lift induced drag and normal force coefficients for the wing
C_{L_s}, C_{D_s}, C_{N_s}	Lift induced drag and normal force coefficients for the slat
$C_{D_{w_T}}$	Drag coefficient due to leading edge suction on the wing
$C_{D_{s_T}}$	Drag coefficient due to leading edge suction on the slat
C_{N_L}	Local normal force-load distribution
c_o	Horizontal position of the Starboard slat) Figure 14
c_1	Semi-span of the slat) Figure 14
d_r (r=1,2,3)	Coefficient of g_r (r=1,3) or Γ_r (r=1,2,3), e.g. equation (44), (47), etc.
e_p (p=1 ... M)	Coefficient of a_p (p=1 ... M), e.g. equation (44), (47), etc.
F	Integration constant
F_B	Integration constant
f_q (q=2 ... N)	Coefficient of b_q (q=2 ... N), e.g. equation (44), (47), etc.
g_1	Unknown in δ_F equation (10)
g_3	Unknown in δ_G equation (14)

CONTENTS

gv_1 (y_A, z_A), gw_1 (y_A, z_A) or gw_1 (θ_A)	Sidewash and upwash velocity influence coeffients due to δ_F in v, w system
gv_{Γ_r} (y_A, z_A) (r=1,2,3)	Sidewash and upwash velocity influence coefficients due to the vortex pairs $\pm \Gamma_r$ (r=1,2,3)
$gv_{\delta_{G_3}}$ (y_B, z_B), $gw_{\delta_{G_3}}$ (y_B, z_B) or $gw_{\delta_{G_3}}$ (θ_B)	Sidewash and upwash velocity influence coefficients due to δ_G in v_B, w_B system
h_o	Vertical position of the starboard slat, Figure 14
k	Wing leading edge parameter in the case of wing-slat configurati alternatively non-dimensionalising parameters = k_3 for slats only configurations
k_2	$= c_o - c_1$
k_3	$= c_o + c_1$
M	Integer limit in series for δ_A equation (11)
N	Integer limit in series for δ_B equation (15)
p	Integer index
q	Integer index
r	Integer index
s	semi-span of the wing s = kx
t	$\sin\alpha$ or $\sin\alpha_B$, e.g. equation (44), (47), etc.
u v w	Perturbation velocities in the xyz axes system, Figure 13
V	Free stream velocity
v_B, w_B	Perturbation velocities in the y_B, z_B axes system, Figure 14
v_r, w_r (r=1,2,3)	Spanwise and upward velocities at a R.H.S. vortex due to the whole flowfield excluding the effect of vortex on itself in the v, w system
v_{Γ_r} (x, y_A, z_A), w_{Γ_r} (x, y_A, z_A) (r=1,2,3)	Sidewash and upwash velocity influence coefficients due to the vortex pair $\pm \Gamma_r$ (r=1,2,3)
v_{δ_w} (x, y_A, z_A), w_{δ_w} (x, y_A, z_A)	Sidewash and upwash induced due to δ_w on the wing A in the v, w system
w_{δ_s} (x, y_A, z_A)	Upwash induced due to δ_s on the slat B in the v, w system
w_{δ_p} (x, y_A, z_A)	Upwash induced due to δ_p on the slat C in the v, w axes system

$v_{\delta_A}(x_A, y_A, z_A)$, $w_{\delta_A}(x_A, y_A, z_A)$	Sidewash and upwash induced due to δ_A on the wing in the v, w system
$v_{\delta_F}(x_A, y_A, z_A)$, $w_{\delta_F}(x_A, y_A, z_A)$	Sidewash and upwash induced due to δ_F on the wing in the v, w system
$w_{B\delta_w}(x_B, y_B, z_B)$	Upwash induced due to δ_w on the wing A in the v_B, w_B system
$v_{B\delta_s}(x_B, y_B, z_B)$, $w_{B\delta_s}(x_B, y_B, z_B)$	Sidewash and upwash induced due to δ_s on slat B in the v_B, w_B system
$v_{B\delta_p}(x_B, y_B, z_B)$, $w_{B\delta_p}(x_B, y_B, z_B)$	Sidewash and upwash induced due to δ_p on Slat C in the v_B, w_B system
$v_{B\delta_B}(x_B, y_B, z_B)$ $w_{B\delta_B}(x_B, y_B, z_B)$	Sidewash and upwash induced due to δ_B on slat B in the v_B, w_B system
$v_{B\delta_G}(x_B, y_B, z_B)$, $w_{B\delta_G}(x_B, y_B, z_B)$	Sidewash and upwash induced due to δ_G on slat B in the v_B, w_B system
x y z	Cartesian co-ordinates axes system (Figure 13)
x_A, y_A, z_A	A general point on wing A in the x y z system
y_B, z_B	Axes system on slat B (Figure 14)
y_C, z_C	Axes system on slat C(Figure 14)
y_{BA}, z_{BA}	Refers to a point y_A, z_A of x-y axes system to the y_B, z_B axes system
y'_{BA}, z'_{BA}	Refers to a point $-y_A$, z_A of x-y axes system to the y_B, z_B axes system
y_{AB}, z_{AB}	Refers to a point y_B, z_B of x_B, y_B axes system to the x, y axes system
y_{BC}, z_{BC}	Refers to a point y_C, z_C of x_C, y_C axes system to the y_B, z_B axes system
y_ℓ, z_ℓ	Position of leading edge or trailing edge
y_r, z_r (r=1,2,3)	Position of vortices 1, 2 and 3
α	Angle of attack of wing
α_B	Effective angle of attack of the slat
Γ_r (r=1,2,3)	Vortex strength
$\frac{\partial \Gamma_r}{\partial x}$ (r=1,2,3)	Vortex feeding sheet - cut strength
γ_w	Total bound vorticity on the wing A
γ_A	Bound vorticity component on the wing A
γ_F	Bound vorticity component on the wing A

γ_S	Total bound vorticity on the slat B	
γ_B	Bound vorticity component on the slat B	
γ_{B_1}	Bound vorticity component on the slat B corresponding to q=1 term - Equation (30)	
γ_G	Bound vorticity component on the slat B	
δ_W	Total trailing vorticity on the wing A	)
δ_A	Trailing vorticity component on the wing A	) Equation (9)
δ_F	Trailing vorticity component on the wing A	)
δ_S	Total trailing vorticity component on the slat B	)
δ_B	Trailing vorticity component on the slat B	) Equation (13)
δ_G	Trailing vorticity component on the slat B	)
ε	Semi-apex angle of the wing	
ε_B	Semi-apex angle of the slat	
θ_A	$= \cos^{-1} (-y/_{kx})$ angular interval on the wing A	
θ_B	$= \cos^{-1} (-{}^{y_B}/_{c_1 x})$ angular interval on the slat B	
θ_C	$= \cos^{-1} (-{}^{y_C}/_{c_1 x})$ angular interval on the slat C	
Λ	Angle of sweepback	
[illegible] or ϕ	Slat inclination	

I. INTRODUCTION

Leading edge devices and slats are applicable to a number of high speed wing planforms with high sweepback or strakes (Fig. 1). This includes aircraft with transonic manoeuvring capability and supersonic cruise vehicles not only for civil or transport functions but also for strategic reconnaissance and advanced air-defence concepts (e.g. against cruise-missile carriers and penetrating bombers). In the far future, liquid hydrogen fuel, if it is to be used, makes more sense for an aircraft with supersonic cruise capability. Leading edge devices may also be used on the canard wing of forward-sweep wing aircraft designs.

The leading edge design on aircraft is subject to compromises between the conflicting requirements of high speed lift/drag efficiency and low speed, and transonic manoeuvring requirements of high lift. The usual way of incorporating leading edge devices is design the wing for cruise or high speed with devices retracted and then to deploy them during the phase of flight when high lift is called for, i.e. at low speed and/or transonic manoeuvres.

Simple leading edge devices in the form of flaps or variable camber may be used, but they allow only one degree of movement and, therefore, a limited scope for optimisation. Leading edge slats offer one extra degree; the position and angle can both be varied for optimised condition.

For conventional aircraft with wings of low sweep-back, there is a considerable amount of information available on the subject of leading edge design with or without devices (Ref. 1). Calculation methods have been devised for treating 2-D geometries (Figs 2 and 3). The methods are strictly applicable only when 3-D effects such as those due to wing-tips or fuselage junctions, are small.

For wings of higher sweep-back, however, there seems to be only a small amount of information available, particularly with regard to leading edge devices. An idea of the order of gains from leading edge devices can be obtained by reference to the work of Ray and Hollingsworth (Ref. 2) on F-4 Fighter aircraft with leading edge sweep-back 51.4^{o} (Fig. 4). They conclude that incorporation of devices resulted in a sizeable 33% improvement on the buffet onset, and L/D performance gain of 35% at $C_L = 0.8$, and improved lateral directional characteristics throughout the test Mach number range of 0.6 to 0.94. The improvements were verified in a subsequent flight evaluation.

Goodmanson and Gratzer (Ref. 3) show in Fig.5, 24% improvement in L/D at $C_L = 0.4$, using droop and slats on a highly swept-back wing (L.E. sweep-back 70^{o} approximately). Experience of NASA Langley on supercruiser and arrow shaped wings also suggests similar improvements.

An idea of complexity of such flowfields can be gained from Fig. 6 which shows multiple vortex separations that arise due to the use of leading edge slats. The vortex separations are, of course, sources for non-linear lift and provided this lift is distributed on forward facing surfaces we have then a mechanism for reducing drag.

In a practical flow situation, compressibility, vortex wake and boundary layers on surfaces introduce further complexity to the flow field.

Recently Cuming and Dickison[4] have investigated flow around delta wings with conical type leading edge slats. Their studies have included flow visualisation using water tank, smoke and surface oil flow patterns. They have also conducted force tests on a selection of wing-slat geometries. They indicate that multiple flow separations and interactions are present and benefits in L/D of 10% - 15% are obtainable for certain conical type geometries.

II. PHYSICAL FLOW FIELDS AND THEORETICAL MODELS

II.1 QUALITATIVE FEATURES OF FLOW

It is instructive to look at the qualitative features of flow that lead to the possible use of leading edge devices, e.g. plain flaps, smooth variable camber or slotted flaps (slats). It is convenient to confine our attention to conical flows in small, moderate and higher incidence ranges. Conical streamline patterns on basis of Ref.9 have been sketch

Small Incidence Range

The simplest situation of attached flow over the wing with the leading edge flap deflected to prevent any separation at a particular incidence is illustrated in Fig. 7(a). This type of flow may be calculated using, for example, techniques such as conformal transformation or panel methods. The flow is susceptible to off-design variation and a shoulder separation as shown in Fig. 7(b) may appear. This shoulder separation may be avoided by using slots near the leading edge as shown in Figs 8(a) and (b). In Fig. 8(a) the 'rolled-up' wake of the flap is shown near its trailing edge whilst in Fig. 8(b) this wake is allowed to extend further over the wing. The qualitative features of the Figs 8(a) and (b), particularly the latter, resemble those of Fig. 7. It is difficult to lay down any rules about lift/drag (L/D) performance of the flows at this stage. Intuitively, we might say that the performance of the wing with the slotted flap would be worse than the calculated performance of Fig. 7(a), but perhaps better than the actual experimental performance of the shoulder flap (Fig. 7(b)).

Moderate Incidence Range

At moderate incidences the flow separates at the leading edge in spite of flap deflection and the flowfield as illustrated in Fig. 9 may appear. The separations near the shoulder and the leading edge may be controlled by using slots, as in Figs 8(a) and (b).

High Incidence Range

At higher incidence the primary vortex moves inboard of the shoulder. A simple model is shown in Fig. 10(a) and a more realistic one in Fig. 10(b) with a secondary separation fixed near the shoulder. This secondary separation could be removed by a slot as in Figs 11(a) and (b). These slots are in the opposite sense to those of Figs 8(a) and (b). They enable the idealized flow of Fig. 10(a) to be realized, however.

It is evident from the foregoing that there are a number of areas in which investigations for understanding the flow are needed, both theoretically and experimentally.

An idea of configurations suitable for modelling by theory can be gained from Figure 12.

II.2 APPLICABLE DESIGN METHODS

As far as the design methods are concerned, the current state of art may be inferred from a paper by Tinoco and Yoshihara[5] in which they have considered separated flow past slender thin wings with leading edge droop and vortex control tabs. The capability of the computer code using panel methods is limited to one vortex separation system only. Any extension of the panel method to simulate the wing and leading edge devices together will require a very large number of panels to permit sufficient resolution; to this must be added the panels required for simulation of multiple flow separations from various edges of the configuration.

The method of leading edge suction analogy is more suited to estimation of overall planform effects and not to detailed description of flow that is required for understanding of leading edge devices.

It is evident from the foregoing that we have some way to go before we can model the flows of Fig. 6 in a fully three-dimensional way. In a number of applications the wing trailing edge effect can be small, e.g. on slender wings the first two-thirds of the flow is nearly conical. On wings with strakes, the strake portion is mainly subject to slender wing principles. Slender wing theory forms a necessary platform for any three-dimensional calculations such as by step-by-step method. A more exact method is by inclusion of chordwise terms thus simulating the 3-D trailing edge effect.

The slender-wing approach is versatile and it can utilize either the conformal transformation method or Fourier type series formulation in the cross-flow plane - or a combination of both of these. The theoretical approaches of Brown and Michael[6], Nangia[7,8], Smith[9], Pullin[10,11] Jones[12], Cohen[13] an form essential background to the method mentioned in this report.

III THEORETICAL MODEL

III.1 Model Geometry

We take a set of Cartesian co-ordinates (x, y, z) with the origin at the apex of the wing (component A of the combination) as shown in Figure 13. The x-axis coincides with the centre line of the wing, the y-axis lies in the plane of the wing measured in the starboard direction and the z-axis is perpendicular to the wing. The angle of attack measured at wing centre-line with respect to the freestream V is α. The leading edges of the wing (component A of the combination) are defined by $y = \pm k x$. The perturbation velocities are denoted by u, v, w in the x, y, z system.

The starboard slat (component B of the combination) is located near the starboard leading edge of wing A. The centre line of the slat lies at $y = c_o.x$, $z = h_o.x$. The semi-span of the slat is $c_1 x$ and its inclination to y-axis is ϕ (measured positive upwards). For convenience, we introduce axes y_B and z_B to measure dimensions along and normal to the slat as shown in Figure 14. The leading edge of the slat lies at $y = (c_o + c_1 \cos \phi) x$ and $z = (h_o + c_1 \sin \phi) x$. The trailing edge of the slat lies at $y = (c_o - c_1 \cos \phi) x$ and $z = (h_o - c_1 \sin \phi) x$. The perturbation velocities are denoted by v_B and w_B along y_B and z_B directions.

The port slat (component C of the combination) is a mirror image of the starboard slat in the xz-plane. We introduce axes y_C and z_C for this slat as shown in Figure 14.

III.2 Boundary Conditions

Boundary conditions on the surfaces, edges and in the field are as follows:-

III.2.1 Surfaces

The problem is restricted to slender-body theory and a solution is desired which satisfies the condition of zero normal velocity in each cross-flow plane on the wing-slat combination surfaces

III.2.2 Edges

At the edges of the configuration, there is a choice of conditions available which depends on the complexity of the model adopted as shown in the following table.

EDGE BI[illegible]		NO EDGE VORTEX SHEETS (LINEAR THEORY)	VORTEX SHEETS REPLACED BY VORTEX-CUT ARRANGEMENTS AS IN BROWN AND MICHAEL MODEL (Ref. 6)	VORTEX SHEETS AS IN SMITH'S MODEL (Ref. 9)
IMPLICATIONS	(a) Velocity	Infinite velocity at the edge (attached flow)	Finite velocity at the edge (flow separates)	Finite velocity at the edge (flow separates)
	(b) Load	Infinite load at the edge	Small finite load at the edge	Zero load at the edge
	(c) Trailing vorticity	Tends to ∞ as $\frac{1}{\sqrt{1-d^2}}$	Tends to zero as $\sqrt{1-d^2}$	δ_B related to bound component to give correct load at the edge
	(d) Complexity of solution	Least complex	Medium complex	Most complex
WING	**Leading Edge**	✓	✓	✓
SLAT	**Trailing Edge**	╳	✓	✓ More appropriate: Pullin (Ref. 11)
	Leading Edge	✓	✓	✓

In the present work, edge vortex sheets are not employed and the choice is restricted to four possible types of wing-slat configurations as shown in Figure 15.

1. Configuration A-S-A Attached flow at wing and slat leading edges, vortex-cut arrangement at slat trailing edge.

2. Configuration S-S-A Attached flow at wing leading edge, vortex-cut arrangements at the slat leading and trailing edges.

3. Configuration A-S-S Attached flow at wing leading edge, vortex-cut arrangements at the slat leading and trailing edges.

4. Configuration S-S-S Vortex-cut arrangements at all edges.

In addition, the configuration of slats only is of interest as a reference. Two possible configurations are (Figure 16):

1. Configuration S-A Attached flow at slat leading edge, vortex-cut arrangement at slat trailing edge.

2. Configuration S-S Vortex-cut arrangements at both edges of the slat.

It is thought that the more complex edge vortex sheet models can be considered once an insight has been gained from the calculation of the foregoing configurations.

In the cross-flow plane, the behaviour of trailing vorticity near the edges can be summarised as follows:

Wing ($\theta_A = \cos^{-1}(-{}^{y}/_{kx})$)

Flow at Wing Leading Edge	Leading Edge Vortex	Form of Vorticity at Edge
Attached	0	$\propto \dfrac{y/(k.x)}{\sqrt{1-\left(\frac{y}{kx}\right)^2}}$ or $\cot\theta_A$
Separated	Γ_1	$\propto \frac{y}{kx}\sqrt{1-\left(\frac{y}{kx}\right)^2}$ or $\sin 2\theta_A$

Starboard Slat ($\theta_B = \sin^{-1} ({}^{y_B}/c_1 x)$)

Flow at Edge	Edge Vortex	Form of Vorticity at the Edge
Attached at Slat Leading Edge Separated at Slat Trailing Edge	0 Γ_2	$\propto \sqrt{\dfrac{c_1 + y_B}{c_1 - y_B}}$ or $\tan \dfrac{\theta_B}{2}$
Separated Flow at Slat Leading Edge Separated Flow at Slat Trailing Edge	Γ_3 Γ_2	$\propto \sqrt{1 - \left(\dfrac{y_B}{c_1 x}\right)^2}$ or $\sin \theta_B$

Port Slat

The behaviour follows from symmetry considerations.

III 2.3 Field

(a) The flow is unperturbed at infinity.

(b) In the case of flow separations idealised as vortex sheets, it is necessary to satisfy that they are stream surfaces of three-dimensional flow. For the vortex-cut arrangement we need to satisfy only that the arrangement as a whole carries no load.

(c) To prevent vorticity being carried through the apex from one element of the wing-slat combination to another, it is required that the total circulation about each element of the combination is zero. The wing by virtue of its symmetry satisfies this condition automatically. The condition needs to be imposed on slats only.

In this report, as mentioned earlier, configurations with and without flow separation from edges are of interest. In the most general case, i.e. configuration S-S-S, it is convenient to define various quantities as follows; we need to refer to starboard slat in the first place (Fig. 17).

Wing

Quantity	Location	Sense
Vortex $\Gamma_1(x)$	$y_1(x)$, $z_1(x)$	Positive anticlockwise
Cut $\dfrac{d\Gamma_1(x)}{dx}$	between (kx, 0) and $\{y_1(x), z_1(x)\}$	
Trailing vorticity $\delta_w\left(\dfrac{y}{kx}\right)$	Along wing surface	Positive anticlockwise about x-axis
Bound vorticity $\gamma_w\left(\dfrac{y}{kx}\right)$	Along wing surface - follows from δ_w, i.e. $\dfrac{\partial \gamma_w}{\partial y} = -\dfrac{\partial \delta_w}{\partial x}$	Positive clockwise about y-axis

Quantity	Location	Sense
Vortex $\Gamma_2(x)$	$\{y_2(x),\ z_2(x)\}$	Positive anticlockwise
Cut $\dfrac{d\Gamma_2(x)}{dx}$	between $\{(c_o-c_1\cos\phi)x,$ $(h_o-c_1\sin\phi)x\}$ and $\{y_2(x),\ z_2(x)\}$	
Vortex $\Gamma_3(x)$	$y_3(x),\ z_3(x)$	Positive anticlockwise
Cut $\dfrac{d\Gamma_3(x)}{dx}$	between $\{(c_o+c_1\cos\phi)x,$ $(h_o+c_1\sin\phi)x\}$ and $\{y_3(x),\ z_3(x)\}$	
Trailing vorticity $\delta_s\left(\dfrac{y}{kx}\right)$	Along slat surface	Positive anticlockwise about x-axis
Bound vorticity $\gamma_s\left(\dfrac{y}{kx}\right)$	Along slat surface - follows from δ_s, i.e. $\dfrac{\partial\gamma_s}{\partial y} = -\dfrac{\partial\delta_s}{\partial x}$	Positive clockwise about y-axis

The quantities on the port side of the configuration are defined on considerations of symmetry. It is convenient, however, to denote the port slat trailing vorticity by δ_p and bound vorticity by γ_p.

As in the Brown and Michael model, the vortex-cut representation leads to a small finite load at the edge under consideration. Zero load at the edge can only be obtained with vortex sheet representation by Smith's[9] model.

IV DEVELOPMENT OF BOUNDARY CONDITIONS

IV 1. Surfaces

We need to consider the cross-flow plane in which the trailing vorticities δ_w, δ_s, δ_p and any or all of the vortices Γ_1, Γ_2, Γ_3 are present.

A general point $(x_A, y_A, 0)$ on the wing

The upwash equation is

$$w_{\delta_W}(x_A, y_A, 0) + w_{\delta_S}(x_A, y_A, 0) + w_{\delta_P}(x_A, y_A, 0)$$

$$+ w_{\Gamma_1}(x_A, y_A, 0) + w_{\Gamma_2}(x_A, y_A, 0) + w_{\Gamma_3}(x_A, y_A, 0) + V\sin\alpha = 0$$

where w_{δ_W} is the upwash induced due to the vorticity δ_W on the wing

w_{δ_S} " " " " " " " " δ_S on the slat B

w_{δ_P} " " " " " " " " δ_P on the slat C

w_{Γ_r} $(r = 1,2,3)$ " " " " " " a pair of vortices $\Gamma_r(x)$ at $\pm y_r(x)$, $z_r(x)$.

Geometry considerations show that

$$w_{\delta_P}(x_A, y_A, 0) = w_{\delta_S}(x_A - y_A, 0).$$

The upwash equation may now be put in more convenient form with slat induced velocities measured in v_B, w_B system.

$$w_{\delta_W}(x_A, y_A, 0) + \left\{ w_{B_{\delta_S}}(x_A, y_{BA}, z_{BA}) + w_{B_{\delta_S}}(x_A, y'_{BA}, z'_{BA}) \right\}\cos\phi$$

$$+ \left\{ v_{B_{\delta_S}}(x_A, y_{BA}, z_{BA}) - v_{B_{\delta_S}}(x_A, y'_{BA}, z'_{BA}) \right\}\sin\phi$$

$$+ w_{\Gamma_1}(x_A, y_A, 0) + w_{\Gamma_2}(x_A, y_A, 0) + w_{\Gamma_3}(x_A, y_A, 0) + V\sin\alpha = 0 \quad \ldots (1)$$

where (x_A, y_{BA}, z_{BA}) is the point $(x_A, y_A, 0)$ in the x, y_B, z_B axes system (Fig. 18) and (x_A, y'_{BA}, z'_{BA}) is the point $(x_A, -y_A, 0)$ in x, y_B, z_B axes system.

Slat B at a general point (x_B, y_B, 0)

The upwashes are measured in w_B direction and we have for the most general case with all Γ_1, Γ_2 and Γ_3 being present

$$w_{B\delta_W}(x_B, y_B, 0) + w_{B\delta_S}(x_B, y_B, 0) + w_{B\delta_P}(x_B, y_B, 0)$$

$$+ w_{B\Gamma_1}(x_B, y_B, 0) + w_{B\Gamma_2}(x_B, y_B, 0) + w_{B\Gamma_3}(x_B, y_B, 0) + V \sin\alpha_B = 0$$

where $w_{B\delta_W}$ is the upwash induced due to the vorticity δ_W on the wing

$w_{B\delta_S}$ " " " " " " " " δ_S on the slat B

$w_{B\delta_P}$ " " " " " " " " δ_P on the slat C

$w_{B\Gamma_r}$ (r=1,2,3) is the upwash induced due to a pair of vortices $\Gamma_r(x)$ at $\pm y_r(x)$, $z_r(x)$

α_B is angle of attack of the slat.

Geometry considerations show that

$$w_{B\delta_P}(x_B, y_B, 0) = w_{B\delta_S}(x_B, y_{Bc}, z_{Bc})\cos 2\phi + v_{B\delta_S}(x_B, y_{Bc}, z_{Bc})\sin 2\phi$$

where $v_{B\delta_S}$ is the sidewash velocity induced due to vorticity δ_S on the slat

y_{Bc}, z_{Bc} are defined in Fig. 19.

The upwash equation may now be put in more convenient form with wing induced and vortices induced velocities measured in v, w system.

$$w_{\delta_W}(x_B, y_{AB}, z_{AB})\cos\phi - v_{\delta_W}(x_B, y_{AB}, z_{AB})\sin\phi$$

$$+ w_{B\delta_S}(x_B, y_B, 0) + w_{B\delta_S}(x_B, y_{Bc}, z_{Bc})\cos 2\phi + v_{B\delta_S}(x_B, y_{Bc}, z_{Bc})\sin 2\phi$$

$$+ \sum_{r=1}^{3} \left\{ w_{\Gamma_r}(x_B, y_{AB}, z_{AB})\cos\phi - v_{\Gamma_r}(x_B, y_{AB}, z_{AB})\sin\phi \right\}$$

$$+ V \sin\alpha_B = 0 \qquad \ldots\ldots (2)$$

where the point (x_B, y_{AB}, z_{AB}) is the x_B, y_B, z_B in the x, y, z system.

IV 2. Field Boundary Conditions of Zero Total Circulation about Slat

If the flow is attached about the slat leading edge then

$$\Gamma_2 + \int_{-c_1 x}^{+c_1 x} \delta_s(y_B)\, dy_B = 0 \qquad \ldots\ldots (3)$$

If the flow is separated at the slat leading edge then

$$\Gamma_2 + \Gamma_3 + \int_{-c_1 x}^{+c_1 x} \delta_s(y_B)\, dy_B = 0 \qquad \ldots\ldots (4)$$

IV 3. Zero Force on Vortex-cut Arrangements

The condition of zero force on vortex-cut arrangement follows from Brown and Michael (Ref. 6) and may be written in the general form for a vortex at $x, y_r(x), z_r(x)$ joined by a cut to an edge at $x, y_\ell(x), z_\ell(x)$ as follows

$$2\frac{y_r}{x} = \frac{v_r}{V} + \frac{y_\ell}{x}$$
$$2\frac{z_r}{x} = \frac{w_r}{V} + \frac{z_\ell}{x} \qquad \ldots\ldots (5)$$

where v_r and w_r are the velocities induced at the vortex position $x, y_r(x), z_r(x)$ due to whole flowfield (excluding the effect of vortex on itself).

We may now write Equation (5) for each edge of the combination

Wing Leading Edge

$$2\frac{y_1}{x} = \frac{v_1}{V} + k_1$$
$$2\frac{z_1}{x} = \frac{w_1}{V} \qquad \ldots\ldots (6)$$

Slat Trailing Edge

$$2\frac{y_2}{x} = \frac{v_2}{V} + c_0 - c_1\cos\phi$$
$$2\frac{z_2}{x} = \frac{w_2}{V} + h_0 - c_1\sin\phi \qquad \ldots\ldots (7)$$

It is interesting to note that for the particular case of $\phi = 0$ and vanishing α, we have

$v_2 \to 0 \quad , \quad w_2 \to V\sin\alpha.$

Therefore

$$y_2/x = \frac{c_0 - c_1}{2}$$
$$z_2/x = \frac{\sin\alpha + h_0}{}$$

Slat Leading Edge

$$2\frac{y_3}{x} = \frac{v_3}{V} + c_0 + c_1\cos\varphi \qquad \ldots\ldots (8)$$

$$2\frac{z_3}{x} = \frac{w_3}{V} + h_0 + c_1\sin\varphi$$

V SOLUTION BY SERIES FORMULATION

The series type approach for determination of vorticity is a convenient way of satisfying the general upwash equations.

V 1. Series Forms for Trailing Vorticities on the Wing and the Slat

We write for the wing with reference to Section III 2.2 splitting δ_W into two contributions δ_F and δ_A.

$$\delta_W(y) \equiv \delta_W(\theta_A) = \delta_F(\theta_A) + \delta_A(\theta_A) \qquad \ldots\ldots (9)$$

where $\theta_A = \cos^{-1}(-y/kx)$

If the flow is attached at the wing leading edge then the first contribution is

$$\delta_F(\theta_A) = -g_1 . V . \cot\theta_A \qquad \ldots\ldots (10)$$

It is implied that $\Gamma_1 = 0$.

If the flow on the wing is separated at the leading edge, then

$\delta_F(\theta_A) = 0$ and $\Gamma_1 \neq 0$.

The second contribution is denoted by

$$\delta_A(\theta_A) = V . \sum_{p=1}^{M} a_p \sin(2p\theta_A) \qquad \ldots\ldots (11)$$

The general form for $\delta_W(\theta_A)$ is given by

$$\delta_W(\theta_A) = -g_1 . V . \cot\theta_A + V \sum_{p=1}^{M} a_p \sin(2p\theta_A) \qquad \ldots\ldots (12)$$

The trailing vorticity δ_S on the starboard slat B comprises two portions with reference to Section III 2.2

$$\delta_S(y_B) \equiv \delta_S(\theta_B) = \delta_G(\theta_B) + \delta_B(\theta_B) \qquad \ldots\ldots (13)$$

where $\theta_B = \sin^{-1}(-y_B/c_1x)$

If the flow is attached at the slat leading edge, then

$$\delta_G(\theta_B) = g_3 . V . \tan\theta_B/2 \quad \text{and} \quad \Gamma_3 = 0 \qquad \ldots\ldots (14)$$

If the flow is separated at the slat leading edge, then

$\delta_G(\theta_B) = 0$ and $\Gamma_3 \neq 0$

The second contribution is denoted by

$$\delta_B(\theta_B) = V . \sum_{q=1}^{N} b_q . \sin(q\theta_B) \quad \ldots . \quad (15)$$

The general form for $\delta_S(\theta_B)$ is given by

$$\delta_S(\theta_B) = V . g_3 . \tan \theta_B/_2 + V . \sum_{q=1}^{N} b_q . \sin(q\theta_B) \quad \ldots . \quad (16)$$

The expressions for trailing vorticity δ_P on the port slat C follow from geometry considerations, i.e.

$$\delta_P(\theta_c) = -\delta_S(\theta_B) \quad \ldots . \quad (17)$$

where θ_C is the image of point θ_B in x z -plane.

$$\theta_C = \sin^{-1}\left(\underline{y_c}/_{c_1x} \right)$$

V 2. <u>Series Forms for Zero Total Circulation on the Slat</u>

(a) Attached flow about slat L.E.

Equation (3) becomes

$$\Gamma_2 + \int_{-c_1x}^{c_1x} \delta_G \, dy_B + \int_{-c_1x}^{c_1x} \delta_B \, dy_B = 0$$

On substitution of $y_B = -c_1x . \cos\theta$ we obtain

$$\Gamma_2 - c_1x \int_{-1}^{+1} \delta_G\left(-\frac{y_B}{c_1x}\right) d\left(-\frac{y_B}{c_1x}\right) - c_1x \int_{-1}^{+1} \delta_B\left(-\frac{y_B}{c_1x}\right) d\left(-\frac{y_B}{c_1x}\right) = 0$$

or

$$\Gamma_2 + c_1x \int_0^{\pi} \delta_G(\theta_B) \sin\theta_B \, d\theta_B + c_1x \int_0^{\pi} \delta_B(\theta_B) \sin\theta_B \, d\theta_B = 0$$

Substituting Equations (14) and (15)

$$\Gamma_2 + c_1x . g_3 . V \int_0^{\pi} \tan\frac{\theta_B}{2} \sin\theta_B . d\theta_B + c_1x . V \sum_{q=1}^{N} b_q . \int_0^{\pi} \sin(q\theta_B) \sin\theta_B . d\theta_B = 0$$

i.e.

$$\Gamma_2 + V . g_3 . c_1x . \pi + V . c_1x . b . \frac{\pi}{2} = 0$$

In non-dimensional terms

$$\frac{\Gamma_2}{V.\,k\,x} + g_3 \cdot \frac{c_1}{k_1} \cdot \pi + \frac{c_1}{k} \cdot b_1 \cdot \frac{\pi}{2} = 0 \qquad \ldots\ldots (18)$$

(b) Separated flow about slat L.E.

Equation (4) becomes

$$\Gamma_2 + \Gamma_3 + \int_{-c_1 x}^{c_1 x} \delta_B \, dy_B = 0$$

which on using similar analysis as in the previous case yields

$$\Gamma_2 + \Gamma_3 + c_1 x \cdot V \cdot b_1 \cdot \pi/2 = 0$$

In non-dimensional terms

$$\frac{\Gamma_2}{V.\,k\,x} + \frac{\Gamma_3}{V.\,k_x} + \frac{c_1}{k} \cdot b_1 \cdot \pi/2 = 0 \qquad \ldots\ldots (19)$$

Equations (18) and (19) therefore offer convenient relationships to remove one of the unknowns, say b_1, from the calculations.

V 3. <u>Series Forms for Bound Vorticities</u>

The expressions for bound vorticities follow from application of the equation of conservation of vorticity, i.e.

$$\frac{\partial \delta}{\partial x} + \frac{\partial \gamma}{\partial y} = 0 \qquad \ldots\ldots (20)$$

<u>Wing</u>

On the wing we have

$$\cos\theta_A = -y/k\,x$$

i.e. $\sin\theta_A \cdot \dfrac{d\theta_A}{\partial x} = \dfrac{y}{k\,x^2}$ and $\sin\theta_A \dfrac{\partial\theta_A}{\partial y} = -\dfrac{1}{k\,x}$

Equation (20) becomes

$$\frac{\partial \gamma_W}{\partial \theta_A} = -\,\partial\theta/\partial x \Big/ \frac{\partial\theta_A}{\partial y} \cdot \frac{\partial \delta_W}{\partial \theta_A} = y/x \,\frac{\partial \delta_W}{\partial \theta_A} = -k\cos\theta_A \frac{\partial \delta_W}{\partial \theta_A} \qquad \ldots\ldots (21)$$

We split $\gamma_W(\theta_A)$ into three contributions as follows

$$\gamma_W(\theta_A) = \gamma_F(\theta_A) + \gamma_B(\theta_A) + \frac{d\Gamma_1}{dx} \qquad \ldots\ldots (22)$$

$\gamma_F(\theta_A)$ corresponds to $\delta_F(\theta_A)$ and arises only when the flow is attached at the wing leading edge. $\gamma_B(\theta_A)$ corresponds to $\delta_B(\theta_A)$ $\frac{d\Gamma_1}{dx}$ arises only when the flow is separated at the wing leading edge.

On partial differentiation with respect to θ_A, equation (22) yields

$$\frac{\partial \gamma_W(\theta_A)}{\partial \theta_A} = \frac{\partial \gamma_F(\theta_A)}{\partial \theta_A} + \frac{\partial \gamma_B(\theta_A)}{\partial \theta_A} \quad \ldots\ldots \quad (23)$$

<u>Derivation of $\gamma_F(\theta_A)$</u>

Using Equations (10) and (21)

$$\frac{\partial \gamma_F(\theta_A)}{\partial \theta_A} = -k \cos\theta_A \cdot g_1 \cdot V \operatorname{cosec}^2\theta_A$$

which gives by integration with respect to θ_A within limits of 0 and θ_A an expression for $\gamma_F(\theta_A)$.

$$\gamma_F(\theta_A) = -k \cdot g_1 \cdot V \cdot \int_0^{\theta_A} \frac{\cos\theta_A}{\sin^2\theta_A}\, d\theta_A \quad \ldots\ldots \quad (24)$$

$$= k \cdot g_1 \cdot V/\sin\theta_A$$

We may also write this in form

$$\gamma_F\left(-\frac{y}{kx}\right) = k \cdot g_1 \, V \Big/ \sqrt{1 - \left(\frac{y}{kx}\right)^2}$$

which corresponds to linear attached flow solution of Jones slender wing approach.

<u>Derivation of $\gamma_B(\theta_A)$</u>

Using Equations (15) and (21)

$$\frac{\partial \gamma_B(\theta_A)}{\partial \theta_A} = -k \cos\theta_A \cdot V. \sum_{p=1}^{M} 2p \cdot a_p \cdot \cos 2p\,\theta_A$$

$$= -k.V. \sum_{p=1}^{M} p.\, a_p \left\{ \cos(2p+1)\theta + \cos(2p-1)\theta \right\}$$

which gives by integration with respect to θ_A within limits of 0 and θ_A an expression for $\gamma_B(\theta_A)$

$$\gamma_B(\theta_A) = -k.V. \sum_{p=1}^{M} a_p \left\{ \frac{\sin(2p+1)\theta_A}{2p+1} + \frac{\sin(2p-1)\theta_A}{2p-1} \right\} \quad \ldots\ldots \quad (25)$$

Slat B

To obtain expressions for γ_S from δ_S we need to apply the equation of conservation of vorticity (equation 20)) in terms of co-ordinates x, y_O, z_O as in Figure 20. This approach then allows for inclination φ of the slat

$$y_o = (c_o \cos\varphi + h_o \sin\varphi - c_1 \cos\theta_B)\, x$$

or

$$\cos\theta_B = \frac{y_o}{c_1 x} - \frac{c_o}{c_1}\cos\varphi - \frac{h_o}{c_1}\sin\varphi$$

i.e. $\sin\theta_B \cdot \dfrac{\partial\theta_B}{\partial x} = \dfrac{y}{c_1 x^2}$ and $\cos\theta_B \cdot \dfrac{\partial\theta_B}{\partial y_o} = -\dfrac{1}{c_1 x}$

Equation (21) becomes

$$\frac{\partial\gamma_S(\theta_B)}{\partial\theta_B} = -\frac{\partial\theta_B}{\partial x}\Big/\frac{\partial\theta_B}{\partial y_o} \cdot \frac{\partial\delta_S(\theta_B)}{\partial\theta_B}$$

$$= y/x\,\frac{\partial\delta_S(\theta_B)}{\partial\theta_B} = (c_o\cos\varphi + h_o\sin\varphi - c_1\cos\theta_B)\frac{\partial\delta_S(\theta_B)}{\partial\theta_B} \quad \ldots \quad (26)$$

Derivation of $\gamma_G(\theta_B)$

Using Equations (14) and (26)

$$\frac{\partial\gamma_G(\theta_B)}{\partial\theta_B} = (c_o\cos\varphi + h_o\sin\varphi - c_1\cos\theta_B)\cdot g_3 \cdot V \cdot \frac{1}{2}\sec^2\left(\frac{\theta_B}{2}\right)$$

$$= g_3 \cdot V \cdot \frac{1}{2}\left\{(c_o\cos\varphi + h_o\sin\varphi)\sec^2\left(\frac{\theta_B}{2}\right) - c_1\left(2 - \sec^2(\theta_B/2)\right)\right\}$$

which gives on integration with respect to θ_B

$$\gamma_G(\theta_B) = g_3 \cdot V \cdot \left\{(c_o\cos\varphi + h_o\sin\varphi + c_1)\tan\left(\frac{\theta_B}{2}\right) - c_1\theta_B\right\} + V \cdot F \quad \ldots \quad (27)$$

where F is a constant of integration and it is evaluated by using the Field condition (equations (3, 4)).

At $\theta_B = 0$ we have

$$\gamma_G(\theta_B = 0) = V \cdot F. \quad \ldots \quad (28)$$

Derivation of $\gamma_B(\theta_B)$

Using Equations (15) and (26)

$$\frac{\partial \gamma_B(\theta_B)}{\partial \theta_B} = V.\left(c_0\cos\varphi + h_0\sin\varphi - c_1\cos\theta_B\right)\sum_{q=1}^{M} b_q \cdot q \cdot \cos\theta_B$$

$$= V\sum_{q=1}^{N} b_q \cdot q \cdot \left[\left(c_0\cos\varphi + h_0\sin\varphi\right)\cos q\theta_B - c_1\cos\theta_B\,\cos q\theta_B\right]$$

$$= V\sum_{q=1}^{N} b_q \cdot q\left[\left(c_0\cos\varphi + h_0\sin\varphi\right)\cos q\theta_B - \frac{c_1}{2}\left\{\cos(q+1)\theta_B + \sin(q-1)\theta_B\right\}\right]$$

which gives on integration with respect to θ_B

$$\gamma_B(\theta_B) = V.\sum_{q=1}^{N} b_q \cdot \left[\left(c_0\cos\varphi + h_0\sin\varphi\right)\sin q\theta_B - \frac{q}{2}c_1\left\{\frac{\sin(q+1)\theta_B}{q+1} + \frac{\sin(q-1)\theta_B}{q-1}\right\}\right] + V.F_B \quad \ldots \ (29)$$

where F_B is a constant of integration and it is determined from boundary conditions at the edges of the slat. It arises from q = 1 term only when $\frac{\sin(q-1)\theta_B}{q-1}$ reduces to θ_B.

We examine q = 1 term

$$\gamma_{B_1}(\theta_B) = V.\,b_1\left\{\left(c_0\cos\varphi + h_0\sin\varphi\right)\sin\theta_B - \frac{c_1}{2}\left(\frac{\sin 2\theta_B}{2} + \theta\right)\right\} + V.F_B \quad \ldots \ (30)$$

If the flow is separated at both edges of the slat then we allow for two vortex "feeding" cuts and write

$$\gamma_{B_1}(\theta_B = 0) = -\frac{\partial\Gamma_2}{\partial x}, \qquad \gamma_{B_1}(\theta_B = \pi) = \frac{\partial\Gamma_3}{\partial x}$$

i.e.

$$\frac{\partial\Gamma_2}{\partial x} = -V.\,F_B$$

and

$$\frac{\partial\Gamma_3}{\partial x} = -V.\,b_1\,\frac{c_1}{2}\pi + V.\,F_B$$

We now have a relationship between

Γ_3, Γ_2 and b_1, i.e.

$$\frac{\partial \Gamma_3}{\partial x} = - V b_1 . c_1 . \frac{\pi}{2} - \frac{\partial \Gamma_2}{x} \quad \ldots \ldots (31)$$

or $$b_1 = - \left(\frac{\partial \Gamma_2}{\partial x} + \frac{\partial \Gamma_3}{\partial x} \right) . \frac{2}{\pi c_1}$$

This relationship satisfies the field condition of zero total circulation about the slat.

If the flow is attached at the slat leading edge but separated at its trailing edge, then we allow only for one vortex "feeding" cut and write

$$\gamma_{B_1} (\theta_B = \pi) = 0$$

Equation (30) then yields

$$\gamma_{B_1} (\theta_B = \pi) = 0 = -V . b_1 \frac{c_1}{2} \pi + V . F_B$$

or $$F_B = b_1 . c_1 . \pi/2$$

Substituting for F_B in Equation (30), we get

$$\gamma_{B_1} (\theta_B) = V . b_1 \left\{ (c_0 \cos\phi + h_0 \sin\phi) \sin\theta_B - \frac{c_1}{2} \left(\frac{\sin 2\theta_B}{2} + \theta_B - \pi \right) \right\} \quad \ldots (32)$$

At $\theta_B = 0$, we have

$$\gamma_{B_1} (\theta_B = 0) = V . b_1 . c_1 . \pi/2$$

Total bound vorticity at slat trailing edge $\theta_B = 0$ is given from

$$\gamma_S (\theta_B = 0) = \gamma_G (\theta_B = 0) + \gamma_B (\theta_B = 0)$$
$$= V . F . + V . b_1 . c_1 . \pi/2$$

By continuity this is fed into the vortex Γ_2 using the appropriate sign at the slat trailing edge

$$\gamma_S (\theta_B = 0) = - \frac{\partial \Gamma_2}{\partial x} = - \frac{\Gamma_2}{x}$$

or $$- \frac{\Gamma_2}{x} = V . F . + V . b_1 . c_1 . \pi/2$$

or $$\Gamma_2 + x . V . F + V . c_1 x . b_1 . \pi/2 = 0$$

Comparing this with Equation (28), we obtain

$$F = g_3 \cdot c_1 \cdot \pi$$

$\gamma_G(\theta_B)$ from Equation (27) is

$$\gamma_G(\theta_B) = g_3 \cdot V \cdot \left\{ \left(c_0 \cos\varphi + h_0 \sin\varphi + c_1 \right) \tan\frac{\theta_B}{2} - c_1 (\theta_B - \pi) \right\} \quad \ldots\ldots \quad (33)$$

V.4 Upwash Equation for Wing

The series forms for δ_w, δ_s and δ_p are substituted in Equation (1). We distinguish now between the four possible configurations A-S-A, S-S-A, A-S-S and S-S-S.

(a) Configuration A-S-A

Using Equations (1), (9), (13)

$$\begin{aligned}
& w_{\delta_F}(x_A, y_A, 0) + w_{\delta_A}(x_A, y_A, 0) \\
& \quad + \cos\varphi \left\{ w_{B\delta_G}(x_A, y_{BA}, z_{BA}) + w_{B\delta_B}(x_A, y_{BA}, z_{BA}) \right. \\
& \qquad \left. + w_{B\delta_G}(x_A, y'_{BA}, z'_{BA}) + w_{B\delta_B}(x_A, y'_{BA}, z'_{BA}) \right\} \\
& \quad + \sin\varphi \left\{ v_{B\delta_G}(x_A, y_{BA}, z_{BA}) + v_{B\delta_B}(x_A, y_{BA}, z_{BA}) \right. \\
& \qquad \left. - v_{B\delta_G}(x_A, y'_{BA}, z'_{BA}) - v_{B\delta_G}(x_A, y'_{BA}, z'_{BA}) \right\} \\
& \quad + w_{\Gamma_2}(x_A, y_A, 0) + V \sin\alpha = 0
\end{aligned}$$

Using series froms for trailing vorticity distributions from Equations (12), (16) and writing for constant x_A in the crossflow plane. All distances y and z are non-dimensionalized by dividing by kx.

$$g_1 \cdot gw_1(\theta_A) + \sum_{p=1}^{M} a_p \cdot aw_{\delta_A}(p, \theta_A)$$

$$+ g_3 \left[\left\{ gw_{\delta_{G_3}}(y_{BA}, z_{BA}) + gw_{\delta_{G_3}}(y'_{BA}, z'_{BA}) \right\} \cos\phi + \left\{ gv_{\delta_{G_3}}(y_{BA}, z_{BA}) - gv_{\delta_{G_3}}(y'_{BA}, z'_{BA}) \right\} \sin\phi \right]$$

$$+ \sum_{q=1}^{N} b_q \cdot \left[\left\{ bw_{\delta_B}(q, y_{BA}, z_{BA}) + bw_{\delta_B}(q, y'_{BA}, z'_{BA}) \right\} \cos\phi + \left\{ bv_{\delta_B}(q, y_{BA}, z_{BA}) - bv_{\delta_B}(q, y'_{BA}, z'_{BA}) \right\} \sin\phi \right]$$

$$+ \frac{\Gamma_2}{V.\,kx} \cdot gw_{\Gamma_2}(y_A, 0) = -\sin\alpha \qquad \ldots . \quad (34)$$

where the unknowns are g_1, a_p, b_q, g_3 and Γ_2. The other multiplying terms are velocity influence coefficients which are defined in the Appendix. I·

(b) <u>Configuration S-S-A</u>

$$w_{\delta_A}(x_A, y_A, 0) + \cos\phi \left\{ w_{B\delta_B}(x_A, y_{BA}, z_{BA}) + w_{B\delta_B}(x_A, y'_{BA}, z'_{BA}) \right\} + \sin\phi \left\{ v_{B\delta_B}(x_A, y_{BA}, z_{BA}) + v_{B\delta_B}(x_A, y'_{BA}, z'_{BA}) \right\}$$

$$+ w_{\Gamma_1}(x_A, y_A, 0) + w_{\Gamma_2}(x_A, y_A, 0) + V\sin\alpha = 0$$

Using series froms for trailing vorticity distributions from Equations (12), (16), we have for constant x_A in the crossflow plane

$$\sum_{p=1}^{M} a_p \cdot aw_{\delta_A}(p, \theta_A)$$

$$+ g_3 \Big[\Big\{ gw_{\delta_{G_3}}(y_{BA}, z_{BA}) + gw_{\delta_{G_3}}(y'_{BA}, z'_{BA}) \Big\} \cos\phi$$

$$+ \Big\{ gv_{\delta_{G_3}}(y_{BA}, z_{BA}) - gv_{\delta_{G_3}}(y'_{BA}, z'_{BA}) \Big\} \sin\phi \Big]$$

$$+ \sum_{q=1}^{N} b_q \cdot \Big[\Big\{ bw_{\delta_B}(q, y_{BA}, z_{BA}) + bw_{\delta_B}(q, y'_{BA}, z'_{BA}) \Big\} \cos\phi$$

$$+ \Big\{ bv_{\delta_B}(q, y_{BA}, z_{BA}) - bv_{\delta_B}(q, y'_{BA}, z'_{BA}) \Big\} \sin\phi \Big]$$

$$+ \frac{\Gamma_1}{V \cdot kx} \cdot gw_{\Gamma_1}(y_A, 0) + \frac{\Gamma_2}{V \cdot kx} \cdot gw_{\Gamma_2}(y_A, 0)$$

$$= -\sin\alpha$$

. . . . (35)

where the unknowns are a_p, g_3, b_q, Γ_1 and Γ_2. The multiplying terms are the velocity influence coefficients which are defined in Appendix I.

(c) Configuration A-S-S

$$w_{\delta_F}(x_A, y_A, 0) + w_{\delta_A}(x_A, y_A, 0)$$

$$+ \cos\phi \cdot \Big\{ w_{B_{\delta_B}}(x_A, y_{BA}, z_{BA}) + w_{B_{\delta_B}}(x_A, y'_{BA}, z'_{BA}) \Big\}$$

$$+ \sin\phi \Big\{ v_{B_{\delta_B}}(x_A, y_{BA}, z_{BA}) - v_{B_{\delta_B}}(x_A, y'_{BA}, z'_{BA}) \Big\}$$

$$+ w_{\Gamma_2}(x_A, y_A, 0) + w_{\Gamma_3}(x_A, y_A, 0) + V \sin\alpha = 0$$

Using series forms for trailing vorticity distributions as in the previous case, we have for constant x_A in the cross-flow plane

$$g_1 \cdot gw_1(\theta_A) + \sum_{p=1}^{M} a_p \cdot aw_{\delta_A}(p, \theta_A)$$

$$+ \sum_{q=1}^{N} b_q \cdot \left[\left\{ bw_{\delta_B}(q, y_{BA}, z_{BA}) + bw_{\delta_B}(q, y'_{BA}, z'_{BA}) \right\} \cos\phi \right.$$

$$\left. + \left\{ bv_{\delta_B}(q, y_{BA}, z_{BA}) - bv_{\delta_B}(q, y'_{BA}, z'_{BA}) \right\} \sin\phi \right]$$

$$+ \frac{\Gamma_2}{V \cdot k_z} gw_{\Gamma_2}(y_A, 0) + \frac{\Gamma_3}{V \cdot k_z} \cdot gw_{\Gamma_3}(y_A, 0) =$$

$$- \sin\alpha$$

. . . . (36)

where the unknowns are g_1, a_p, b_q, Γ_2 and Γ_3. The multiplying terms are velocity influence coefficients, which are defined in Appendix I.

(d) Configuration S-S-S

$$w_{\delta_A}(x_A, y_A, 0) + \cos\phi \left\{ w_{B_{\delta_B}}(x_A, y_{BA}, z_{BA}) + w_{B_{\delta_B}}(x_A, y'_{BA}, z'_{BA}) \right\}$$

$$+ \sin\phi \left\{ v_{B_{\delta_B}}(x_A, y_{BA}, z_{BA}) - v_{B_{\delta_B}}(x_A, y'_{BA}, z'_{BA}) \right\}$$

$$+ w_{\Gamma_1}(x_A, y_A, 0) + w_{\Gamma_2}(x_A, y_A, 0) + w_{\Gamma_3}(x_A, y_A, 0)$$

$$+ V \sin\alpha = 0$$

Using series forms for trailing vorticity distributions as in the previous case, we have for constant x_A in the cross-flow plane.

$$\sum_{p=1}^{M} a_p \cdot a w_{\delta_A}(p, \theta_A)$$
$$+ \sum_{q=1}^{N} b_q \cdot \Big[\Big\{ b w_{\delta_B}(q, y_{BA}, z_{BA}) + b w_{\delta_B}(q, y'_{BA}, z'_{BA}) \Big\} \cos\phi$$
$$+ \Big\{ b v_{\delta_B}(q, y_{BA}, z_{BA}) - b v_{\delta_B}(q, y'_{BA}, z'_{BA}) \Big\} \sin\phi$$
$$+ \frac{\Gamma_1}{V \cdot k_z} g w_{\Gamma_1}(y_A, 0) + \frac{\Gamma_2}{V \cdot k_z} g w_{\Gamma_2}(y_A, 0) + \frac{\Gamma_3}{V \cdot k_z} g w_{\Gamma_3}(y_A, 0)$$
$$= - \sin\alpha \qquad \ldots\ldots \quad (37)$$

where the unknowns are a_p, b_q, Γ_1 , Γ_2 and Γ_3 . The multiplying terms are velocity influence coefficients which are defined in Appendix I.

V 5. Upwash Equation for Slat

The series forms for δ_W , δ_S and δ_F are substituted in Equation (2). We distinguish as in Section V.4 between the four possible configurations A-S-A, S-S-A, A-S-S and S-S-S.

(a) Configuration A-S-A

Using Equations (2), (9), (13)

$$\cos\phi \Big\{ w_{\delta_F}(x_B, y_{AB}, z_{AB}) + w_{\delta_A}(x_B, y_{AB}, z_{AB}) \Big\}$$
$$- \sin\phi \Big\{ v_{\delta_F}(x_B, y_{AB}, z_{AB}) + v_{\delta_A}(x_B, y_{AB}, z_{AB}) \Big\}$$
$$+ w_{B\delta_G}(x_B, y_B, 0) + w_{B\delta_B}(x_B, y_B, 0)$$
$$+ \Big\{ w_{B\delta_G}(x_B, y_{BC}, z_{BC}) + w_{B\delta_B}(x_B, y_{BC}, z_{BC}) \Big\} \cos 2\phi$$
$$+ \Big\{ v_{B\delta_G}(x_B, y_{BC}, z_{BC}) + v_{B\delta_B}(x_B, y_{BC}, z_{BC}) \Big\} \sin 2\phi$$
$$+ \Big\{ w_{\Gamma_2}(x_B, y_{AB}, z_{AB}) \cos\phi - v_{\Gamma_2}(x_B, y_{AB}, z_{AB}) \sin\phi \Big\} + V \sin\alpha_B = 0$$

Using series forms for trailing vorticity distributions from Equations (12) and (16) and writing for constant x_B in the cross-flow plane

$$
\begin{aligned}
& g_1 \cdot \left\{ g w_1(y_{AB}, z_{AB}) \cos\phi - g v_1(y_{AB}, z_{AB}) \sin\phi \right\} \\
& + \sum_{p=1}^{M} a_p \cdot \left\{ a w_{\delta_A}(p, y_{AB}, z_{AB}) \cos\phi - a v_{\delta_A}(p, y_{AB}, z_{AB}) \sin\phi \right\} \\
& + g_3 \cdot \left\{ g w_{\delta_{G_3}}(\theta_B) + g w_{\delta_{G_3}}(y_{BC}, z_{BC}) \cos 2\phi + g v_{\delta_{G_3}}(y_{BC}, z_{BC}) \sin 2\phi \right\} \\
& + \sum_{q=1}^{N} b_q \cdot \left[b w_{\delta_B}(q, \theta_B) + b w_{\delta_B}(q, y_{BC}, z_{BC}) \cos 2\phi + b v_{\delta_B}(q, y_{BC}, z_{BC}) \sin 2\phi \right] \\
& + \frac{\Gamma_2}{V \cdot k x} \bullet \left\{ g w_{\Gamma_2}(y_{AB}, z_{AB}) \cos\phi - g v_{\Gamma_2}(y_{AB}, z_{AB}) \sin\phi \right\} \\
& \qquad\qquad\qquad = - \sin\alpha_B
\end{aligned}
$$

. . . . (38)

The unknowns are g_1, a_p, g_3, b_q and Γ_2. The other multiplying terms are velocity and the influence coefficients which are defined in Appendix I.

(b) <u>Configuration S-S-A</u>

$$
\begin{aligned}
& \left\{ w_{B\delta_G}(x_B, y_{BC}, z_{BC}) + w_{B\delta_B}(x_B, y_{BC}, z_{BC}) \right\} \cos 2\phi \\
& + \left\{ v_{B\delta_G}(x_B, y_{BC}, z_{BC}) + v_{B\delta_B}(x_B, y_{BC}, z_{BC}) \right\} \sin 2\phi \\
& + w_{B\delta_G}(x_B, y_B, 0) + w_{B\delta_B}(x_B, y_B, 0) \\
& + w_{\delta_A}(x_B, y_{AB}, z_{AB}) \cos\phi - v_{\delta_A}(x_B, y_{AB}, z_{AB}) \sin\phi \\
& + w_{\Gamma_1}(x_B, y_{AB}, z_{AB}) \cos\phi - v_{\Gamma_1}(x_B, y_{AB}, z_{AB}) \sin\phi \\
& + w_{\Gamma_2}(x_B, y_{AB}, z_{AB}) \cos\phi - v_{\Gamma_2}(x_B, y_{AB}, z_{AB}) \sin\phi + V \sin\alpha_B = 0
\end{aligned}
$$

Using series forms for trailing vorticity distributions as in the previous case, we have for constant x_B in the cross-flow plane

$$\sum_{p=1}^{M} a_p \cdot \left\{ aw_{\delta_A}(p, y_{AB}, z_{AB})\cos\phi - av_{\delta_A}(p, y_{AB}, z_{AB})\sin\phi \right\}$$

$$+ \sum_{q=1}^{N} b_q \cdot \left[bw_{\delta_B}(q, \theta_B) + bw_{\delta_B}(q, y_{BC}, z_{BC})\cos 2\phi + bv_{\delta_B}(q, y_{BC}, z_{BC})\sin 2\phi \right]$$

$$+ g_3 \cdot \left[gw_{\delta_{G_3}}(y_{BC}, z_{BC})\cos 2\phi + gv_{\delta_{G_3}}(y_{BC}, z_{BC})\sin 2\phi + gw_{\delta_{G_3}}(y_B, 0) \right]$$

$$+ \frac{\Gamma_1}{V.k_x} \left\{ gw_{\Gamma_1}(y_{AB}, z_{AB})\cos\phi - gv_{\Gamma_1}(y_{AB}, z_{AB})\sin\phi \right\}$$

$$+ \frac{\Gamma_2}{V.k_x} \left\{ gw_{\Gamma_2}(y_{AB}, z_{AB})\cos\phi - gv_{\Gamma_2}(y_{AB}, z_{AB})\sin\phi \right\}$$

$$= -\sin\alpha_B \quad \ldots . \quad (39)$$

The unknowns are a_p, b_q, g_3, Γ_1 and Γ_2. The other multiplying terms are the velocity influence coefficients defined in Appendix I.

(c) Configuration A-S-S

$$\left\{ w_{\delta_F}(x_B, y_{AB}, z_{AB}) + w_{\delta_A}(x_B, y_{AB}, z_{AB}) \right\}\cos\phi$$

$$- \left\{ v_{\delta_F}(x_B, y_{AB}, z_{AB}) + v_{\delta_A}(x_B, y_{AB}, z_{AB}) \right\}\sin\phi$$

$$+ w_{B\delta_B}(x_B, y_B, 0) + w_{B\delta_B}(x_B, y_{BC}, z_{BC})\cos 2\phi$$

$$+ v_{B\delta_B}(x_B, y_{BC}, z_{BC})\sin 2\phi$$

$$+ w_{\Gamma_2}(x_B, y_{AB}, z_{AB})\cos\phi - v_{\Gamma_2}(x_B, y_{AB}, z_{AB})\sin\phi$$

$$+ w_{\Gamma_3}(x_B, y_{AB}, z_{AB})\cos\phi - v_{\Gamma_3}(x_B, y_{AB}, z_{AB})\sin\phi$$

$$+ V\sin\alpha_B = 0$$

Using series forms for trailing vorticity distributions as in the previous case, we have for constant x_B in the cross-flow plane

$$g_1 \cdot \left\{ gw_1(y_{AB}, z_{AB}) - gv_1(y_{AB}, z_{AB}) \sin\varphi \right\}$$

$$+ \sum_{p=1}^{M} a_p \cdot \left\{ aw_{\delta_A}(p, y_{AB}, z_{AB}) \cos\varphi - av_{\delta_A}(p, y_{AB}, z_{AB}) \sin\varphi \right\}$$

$$+ \sum_{q=1}^{N} b_q \cdot \left\{ bw_{\delta_B}(q, \theta_B) + bw_{\delta_B}(q, y_{BC}, z_{BC}) \cos 2\varphi + bv_{\delta_B}(q, y_{BC}, z_{BC}) \sin 2\varphi \right\}$$

$$+ \frac{\Gamma_2}{V \cdot k_x} \left\{ gw_{\Gamma_2}(y_{AB}, z_{AB}) \cos\varphi - gv_{\Gamma_2}(y_{AB}, z_{AB}) \sin\varphi \right\}$$

$$+ \frac{\Gamma_3}{V \cdot k_x} \left\{ gw_{\Gamma_3}(y_{AB}, z_{AB}) \cos\varphi - gv_{\Gamma_3}(y_{AB}, z_{AB}) \sin\varphi \right\} = -\sin\alpha_B$$

. . . . (40)

The unknowns are g_1, a_p, b_q, Γ_2 and Γ_3. The other multiplying terms are velocity influence coefficients which are defined in Appendix I.

(d) Configuration S-S-S

$$w_{\delta_A}(x_B, y_{AB}, z_{AB}) \cos\varphi - v_{\delta_A}(x_B, y_{AB}, z_{AB}) \sin\varphi$$

$$+ w_{\delta_B}(x_B, y_3, 0) + w_{B_{\delta_B}}(x_B, y_{BC}, z_{BC}) \cos 2\varphi + v_{B_{\delta_B}}(x_B, y_{BC}, z_{BC}) \sin 2\varphi$$

$$+ w_{\Gamma_1}(x_B, y_{AB}, z_{AB}) \cos\varphi - v_{\Gamma_1}(x_B, y_{AB}, z_{AB}) \sin\varphi$$

$$+ w_{\Gamma_2}(x_B, y_{AB}, z_{AB}) \cos\varphi - v_{\Gamma_2}(x_B, y_{AB}, z_{AB}) \sin\varphi$$

$$+ w_{\Gamma_3}(x_B, y_{AB}, z_{AB}) \cos\varphi - v_{\Gamma_3}(x_B, y_{AB}, z_{AB}) \sin\varphi$$

$$+ V \sin\alpha_B = 0$$

Using series forms for trailing vorticity distributions as in the previous case, we have for constant x_B in the cross-flow plane

$$\sum_{p=1}^{M} a_p \cdot \left\{ aw_{\delta_A}(p, y_{AB}, z_{AB})\cos\phi - av_{\delta_A}(p, y_{AB}, z_{AB})\sin\phi \right\}$$

$$+ \sum_{q=1}^{N} b_q \cdot \Big[bw_{\delta_B}(q, \theta_B) + bw_{\delta_B}(q, y_{BC}, z_{BC})\cos 2\phi + bv_{\delta_B}(q, y_{BC}, z_{BC})\sin 2\phi \Big]$$

$$+ \frac{\Gamma_1}{V.k_x} \left\{ gw_{\Gamma_1}(y_{AB}, z_{AB})\cos\phi - gv_{\Gamma_1}(y_{AB}, z_{AB})\sin\phi \right\}$$

$$+ \frac{\Gamma_2}{V.k_x} \left\{ gw_{\Gamma_2}(y_{AB}, z_{AB})\cos\phi - gv_{\Gamma_2}(y_{AB}, z_{AB})\sin\phi \right\}$$

$$+ \frac{\Gamma_3}{V.k_x} \left\{ gw_{\Gamma_3}(y_{AB}, z_{AB})\cos\phi - gv_{\Gamma_3}(y_{AB}, z_{AB})\sin\phi \right\}$$

$$= -\sin\alpha_B \quad \ldots\ldots \quad (41)$$

The unknowns are a_p, b_q, Γ_1, Γ_2 and Γ_3. The other multiplying terms are velocity influence coefficients which are derived in Appendix I.

(e) <u>Slats Only Configurations S-A and S-S</u>

The upwash equations can be derived from configurations A-S-A (or S-S-A) and A-S-S (or S-S-S) by omitting the wing effects.

V 6. Combined Upwash Equations

We now incorporate the conditions of zero total circulation on the slat (from Section V.2) into the upwash equations for the wing and slat (from Sections V.4 and V.5).

Configuration A-S-A

(a) <u>Wing</u>

Using Equation (18) we can eliminate b_1 from Equation (34), i.e.

$$g_1 \cdot g\,w_1(\theta_A) + \sum_{p=1}^{M} a_p \cdot a\,w_{\delta_A}(p, \theta_A)$$

$$+ g_3 \cdot \Big[\Big\{ g\,w_{\delta_{G_3}}(y_{BA}, z_{BA}) + g\,w_{\delta_{G_3}}(y'_{BA}, z'_{BA}) \Big\} \cos\phi$$

$$+ \Big\{ g\,v_{\delta_{G_3}}(y_{BA}, z_{BA}) - g\,v_{\delta_{G_3}}(y'_{BA}, z'_{BA}) \Big\} \sin\phi$$

$$- 2 \Big(\Big\{ b\,w_{\delta_B}(1, y_{BA}, z_{BA}) + b\,w_{\delta_B}(1, y'_{BA}, z'_{BA}) \Big\} \cos\phi$$

$$+ \Big\{ b\,v_{\delta_B}(1, y_{BA}, z_{BA}) - b\,v_{\delta_B}(1, y'_{BA}, z'_{BA}) \Big\} \sin\phi \Big) \Big]$$

$$+ \sum_{q=2}^{N} b_q \cdot \Big[\Big\{ b\,w_{\delta_B}(q, y_{BA}, z_{BA}) + b\,w_{\delta_B}(q, y'_{BA}, z'_{BA}) \Big\} \cos\phi$$

$$+ \Big\{ b\,v_{\delta_B}(q, y_{BA}, z_{BA}) - b\,v_{\delta_B}(q, y'_{BA}, z'_{BA}) \Big\} \sin\phi \Big]$$

$$+ \frac{\Gamma_2}{V \cdot k_2} \Big[g\,w_{\Gamma_2}(y_A, 0) - \frac{2k}{C_1 \pi} \Big(\Big\{ b\,w_{\delta_B}(1, y_{BA}, z_{BA}) + b\,w_{\delta_B}(1, y'_{BA}, z'_{BA}) \Big\} \cos\phi$$

$$+ \Big\{ b\,v_{\delta_B}(1, y_{BA}, z_{BA}) - b\,v_{\delta_B}(1, y'_{BA}, z'_{BA}) \Big\} \sin\phi \Big) \Big]$$

$$= - \sin\alpha$$

. . . . (42)

(b) <u>Slat</u>

Using Equation (18), b_1 can be eliminated from Equation (38).

$$g_1 \cdot \left\{ gw_1(y_{AB}, z_{AB})\cos\phi - gv_1(y_{AB}, z_{AB})\sin\phi \right\}$$

$$+ \sum_{p=1}^{M} a_p \cdot \left\{ aw_{\delta_A}(p, y_{AB}, z_{AB})\cos\phi - av_{\delta_A}(p, y_{AB}, z_{AB})\sin\phi \right\}$$

$$+ g_3 \cdot \Big[gw_{\delta_{G_3}}(\theta_B) + gw_{\delta_{G_3}}(y_{BC}, z_{BC})\cos 2\phi + gv_{\delta_{G_3}}(y_{BC}, z_{BC})\sin 2\phi$$

$$- 2\left\{ bw_{\delta_B}(1, \theta_B) + bw_{\delta_B}(1, y_{BC}, z_{BC})\cos 2\phi + bv_{\delta_B}(1, y_{BC}, z_{BC})\sin 2\phi \right\} \Big]$$

$$\sum_{q=2}^{N} b_q \cdot \left[bw_{\delta_B}(q, \theta_B) + bw_{\delta_B}(q, y_{BC}, z_{BC})\cos 2\phi + bv_{\delta_B}(q, y_{BC}, z_{BC})\sin 2\phi \right]$$

$$+ \frac{\Gamma_2}{V \cdot k_x} \Big[\left\{ gw_{\Gamma_2}(y_{AB}, z_{AB})\cos\phi - gv_{\Gamma_2}(y_{AB}, z_{AB})\sin\phi \right\}$$

$$- \frac{2k}{C_1 \pi} \left\{ bw_{\delta_B}(1, \theta_B) + bw_{\delta_B}(1, y_{BC}, z_{BC})\cos 2\phi + bv_{\delta_B}(1, y_{BC}, z_{BC})\sin 2\phi \right\} \Big]$$

$$= -\sin\alpha_B \qquad \ldots\ldots (43)$$

We may write equations (42) and (43) in shorthand form

$$g_1 \cdot d_1 + \sum_{p=1}^{M} a_p \cdot e_p + g_3 \cdot d_3 + \sum_{q=2}^{N} b_q \cdot f_q + \frac{\Gamma_2}{V \cdot k_x} \cdot d_2 = t \qquad \ldots\ldots (44)$$

where the unknowns are

$$g_1 \;,\; a_p \; (p = 1 \cdots M) \;,\; g_3 \;,\; b_q \; (q = 2 \cdots N) \;,\; \frac{\Gamma_2}{V \cdot k_x}$$

and the coefficients d_1, e_p, d_3, f_q, d_2, t have the obvious significance with reference to equations (43) and (44).

Configuration S-S-A

(a) Wing

Using equation (18), b_1 can be eliminated from equation (35), i.e.

$$\sum_{p=1}^{M} a_p \cdot aw_{\delta_A}(p, \theta_A)$$

$$+ g_3 \cdot \Big[\Big\{ gw_{\delta_{G_3}}(y_{BA}, z_{BA}) + gw_{\delta_{G_3}}(y'_{BA}, z'_{BA}) \Big\} \cos\phi$$

$$+ \Big\{ gv_{\delta_{G_3}}(y_{BA}, z_{BA}) - gv_{\delta_{G_3}}(y'_{BA}, z'_{BA}) \Big\} \sin\phi$$

$$- 2 \Big(\Big\{ bw_{\delta_B}(1, y_{BA}, z_{BA}) + bw_{\delta_B}(1, y'_{BA}, z'_{BA}) \Big\} \cos\phi$$

$$+ \Big\{ bv_{\delta_B}(1, y_{BA}, z_{BA}) - bv_{\delta_B}(1, y'_{BA}, z'_{BA}) \Big\} \sin\phi \Big) \Big]$$

$$+ \sum_{q=2}^{N} b_q \cdot \Big[\Big\{ bw_{\delta_B}(q, y_{BA}, z_{BA}) + bw_{\delta_B}(q, y'_{BA}, z'_{BA}) \Big\} \cos\phi$$

$$+ \Big\{ bv_{\delta_B}(q, y_{BA}, z_{BA}) - bv_{\delta_B}(q, y'_{BA}, z'_{BA}) \Big\} \sin\phi \Big]$$

$$+ \frac{\Gamma_1}{V . k_2} \; gw_{\Gamma_1}(y_A, 0)$$

$$+ \frac{\Gamma_2}{V . k_2} \Big[gw_{\Gamma_2}(y_A, 0) - \frac{2k}{c_1 \pi} \Big(\Big\{ bw_{\delta_B}(1, y_{BA}, z_{BA})$$

$$+ bw_{\delta_B}(1, y'_{BA}, z'_{BA}) \Big\} \cos\phi$$

$$+ \Big\{ bv_{\delta_B}(1, y_{BA}, z_{BA}) - bv_{\delta_B}(1, y'_{BA}, z'_{BA}) \Big\} \sin\phi \Big) \Big]$$

$$= - \sin\alpha \qquad \ldots . \quad (45)$$

(b) Slat

Using equation (18), b_1 is eliminated from equation (39).

$$\sum_{p=1}^{M} a_p \cdot \left\{ aw_{\delta_A}(p, y_{AB}, z_{AB})\cos\varphi - av_{\delta_A}(p, y_{AB}, z_{AB})\sin\varphi \right\}$$

$$+ g_3 \cdot \Big[\left\{ gw_{\delta_{G_3}}(y_{BC}, z_{BC})\cos 2\varphi + gv_{\delta_{G_3}}(y_{BC}, z_{BC})\sin 2\varphi + gw_{\delta_{G_3}}(y_B, 0) \right\}$$

$$-2\left\{ bw_{\delta_B}(1, \theta_B) + bw_{\delta_B}(1, y_{BC}, z_{BC})\cos 2\varphi + bv_{\delta_B}(1, y_{BC}, z_{BC})\sin 2\varphi \right\}$$

$$+ \sum_{q=2}^{N} b_q \cdot \Big[bw_{\delta_B}(q, \theta_B) + bw_{\delta_B}(q, y_{BC}, z_{BC})\cos 2\varphi + bv_{\delta_B}(q, y_{BC}, z_{BC}) \ldots$$

$$+ \frac{\Gamma_1}{V \cdot kx} \left\{ gw_{\Gamma_1}(y_{AB}, z_{AB})\cos\varphi - gv_{\Gamma_1}(y_{AB}, z_{AB})\sin\varphi \right\}$$

$$+ \frac{\Gamma_2}{V \cdot kx} \Big[gw_{\Gamma_2}(y_{AB}, z_{AB})\cos\varphi - gv_{\Gamma_2}(y_{AB}, z_{AB})\sin\varphi$$

$$- \frac{2k}{c_1\pi} \left\{ bw_{\delta_B}(1, \theta_B) + bw_{\delta_B}(1, y_{BC}, z_{BC})\cos 2\varphi + bv_{\delta_B}(1, y_{BC}, z_{BC})\sin 2\varphi \right\} \Big]$$

$$= -\sin\alpha_B$$

. . . . (46)

Equations (45) and (46) may be written in shorthand notation.

$$\sum_{p=1}^{M} a_p \cdot e_p + g_3 \cdot d_3 + \sum_{q=2}^{N} b_q \cdot f_q + \frac{\Gamma_1}{V \cdot kx} \cdot d_1 + \frac{\Gamma_2}{V \cdot kx} \cdot d_2 = t \qquad (47)$$

where the unknowns are

$$a_p(p=1\ldots M),\ g_3,\ b_q(q=2\cdots N),\ \frac{\Gamma_1}{V\cdot k_x},\ \frac{\Gamma_2}{V\cdot k_x}$$

and the coefficients e_p, g_3, f_q, d_1, d_2, t have the obvious significance with reference to equation (45) and (46).

Configuration A-S-S

(a) Wing

Using equation (19), b_1 can be eliminated from equation (36), i.e.

$$g_1 \cdot gw_1(\theta_A) + \sum_{p=1}^{M} a_p \cdot aw_{\delta_A}(p,\theta_A)$$

$$+ \sum_{q=2}^{N} b_q \cdot \Big[\Big\{ bw_{\delta_B}(q, y_{BA}, z_{BA}) + bw_{\delta_B}(q, y'_{BA}, z'_{BA}) \Big\} \cos\phi + \Big\{ bv_{\delta_B}(q, y_{BA}, z_{BA}) - bv_{\delta_B}(q, y'_{BA}, z'_{BA}) \Big\} \sin\phi \Big]$$

$$+ \frac{\Gamma_2}{V.k_x} \Big[gw_{\Gamma_2}(y_A, 0) - \frac{2k}{c_1\pi} \Big(\Big\{ bw_{\delta_B}(1, y_{BA}, z_{BA}) + bw_{\delta_B}(1, y'_{BA}, z'_{BA}) \Big\} \cos\phi + \Big\{ bv_{\delta_B}(1, y_{BA}, z_{BA}) - bv_{\delta_B}(1, y'_{BA}, z'_{BA}) \Big\} \sin\phi \Big) \Big]$$

$$+ \frac{\Gamma_3}{V.k_x} \Big[gw_{\Gamma_3}(y_A, 0) - \frac{2k}{c_1\pi} \Big(\Big\{ bw_{\delta_B}(1, y_{BA}, z_{BA}) + bw_{\delta_B}(1, y'_{BA}, z'_{BA}) \Big\} \cos\phi + \Big\{ bv_{\delta_B}(1, y_{BA}, z_{BA}) - bv_{\delta_B}(1, y'_{BA}, z'_{BA}) \Big\} \sin\phi \Big) \Big]$$

$$= -\sin\alpha \qquad \ldots\ldots (48)$$

(b) Slat

Using equation (19) b_1 can be eliminated from equation (40), i.e.

$$g_1 \cdot \Big\{ gw_1(y_{AB}, z_{AB}) - gv_1(y_{AB}, z_{AB}) \sin\phi$$

$$+ \sum_{p=1}^{M} a_p \cdot \Big\{ aw_{\delta_A}(p, y_{AB}, z_{AB}) \cos\phi - av_{\delta_A}(p, y_{AB}, z_{AB}) \sin\phi \Big\}$$

$$+ \sum_{q=2}^{N} b_q \cdot \Big[bw_{\delta_B}(q, \theta_B) + bw_{\delta_B}(q, y_{BC}, z_{BC}) \cos 2\phi$$
$$+ bv_{\delta_B}(q, y_{BC}, z_{BC}) \sin 2\phi \Big]$$

$$+ \frac{\Gamma_2}{V.k_x} \Big[\Big\{ gw_{\Gamma_2}(y_{AB}, z_{AB}) \cos\phi - gv_{\Gamma_2}(y_{AB}, z_{AB}) \sin\phi \Big\}$$

$$- \frac{2k}{C_1 \pi} \Big\{ bw_{\delta_B}(1, \theta_B) + bw\delta_B(1, y_{BC}, z_{BC}) \cos 2\phi$$
$$+ bv_{\delta_B}(1, y_{BC}, z_{BC}) \sin 2\phi \Big\} \Big]$$

$$+ \frac{\Gamma_3}{V.k_x} \Big[\Big\{ gw_{\Gamma_3}(y_{AB}, z_{AB}) \cos\phi - gv_{\Gamma_3}(y_{AB}, z_{AB}) \sin\phi \Big\}$$

$$- \frac{2k}{C_1 \pi} \Big\{ bw_{\delta_B}(1, \theta_B) + bw_{\delta_B}(1, y_{BC}, z_{BC}) \cos 2\phi$$
$$+ bv_{\delta_B}(1, y_{BC}, z_{BC}) \sin 2\phi \Big\} \Big]$$

$$= - \sin \alpha_B$$

. . . . (49)

Equations (49) and (49) may be written in shorthand notation

$$g_1 \cdot d_1 + \sum_{p=1}^{M} a_p \cdot e_p + \sum_{q=2}^{N} b_q \cdot f_q + \frac{\Gamma_2}{V.k_x} . d_2 + \frac{\Gamma_3}{V.k_x} . d_3 = t \quad \text{. . . . (50)}$$

where the unknowns are g_1 , a_p (p = 1 ... M), b_q (q = 2 ... N), $\Gamma_2/V.k_x$, $\Gamma_3/V.k_x$ and the coefficients d_1, e_p, f_q , d_2 , d_3 have the obvious significance with reference to equations (48) and (49).

Configuration S-S-S

(a) Wing

Using Equation (19), b_1 can be eliminated from equation (37).

$$\sum_{p=1}^{M} a_p \cdot aw_{\delta_A}(p, \theta_A)$$

$$+ \sum_{q=2}^{N} b_q \cdot \Big[\Big\{ bw_{\delta_B}(q, y_{BA}, z_{BA}) + bw_{\delta_B}(q, y'_{BA}, z'_{BA}) \Big\} \cos\phi$$

$$+ \Big\{ bv_{\delta_B}(q, y_{BA}, z_{BA}) - bv_{\delta_B}(q, y'_{BA}, z'_{BA}) \Big\} \sin\phi \Big]$$

$$+ \frac{\Gamma_1}{V.k_x} \; gw_{\Gamma_1}(y_A, 0)$$

$$+ \frac{\Gamma_2}{V.k_x} \Big[gw_{\Gamma_2}(y_A, 0) - \frac{2k}{c_1 \pi} \Big(\Big\{ bw_{\delta_B}(1, y_{BA}, z_{BA})$$

$$+ bw_{\delta_B}(1, y'_{BA}, z'_{BA}) \Big\} \cos\phi$$

$$+ \Big\{ bv_{\delta_B}(1, y_{BA}, z_{BA}) - bv_{\delta_B}(1, y'_{BA}, z'_{BA}) \Big\} \sin\phi \Big) \Big]$$

$$+ \frac{\Gamma_3}{V.k_x} \Big[gw_{\Gamma_3}(y_A, 0) - \frac{2k}{c_1 \pi} \Big(\Big\{ bw_{\delta_B}(1, y_{BA}, z_{BA})$$

$$+ bw_{\delta_B}(1, y'_{BA}, z'_{BA}) \Big\} \cos\phi$$

$$+ \Big\{ bv_{\delta_B}(1, y_{BA}, z_{BA}) - bv_{\delta_B}(1, y'_{BA}, z'_{BA}) \Big\} \sin\phi \Big) \Big] \quad \ldots\ldots (51)$$

$$= - \sin\alpha$$

(b) <u>Slat</u>

Using Equation (19) b_1 can be eliminated from (41).

$$\sum_{p=1}^{M} a_p \cdot \left\{ a w_{\delta_A}(p, y_{AB}, z_{AB}) \cos\phi - a v_{\delta_A}(p, y_{AB}, z_{AB}) \sin\phi \right\}$$

$$+ \sum_{q=2}^{N} b_q \cdot \Big[b w_{\delta_B}(q, \theta_B) + b w_{\delta_B}(q, y_{BC}, z_{BC}) \cos 2\phi + b v_{\delta_B}(q, y_{BC}, z_{BC}) \sin 2\phi \Big]$$

$$+ \frac{\Gamma_1}{V \cdot k_x} \cdot \Big[g w_{\Gamma_1}(y_{AB}, z_{AB}) \cos\phi - g v_{\Gamma_1}(y_{AB}, z_{AB}) \sin\phi \Big]$$

$$+ \frac{\Gamma_2}{V \cdot k_x} \cdot \Big[g w_{\Gamma_2}(y_{AB}, z_{AB}) \cos\phi - g v_{\Gamma_2}(y_{AB}, z_{AB}) \sin\phi - \frac{2k}{C_1 \pi} \left\{ b w_{\delta_B}(1, \theta_B) + b w_{\delta_B}(1, y_{BC}, z_{BC}) \cos 2\phi + b v_{\delta_B}(1, y_{BC}, z_{BC}) \sin 2\phi \right\} \Big]$$

$$+ \frac{\Gamma_3}{V \cdot k_x} \cdot \Big[g w_{\Gamma_3}(y_{AB}, z_{AB}) \cos\phi - g v_{\Gamma_3}(y_{AB}, z_{AB}) \sin\phi - \frac{2k}{C_1 \pi} \left\{ b w_{\delta_B}(1, \theta_B) + b w_{\delta_B}(1, y_{BC}, z_{BC}) \cos 2\phi + b v_{\delta_B}(1, y_{BC}, z_{BC}) \sin 2\phi \right\} \Big]$$

$$= - \sin \alpha_B \quad \ldots \quad (52)$$

Equations (51) and (52) may be written in shorthand notation

$$\sum_{p=1}^{M} a_p \cdot e_p + \sum_{q=2}^{N} b_q \cdot f_q + \frac{\Gamma_1}{V \cdot k_x} \cdot d_1 + \frac{\Gamma_2}{V \cdot k_x} \cdot d_2 + \frac{\Gamma_3}{V \cdot k_x} \cdot d_3 = t \quad \ldots \quad (53)$$

where the unknowns are a_p (p = 1 ... M), b_q (q = 2 ... N), $\frac{\Gamma_1}{V \cdot k_x}$, $\frac{\Gamma_2}{V \cdot k_x}$, $\frac{\Gamma_3}{V \cdot k_x}$ and the coefficients e_p, f_q, d_1, d_2, d_3 have the obvious significance with reference to equations (51) and (52).

Slats Only Configurations S-A and S-S

The combined upwash equations including the relationship of Equation (18) for Configuration S-A and Equation (19) for Configuration S-S are derived by omitting the wing effects in Equation (44) for Configuration S-A and Equation (47) for the Configuration S-S.

V 7. Solution Procedure

The combined upwash equations (44), (47), (50) and (53) for the various types of configurations are all sets of linear simultaneous equations. The procedure for solution by collocation at a number of points on the surfaces of wing and slat is illustrated in Figure 21. The various steps are as follows:

(a) Choose type of configuration (i.e. edge conditions).

(b) Choose wing and slat geometry parameters.

(c) Select (M + 1) points along wing semi-span (equal intervals in θ_A).

(d) Select (N + 1) points along the slat span (equal intervals in θ_B).

(e) Calculate wing and slat vorticity induced velocity influence coefficients.

(f) Locate initial vortex positions.

(g) Calculate vortices induced velocity influence coefficients.

(h) Solve the appropriate upwash equation to determine the unknowns - vorticity strength and vortex strength.

(i) Evaluate velocities at vortex positions for applying the equations for zero force on vortex-cut arrangements.

(j) Estimate predicted positions of vortices.

(k) If predicted positions of vortices are not within a pre-specified small tolerance on the initial assumed vortex positions, then the vortices are re-located. This re-location procedure is optimised for the best direction of movement. Calculation is taken back to step (g).

(l) Bound vorticity, lift distribution, lift and drag are calculated (see Appendix II).

V 8. Similarity Parameters

In conical wing theory problems, the similarity parameters are generally taken as follows:

$\frac{\sin\alpha}{k}$ is the angle of attack parameter which is the main variable of the problem and defines a family of solutions related to wing sweepback and α.

The parameters $\frac{\Gamma_2}{V.kx.k^2}$ for vortex strength and $\frac{C_L}{k^2}$ for lift are dependent on $\sin\alpha/k$.

For wing-slat configurations also, these parameters are applicable. The angle of attack parameter that is more appropriate is $\sin\alpha/k_3$ referred to slat leading edge. A family of solutions is therefore implied in each calculation for given values of α and k_3. Additional geometry parameters defining the gap between the wing and slat may also be identified. An understanding of these will lead to reducing the computations required.

V 9. Computer Calculations

Computations were performed on the University of Bristol system 4-75 computer. The time taken for each case depended on the number of collocation points on the wing-slat geometry and the accuracy of starting positions of the vortices. In the order of numerical computation time required to attain reasonable convergence, the various configurations stand as follows:-

(i)	Slats only configuration	S - A
(ii)	Slats only configuration	S - S
(iii)	Wing-slat configuration	A - S - A
(iv)	Wing-slat configuration	S - S - A
(v)	Wing-slat configuration	A - S - S
(vi)	Wing-slat configuration	S - S - S

It must be mentioned that for configurations A - S - S and S - S - S, the convergence rates were rather slow. An improved iteration procedure may be required based on "nested" iterations for each vortex in turn. A different form for series distributions of vorticity can also be used. These may have a favourable influence on the convergence rates (see Reference 7).

VI RESULTS

An understanding of the slats only configuration is an essential prelude to the wing-slat configurations.

VI.1 SLATS ONLY CONFIGURATIONS

A series of slat geometries S1-S3 as illustrated in Figure 22 have been used. The slat leading edge has been defined by $y = 0.25\,x$ (angle of sweep-back 75.964°). The trailing edges are given by $y = 0.05\,x$, $0.1\,x$ and $0.2\,x$. This forms a sequence with the limiting case of the wing only configuration.

Configuration S-A refers to the attached flow on the slat leading edge whilst in S-S, flow separation at the leading edge is included (see Figure 16).

VI 1.1 Configuration S-A

The effects of angle of attack α on slat combination S1-S2 are illustrated through Figures 23 and 24. The variations of load distributions, vortex height, vortex strength and lift coefficient C_{L_S} have been considered. The effects of increasing α are as follows:-

(i) The magnitude of slat wake vortex strength increases linearly.

(ii) The vortex moves inwards and outwards starting from a spanwise location $y_2 = \frac{1}{2}(c_o - c_1)\,x$, $z_2 = 0$ at $\alpha = 0$.

(iii) C_{L_S} increases linearly.

The effect of slat span on load distributions and wake vortex at $\alpha = 5^{\circ}$ and 10° for $\phi = 0^{\circ}$ is illustrated in Figure 25 (a) and (b). This is conveniently interpreted as the effect of introducing a symmetrical concial gap near the centreline of a flat delta wing. The load distributions therefore follow a plausible sequence.

Movement of the trailing edge outwards, i.e. increasing the gap in the wing leads to the following effects at fixed α (see Figs 26 and 27).

(i) Vortex strength magnitude $\Gamma_2/\{V.(c_0+c_1)x\}$ reduces. However vortex strength magnitude $\Gamma_2/\{V.\,2c_1 x\}$ based on slat span increases slightly and then reduces.

(ii) Vortex position moves outwards and downwards, the limiting values being $y_2 = 0$, $z_2 = \infty$ for no gap and $y_2 = 0.5$, $z_2 = \sin\alpha/\{2(c_0+c_1)\}$ for vanishing slat span.

(iii) the total lift decreases, however, lift coefficient based on local span increases slightly and then tends to a limiting value $2\pi.\sin\alpha.\cos\Lambda$ (for an infinite sheared wing of sweepback angle Λ).

The effect of slat inclination ϕ is shown for slat combination S1 and S2 in Figures 28 and 29.

The effective angle of attack α_B increases with ϕ increasing and aerodynamic effects may be interpreted on this basis, e.g.

(i) The vortex strength magnitude and lift increase with ϕ.

(ii) The vortex spanwise position moves outwards for both increasing and decreasing ϕ. Vortex height increases with reducing ϕ and conversely.

(iii) On lift coefficient basis (based on actual area and not the projected area), $C_{L_S}/C_{D_{S_i}}$ improves with decreasing ϕ (i.e. same sense as leading edge droop). It must be mentioned that leading edge suction effect on induced drag C_{D_i} has not been included.

VI 1.2 Configuration S-S

A few selected combinations S1-S3 from Figure 22 have been used.

The effect of slat size on load distributions and vortices is depicted in Figure 30. This is conveniently interpreted as the effect of introducing a symmetrical conical gap near the centre-line of the flat delta wing. It is interesting to note that peak loads are of the same order, i.e. leading edge vortex lift dominates and this is not substantially altered by the vicinity of the slat trailing edge.

The vortex strength Γ_2 and Γ_3 are shown in Figure 31. The magnitude of Γ_2 reduces with reduction in slat span but tends to a constant value for vanishing span. Γ_3 reaches a peak for $k_2/k_3 \simeq 0.2$ and then decreases with increasing k_2/k_3 but tends to constant value for vanishing span.

Lift coefficient based on $(c_0+c_1)x$ decreases with increasing k_2/k_3 (Figure 32) and tends to a constant value for vanishing slat size. Based on local span $2c_1x$ the curve as shown in Figure 32 is obtained, which tends to infinity for vanishing slat size. This behaviour for vanishing slat size appears to be reasonable since the usual incidence parameter $\sin \alpha/c_1$ for slat will also tend to infinity and non-linear lift is a direct function of this incidence parameter.

The effect of angle of attack $\alpha = 2.5^{\circ}$ to 8° on load distributions and the vortices for slats geometry S1 is shown in Figure 33. The peak load moves inwards with increasing α. Γ_2 and Γ_3 both move inwards and upwards with increasing α. Vortex height for all geometries increases with α increasing.

For $\alpha = 5^{\circ}$ case, a comparison of configuration S-A and S-S is presented in Figure 34 (i.e. this is the effect of including Γ_3 at the slat leading edge). We note that with Γ_3 present, large increases in lift distribution (non-linear lift) and hence wake vortex strength are obtained.

It is of interest also to compare the vortex and lift characteristics for the two configurations S-A and S-S throughout the incidence range (Figures 35 and 36). We note that by including Γ_3, large benefits in non-linear lift are obtained. Γ_3 approaches the strength given by Brown and Michael (for the wing with the same leading edge). This is particularly interesting and shows that the effect of slat trailing edge on Γ_3 and hence on non-linear lift is small.

The magnitude of Γ_2 for the configuration S-S is higher and increases non-linearly with α. This is in line with total zero circulation condition about the slat.

An idea of the C_{L_S}/C_{D_S} characteristics can be gained from Figure 37. As the slat span reduces (i.e. it approaches the case of infinite sheared wing), its performance increases, as might be expected. As the slat gap vanishes, the limit is the Brown and Michael curve.

The comparison of vortex locations of Γ_2 and Γ_3 presented in Figure 38 refers to the case of twin slats (combination S3) compared with the case of one slat only (i.e. yawed delta wing results from Cohen[13]). It is noted that although Γ_3 locations are comparable, Γ_2 location for the twin slats combination is higher because of the mutual influence of one slat on the other.

VI 2. WING-SLAT CONFIGURATIONS

A series of wing-slat geometries WS1-WS20, as shown in Table I , have been used for analysis and comparison. In most cases the slat leading edge (at $\phi = 0^{\circ}$) is at $y = k_3 x = 0.25x$ and the maximum angle of attack α is of the order of 15°. This gives the maximum value for angle of attack similarity parameter $(\sin\alpha/k_3)$ as 1.034.

There are four configurations of Figure 15 to be considered (A-S-A, A-S-S, S-S-A and S-S-S) all with different combinations of edge conditions.

VI 2.1 Configuration A-S-A

The conical streamline pattern sketched in Figure 39 results from the effect of introducing a conical gap in a flat delta wing away from the wing centre-line (constituting thus a wing-slat configuration). Load distributions for a typical case at $\alpha = 5^{\circ}$ are shown in Figure 40. These have been compared with the cases of slats only (Configuration S-A) and wing only (no gap - Jones' linear theory result). It is evident that wing and slat in combination produce more lift than the sum of their individual lift values, but it is less than the value for the wing only as might be anticipated. The appearance of non-linear lift on the wing under the slat trailing edge wake vortex is also noted.

The effect of angle of attack $\alpha = 2.5^{\circ}$ to 15° on load distributions and vortex position is shown in Figure 41. The slat wake vortex moves inwards and upwards with increasing α as its magnitude increases (Figure 42). It is interesting to compare this strength with the equivalent value from slats only configuration S-A and it is noted that the presence of the wing leads to an increase in the vortex strength magnitude.

Lift coefficient, angle of attack relationships are shown in Figure 43. It is convenient to distinguish between the lift coefficients based on the total projected area (between the slat leading edges at $\phi = 0^{\circ}$) and the actual exposed surface area (i.e. allowing for the slot). It is noted that the wing slat case offers lift of the same order as the wing with the same exposed surface area.

The effect of slat inclination $\phi = 0$ to -20° (in the same sense as wing leading edge droop) is shown in Figure 44. It is noted that the gap between the wing leading edge and the slat trailing edge increases as ϕ decreases. The lift distribution on the slat and hence the magnitude of the slat wake vortex decreases with decrease in ϕ. Similarly the effect of slat wake vortex on the wing load distribution also decreases as ϕ decreases.

The effect of gap size for various ϕ has also been examined (Figure 45a, b, c). Widening of the gap leads to loss of lift distribution on the slat as may be expected and this leads to a reduction in non-linear peak loading induced on the wing. For the $\phi = 0^{\circ}$ case, the limiting lift distribution for vanishing gap (overall wing) case is also illustrated as a reference curve.

The effect of the slat height is depicted in Figure 46. We note that as the slat distance reduces, the slat loading and its effect on the wing increases, i.e. the loading near the wing leading edge decreases and the peak load on the wing under the slat wake vortex increases. For negative slat height the slat wake vortex lies nearer to the wing leading edge.

It is of interest next to consider the efficiency of wing-slat configurations.

Figure 47 shows the possible design approach for a high speed wing. It might, for example, feature:

(1) a hinged flap;
(2) leading edge slat which can have a variable gap and deflection;
(3) leading edge deflection and extension with major geometry changes.

(1) and (2) above are comparable since there is no change in plan-form area, but (3) really means an increased wing area.

Results from a selection of geometries ($k = 0.18$, $c_o = 0.2$ and $c_1 =$ [illegible]) have been compared on C_L/C_{D_i} and C_L basis with a flat wing of the same area in Figs. 48 and 49. The leading edge suction thrust term has been discounted in Fig.48 but retained in Fig.49. It appears that for the configuration A-S-A, the benefits of the slat are dependent on the realisation of leading edge suction thrust. If the suction thrust is fully realised at the leading edges then the wing only case is superior throughout the C_L range. In practice, however, it is difficult to achieve the idealised case of 100% suction and a 20% - 30% figure may be more realistic. Furthermore, flow separations will occur and alter the configuration assumptions at the leading edges. It is therefore of interest to look at the basic case of Fig.48 without leading edge suction.

(i) For $\phi = 0^o$, improvements in (pressure) C_L/C_{D_i} are possible for $C_L > 0.13$, e.g. 15% at $C_L = 0.3$.

(ii) With regard to slat height at $\phi = 0^o$, there appears to be an optimum position for the best C_L/C_{D_i}.

(iii) The C_L/C_{D_i} values are appreciably enhanced (about 15%) by combining height h_o and inclination ϕ of the slat (in the sense of leading edge droop).

(iv) There is a further 8% gain in C_L if the curves for wing-slat are based on the total exposed area of the wing and slat (i.e. discounting the gap).

(v) More optimum configurations may be derived by allowing slat span as an additional variable.

It may be interpreted that gains in C_L/C_{D_i} are due to higher operating efficiency of the slat which may operate at a higher value of incidence parameter α_B/ε_B than the comparable figure for the wing, i.e. α/ε,

where ε is semi-apex angle of the wing $= \tan^{-1} k$
and ε_B is semi-apex angle of the slat.

In the configuration A-S-A, the wing basic lift-incidence realtionship is given by

$$C_{L_w} = 2\pi k \sin\alpha \quad \text{(based on } kx\text{)}$$

whilst the slat lift-incidence relationship is more akin to an infinite apect ratio yawed wing

$$C_{L_S} = 2\pi \cos\Lambda \,.\, \alpha_B \quad \text{(based on } 2c_1 x\text{)}.$$

For certain combinations of α, ε, α_B and ε_B therefore the wing and slat provide improvements in efficiency compared with the wing alone.

VI 2.2 Configuration A-S-S

The conical streamline pattern for this class of flow is sketched in Figure 50. Compared with configuration A-S-A, the slat leading edge and trailing edge vortices are expected to be stronger and this will increase the downwash effect at the wing leading edge.

The effect of angle of attack $\alpha = 2.5$ to 6.5° on load distributions and vortex positions is illustrated in Figure 51. Both slat vortices move inwards and upwards with increasing α. The peak loads induced on the wing and the slat under the two vortices both increase as α increases.

Load distribution for a typical case at $\alpha = 5^{\circ}$ have been compared with cases of slats only (Configuration S-S) and wing only (no gap - Brown and Michael theory result) in Figure 52. It is evident that wing and slat in combination produce more lift than the sum of their individual lift values, but it is less than the value for the wing only as might be anticipated. The load near the wing leading edge is reduced under the strong downwash effect of the slat, but the central portion of the wing carries increased loading.

Load distributions and vortex positions for $\alpha = 2.5$ and 5° have been compared with those of configuration A-S-A in Figure 53. This demonstrates the effect of including the vortex Γ_3 at the slat leading edge. The slat in the configuration A-S-S carries increased load at the expense of reduced load on the wing near the leading edge. The peak load near the centre of the wing for A-S-S under the stronger influence of Γ_2 is also higher.

The vortex strengths Γ_2 and Γ_3 for Configuration A-S-S have been compared with the case of slats only Configuration S-S in Figure 54. The Brown and Michael curve for Γ_3 has also been shown, as well as the curve for Γ_2 from Configuration A-S-A. It is noted that at a given α, the value of Γ_3 required for Configuration A-S-S lies between the narrow band for the slats only Configuration S-S and Brown and Michael, indicating that the slat trailing edge has a small effect on the slat leading edge vortex. The magnitude of Γ_2 for Configuration A-S-S is greater than that for either Configurations A-S-A or S-S.

Lift coefficient, angle of attack relationships are shown in Fig.55. It is noted that the wing-slat configuration A-S-S offers an appreciable increase in lift compared with the wing of same area according to the Brown and Michael theory. In fact it approaches the Brown and Michael curve discounting the gap. Linear theory curves are shown as a reference.

The effect of slat inclination $\phi = 0^{\circ}$ to -10° (in the same sense as wing leading edge droop) is shown in Fig. 56. With decrease in ϕ, the lift distribution on the slat and hence magnitudes of both Γ_2 and Γ_3 decrease. The effect of slat wake vortex on the wing load distribution also decreases.

Results from a few calculations have been compared on C_L/C_{D_i} and C_L basis with a flat wing of the same area in Fig.57. Leading edge suction thrust at the wing leading edge has been included. It is noted that the wing slat configuration offers 15% - 20% gain in C_L/C_{D_i} at C_L about 0.3.

VI 2.3 Configuration S-S-A

The conical streamline pattern for this class of flow is shown in Figure 58. Although the wing leading edge vortex is shown above the wing surface, it is possible for the vortex to appear under the wing surface because of the strong downwash effect of the slat.

The effect of angle of attack $\alpha = 2.5^\circ$ to 15° on load distributions and vortex positions is illustrated in Figure 59. Both vortices Γ_1 and Γ_2 move inwards and upwards with increasing α. The peak loads induced on the wing under the two vortices both increase as α increases. It is of interest to compare the two vortex strengths with corresponding values from slats only configuration S-A and Brown and Michael wing only case (Figure 60). The presence of wing leads to an increase in magnitude of the slat wake vortex Γ_2 as also noted in configuration A-S-A. The slats cause the wing vortex Γ_1 to decrease in strength.

Load distributions and vortex positions for $\alpha = 2.5^\circ$ and 5° have been compared with those of configurations A-S-A and A-S-S in Fig. 61(a) and (b). Configurations S-S-A and A-S-A are more readily comparable because slat loadings are similar and the difference can be interpreted as the effect due to the inclusion of wing leading edge vortex Γ_1. The presence of Γ_1 implies therefore an increase in loading near the wing leading edge. In configuration A-S-S the slat loadings are higher and therefore the wing leading edge loads are much reduced.

Lift coefficient, angle of attack relationships are shown in Fig. 62. It is noted that the wing-slat configuration S-S-A offers an appreciable increase in lift compared with linear theory based on both types of reference areas (i.e. with and without the inclusion of the slat gap).

Results from a few calculations have been compared on C_L/C_{D_i} and C_L basis with a flat wing of the same area in Figure 63. Curves with and without leading edge suction thrust have been shown; Brown and Michael curve is also shown for reference. It is noted that

(i) with realisation of 100% leading edge suction the configuration S-S-A is not superior to the wing only case with attached flow, but it is superior to the Brown and Michael curve at $C_L > 0.3$.

(ii) If the leading edge suction thrust is not included, then there is an appreciable gain in C_L/C_{D_i} at higher values of C_L (e.g. 40% at $C_L > 0.5$).

IV 2.4 Configuration S-S-S

The conical streamline pattern for this class of flow is shown in Figure 64. Although the wing leading edge vortex is shown above the wing surface, it is possible for it to appear under the wing surface due to the strong downwash effect of the slat. Because of the highly non-linear nature of the flow, convergence of the solution, i.e. the three vortices, was found to be extremely slow and only a few examples have been attempted.

Figure 65 shows the load distribution and vortex positions at $\alpha = 2.5^{o}$. This has also been compared with configuration A-S-S to show the effect of including wing leading edge vortex Γ_1. The presence of Γ_1 appears to imply a reduction in loading near the wing leading edge and an inward and upward movement of Γ_3 with an appropriate movement of suction peak loading on the slat. It must be emphasised that since these effects are highly non-linear and interdependent, behaviour cannot be easily extrapolated to other geometries.

The effect of slat height is depicted in Figure 66 for $\alpha = 5^{o}$. Results for smaller slat heights were found very difficult to obtain and therefore only two heights have been considered. It is noted that as the slat height reduces, the slat loading and its effect on the wing increases, i.e. the loading near the wing leading edge decreases and the peak load on the wing under the slat wake vortex increases.

It is interesting to look at the significance of leading edge conditions for a given slat height. Figure 67 shows a comparison of configuration A-S-A with S-S-S and we note the large changes in lift distribution near the wing leading edge (due to Γ_1) and the slat leading edge (due to Γ_3). The slat trailing edge vortex Γ_2 is increased in strength for configuration S-S-S and therefore causes a larger peak loading on the wing.

Results from a few calculations have been compared in Figure 68 on a C_L/C_{D_i} and C_L basis with a flat wing according to Brown and Michael theory for both types of reference areas (i.e. with and without the inclusion of the slat gap). These results indicate a very appreciable 30-40% gain in C_L/C_{D_i} at C_L values above 0.2.

VII CONCLUSIONS

The conical type approach gives an insight into flows around swept-back slender wings with leading edge devices-slats. The prevailing conditions at the edges (flow attached or separated) of the configurations have a marked effect on the performance. Separated flow conditions generally lead to appreciable benefits in lift-drag ratio, e.g. 30-40 % at higher lift coefficients.

The method of this report allows a large number of possibilities for variation of geometry, and further optimisation studies can be undertaken. From some of the cases considered, it can be inferred that theoretical gains in performance are of the same order as those measured in experiments.

The leading edge devices-slats can, therefore, be useful not only in the obvious case where high lift is required, e.g. near an airfield, but also for transonic manoeuvrability and increased performance and controllability at both low and high speeds.

VIII FUTURE WORK AND RECOMMENDATIONS

There are several areas of work, both theoretical and experimental, that emerge from the present report and it appears that there is some way to go before configurations such as those of Figures 6 and 69, Reference 14, can be tackled successfully.

(a) Theoretical

The slender wing methods may be developed as follows:-

(i) Incorporation of wing camber. An approach using conformal transformations is illustrated in Figure 70. The method mentioned by Nangia[15] may be used to develop realistic leading edge camber. In addition to vorticity distributions, source distributions will also be required. Calculations are performed in the simpler transformed plane.

(ii) Incorporation of wing and slat thickness and camber. Multiple aerofoil type conformal transformation methods (Ref. 16, 17) can be used to simplify the thickness problems (Figure 71).

(iii) Vortex sheet representation of separations. This is an important aspect and has a significant bearing on the flow near the leading edges. The work of Pullin[10,11] and Jones[12] is of interest. The first case to consider in the inclusion of vortex sheet at the slat trailing edge.

(iv) Multiple slats are a fairly common feature of conventional wings of large aspect ratio. They offer large gains in lift. A theoretical study within the framework of slender wing theory can be formulated to assess their potential (Figure 72). Conformal transformation method aids in simplifying the geometry.

(v) Incorporation of planform effects. Step-by-step methods, e.g. Smith[18] and Clarke[19] for wings only may be extended (Figure 73). This will be the first approximation to the treatment of planform exactly by inclusion of chordwise terms, e.g. as in methods of Nangia[8] and Tinoco and Yoshihara[4].

(vi) Assessment of viscid phenomenon and interactions - this is obviously a difficult area, but some work with conical type boundary layers is in order.

The theoretical programme should provide a good understanding of the flow in realistic wing-slat configurations and also aid in definition of limits of parametric variation in experimental studies.

(b) Experimental

In view of the fact that there is really a scarcity of data on slender wings with leading edge devices, a number of models can be devised with varying degrees of sophistication starting from conical type models.

(i) Conical type Models (Figure 74) enable an understanding of the physical flow features with relatively low cost. Force and pressure plotting models are of interest here. Systematic flow visualisation studies are also required.

(ii) Non-conical Models (Figure 75). A simple geometry that needs to be tested is the effect of non-conical slats on a delta wing. The relative merits of various types of slats can then be assessed.

The effect of part span slats on a general planform is the next study required. It may be argued that high lift device is best employed ahead of the wing aerodynamic centre along with a flap type trimming surface near the wing trailing edge.

(iii) Multiple slats. An experimental study on slender wings is required to assess their application potential and also for evaluation of possible theoretical results.

(iv) Viscid and Interaction Effects. Detailed flow survey type studies are required to give an idea of the vortex wake and boundary layer interactions.

APPENDIX I

INDUCED VELOCITIES AND INFLUENCE COEFFICIENTS

Wing Vorticity δ_w

The velocity components v and w induced at a general point (y_G, z_G) in the cross-flow plane are

$$v(y_G, z_G) = -\frac{z_G}{2\pi}\int_{-kx}^{kx}\frac{\delta_W(y)\,dy}{(y-y_G)^2+z_G^2}$$

$$w(y_G, z_G) = -\frac{1}{2\pi}\int_{-kx}^{kx}\frac{(y-y_G)\,\delta_W(y)\,dy}{(y-y_G)^2+z_G^2}$$

In non-dimensional terms (length kx) these become

$$v(y_G^*, z_G^*) = -\frac{z_G^*}{2\pi}\int_{-1}^{+1}\frac{\delta_W(y^*)\,dy^*}{(y^*-y_G^*)^2+z_G^{*2}}$$

$$w(y_G^*, z_G^*) = -\frac{1}{2\pi}\int_{-1}^{+1}\frac{(y^*-y_G^*)\,\delta_W(y^*)\,dy^*}{(y^*-y_G^*)^2+z_G^{*2}}$$

By substituting for the components of δ_W, the velocity influence coefficients can be written as follows:

(a) component $\delta_F(y^*) \equiv \delta_F(\theta) \equiv V \cdot g_1 \cdot \cot\theta_A \equiv V \cdot g_1\left(\frac{-y^*}{\sqrt{1-y^{*2}}}\right)$

$\cos\theta = -y^*$

$$v_{\delta_F}(y_G^*, z_G^*) = V \cdot g_1 \cdot g v_1 (y_G^*, z_G^*)$$

$$w_{\delta_F}(y_G^*, z_G^*) = V \cdot g_1 \cdot g w_1 (y_G^*, z_G^*)$$

Configurations A-S-A and A-S-S

where

$$g v_1 \,(y_G^*, z_G^*) = -\frac{z_G^*}{2\pi} \int_{-1}^{+1} \frac{\left(-\frac{y^*}{\sqrt{1-y^{*2}}}\right) dy^*}{(y^*-y_G^*)^2 + z_G^{*2}}$$

and •

$$g w_1 \,(y_G^*, z_G^*) = -\frac{1}{2\pi} \int_{-1}^{+1} \frac{(y^*-y_G^*)\left(-\frac{y^*}{\sqrt{1-y^{*2}}}\right) dy^*}{(y^*-y_G^{*2}) + z_G^{*2}}$$

on the surface of wing, $z_G^* = 0$

$$g w_1 \,(y_G^*, 0) = -\frac{1}{2\pi} \int_{-1}^{+1} \frac{\left(-\frac{y^{*2}}{\sqrt{1-y^{*2}}}\right) dy^*}{y^*-y_G^*} \quad \text{where } \cos\theta_G = -y_G^*$$

$$= -\frac{1}{2\pi} \int_0^{\pi} \frac{\cos\theta \, d\theta}{\cos\theta - \cos\theta_G} = \frac{1}{2}$$

The expressions for $g v_1$ and $g w_1$ can also be derived from potential theory using complex variables. These are exact.

$$Z_G^* = y_G^* + i\, z_G^*$$

$$g v_1 \,(Z_G^*) = \left(\frac{i}{2} \frac{Z_G^*}{\sqrt{Z_G^{*2}-1}} - \frac{i}{2}\right)$$

$$g w_1 \,(Z_G^*) = g \left(-\frac{i}{2} \frac{Z_G^*}{\sqrt{Z_G^{*2}-1}} + \frac{i}{2}\right)$$

(b) component $\delta_A(y^*) \equiv \delta_A(\theta) \equiv V. \sum_{p=1}^{NA} a_p \cdot \sin(2p\cdot\theta)$

$$\cos\theta = -y^*$$

$$v_{\delta_A}(y_G^*, z_G^*) = V \sum_{p=1}^{N} a_p \cdot a v_{\delta_A}(P, y_G^*, z_G^*)$$

$$w_{\delta_A}(y_G^*, z_G^*) = V \sum_{p=1}^{N} a_p \cdot a w_{\delta_A}(P, y_G^*, z_G^*)$$

where

$$a v_{\delta_A}(p, y_G^*, z_G^*) = -\frac{z_G^*}{2\pi}\int_{-1}^{+1} \frac{\sin\{2p(-\cos^{-1}y^*)\}\,dy^*}{(y^*-y_G^*)^2 + z_G^{*2}}$$

$$a w_{\delta_A}(p, y_G^*, z_G^*) = -\frac{1}{2\pi}\int_{-1}^{1} \frac{(y^*-y_G^*)\sin\{2p(-\cos^{-1}y^*)\}\,dy^*}{(y^*-y_G^*)^2 + z_G^{*2}}$$

on the surface of the wing , $z_G^* = 0$

$$a w_{\delta_A}(p, y_G^*, 0) = -\frac{1}{2\pi}\int_0^{\pi} \frac{\sin(2p\theta)\sin\theta}{\cos\theta - \cos\theta_G}\,d\theta$$

where $\cos\theta_G = -y_G^*$

$$= \frac{1}{2\pi}\int_0^{\pi} \frac{\frac{1}{2}\{\cos(2p-1)\theta - \cos(2p+1)\theta\}\,d\theta}{\cos\theta - \cos\theta_G}$$

$$= \frac{1}{2\pi}\left[\pi\left\{\frac{\sin(2p-1)\theta - \sin(2p+1)\theta}{\sin\theta_G}\right\}\right]_0^{\pi}$$

$$= -\frac{1}{2}\cos(2p\theta_G)$$

Starboard Slat Vorticity δ_s

The velocity components v_B and w_B induced at general point (y_{B_G} , z_{B_G}) in the cross flow plane (in slat axes system y_B , z_B).

$$v_B(y_{B_G}, z_{B_G}) = -\frac{z_{B_G}}{2\pi}\int_{-c_{ox}}^{c_{ox}} \frac{\delta_s(y_B)\,dy_B}{(y_B - y_{B_G})^2 + z_{B_G}^2}$$

$$w_B(y_{BG}, z_{BG}) = -\frac{1}{2\pi}\int_{-c_1 x}^{c_1 x} \frac{(y_B - y_{BG})\,\delta_S(y_B)\,dy_B}{(y_B - y_{BG})^2 + z_{BG}^2}$$

In non-dimensional terms (length kx) these become

$$v_B(y^*_{BG}, z^*_{BG}) = -\frac{z^*_{BG}}{2\pi}\int_{-c_1/k}^{c_1/k} \frac{\delta_S(y^*_B)\,dy^*_B}{(y^*_B - y^*_{BG})^2 + z^{*2}_{BG}}$$

$$w_B(y^*_{BG}, z^*_{BG}) = -\frac{1}{2\pi}\int_{-c_1/k}^{c_1/k} \frac{(y^*_B - y^*_{BG})\,\delta_S(y^*_B)\,dy^*_B}{(y^*_B - y^*_{BG})^2 + z^{*2}_{BG}}$$

By substituting for the components of δ_S, the velocity influence coefficients can be written as follows:

(a) component $\delta_G(y^*_B) \equiv \delta_G(\theta_B) = V \cdot g_3 \cdot \tan \theta_B/2$

$$\cos\theta_B = -y^*_B \cdot \frac{k_1}{c_1}$$

$$v_{B\delta_G}(y^*_{BG}, z^*_{BG}) = V \cdot g_3 \cdot g v_{\delta_{G_3}}(y^*_{BG}, z^*_{BG})$$

$$w_{B\delta_G}(y^*_{BG}, z^*_{BG}) = V \cdot g_3 \cdot g w_{\delta_{G_3}}(y^*_{BG}, z^*_{BG})$$

(Configurations A-S-A and S-S-A)

where

$$g v_{\delta g_3}(y^*_{BG}, z^*_{BG}) = -\frac{z^*_{BG}}{2\pi}\int_{-c_1/k}^{c_1/k}\frac{\delta_G(y^*_B)\,dy^*_B}{(y^*_B - y^*_{BG})^2 + z^{*2}_{BG}}$$

and

$$g w_{\delta g_3}(y^*_{BG}, z^*_{BG}) = -\frac{1}{2\pi}\int_{-c_1/k}^{c_1/k}\frac{(y^*_B - y^*_{BG})\,\delta_G(y^*_B)\,dy^*_B}{(y^*_B - y^*_{BG})^2 + z^{*2}_{BG}}$$

on the surface of the slat, $z^*_{BG} = 0$

$$g w_{\delta g_3}(y^*_{BG}, 0) = -\frac{1}{2\pi}\int_{-c_1/k}^{c_1/k}\frac{\delta_G(y^*_B)\,dy^*_B}{(y^*_B - y^*_{BG})}$$

The expressions for $g v_{B\delta_G}$ and $g w_{B\delta_G}$ can also be derived from potential theory using complex variables. These are exact.

$$Z^*_{BG} = y^*_{BG} + i\,z^*_{BG}$$

$$g v_{\delta g_3}(Z^*_{BG}) = \left(-\frac{i}{2}\sqrt{\frac{Z^*_{BG} + c_1/k_1}{Z^*_{BG} - c_1/k_1}} + \frac{i}{2}\right)$$

and

$$g w_{\delta g_3}(Z^*_{BG}) = g\left(\frac{i}{2}\sqrt{\frac{Z^*_{BG} + c_1/k_1}{Z^*_{BG} - c_1/k_1}} - \frac{i}{2}\right)$$

(b) component $\delta_B(y_B^*) \equiv \delta_B(\theta_B) = V \sum_{q=1}^{N} b_q \cdot \sin(q\theta_B)$

$$\cos\theta_B = -y_B^* \frac{k}{c_1}$$

$$v_{B\delta_B}(y_{BG}^*, z_{BG}^*) = V \sum_{q=1}^{N} b_q \cdot bv_{\delta_B}(q, y_{BG}^*, z_{BG}^*)$$

$$w_B(y_{BG}^*, z_{BG}^*) = V \sum_{q=1}^{N} b_q \cdot bw_{\delta_B}(q, y_{BG}^*, z_{BG}^*)$$

..ere

$$bv_{\delta_B}(q, y_{BG}^*, z_{BG}^*) = -\frac{z_{BG}^*}{2\pi} \int_{-c_1/k}^{c_1/k} \frac{\sin\left(q \cdot \cos^{-1}\left(-y_B^* \frac{k_1}{c_1}\right)\right) dy_B^*}{(y_B^* - y_{BG}^*)^2 + z_{BG}^{*2}}$$

$$bw_{\delta_B}(q, y_{BG}^*, z_{BG}^*) = -\frac{1}{2\pi} \int_{c_1/k}^{c_1/k} \frac{(y_B^* - y_{BG}^*) \sin\left(q \cdot \cos^{-1}\left(-y_B^* \cdot \frac{k}{c_1}\right)\right) dy_B}{(y_B^* - y_{BG}^*)^2 + z_{BG}^{*2}}$$

on the surface of the slat, $z_{BG}^* = 0$

$$b\,w_{\delta_B}(\nu, y^*_{BG}, 0) = -\frac{1}{2\pi}\int_0^{\pi} \frac{\sin(\nu\theta_B)\sin\theta_B \, d\theta_B}{\cos\theta_B - \cos\theta_{BG}}$$

or
$$b\,w_{\delta_B}(\nu, \theta_B) = -\frac{1}{2\pi}\left[\frac{\pi\sin(\nu-1)\theta_B - \pi\sin(\nu+1)\theta_B}{\sin\theta_{BG}}\right]_0^{\pi}$$

$$= -\frac{1}{2}\cos\nu\theta_{BG}$$

Vortex pairs, $\pm\Gamma_1 \pm \Gamma_2 \pm\Gamma_3$

The velocity components v and w induced due to a pair of vortices $\pm\Gamma_i$ at $(\pm y_{v_i}, z_{v_i})$ (i = 1, 2 or 3), at a general point (y_G, z_G) in the cross flow plane are

$$v_{\Gamma_i}(y_G, z_G) = \Gamma_i \cdot g v_{\Gamma_i}(y_G, z_G) = \Gamma_i \cdot \frac{1}{2\pi}(z_{v_i} - z_G)\left[\frac{1}{(y_{v_i}-y_G)^2 + (z_{v_i}-z_G)^2} - \frac{1}{(y_{v_i}+y_G)^2 + (z_{v_i}-z_G)^2}\right]$$

$$w_{\Gamma_i}(y_G, z_G) = \Gamma_i \cdot g w_{\Gamma_i}(y_G, z_G) = \Gamma_i \cdot \frac{1}{2\pi}\left[\frac{-(y_{v_i}-y_G)}{(y_{v_i}-y_G)^2 + (z_{v_i}-z_G)^2} - \frac{y_{v_i}+y_G}{(y_{v_i}-y_G)^2 + (z_{v_i}-z_G)^2}\right]$$

These may be non-dimensionalised with respect to length kx, and velocity V.

$$\frac{v_{\Gamma_i}(y^*_G, z^*_G)}{V} = \left(\frac{\Gamma_i}{V.k_x}\right) \cdot g v_{\Gamma_i}(y^*_G, z^*_G) = \left(\frac{\Gamma_i}{V.k_x}\right) \cdot \frac{(z^*_{v_i} - z^*_G)}{2\pi}\left[\frac{1}{(y^*_{v_i}-y^*_G)^2 + (z^*_{v_i}-z^*_G)^2} - \frac{1}{(y^*_{v_i}+y^*_G)^2 + (z^*_{v_i}-z^*_G)^2}\right]$$

and

$$\frac{w_{\Gamma_i}(y^*_G, z^*_G)}{V} = \frac{\Gamma_i}{V.k_x} \cdot g w_{\Gamma_i}(y^*_G, z^*_G) = \left(\frac{\Gamma_i}{V.k_x}\right) \cdot \frac{1}{2\pi}\left[\frac{-(y^*_{v_i}-y^*_G)}{(y^*_{v_i}-y^*_G)^2 + (z^*_{v_i}-z^*_G)^2} - \frac{y^*_{v_i}+y^*_G}{(y^*_{v_i}-y^*_G)^2 + (z^*_{v_i}-z^*_G)^2}\right]$$

APPENDIX II

FORCES AND FORCE DISTRIBUTIONS

Forces on the Wing

The normal force coefficient distribution on the wing is given by

$$C_{N_L}(y_A) = \frac{2}{V}\left\{\gamma_W(y_A) - \frac{v(y_A)}{V}\cdot\delta_W(y_A)\right\}$$

where $v(y_A)$ is the total spanwise velocity induced at the point y_A.

The total normal force coefficient on the wing C_{N_W} is obtained by integration of C_{N_L} along the wing span. Lift coefficient - C_{L_W} and Drag coefficient - C_{D_W} (not including the profile drag) follow from

$$C_{L_W} = C_{N_W}\cos\alpha$$

$$C_{D_W} = C_{N_W}\sin\alpha + C_{D_{W_T}}$$

where $C_{D_{W_T}}$ is the drag due to leading edge suction on the wing (if present, i.e. the configurations A-S-A and A-S-S). $C_{D_{W_T}}$ may be calculated according to methods indicated in Ref. 20. It depends on the value of coefficient g_1

$$C_{D_{W_T}} = \frac{g_1}{2}\cdot\sin\alpha\cdot\pi\, k\cdot\sqrt{1-k^2}\cdot\frac{k}{k_{ref}}$$

where k_{ref} refers to reference planform with semi-span $k_{ref}.x$

Forces on the Slat

The normal force coefficient distribution on each slat is given by

$$C_{N_L}(y_B) = \frac{2}{V}\left\{\gamma_S(y_B) - \frac{v_B(y_B)}{V}\cdot\delta_S(y_B)\right\}$$

where $v_B(y_B)$ is the total velocity induced in the v_B direction at the point y_B.

The total normal force coefficient on the slat C_{N_S} is obtained by integration of C_{N_L} along the slat span.

Lift coefficient (C_{L_S}) and drag coefficient (C_{D_S}) follow from

$$C_{L_S} = C_{N_S}\cos\alpha_S$$

$$C_{D_S} = C_{N_S}\sin\alpha_S + C_{D_{S_S}}$$

The profile drag has not been included.

where $C_{D_{S_S}}$ is the drag due to leading edge suction on the slat (if present i.e. in the configurations A-S-A and S-S-A). $C_{D_{S_S}}$ may be derived on the basis of Ref. 14 and its value depends on the coefficient g_3.

For one slat, and based on non-dimensionalising semi-span $k_e\,x$, (Fig. 20) $C_{D_{S_S}}$ referred to reference planform of semi-span $k_{ref}.x$ is given by

$$C_{D_{S_S}} = -\frac{g_3}{2} \cdot \sin\alpha_S \cdot \pi \cdot \frac{1}{2} \cdot k_e\sqrt{1-k_e^2} \cdot \frac{k}{k_{ref}}$$

where $\quad k_e = c_0 \cos\varphi + h_0 \sin\varphi + c_1 - \sin\alpha_S \sin\varphi$

<u>Total Forces on Wing-Slat Configuration</u>

Total lift (C_L) and Induced Drag Coefficient (C_D) are given by adding the wing and slat contributions.

$$C_L = C_{L_W} + C_{L_S}$$

$$C_D = C_{D_W} + C_{D_S}$$

The reference lengths should be consistent.

REFERENCES

1. SMITH, A. M. O. — High Lift Aerodynamics, J. of Air. Vol. 12, No. 6, pp. 5-30 (June 1975).

2. RAY, E. J. and HOLLINGSWORTH, E. G. — Subsonic Characteristics of a Twin-Jet Swept-Wing Fighter Model with Manoeuvring Devices. N.A.S.A. TN D-6921.

3. GOODMANSON, L. T. and GRATZER, L. B. — Recent Advances in Aerodynamics for Transport Aircraft, Part 1. A.I.A.A. Astro. & Aero., Dec. 1973.

4. CUMING, M. F. and DICKISON, J. G. — Leading Edge Devices on Slender Wings, University of Bristol, Aero. Eng. Undergraduate Report No.250, 1980.

5. TINOCO, E. N. and YOSHIHARA, H. — Subcritical Drag Minimisation for Highly Swept Wings with Leading Edge Vortices. AGARD CP-247 (1979).

6. BROWN, C. E. and MICHAEL, W. H., Jr. — Effect of Leading Edge Separation on the Lift of a Delta Wing. J. Aero. Sci., Vol. 21, pp.690-694 and 706. 1954. NACA TN.3430 (1955).

7. NANGIA, R. K. — The Effects of Longitudinal Camber on Slender Wings. Ph.D. Thesis, University of London, June 1967.

8. NANGIA, R. K. and HANCOCK, G.J. — A Theoretical Investigation of Delta Wings with Leading Edge Separation at Low Speeds. ARC CP.1086 (1968).

9. SMITH, J. H. B. — Improved Calculations of Leading-Edge Separation from Slender Delta Wings. Proc. Roy. Soc. London, Series A, Vol. 306, pp.67-90 (1968). RAE TR.66070 (1966).

10. PULLIN, D. I. — A Method for Calculating Inviscid Separated Flows about Conical Slender Bodies. Australian Report ARL/A 140, May 1973.

11. PULLIN, D. I. — Calculation of Steady Conical Flow Past a Yawed Slender Delta Wing with Leading Edge Separation. Imperial College London, Aero. Report 72-17 (1972).

12. JONES, I. P. — Flow Separation from Yawed Delta Wings. Computers and Fluids Vol. 3, pp.155-177 (1975).

13. COHEN, M. J. — Aerodynamics of Sideslipping Delta Wings at Incidence with Leading Edge Separation. J. of Aircraft, Vol. 13, No. 12, pp.1020-2, Dec. 1976.

14. SWEETMAN, W. — The Next Supersonic Transport. Flight International. 24 Nov. 1979, pp.1772-9.

15. NANGIA, R. K. — A Study of Slender, Thin, Conically Cambered Wings with Flow Separation. University of Bristol, Dept. of Aero. Eng. Report RKN/7701 (October 1977).

16. NANGIA, R. K. Slender, Thick, Sharp-Edged Conically Cambered Wings with Flow Separation. University of Bristol, Dept. of Aero. Eng. Report RKN/7801 (June 1978).

17. HALSEY, N. D. Potential Flow Analysis of Multi-element Airfoils Using Conformal Mappings. AIAA Jl. Vol. 17, No.12 pp 1281-8 (December 1979).

18. SMITH, J. H. B. A Theory of the Separated Flow from the Curved Leading Edge of a Slender Wing. ARC R&M 3116 (1957).

19. CLARK, R. W. Non-conical Flow Past Slender Wings with Leading-Edge Vortex Sheets. ARC R&M 3814 (March 1976)

20. SEARS, W. R. (Ed.) General Theory of High Speed Aerodynamics. Oxford University Press (1955) pp 218-235.

TABLE I WING SLAT CONFIGURATIONS

Geometry	$k=k_1$	c_o	c_1	h_o	ϕ	k_2 c_1-c_o	k_3 c_1+c_o	Remarks
WS1	.18	.2	.05	0	0	.2	.25	Effect of Slat Inclination ϕ
WS2					-5			
WS3					-10			
WS4					-15			
WS5				-.06	0			Effect of Slat height h_o
WS6				-.036				
WS7				-.02				
WS8				-.005				
WS9				.005				
WS10				.02				
WS11				.036				
WS12				.06				
WS13				.08715				
WS14				-.005	-10			Effect of Slat height h_o and its inclination ϕ
WS15				.005	-10			
WS16				.005	-20			
WS17				.06	-10			
WS18				.06	-20			
WS19	.1	.2	.05	0	0	.1	.25	Effect of reducing wing size
WS20					-10			
WS21					-20			

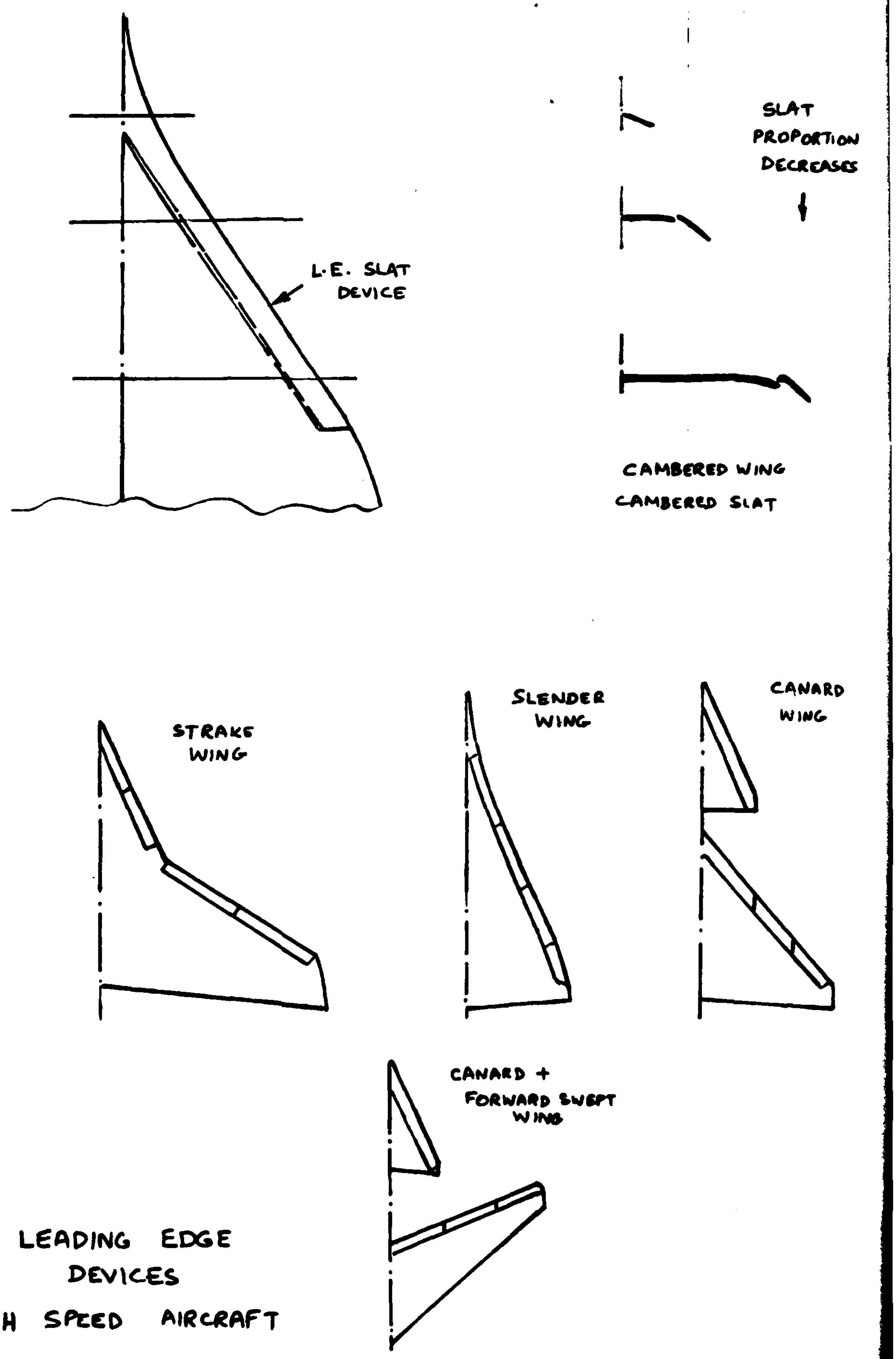

FIG.1. LEADING EDGE DEVICES HIGH SPEED AIRCRAFT

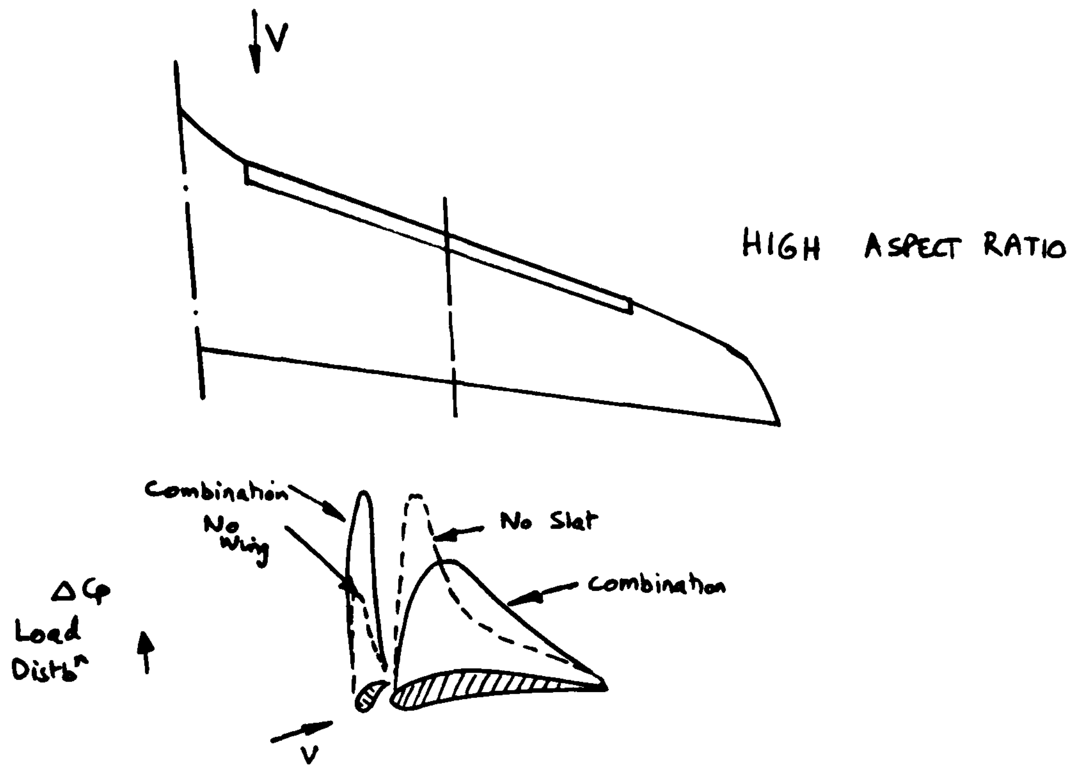

FIG.2 (a) 'CONVENTIONAL' AIRCRAFT WING WITH SLATS AND L.E. DROOP

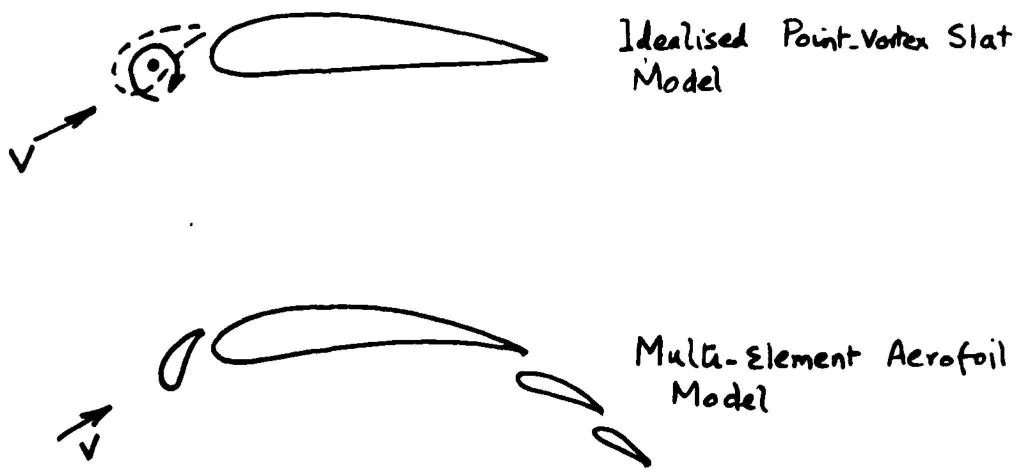

FIG.2 (b) 2-D AEROFOIL METHODS

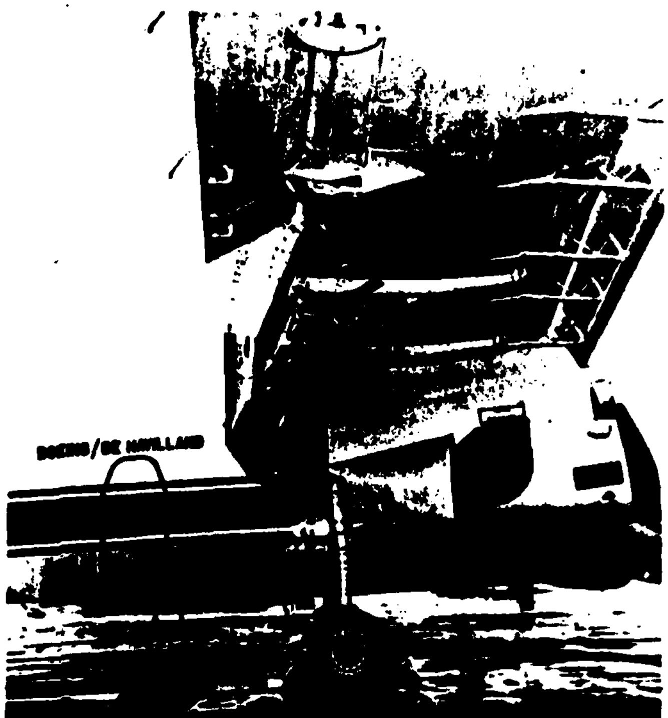

NASA augmenter-wing research airplane.

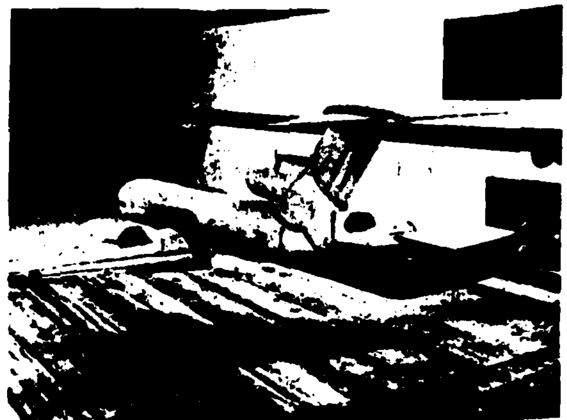

Low-speed USB model in the Boeing-Vertol wind tunnel.

747 HIGH-LIFT SYSTEM

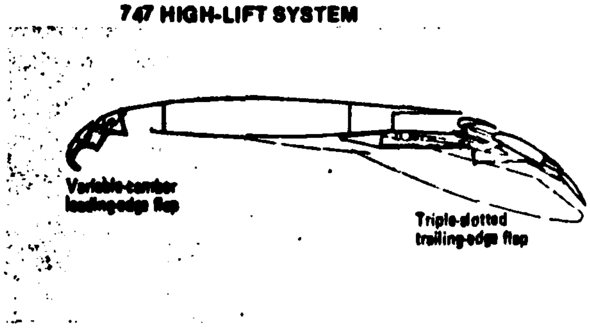

ADVANCED HIGH-LIFT SYSTEM

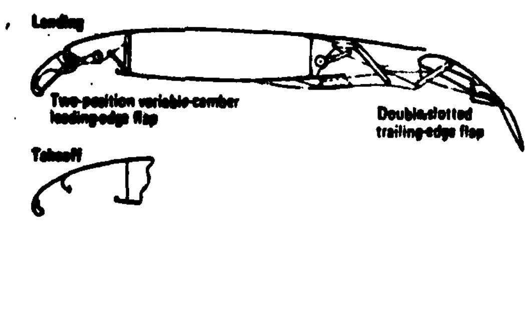

HIGH-LIFT SYSTEM IMPROVEMENT POTENTIAL

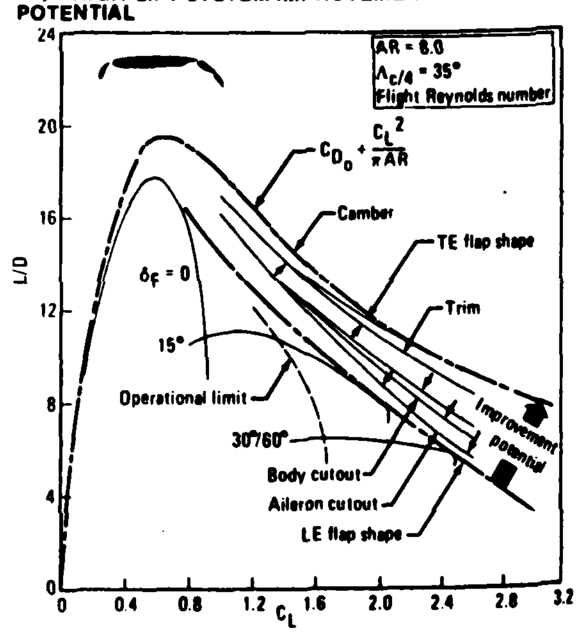

LARGE ASPECT-RATIO, LOW SWEEPBACK

FIG. 3. 'TWO-DIMENSIONAL' WINGS

HIGH-LIFT POTENTIAL (REF. 3)

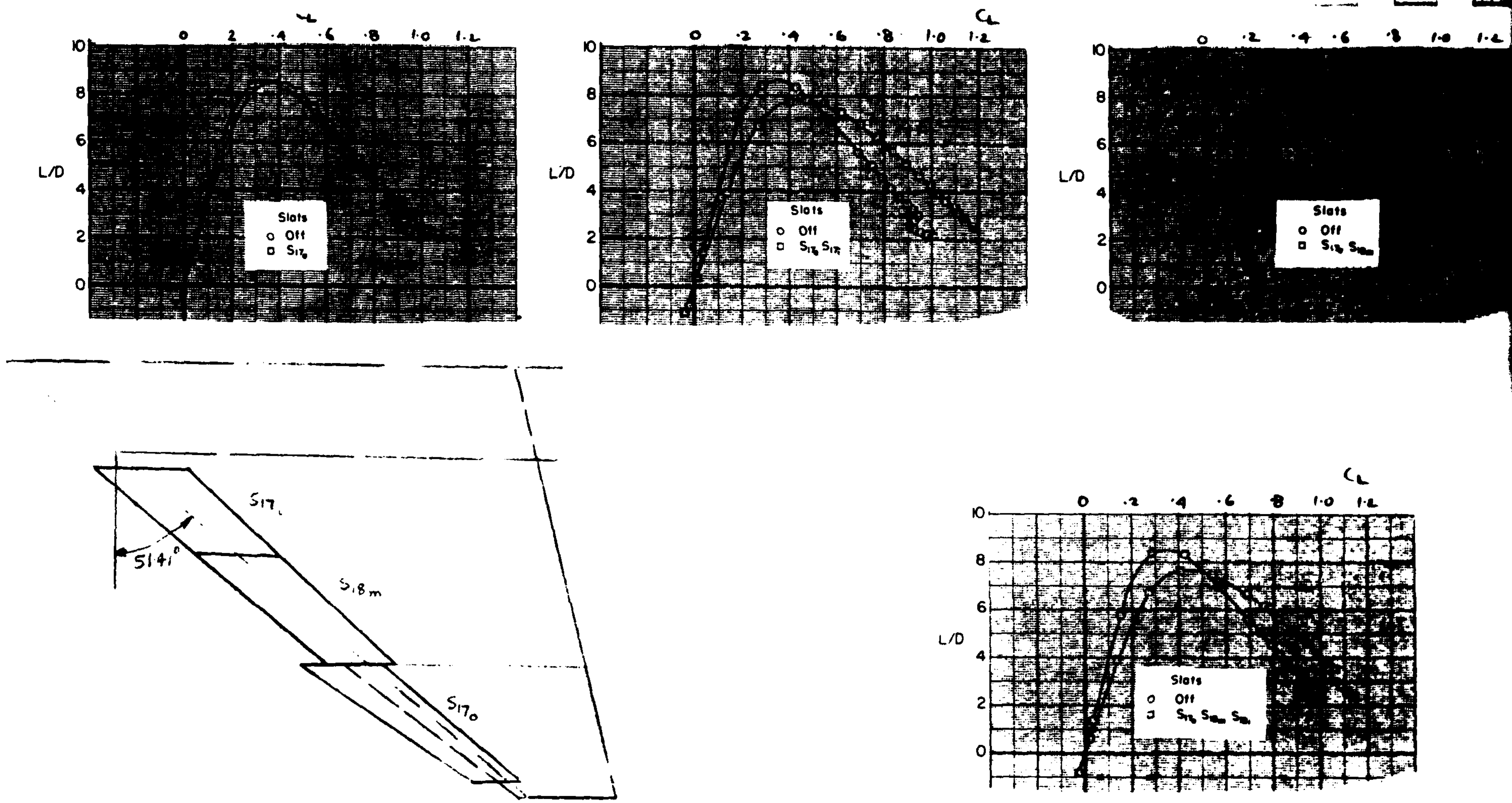

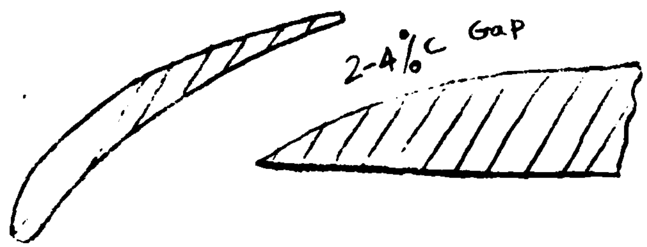

(a) M = 0·6

FIG.4. L.E. DEVICES ON F-4 (REF.2)

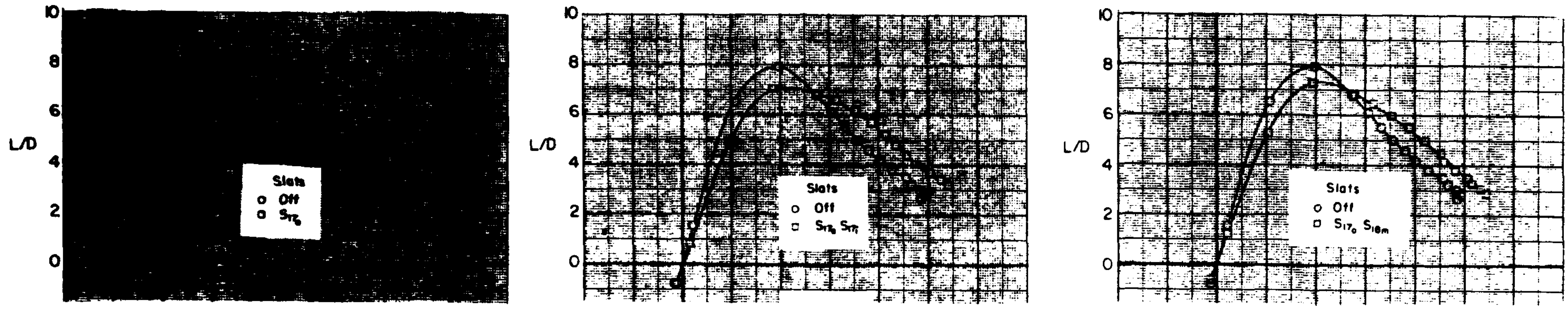

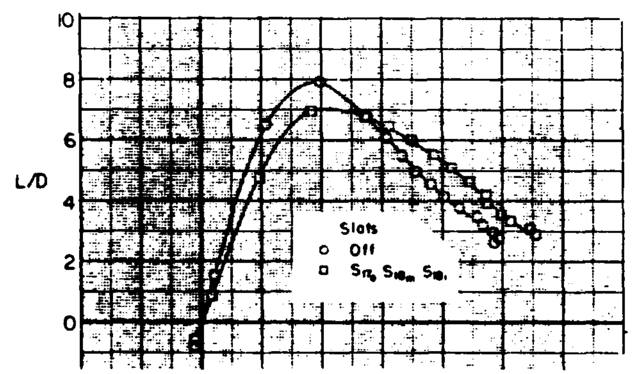

(b) M= 0.9

FIG. 4 CONT'D

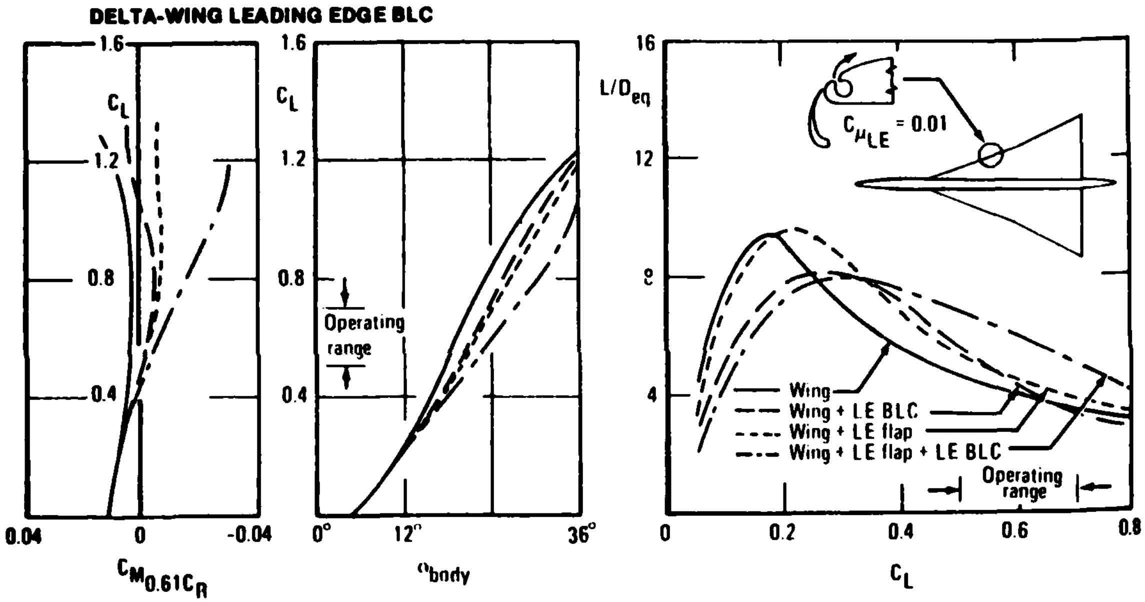

FIG. 5. L.E. DEVICES ON A HIGHLY SWEPT BACK "DELTA" WING (WITH & WITHOUT BOUNDARY LAYER CONTROL)

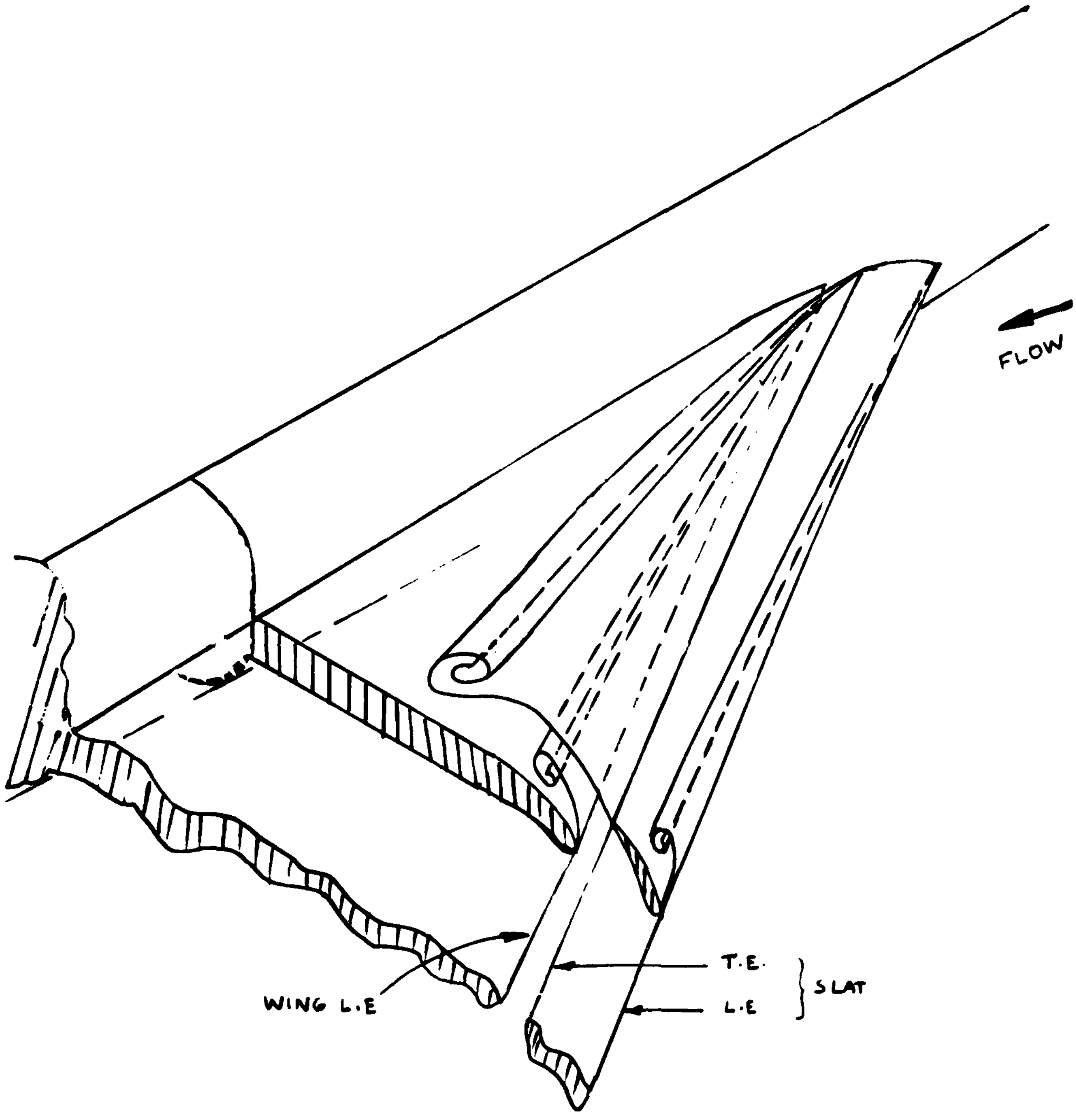

FIG. 6. L.E. DEVICES FLOWFIELD

ADDITIONAL SECONDARY SEPARATIONS MAY BE PRESENT NEAR THE WING L.E & SLAT T.E.

CONICAL STREAMLINES

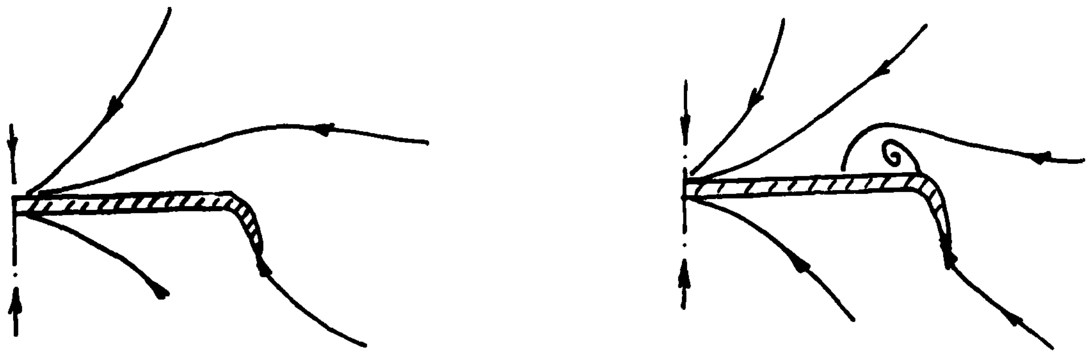

(a) Attached Flow (b) 'Real' Flow

FIG. 7. LARGE DEFLECTION 'SHOULDER FLAP
SMALL INCIDENCE RANGE

(a) (b)

FIG. 8 LARGE DEFLECTION SLOTTED FLAP - FLOW ATTACHED AT LEADING EDGES

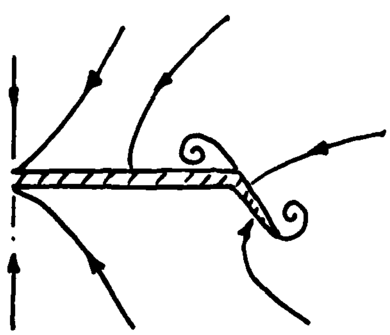

FIG. 9. HINGED FLAP AT MODERATE INCIDENCE

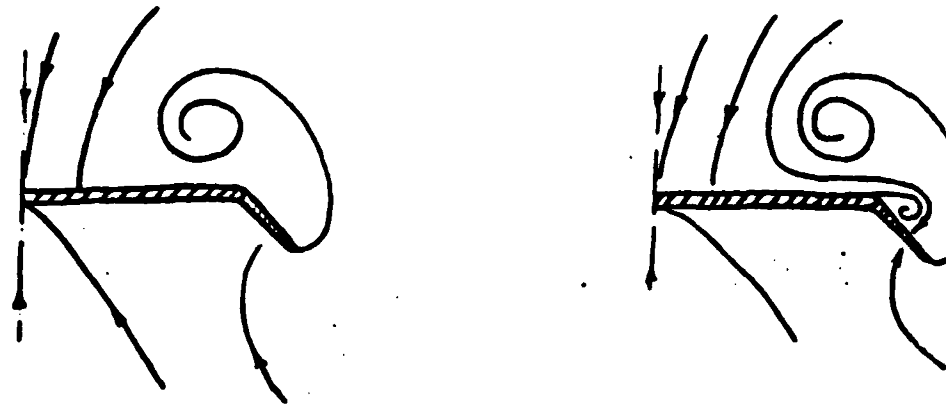

(a) Simple Model

(b) Model with Secondary Separation at Shoulder

FIG. 10 HINGED FLAP AT HIGH INCIDENCE

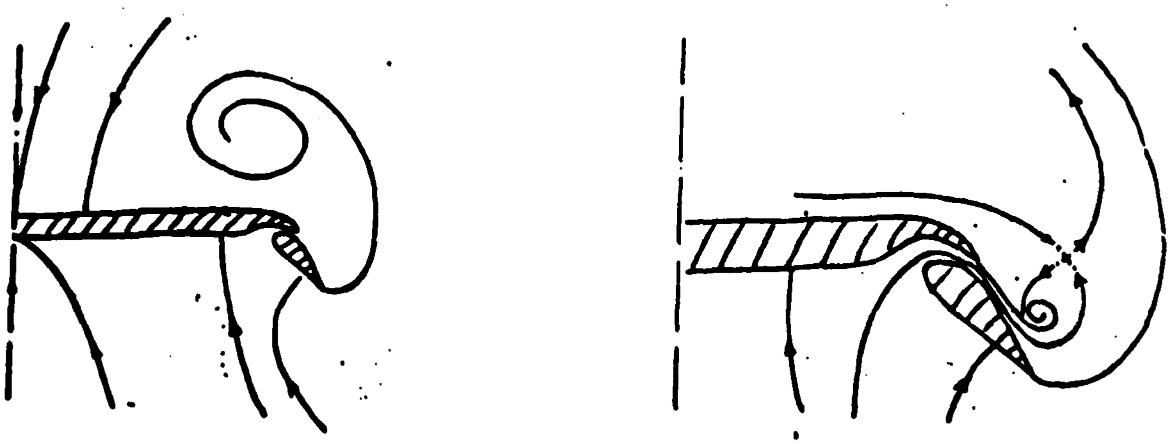

(a)

(b)

FIG. 11. SLOTTED FLAP AT HIGH INCIDENCE

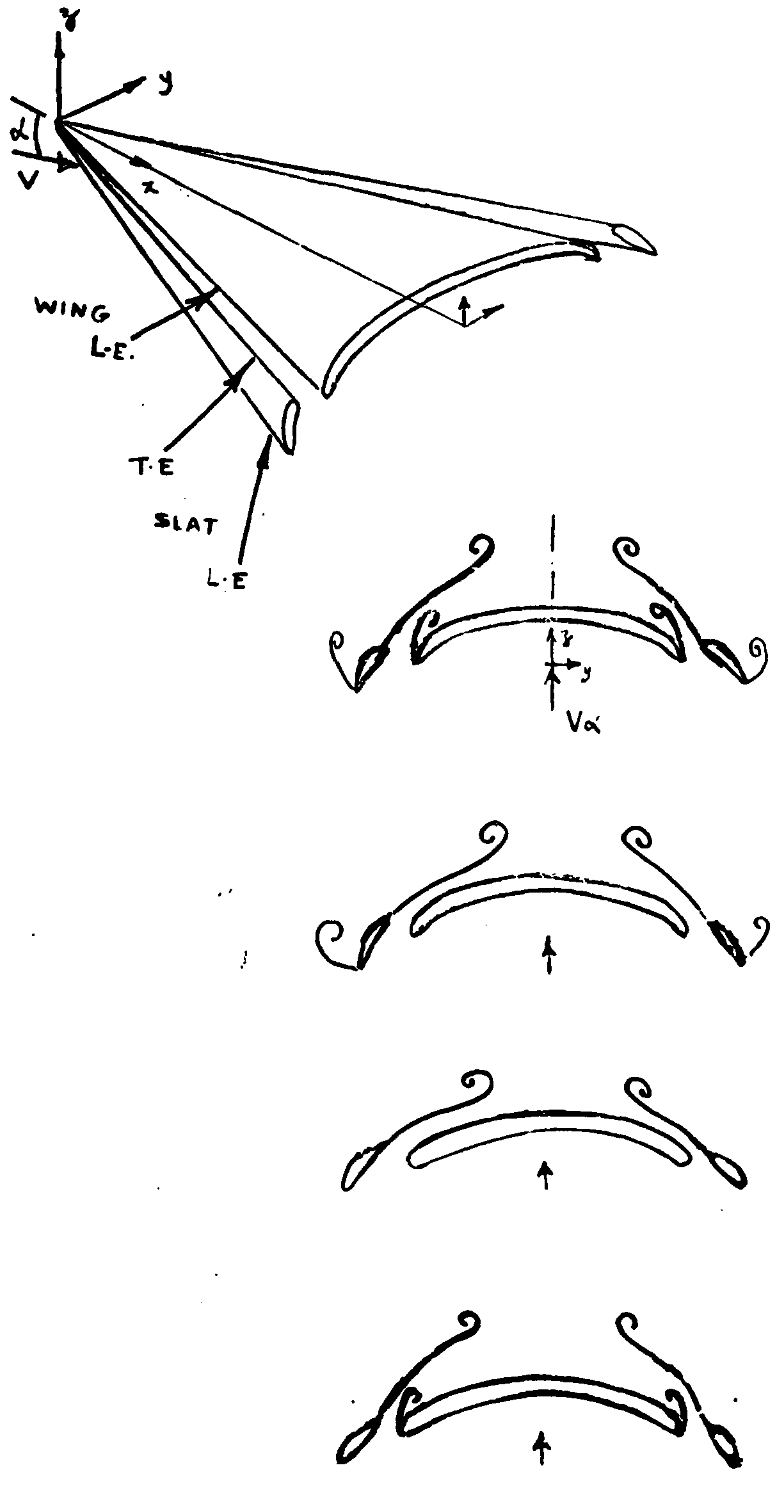

FIG. 12 POSSIBLE FLOWS

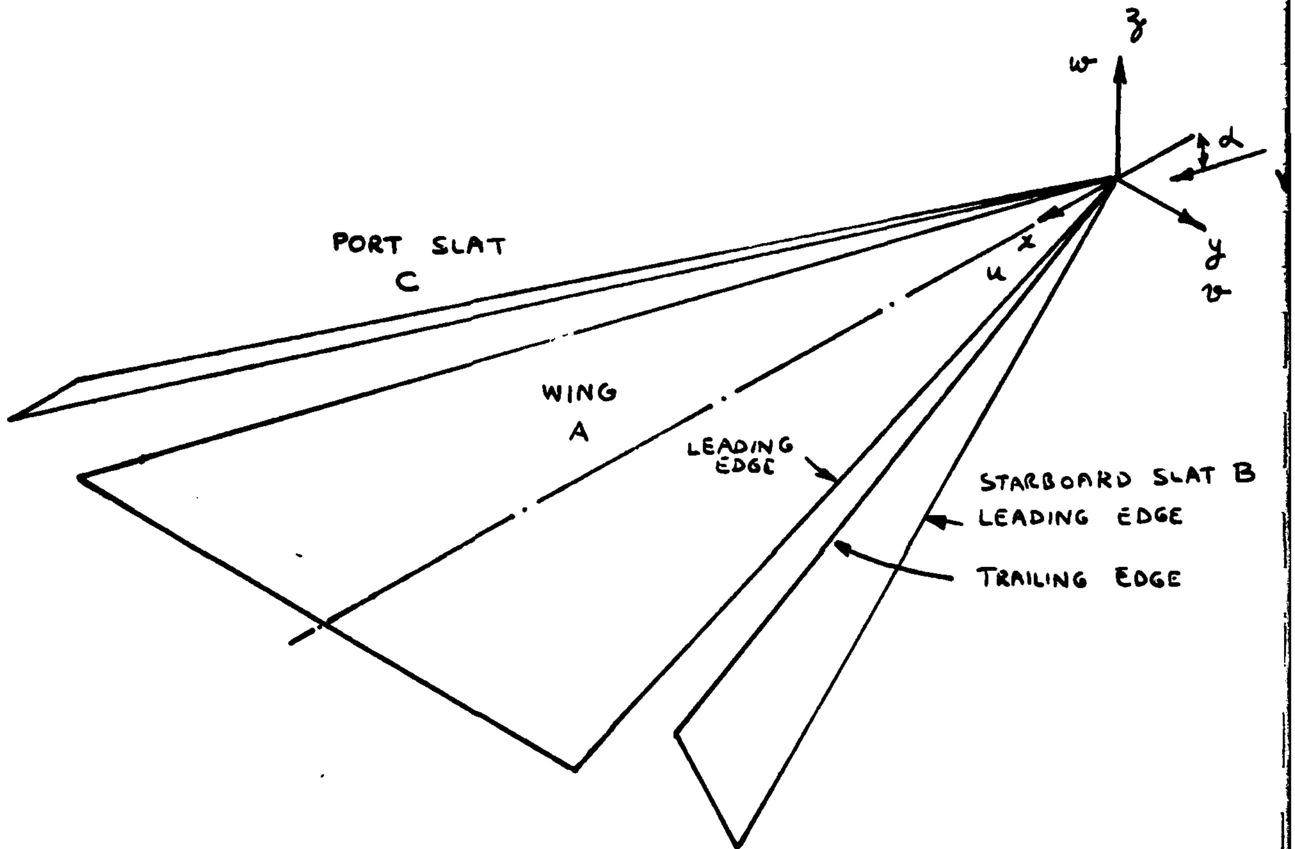

CROSS-FLOW PLANE

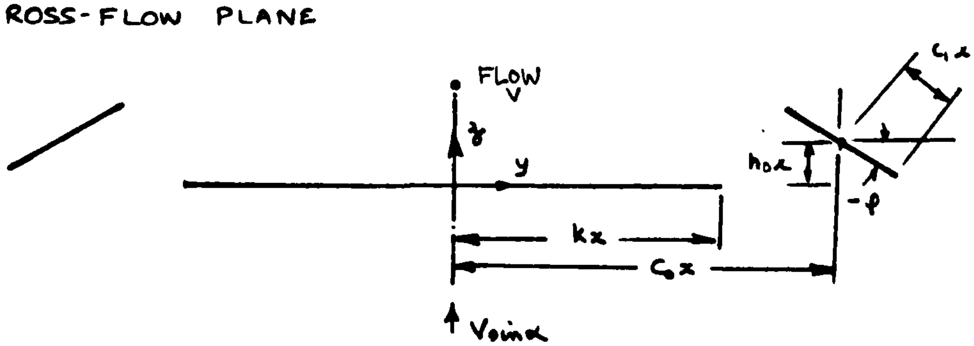

FIG. 13. WING - SLAT GEOMETRY

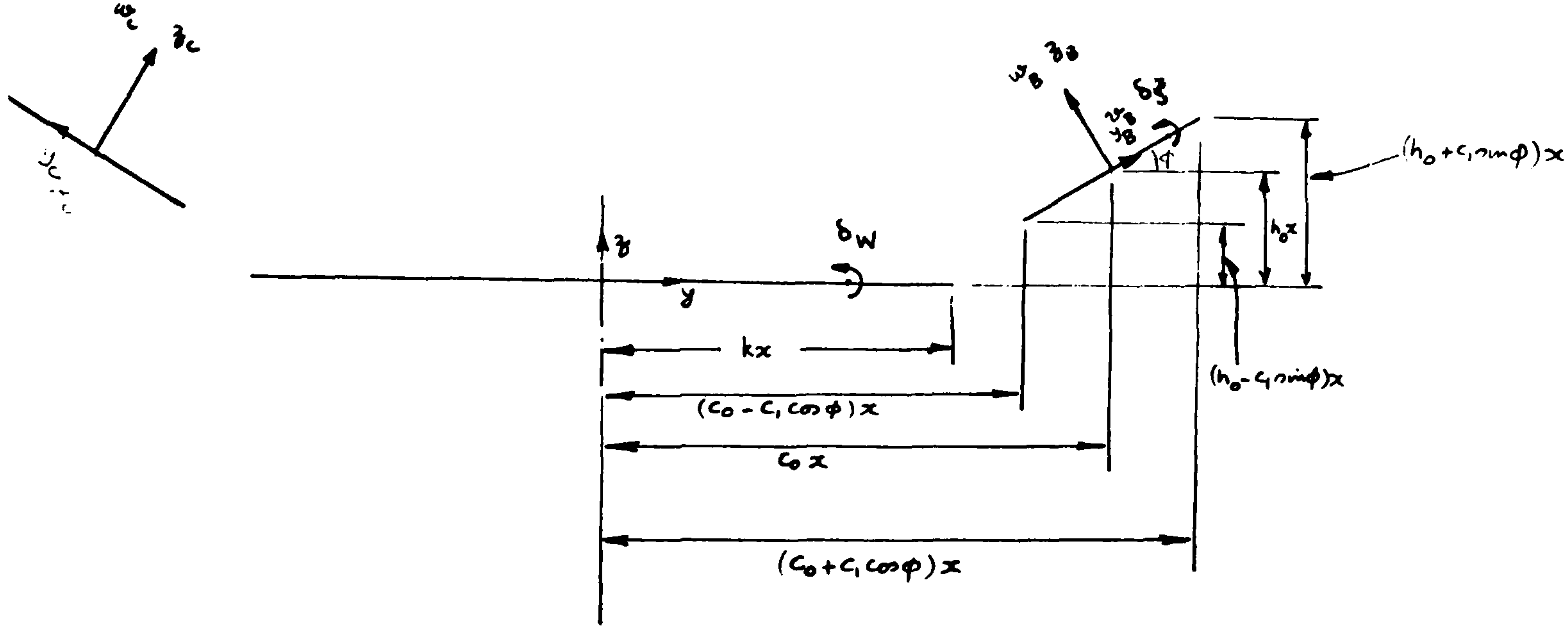

FIG. 14. MODEL GEOMETRY

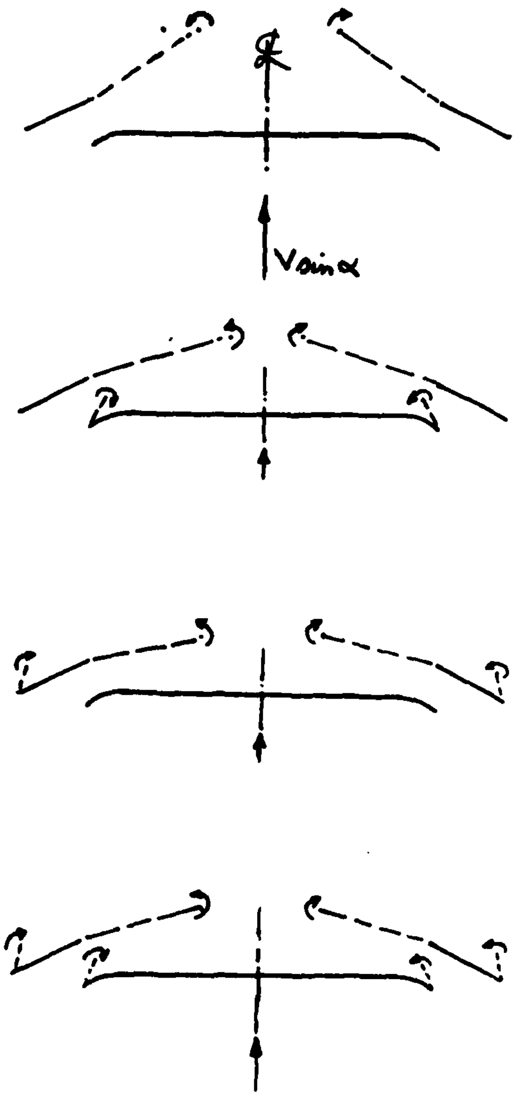

A-S-A
Vortex-cut at Slat T.E. only

S-S-A
Vortex-cuts at Wing L.E & Slat T.E. only

A-S-S
Vortex-cuts at Slat L.E & T.E

S-S-S
Vortex-cuts at Wing L.E, Slat L.E. & T.E.

FIG. 15. FOUR POSSIBLE WING-SLAT CONFIGURATIONS

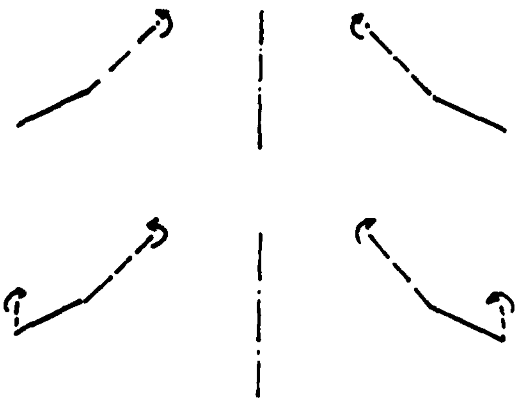

S-A
Vortex-cut at Slat T.E

S-S
Vortex-cuts at Slat L.E & T.E.

FIG. 16. TWO POSSIBLE SLATS ONLY CONFIGURATIONS

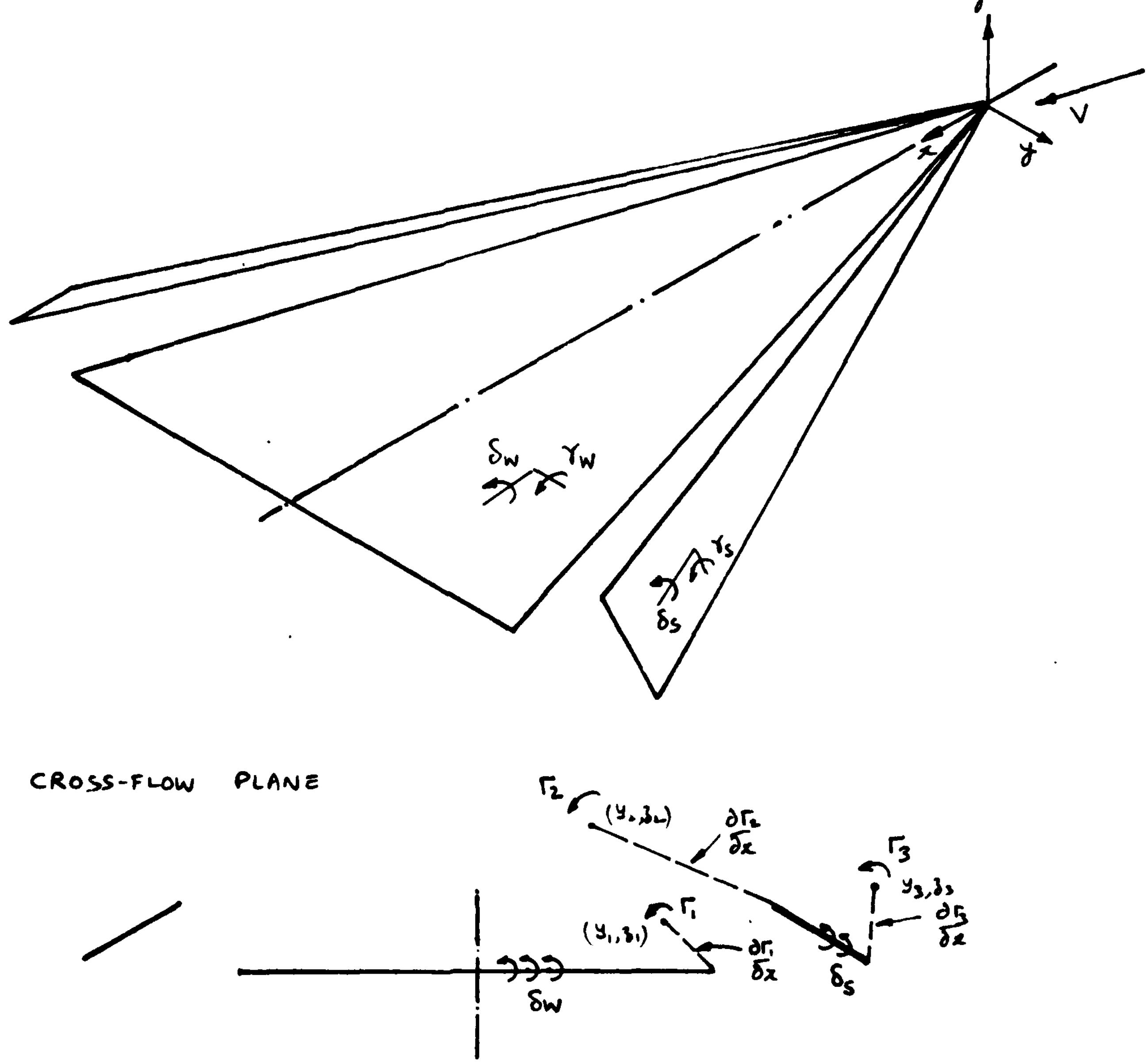

FIG. 17. REPRESENTATION OF VORTICES AND VORTICITY DISTRIBUTION

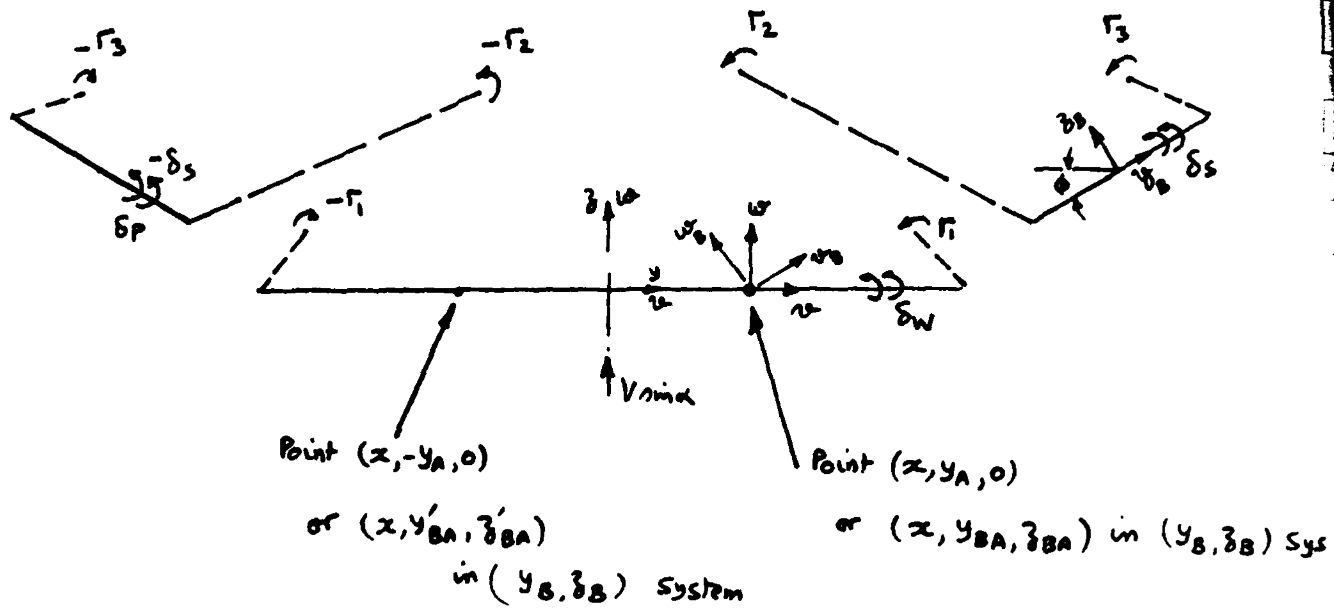

FIG. 18. VELOCITIES INDUCED AT A GENERAL POINT ON THE WING

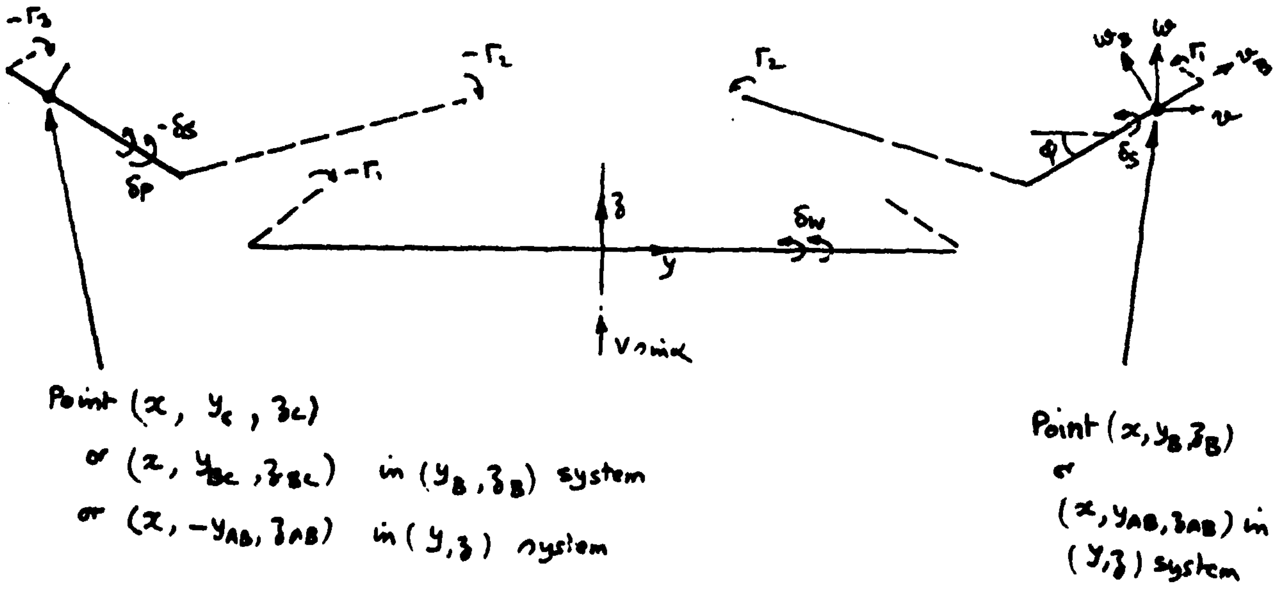

FIG. 19 VELOCITIES INDUCED AT A GENERAL POINT ON THE SLAT

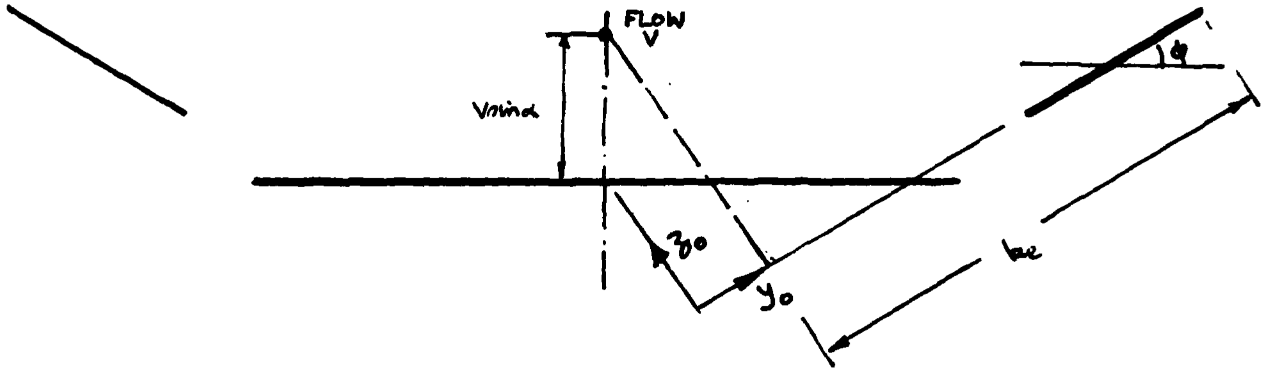

FIG. 20. CO-ORDINATES y_0, z_0

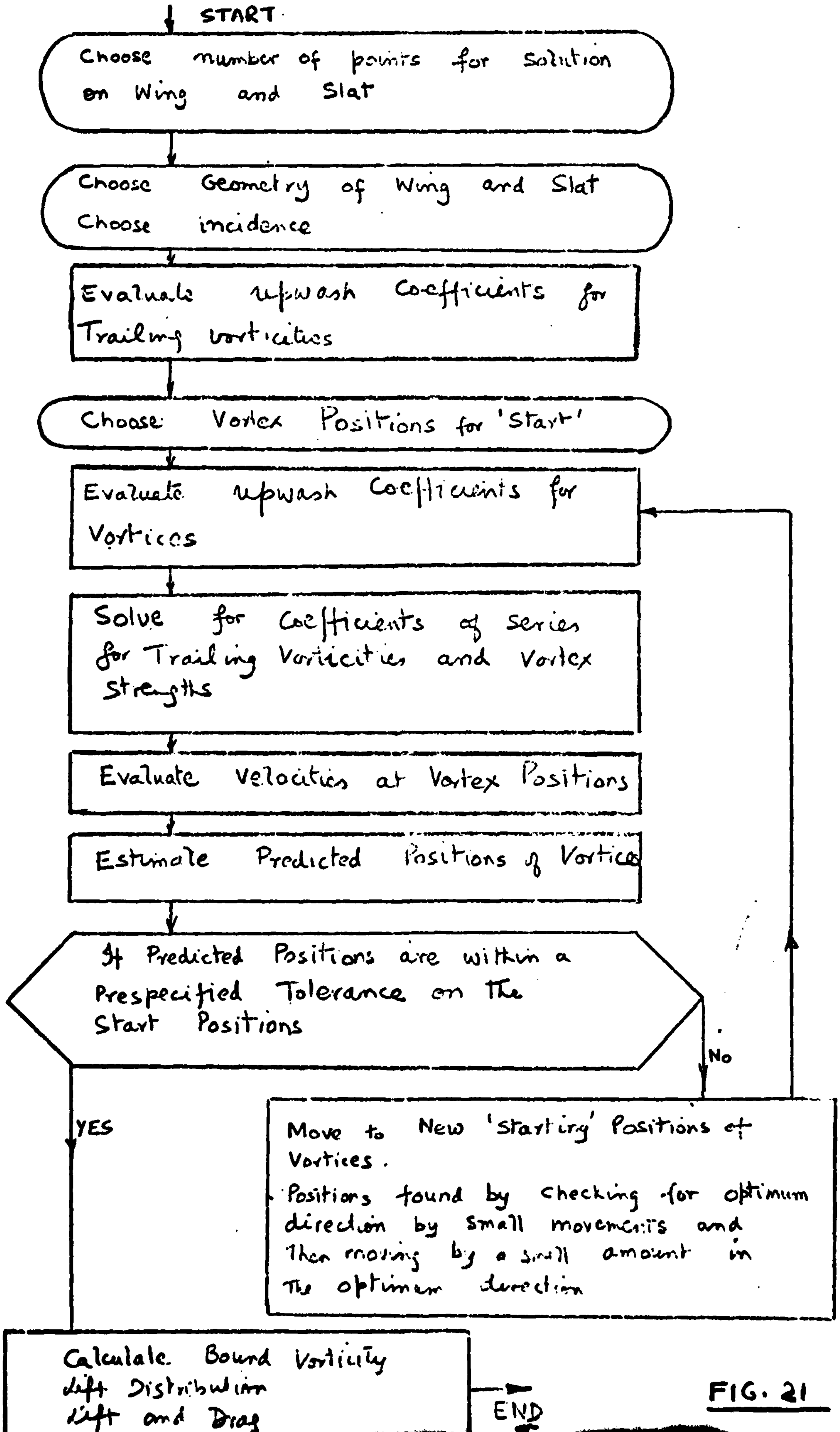
START
Choose number of points for solution on Wing and Slat
Choose Geometry of Wing and Slat
Choose incidence
Evaluate upwash Coefficients for Trailing vorticities
Choose Vortex Positions for 'Start'
Evaluate upwash Coefficients for Vortices
Solve for Coefficients of series for Trailing Vorticities and Vortex strengths
Evaluate velocities at Vortex Positions
Estimate Predicted Positions of Vortices
If Predicted Positions are within a Prespecified Tolerance on the Start Positions
No
YES
Move to New 'starting' Positions of Vortices.
Positions found by checking for optimum direction by small movements and then moving by a small amount in the optimum direction
Calculate Bound Vorticity
Lift Distribution
Lift and Drag
END

FIG. 21

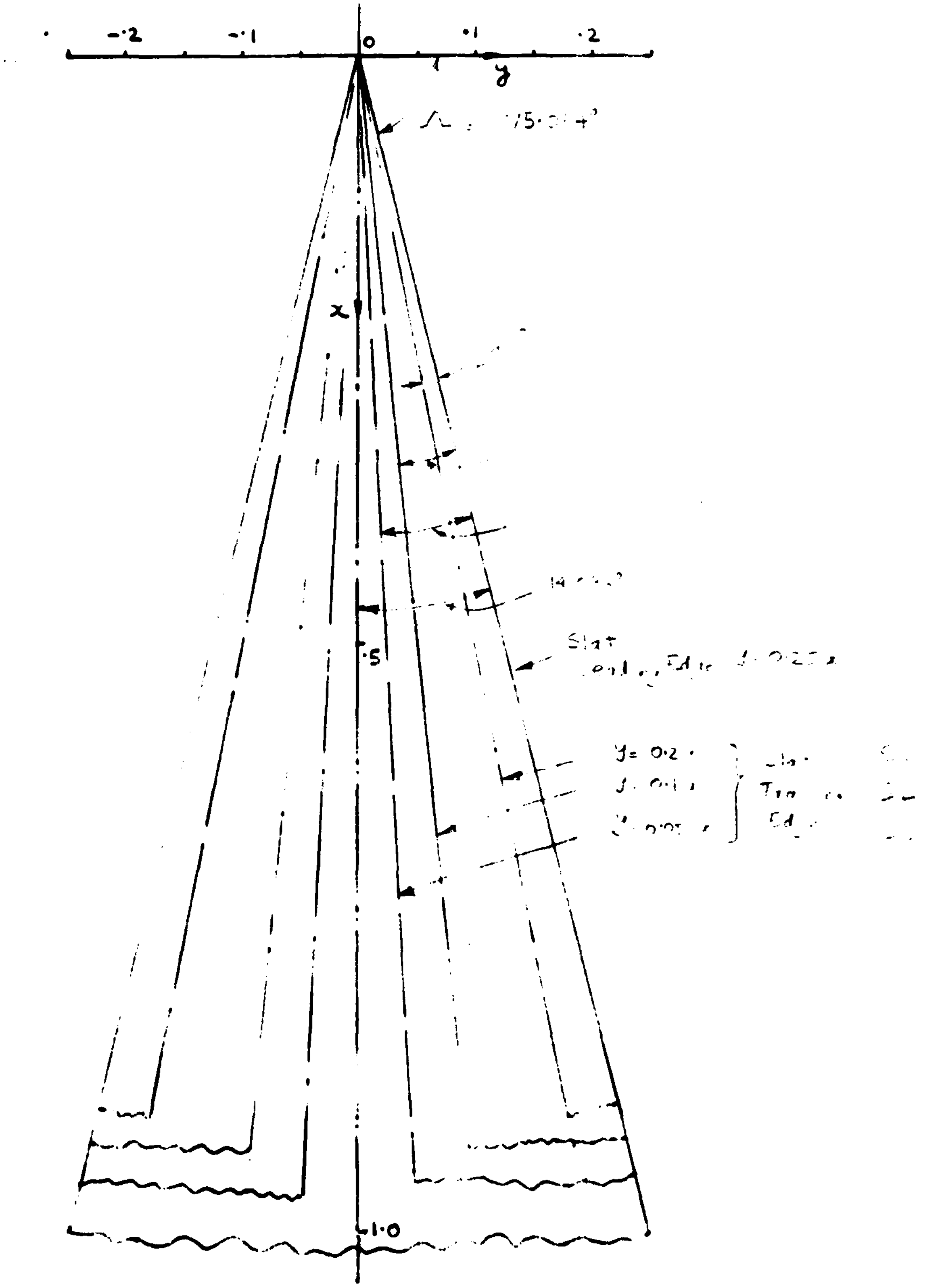

FIG. 22. SLATS ONLY GEOMETRY

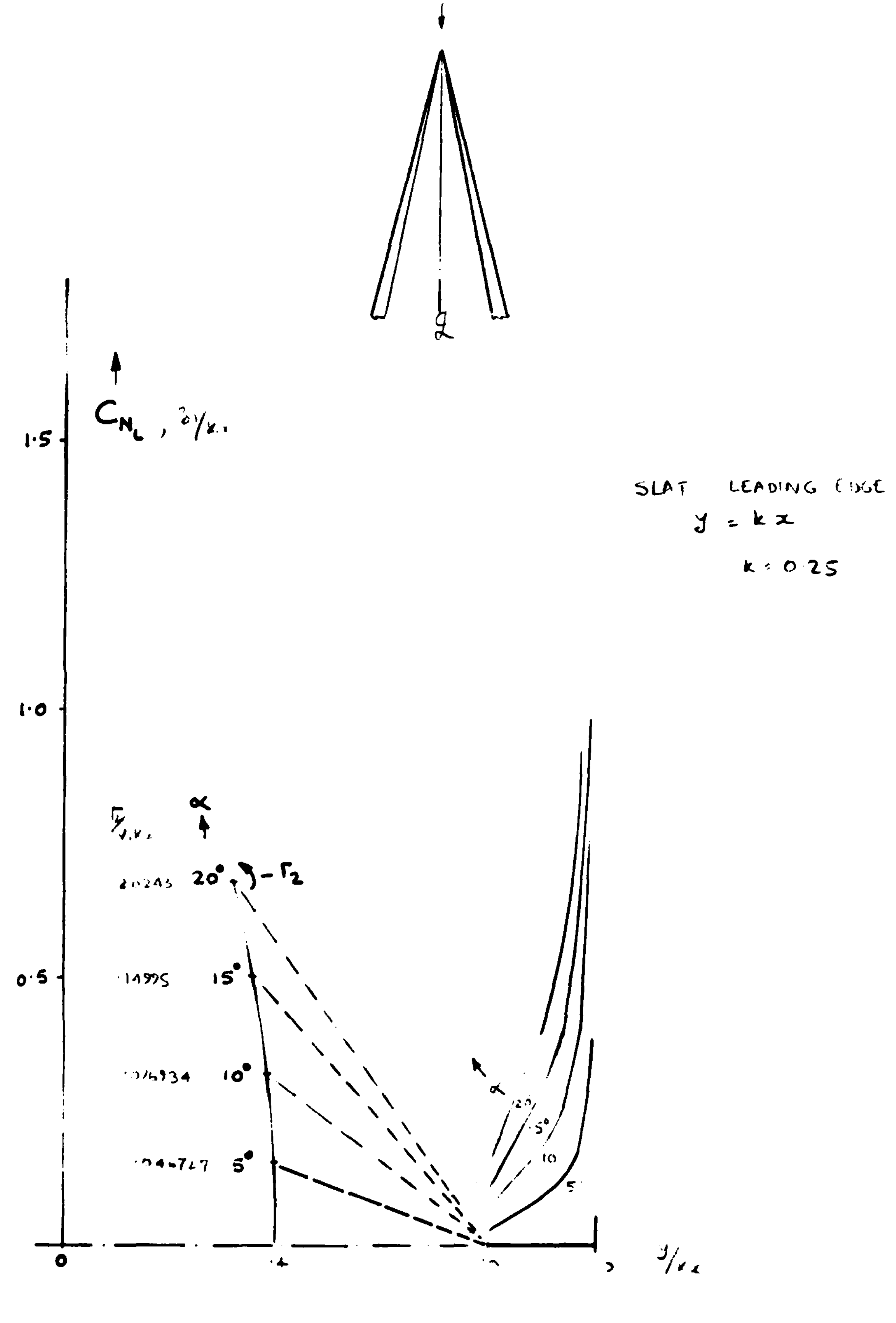

(a) EFFECT OF α

FIG. 23 CONFIGURATION S-A SLATS ONLY
GEOMETRY S-1

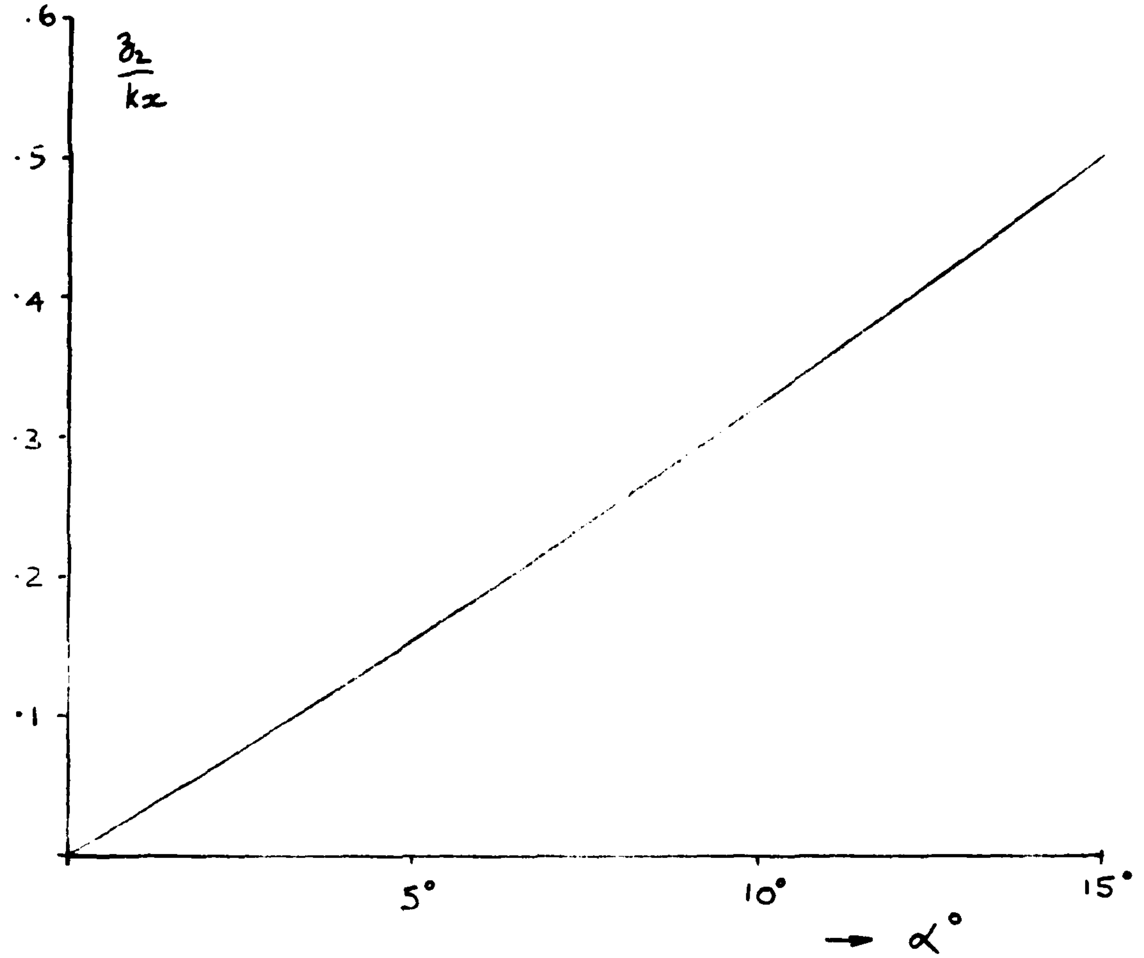

(b) Vortex height $z_2 \sim \alpha$

FIG 23 CONT'D

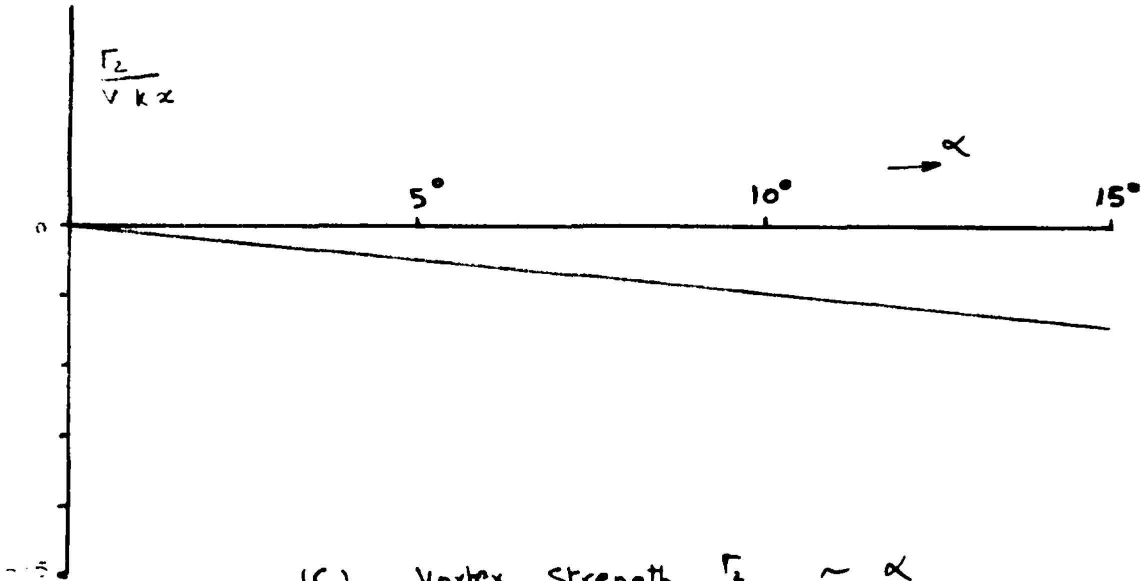

(c) Vortex Strength Γ_2 ~ α

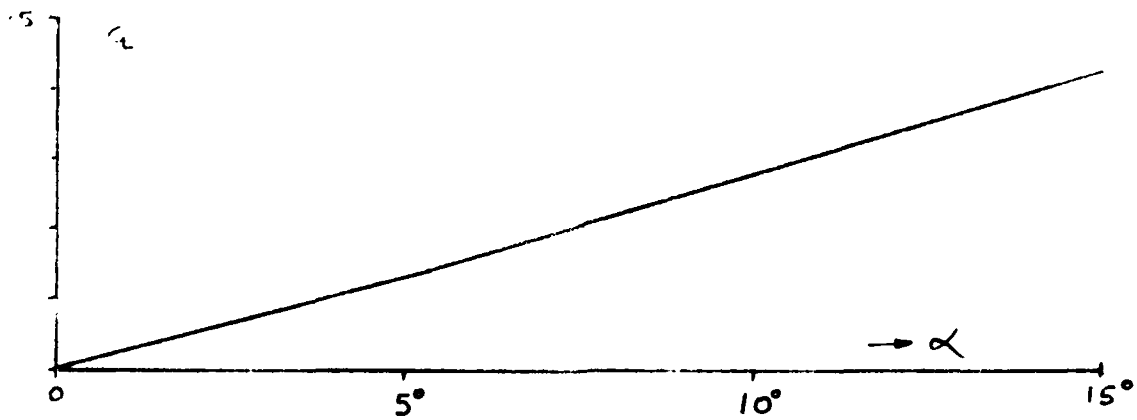

(d) Lift Coefficient ~ α

FIG. 23. CONT'D

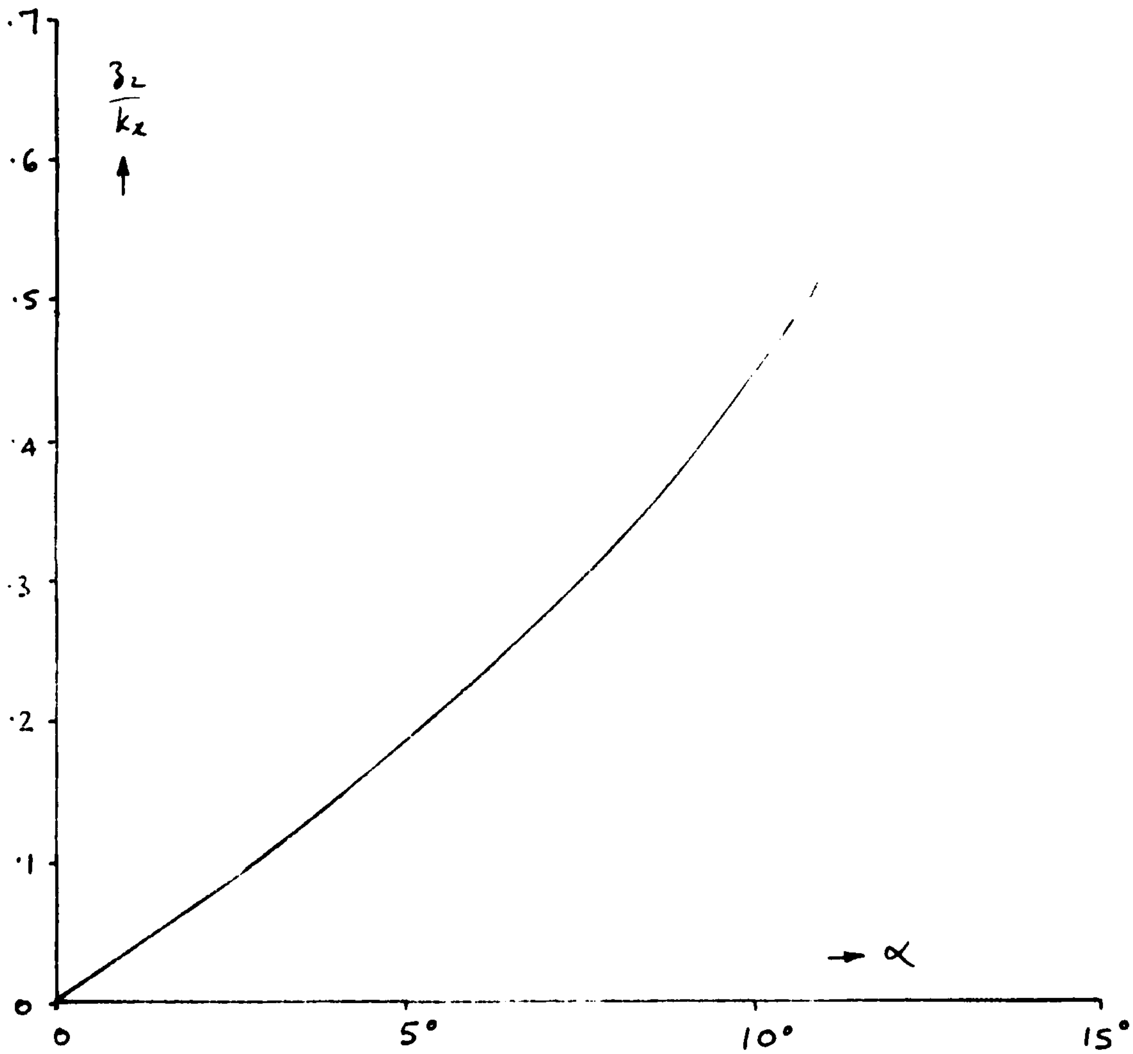

(b) VORTEX HEIGHT $z_2 \sim \alpha$

FIG. 24 CONT'D

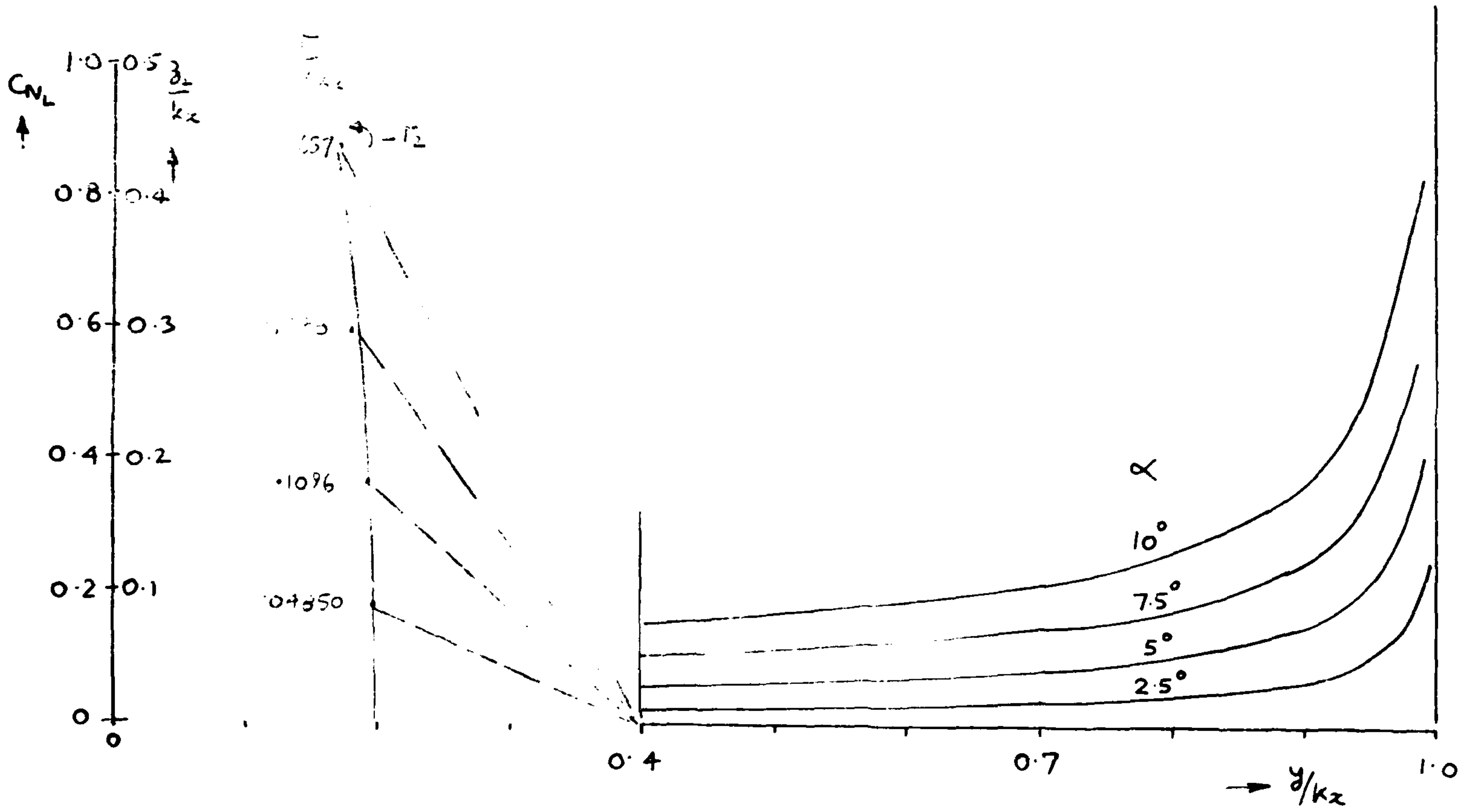

(a) Effect of α

FIG. 24. SLATS ONLY CONFIGURATION S-A
GEOMETRY S-2

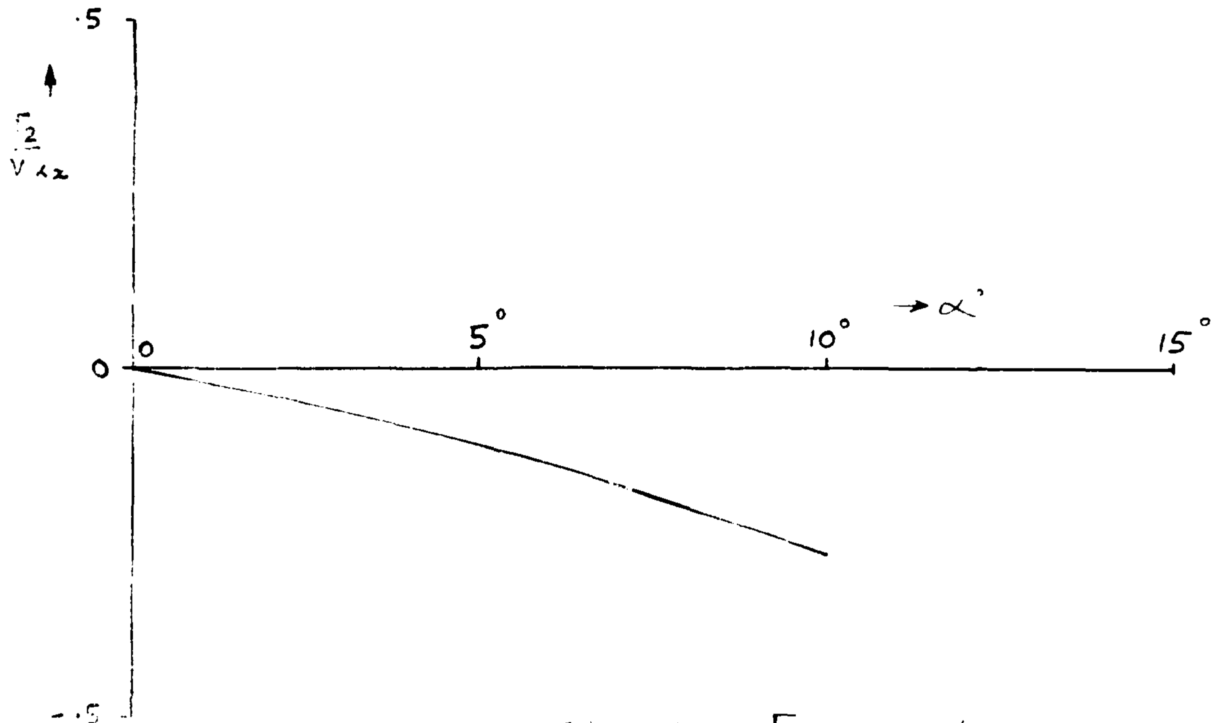

(c) Vortex Strength $\Gamma_2 \sim \alpha$

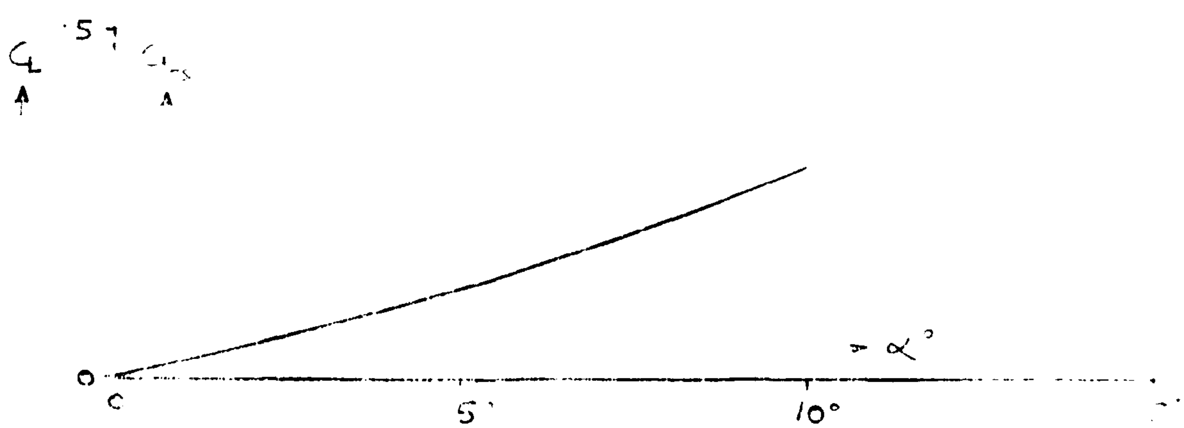

(d) Lift Coefficient ~ α

FIG. 2.4 (CONT.)

AD-A138 530 LEADING EDGE DEVICES SLATS ON SWEPT-BACK SLENDER WINGS WITH FLOW SEPARATI..(U) BRISTOL UNIV (ENGLAND) DEPT OF AERONAUTICAL ENGINEERING R K NANGIA JUN 80 RKN/8001 2/2

UNCLASSIFIED F49620-79-C-0075 F/G 20/4 NL

END

DATE FILMED

3-84

DTIC

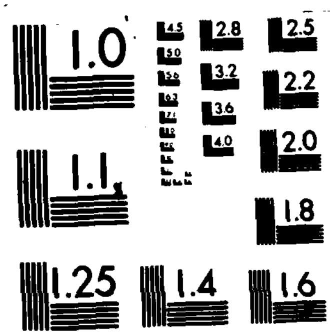

MICROCOPY RESOLUTION TEST CHART
NATIONAL BUREAU OF STANDARDS-1963-A

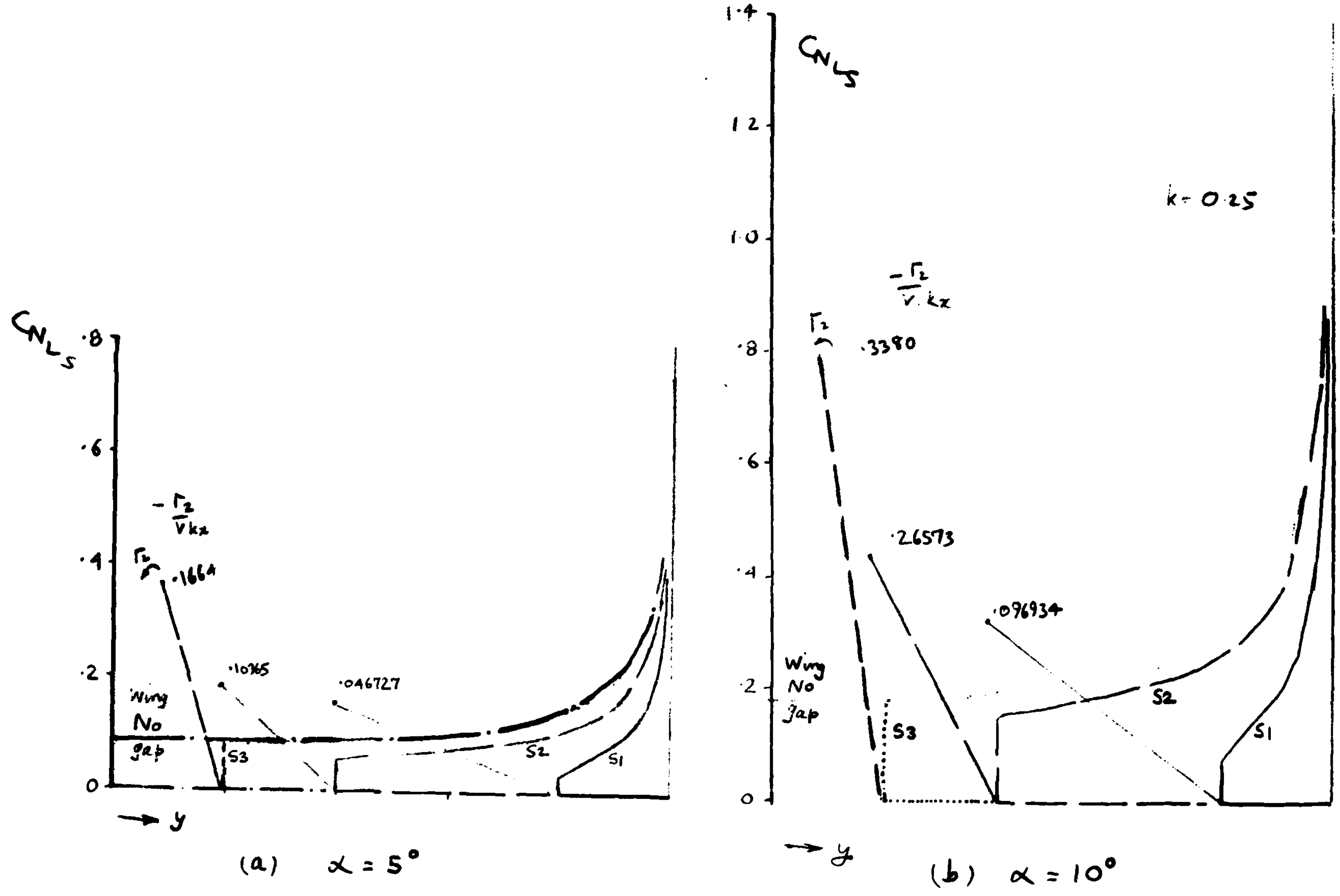

FIG. 25 SLATS ONLY CONFIGURATION S-A
Effect of Slat span

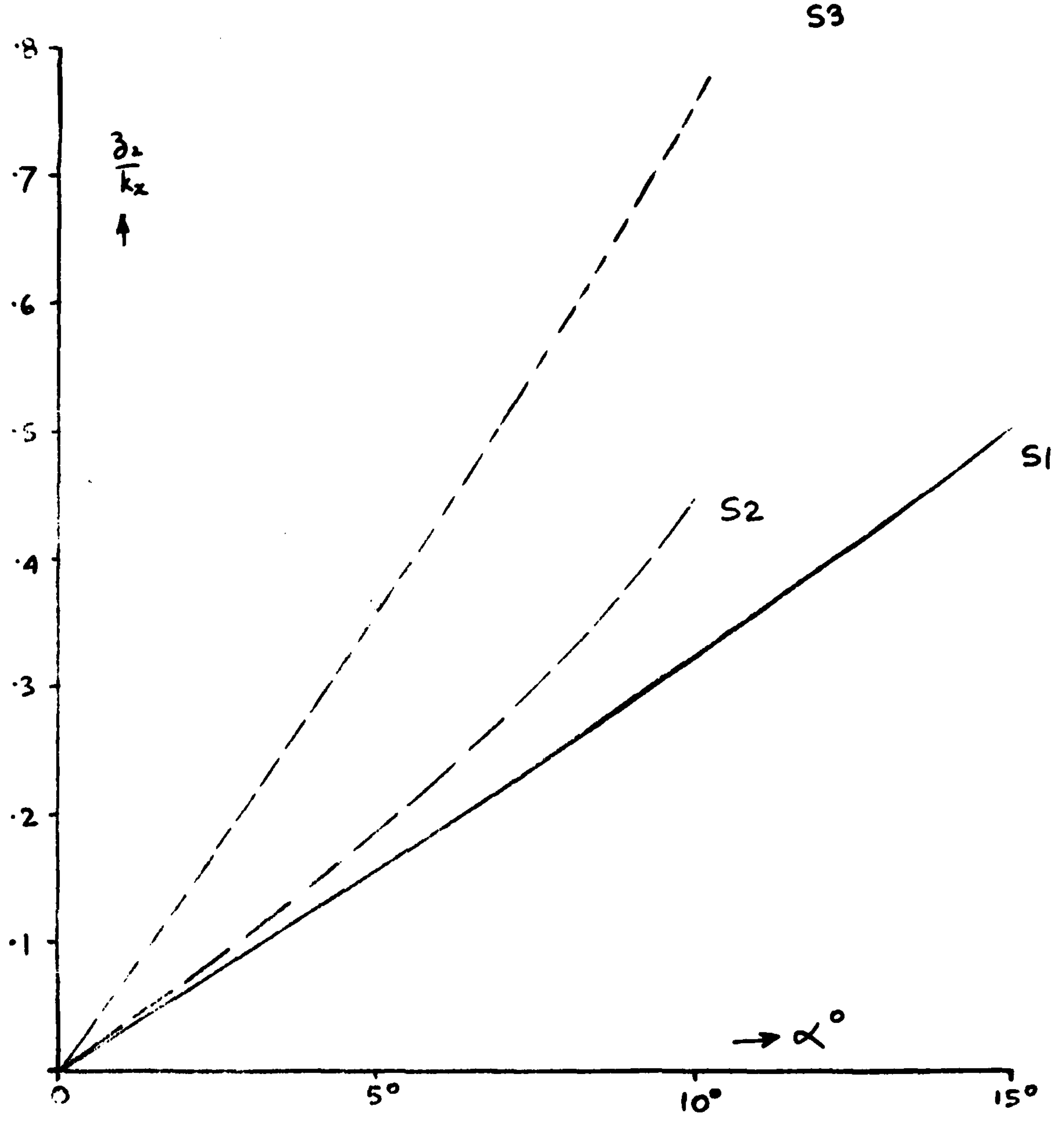

FIG 26. SLATS ONLY CONFIGURATION S-A

(a) Vortex height $z_2 \sim \alpha$

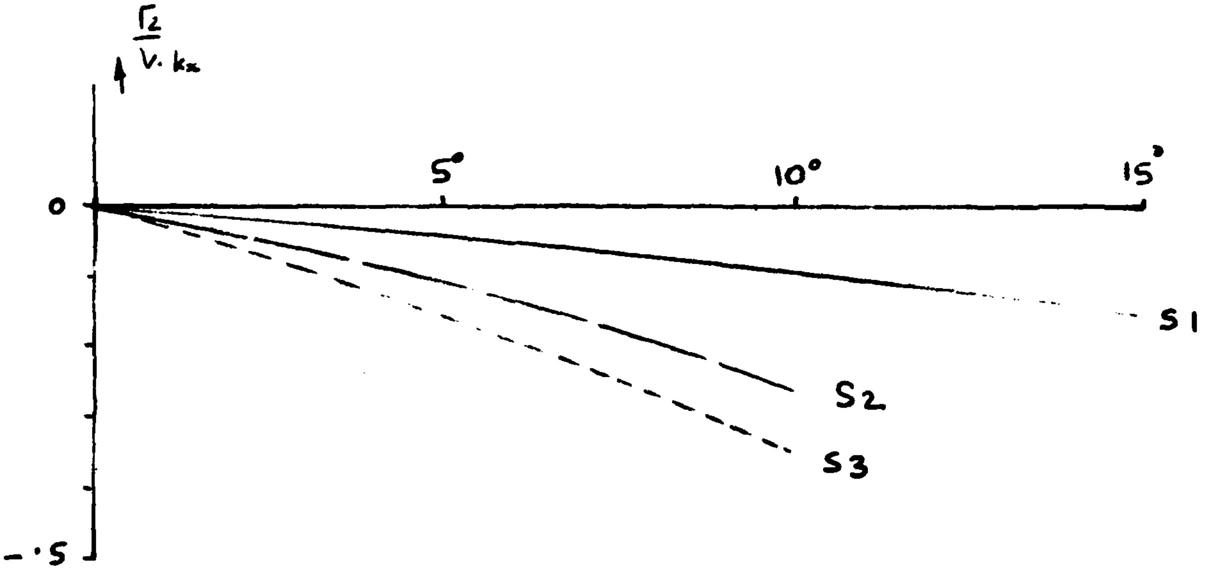

(b) Vortex Strength $\Gamma_2 \sim \alpha$

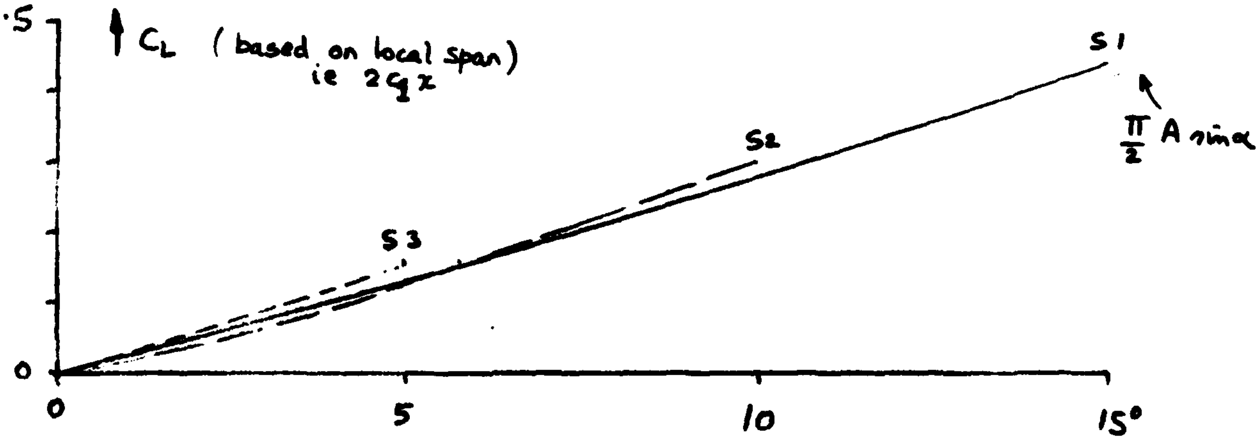

(c) Lift Coefficient $C_L \sim \alpha$

FIG. 26. CONT'D.

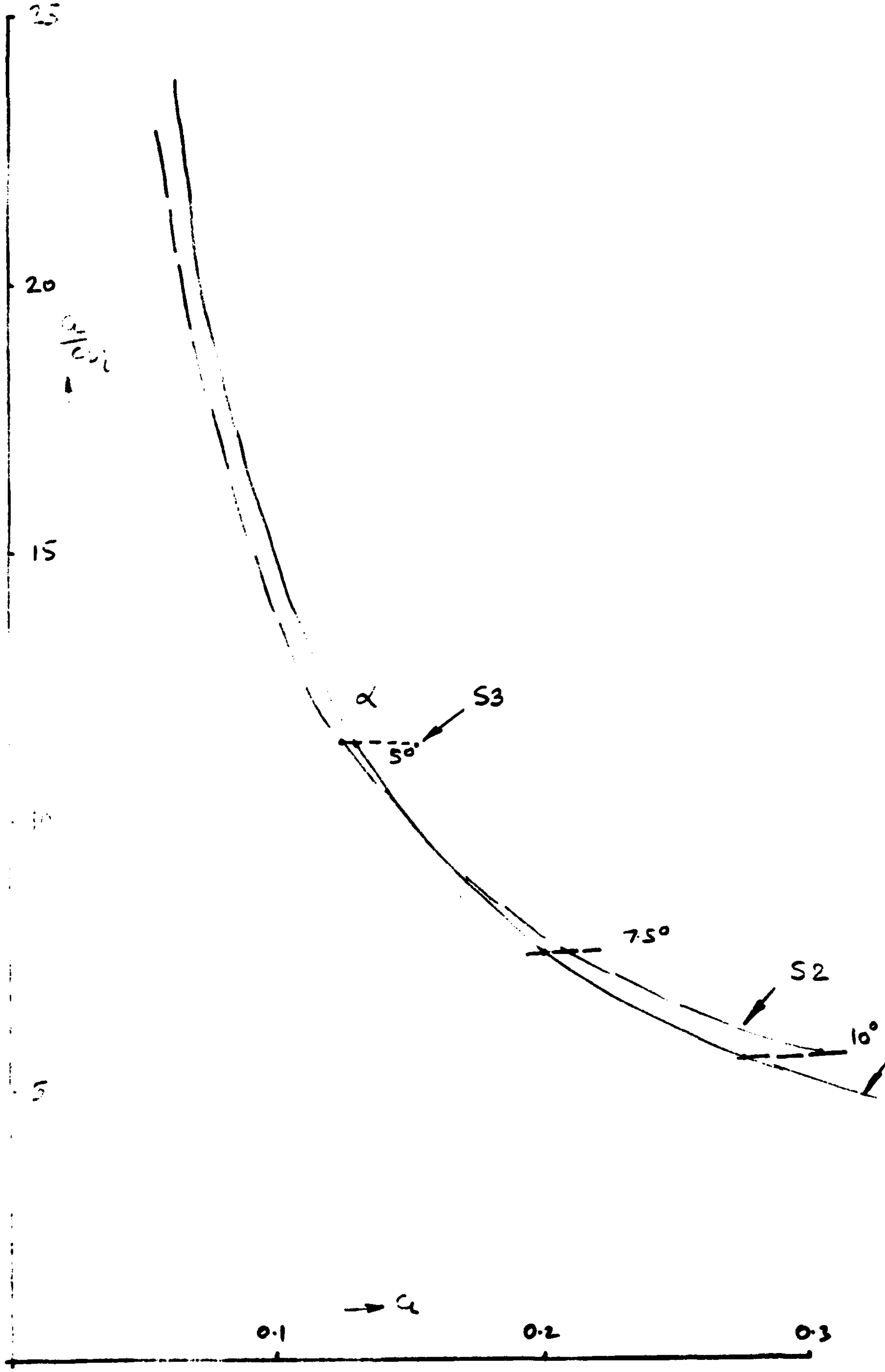

(d) $C_L/C_D \sim \alpha$

FIG 26. CONT'D

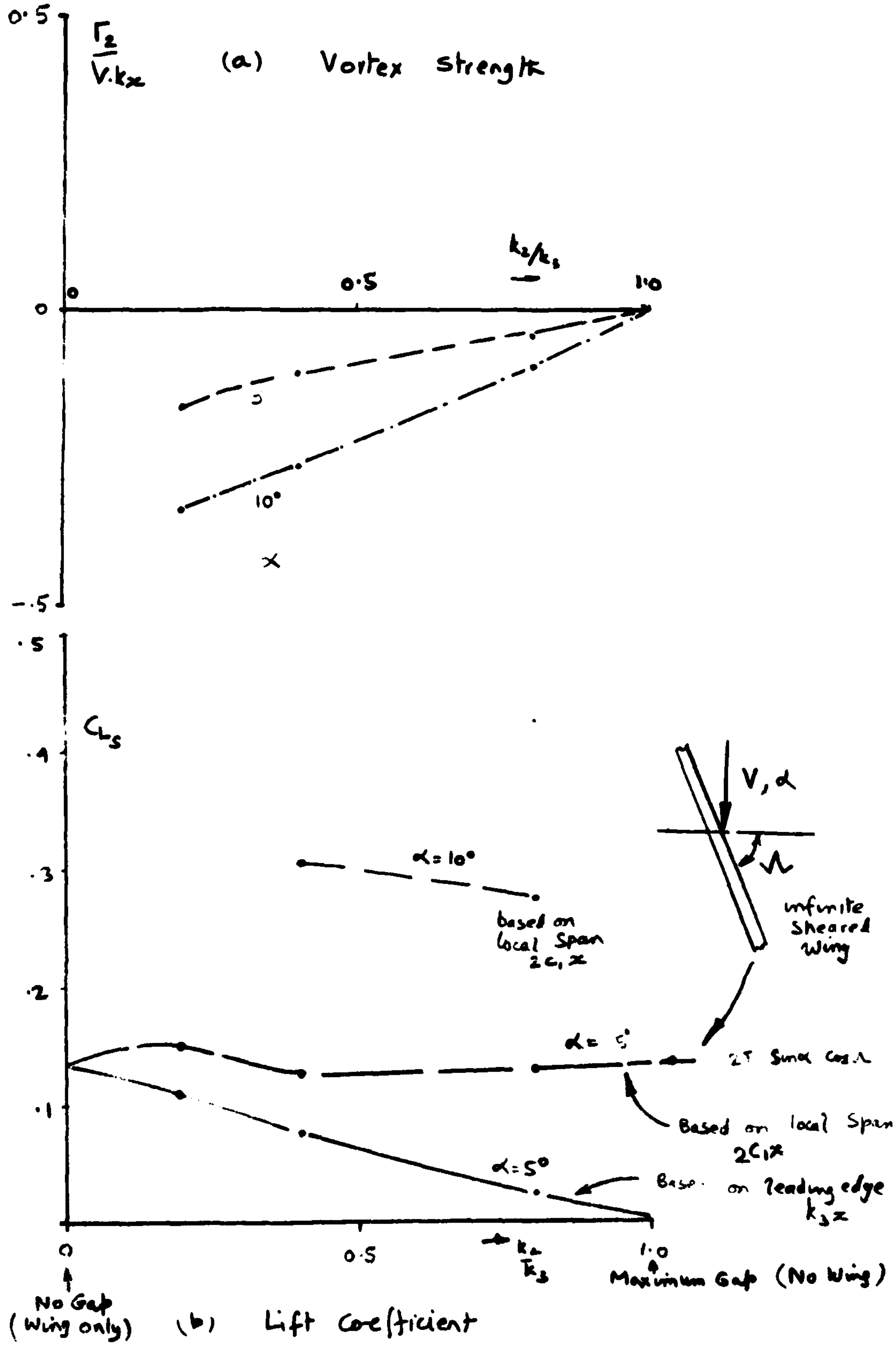

FIG. 27 SLATS ONLY CONFIGURATION S-A

Effect of Slat Span

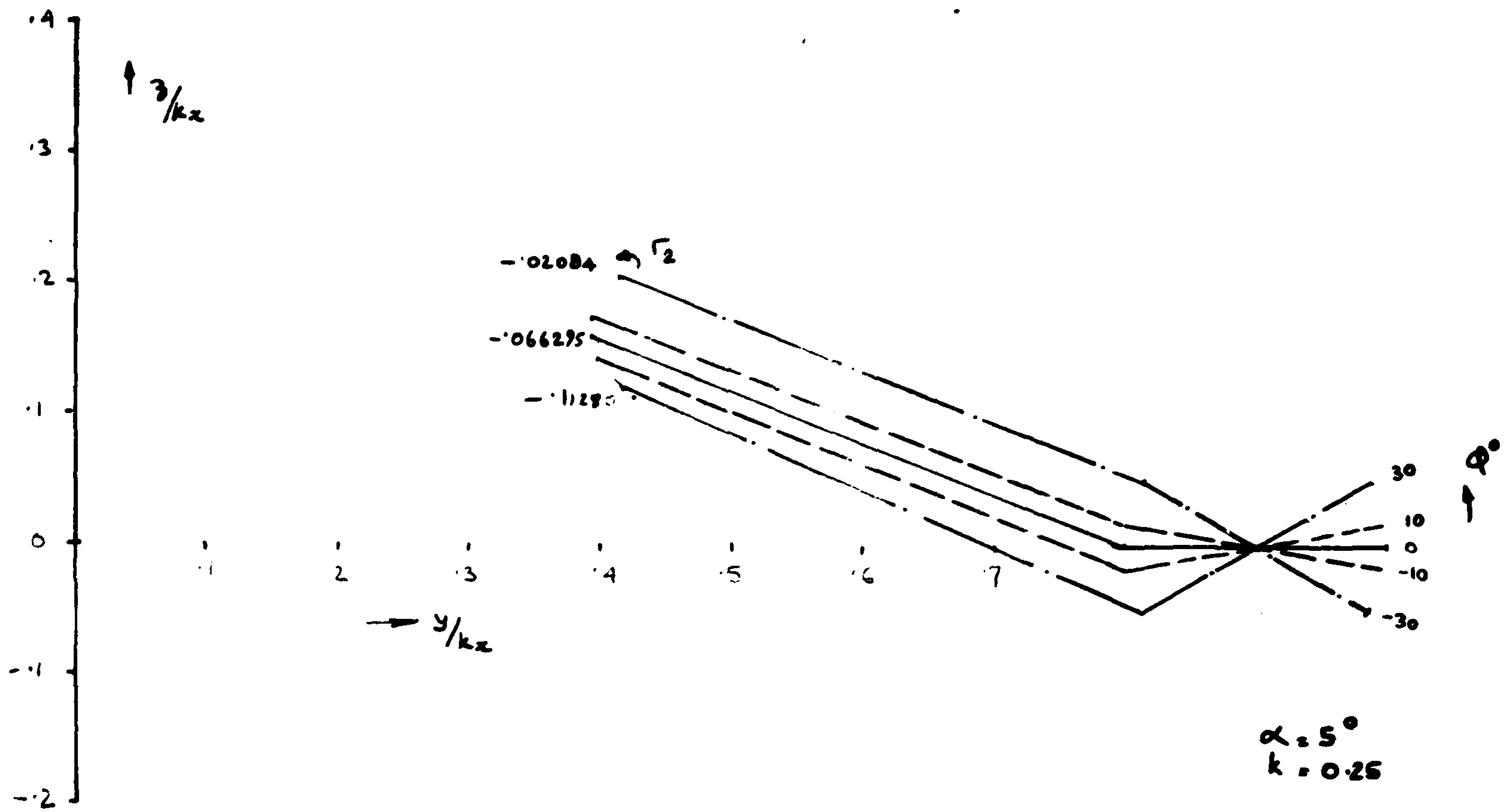

(a) VORTEX POSITION & STRENGTH

FIG. 28. SLATS ONLY CONFIGURATION S-A
GEOMETRY S-1
EFFECT OF SLAT INCLINATION φ

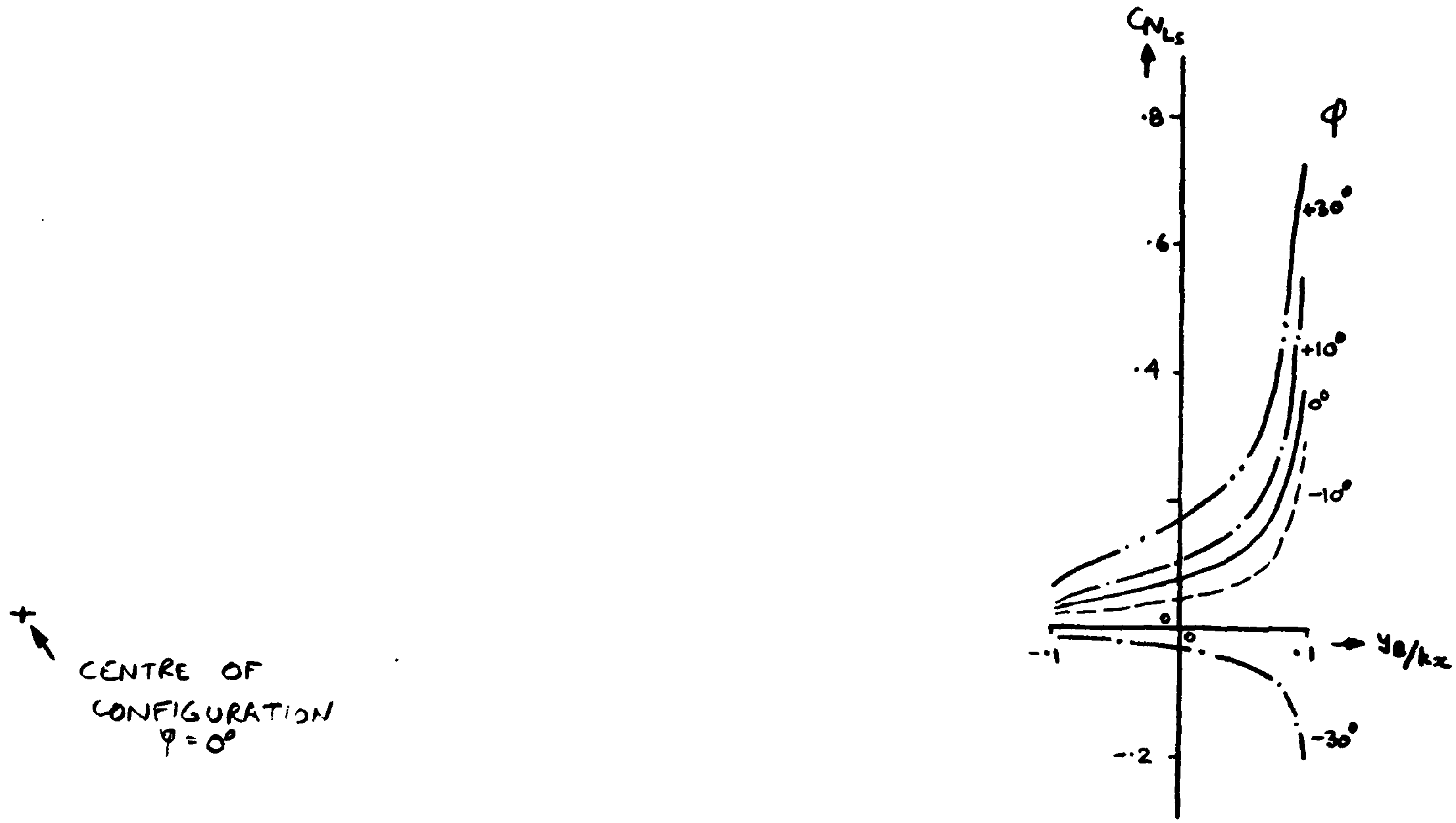

(b) Lift Distribution ~ y_B

FIG. 28 CONT'D

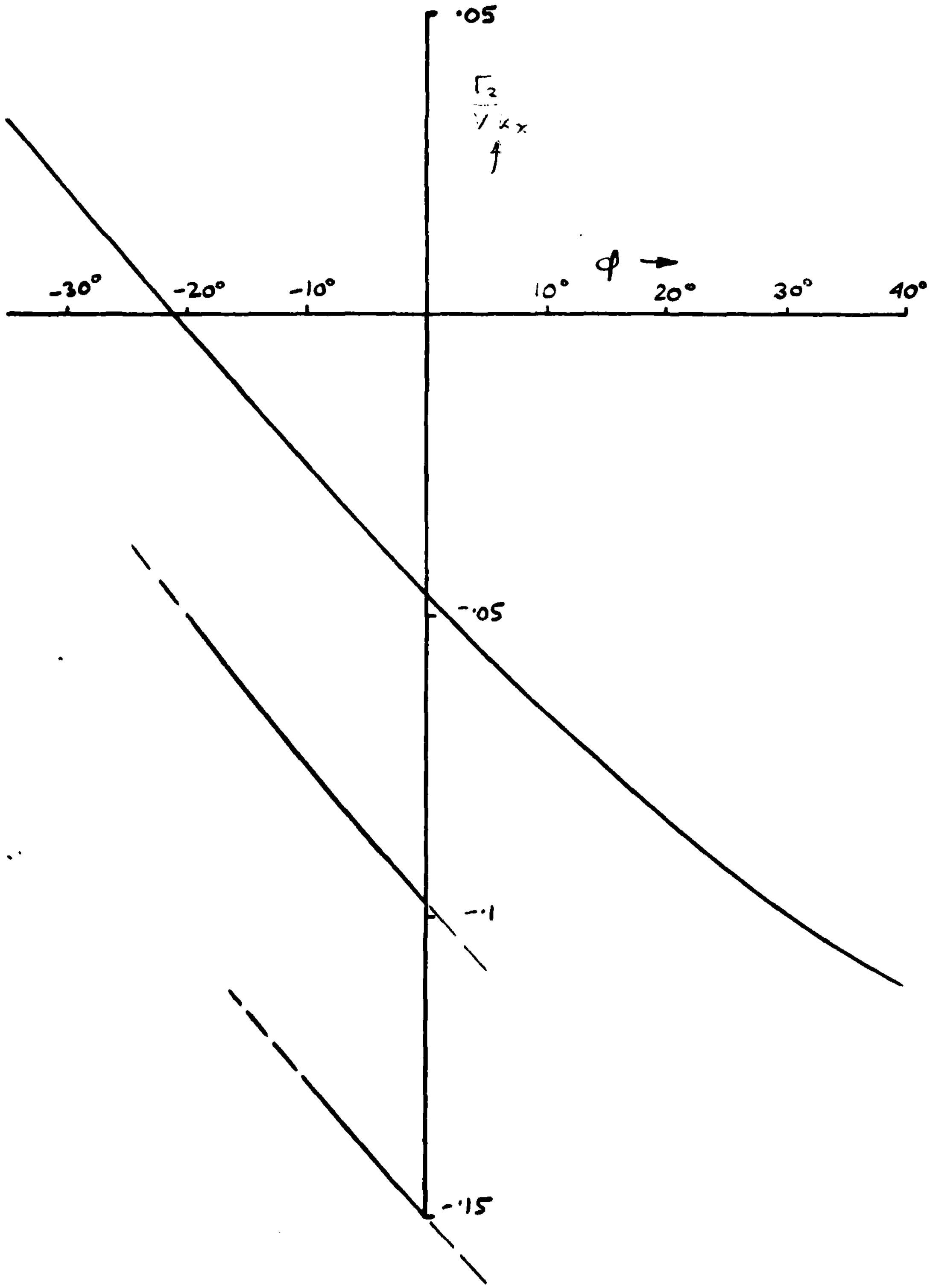

(c) Vortex strength ~ φ

FIG. 28 CONT'D

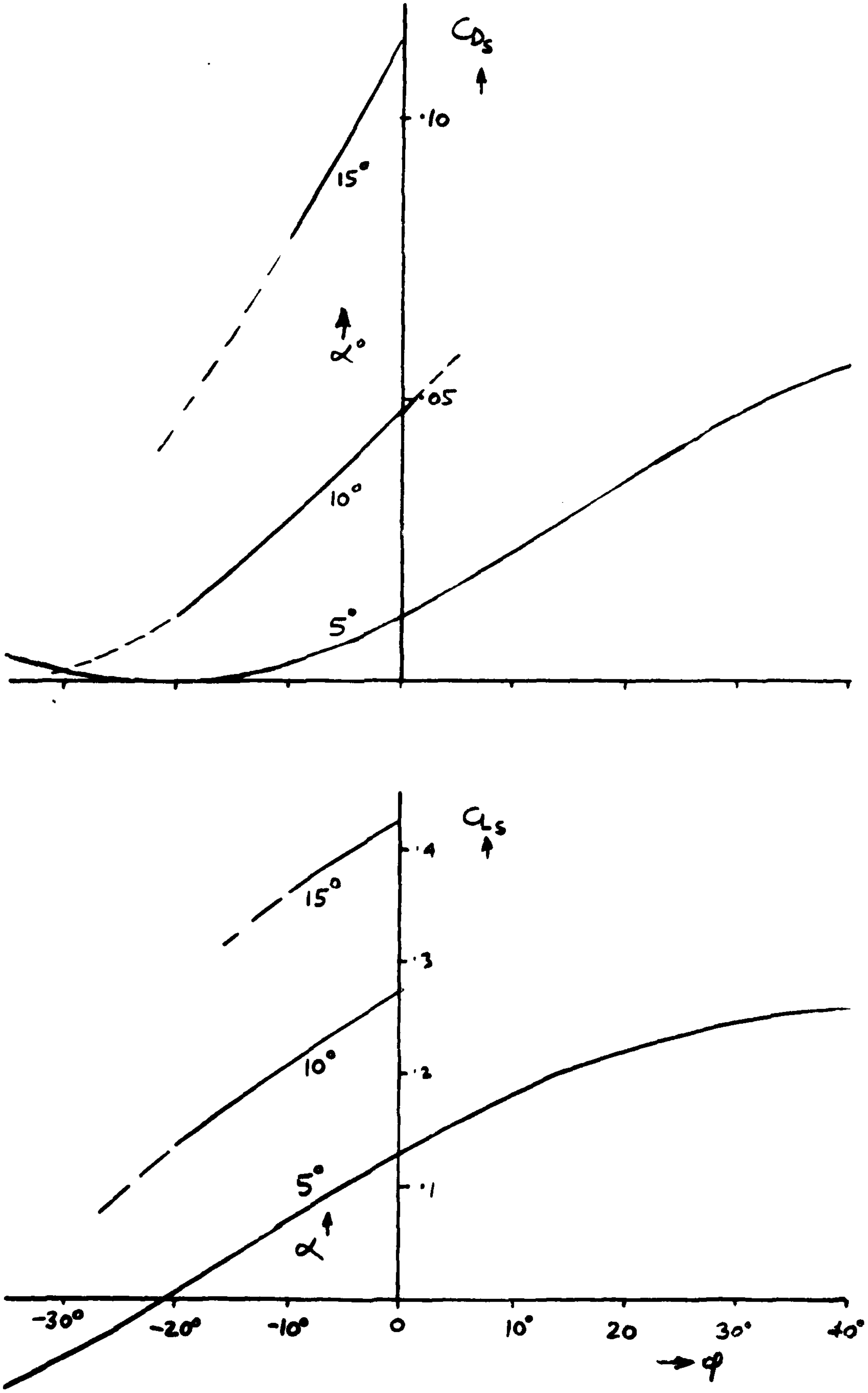

(d) C_{D_S} & $C_{L_S} \sim \varphi$

FIG. 28 CONT'D

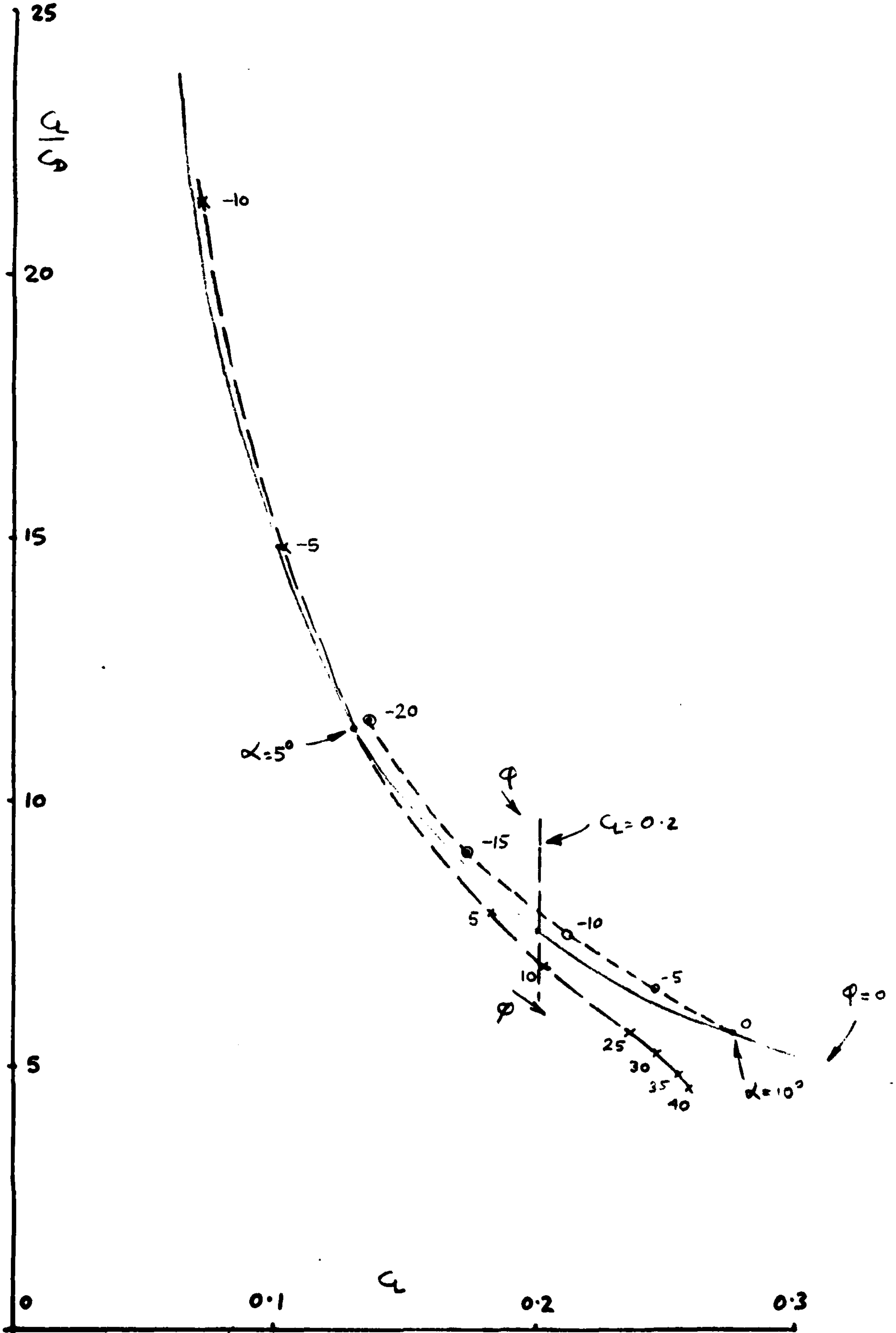

ie. $C_L/C_{D_i} \sim C_L$

FIG 28 CONT'D

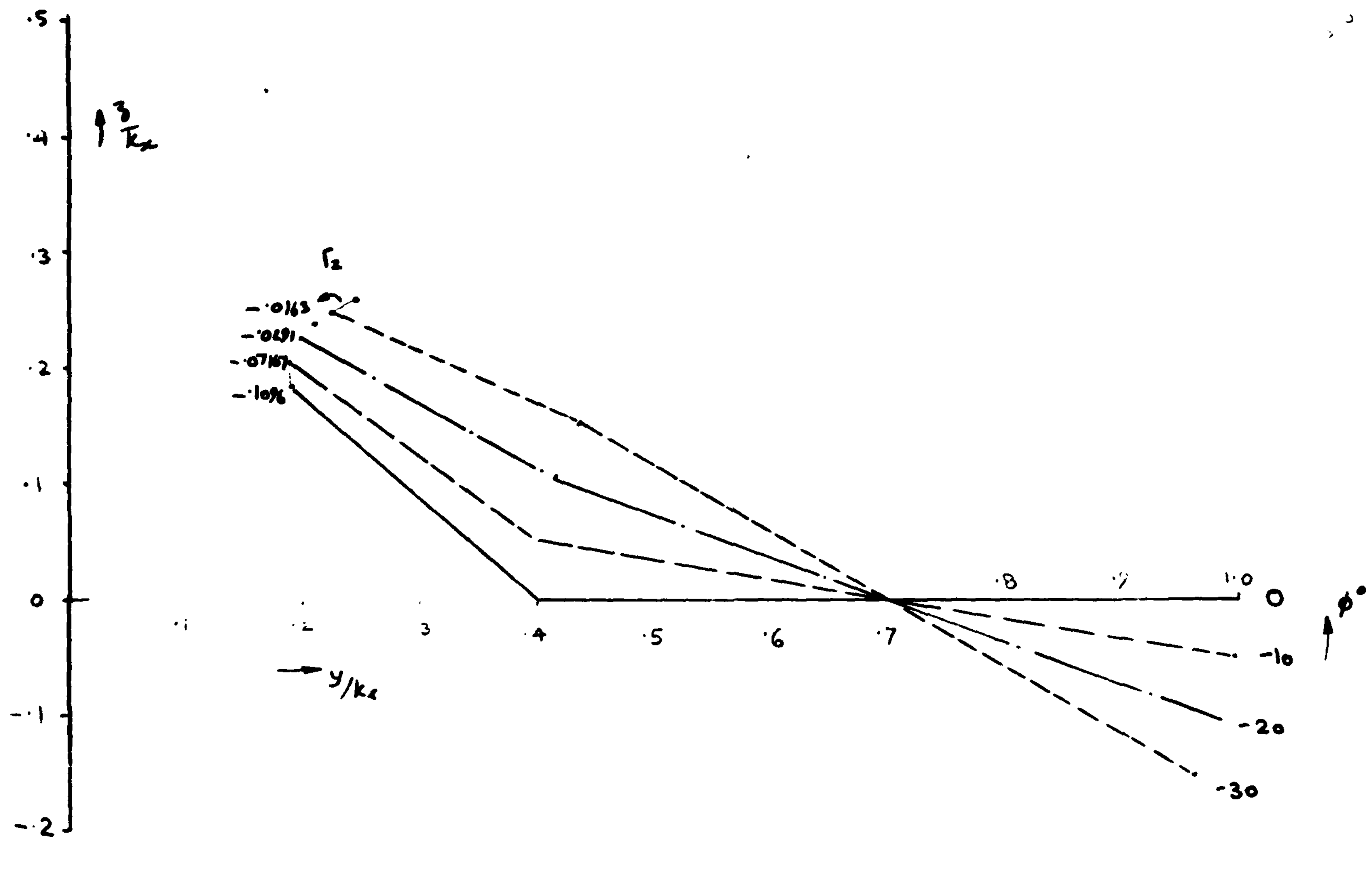

(a) VORTEX POSITION & STRENGTH

FIG. 29. SLATS ONLY CONFIGURATION S·A
GEOMETRY S·2
EFFECT OF SLAT INCLINATION ϕ

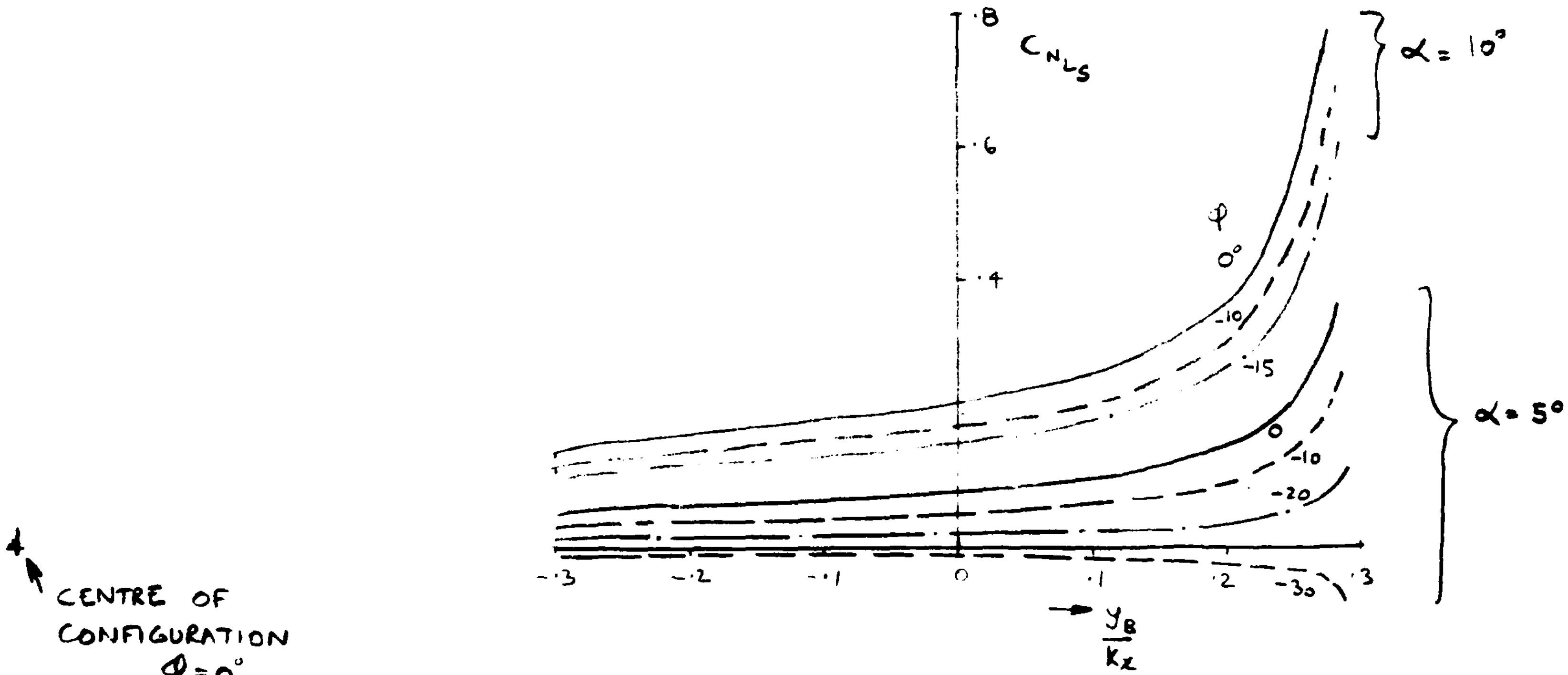

(b) Lift Distribution ~ y_B

FIG. 29 CONT'D

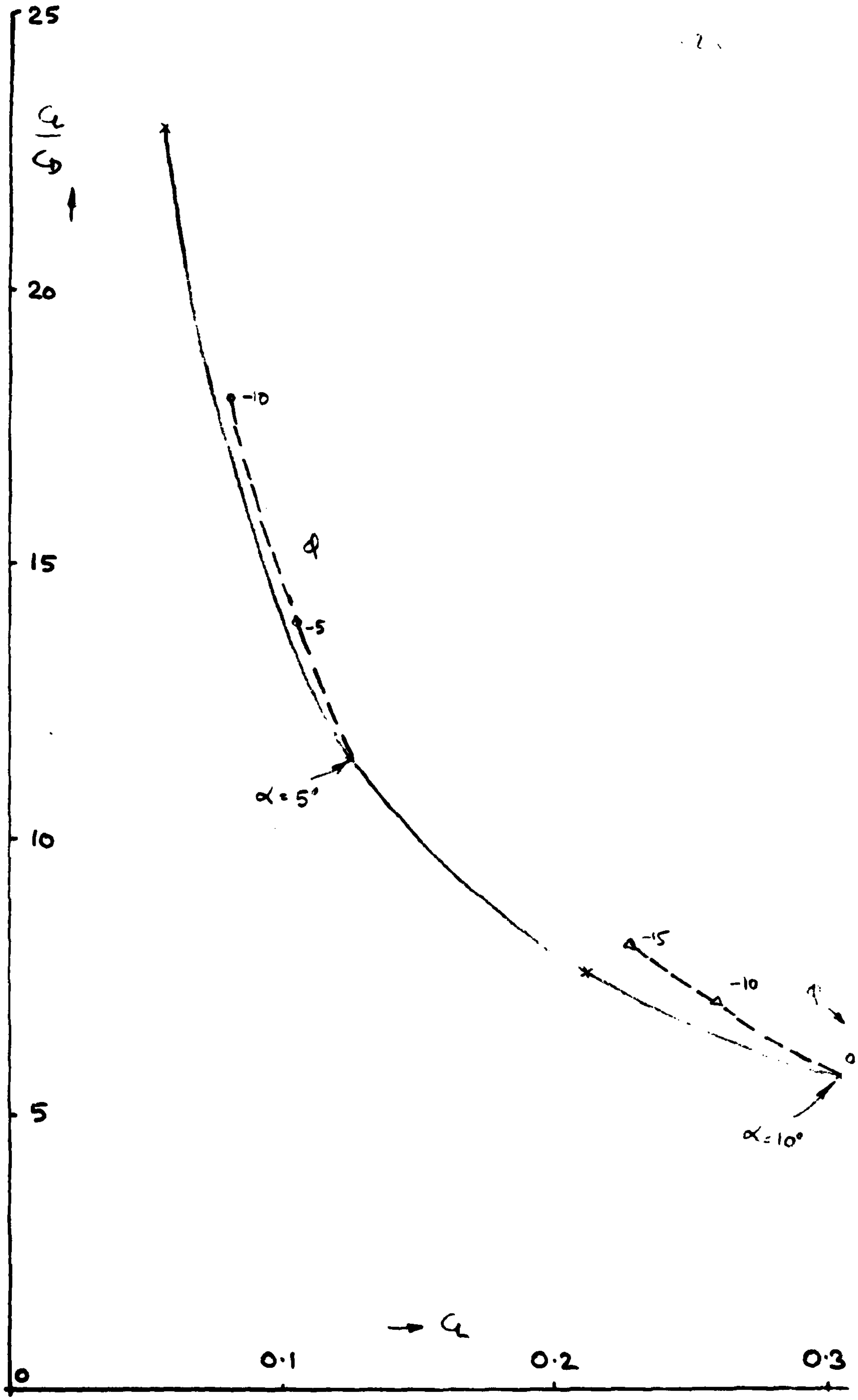

(C) $C_L / C_D \sim C_L$

FIG. 29. CONT'D

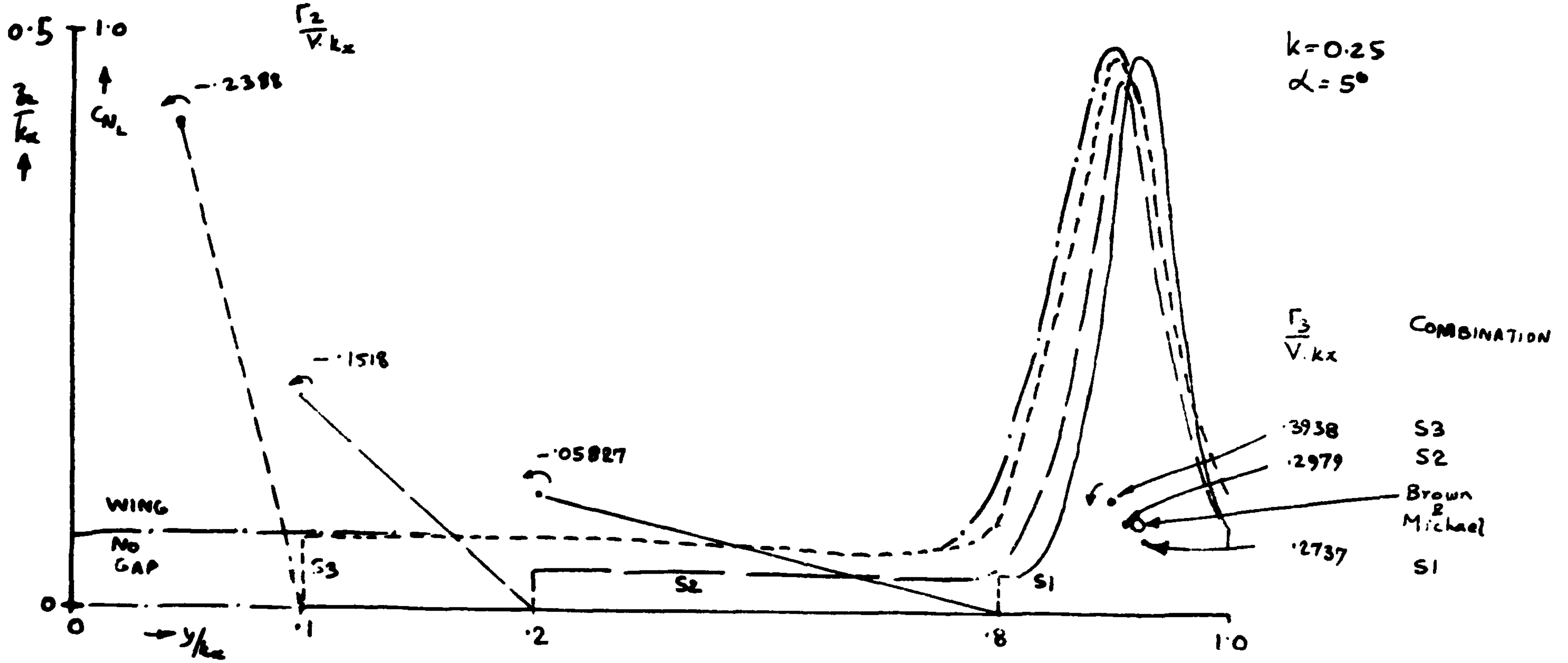

EFFECT OF SLAT SPAN

FIG. 30. SLATS ONLY CONFIGURATION S-S

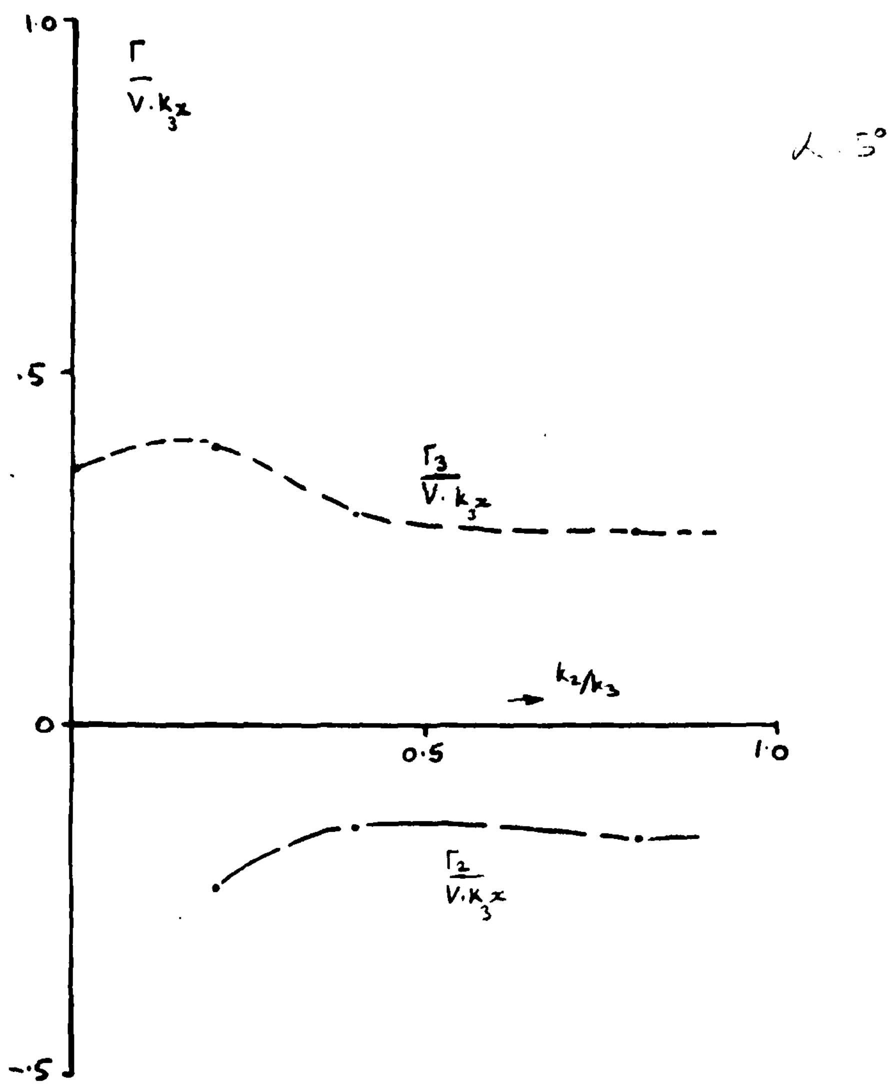

Vortex Strengths ~ Sla: Span

FIG. 31 SLATS ONLY CONFIGURATION S-S

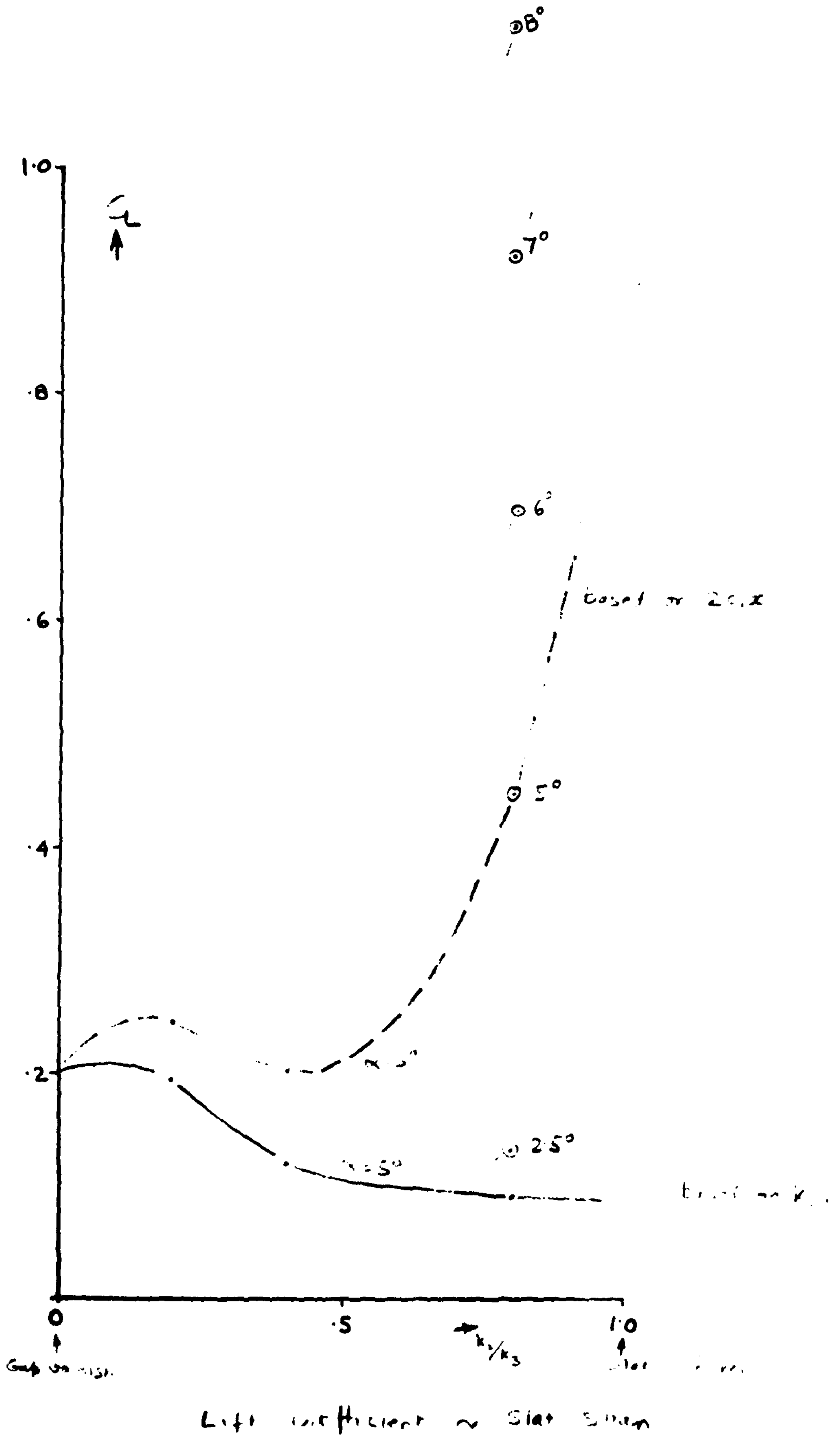

FIG. 32.

FIG. 33. SLATS ONLY CONFIGURATION S-S

GEOMETRY S-1

(a) Effect of α

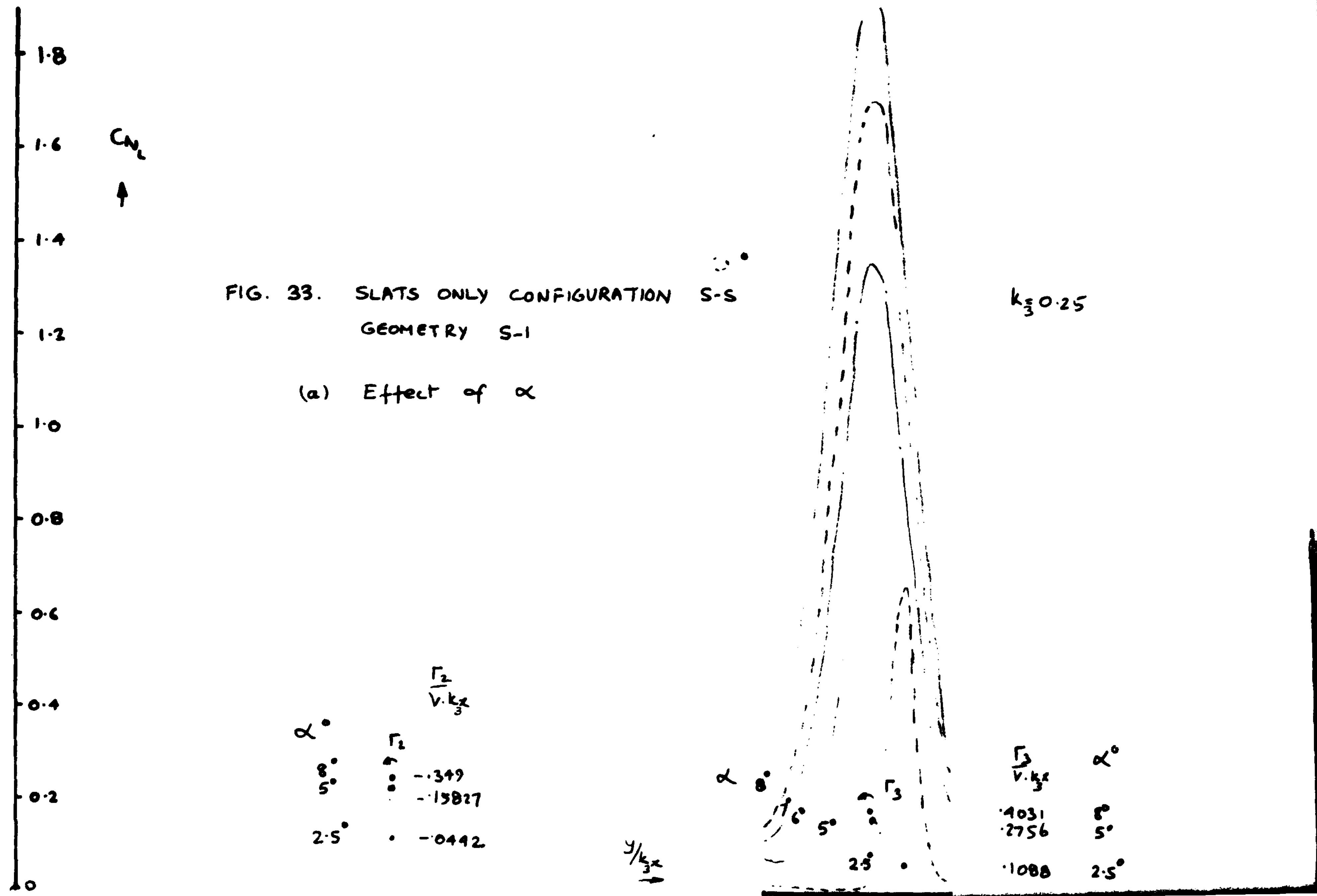

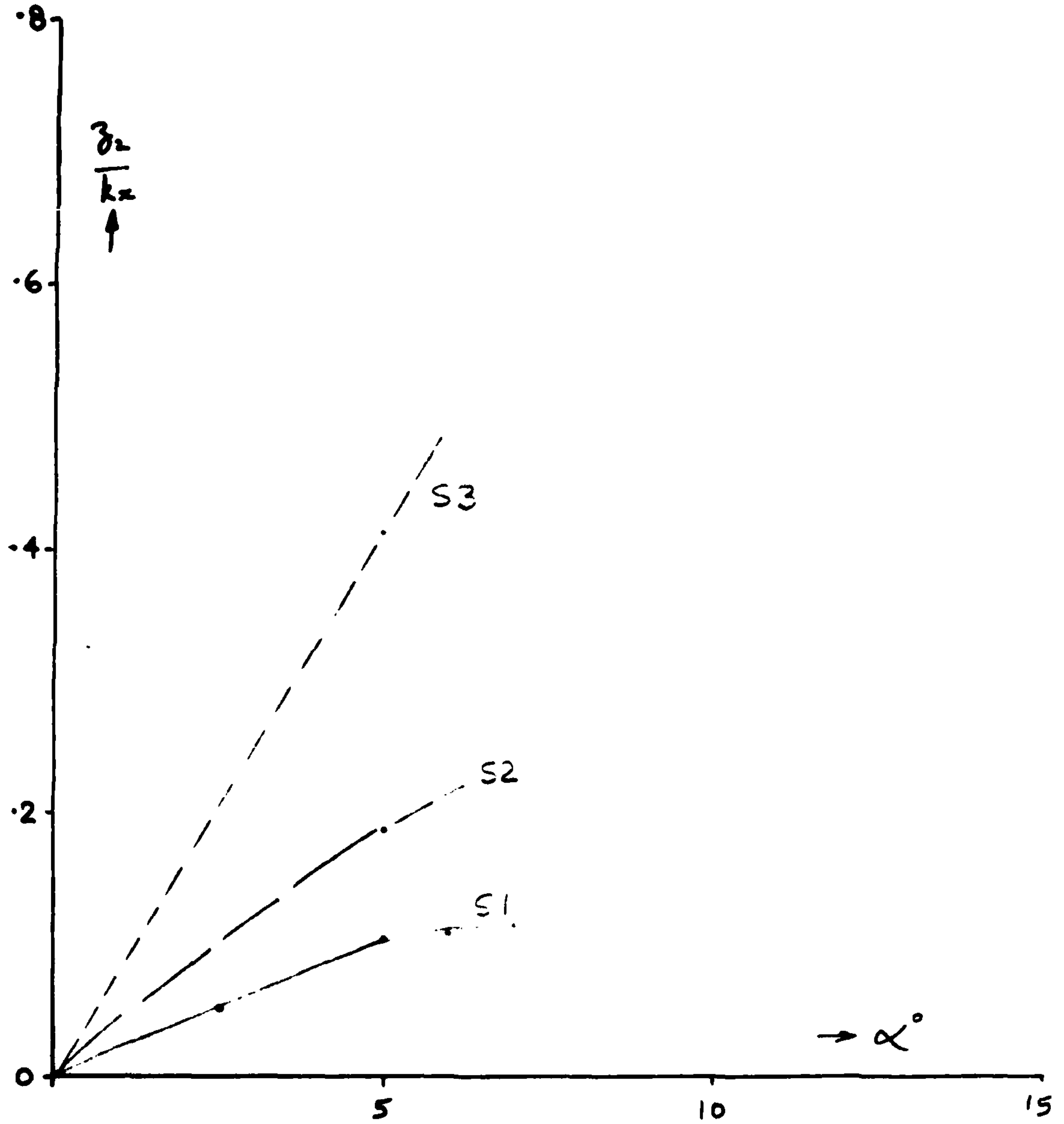

(b) $\gamma_2 \sim \alpha$

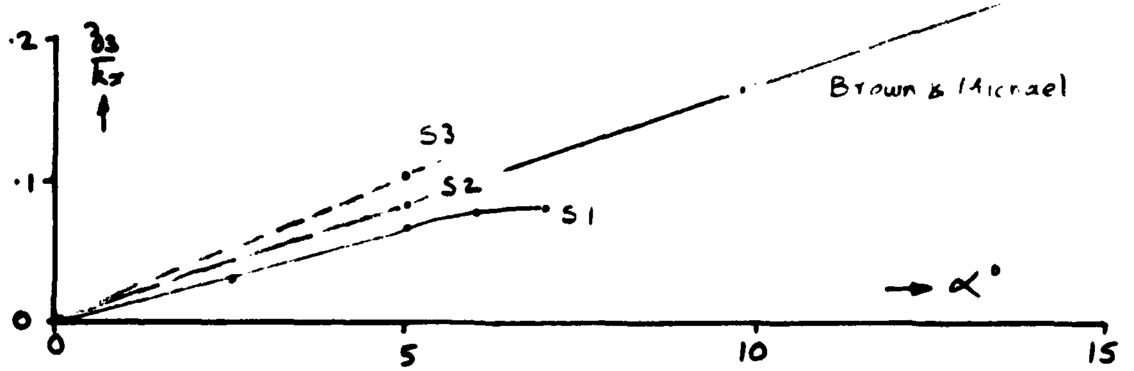

(c) $\gamma_3 \sim \alpha$

FIG 33 CONT'D

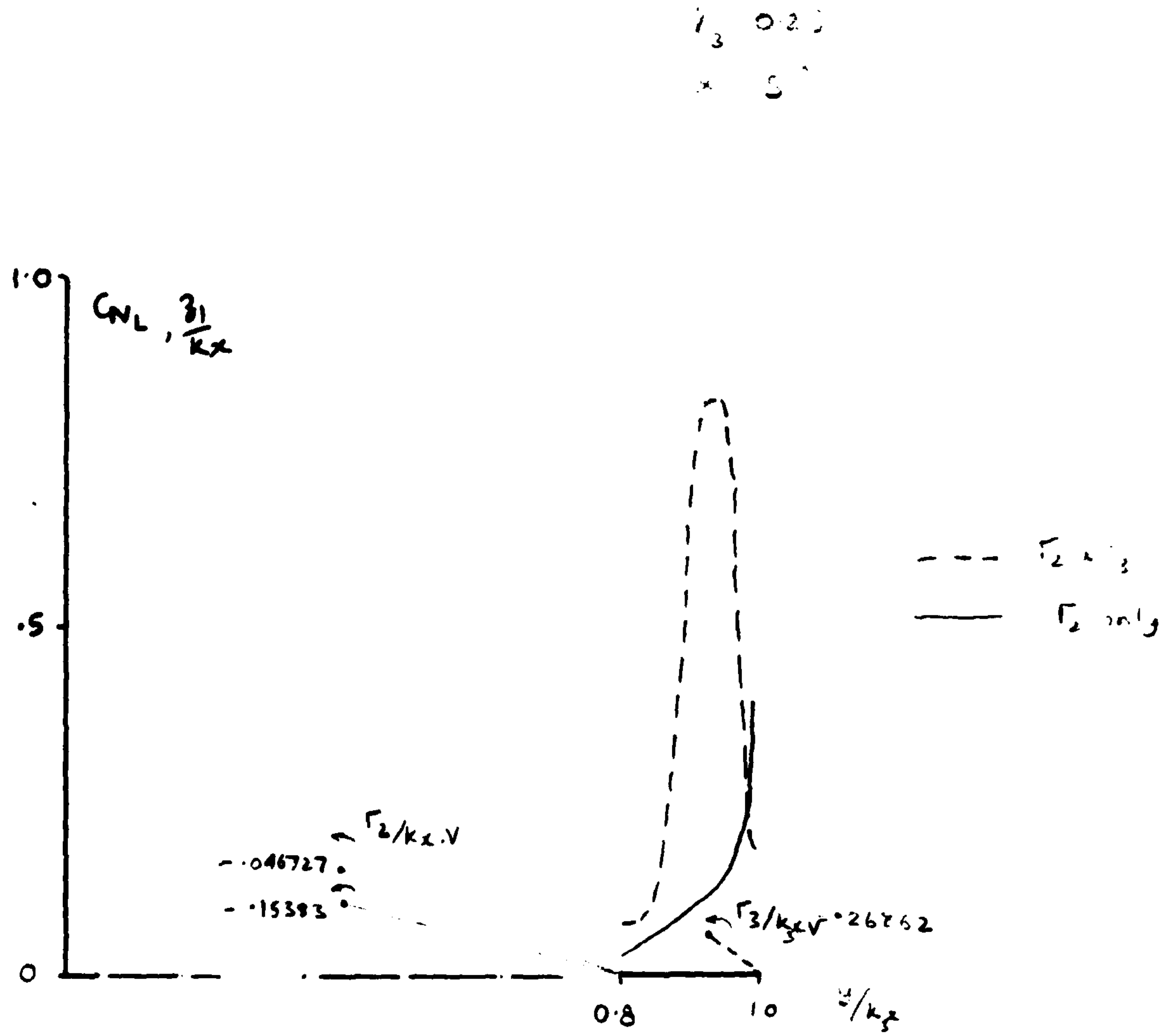

FIG. 34. SLATS ONLY CONFIGURATIONS
COMPARISON OF S-A & S-S
GEOMETRY S-1
(Effect of including Γ_3)

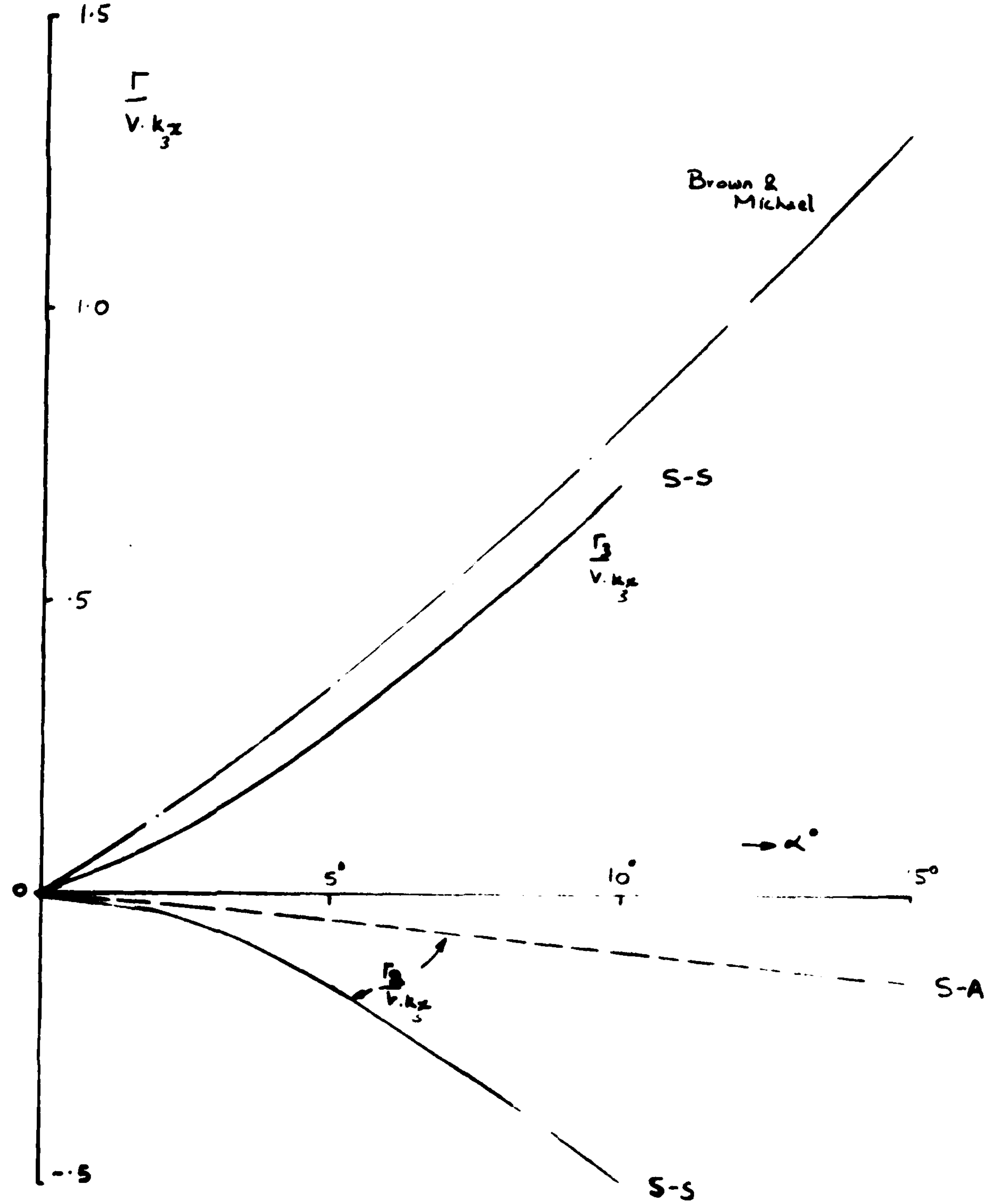

FIG. 35. SLATS ONLY CONFIGURATIONS
COMPARISON OF S-A & S-S
GEOMETRY S-1
Vortex strength ∼ α

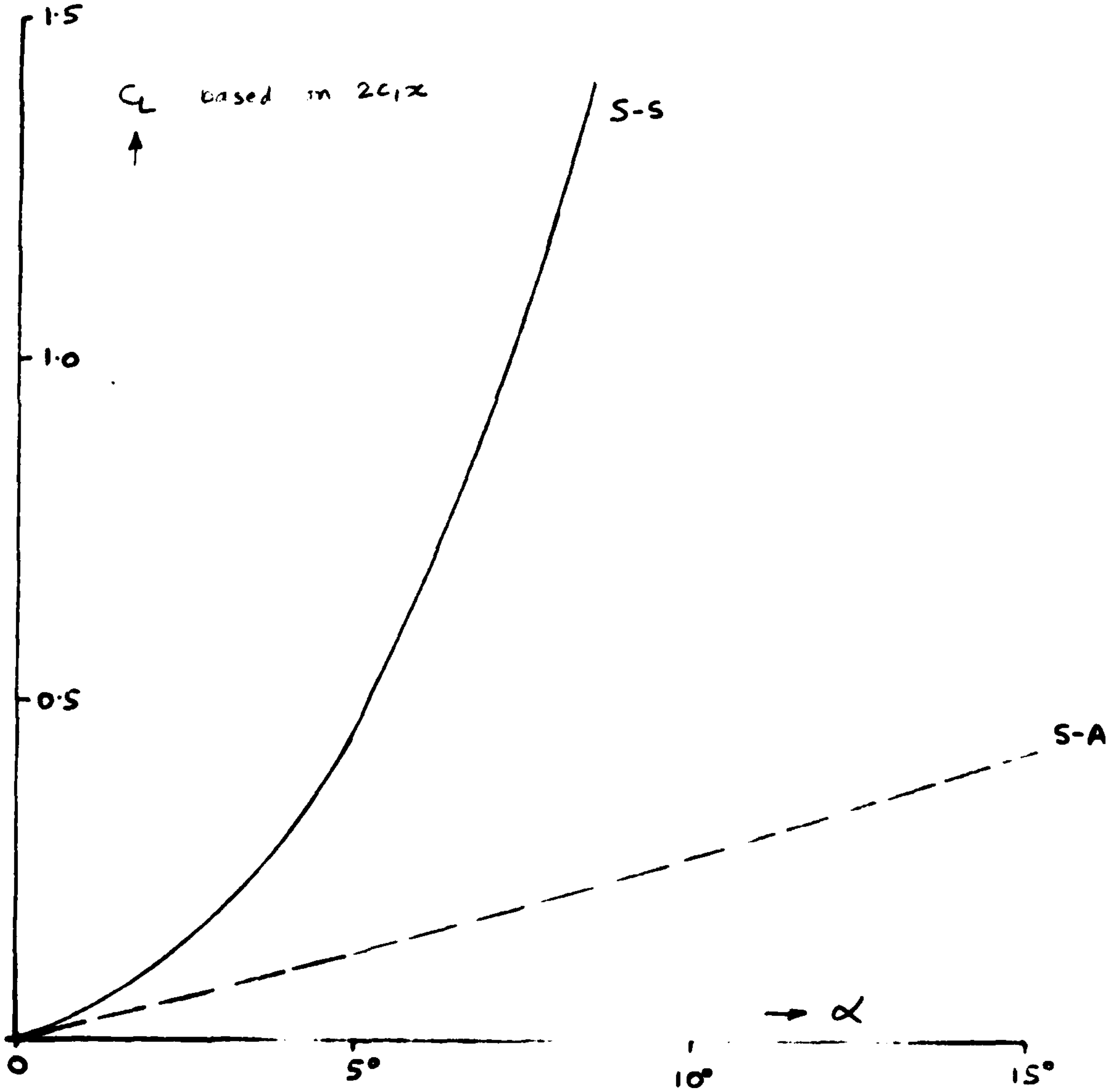

FIG. 36. SLATS ONLY CONFIGURATIONS
COMPARISON OF S-A & S-S
GEOMETRY S-1
Lift Coefficient ~ α

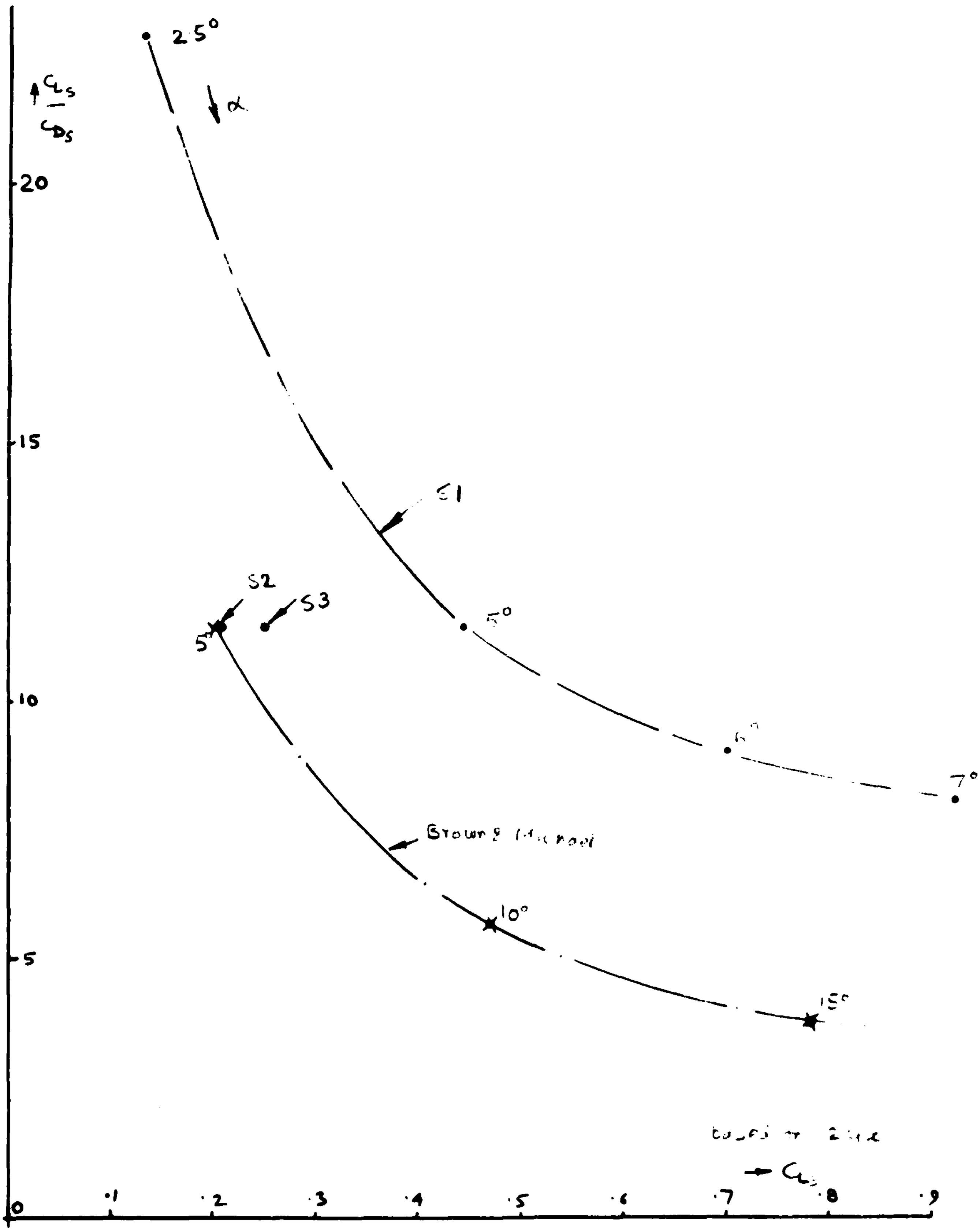

FIG. 37 SLATS ONLY CONFIGURATION S-S

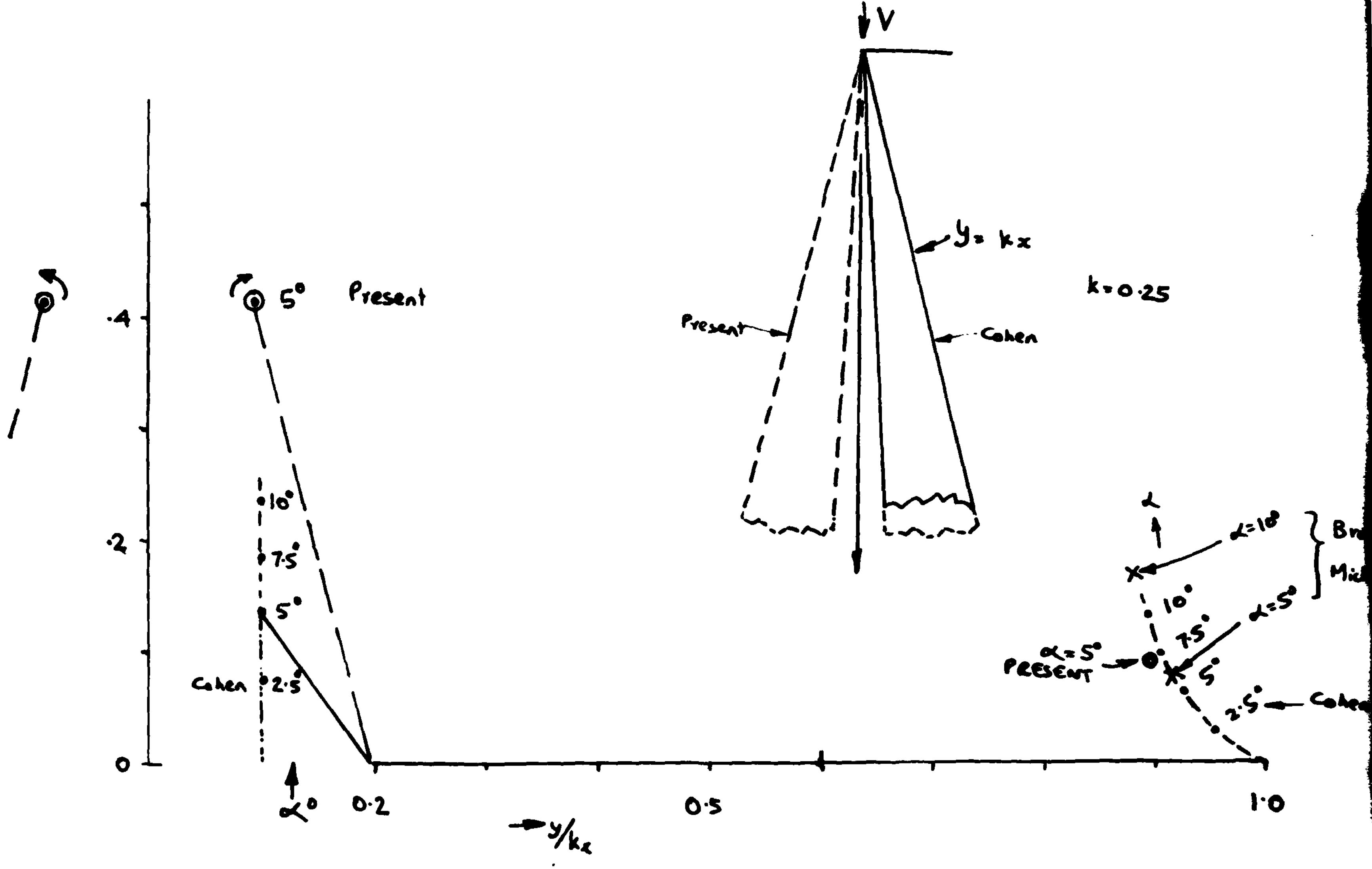

FIG. 38. COMPARISON TWIN SLATS WITH ONE SLAT (COHEN)

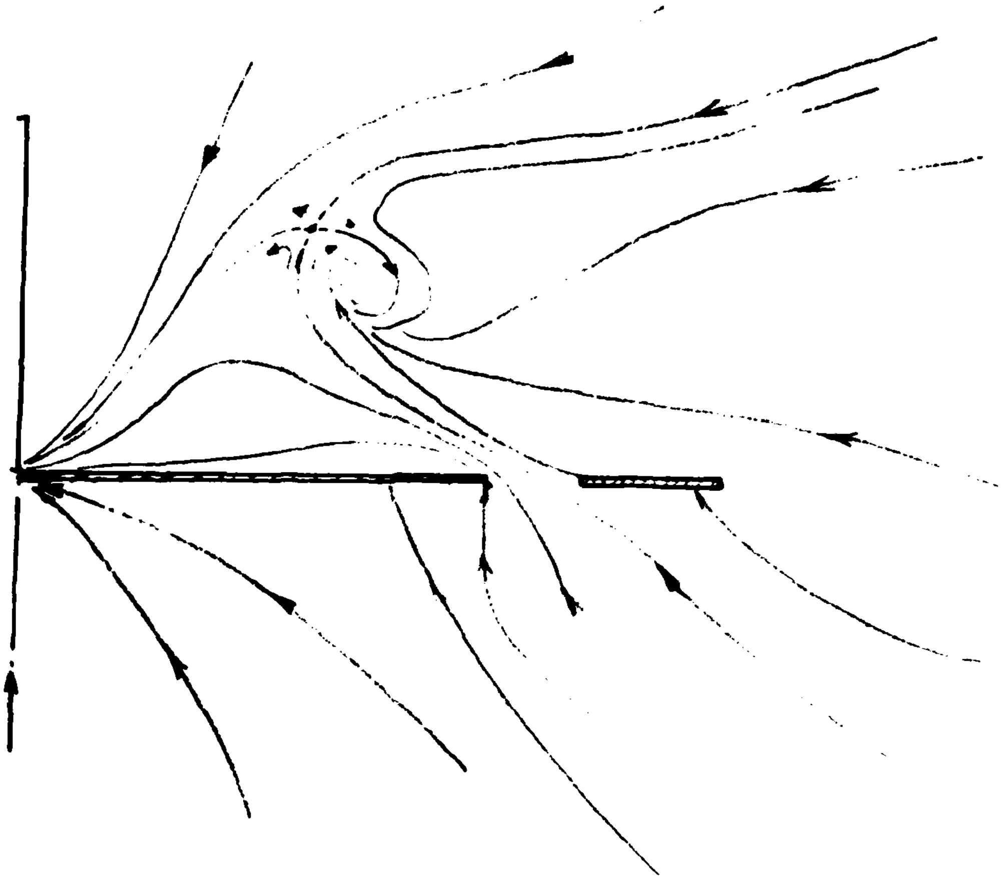

FIG 39 WING-SLAT CONFIGURATION A-S-A

CONICAL STREAMLINES

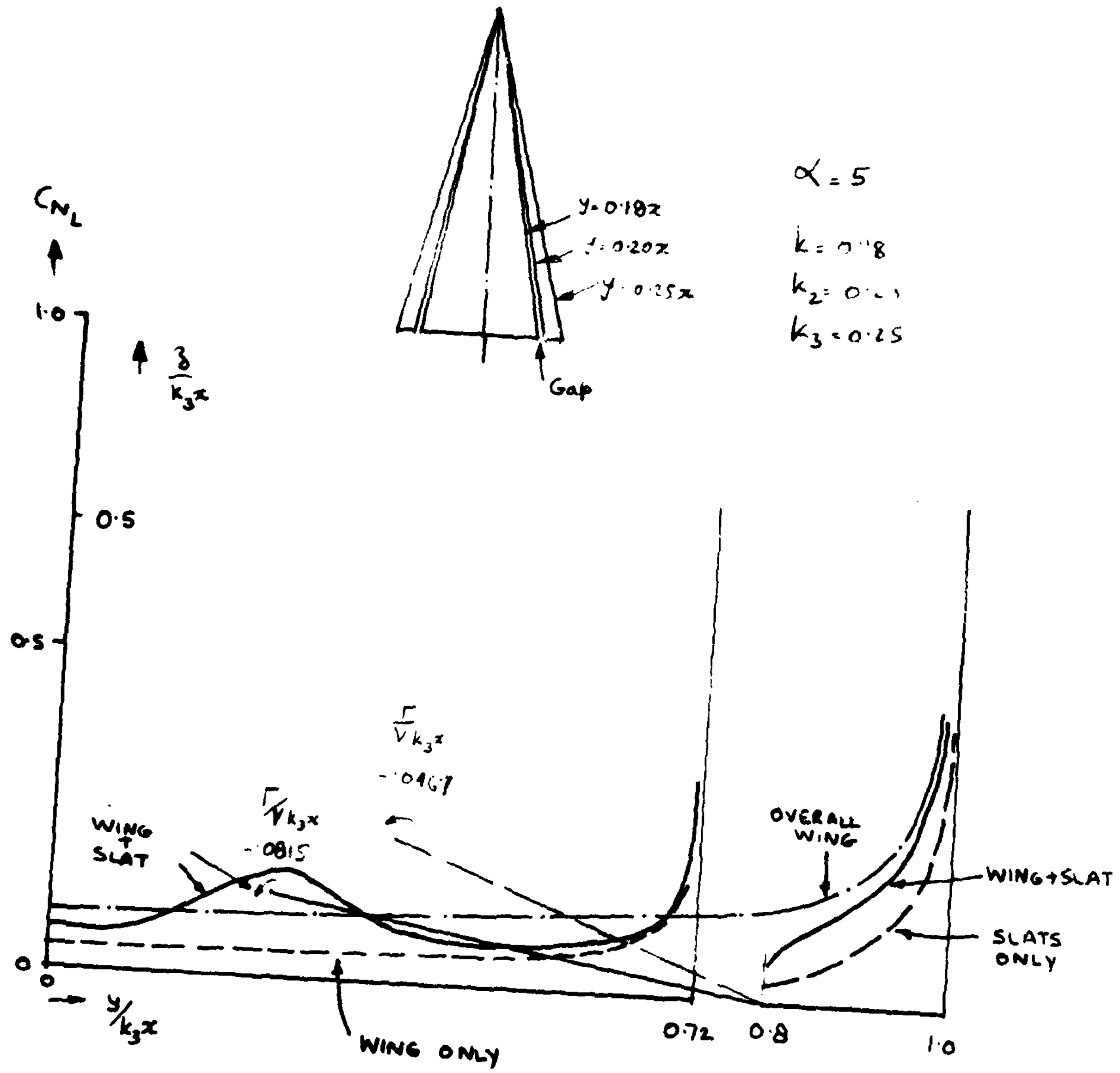

FIG. 40. WING - SLAT CONFIGURATION A-S-A

Effect of a Conical gap away from Centre-line of a Delta Wing

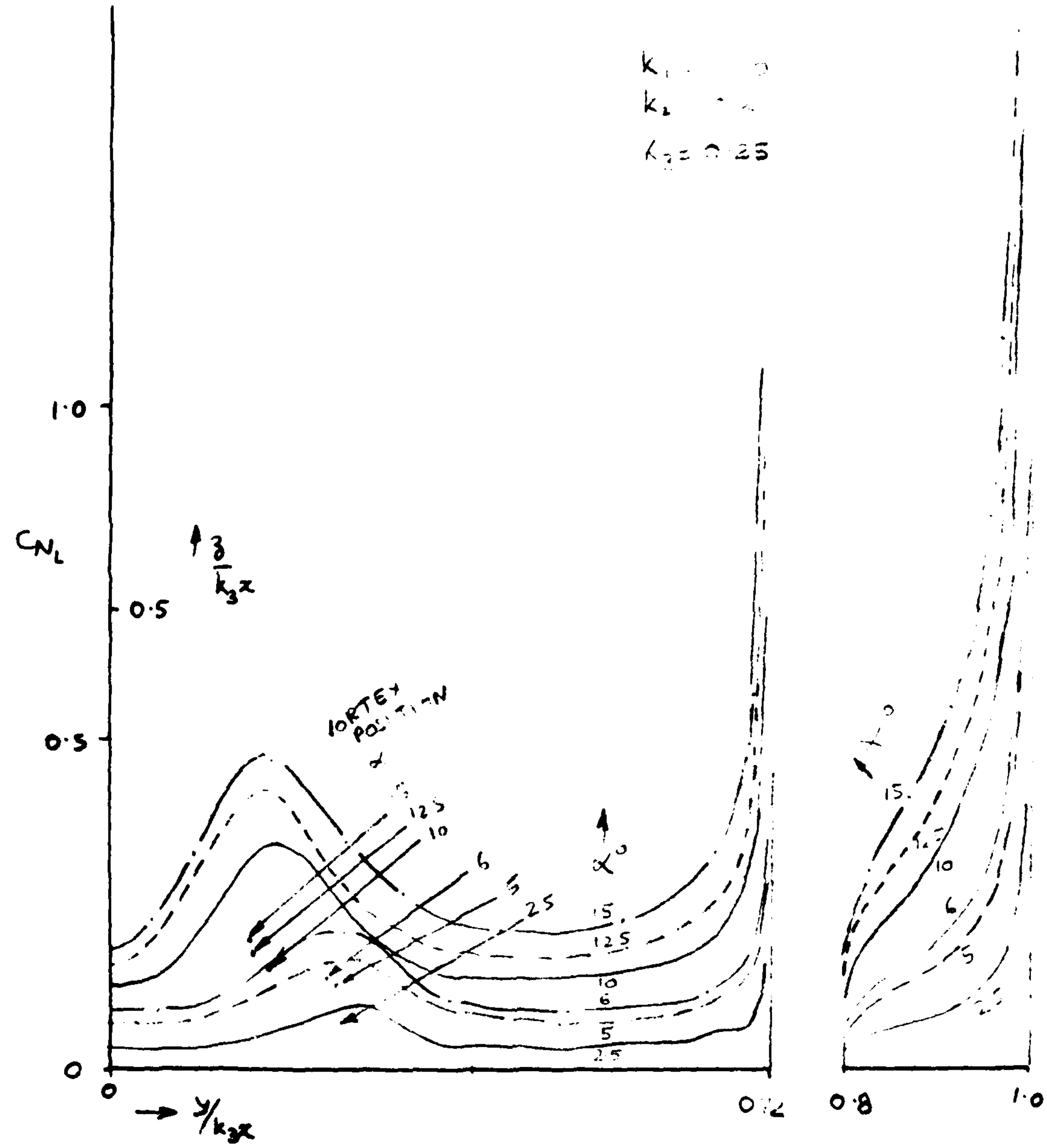

FIG. 41. WING-SLAT CONFIGURATION A-S-A

Effect of α

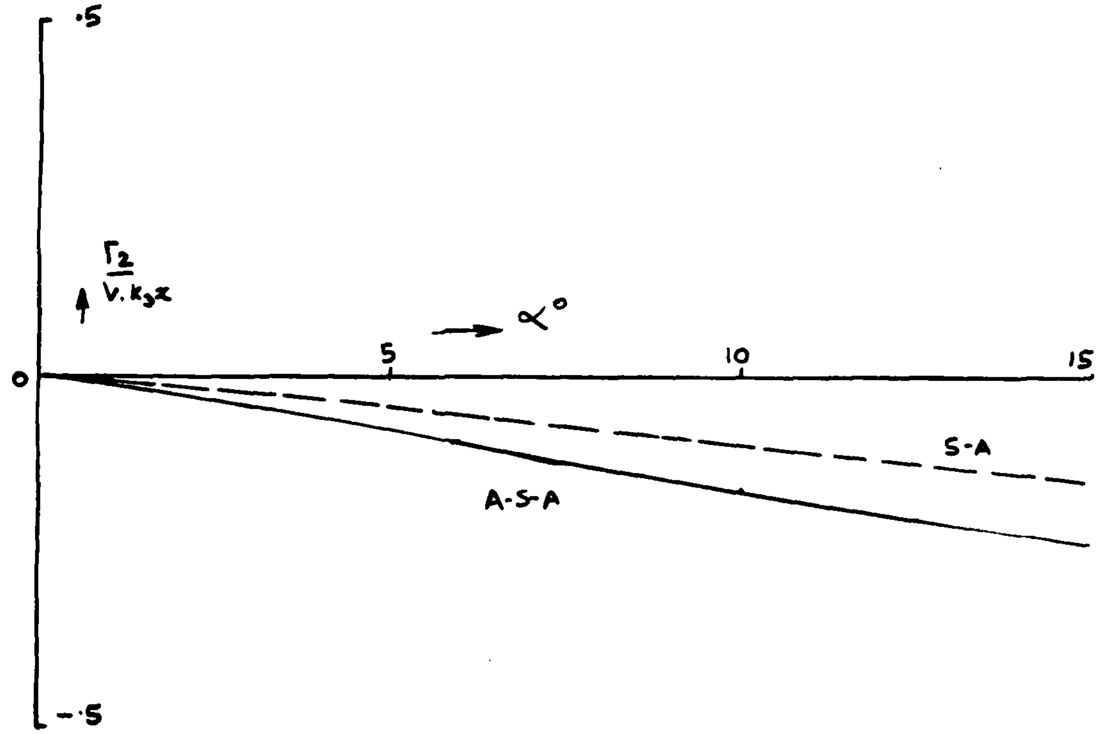

FIG. 42. WING-SLAT CONFIGURATION A-S-A
& SLAT CONFIGURATION S A
VORTEX STRENGTH ~ α

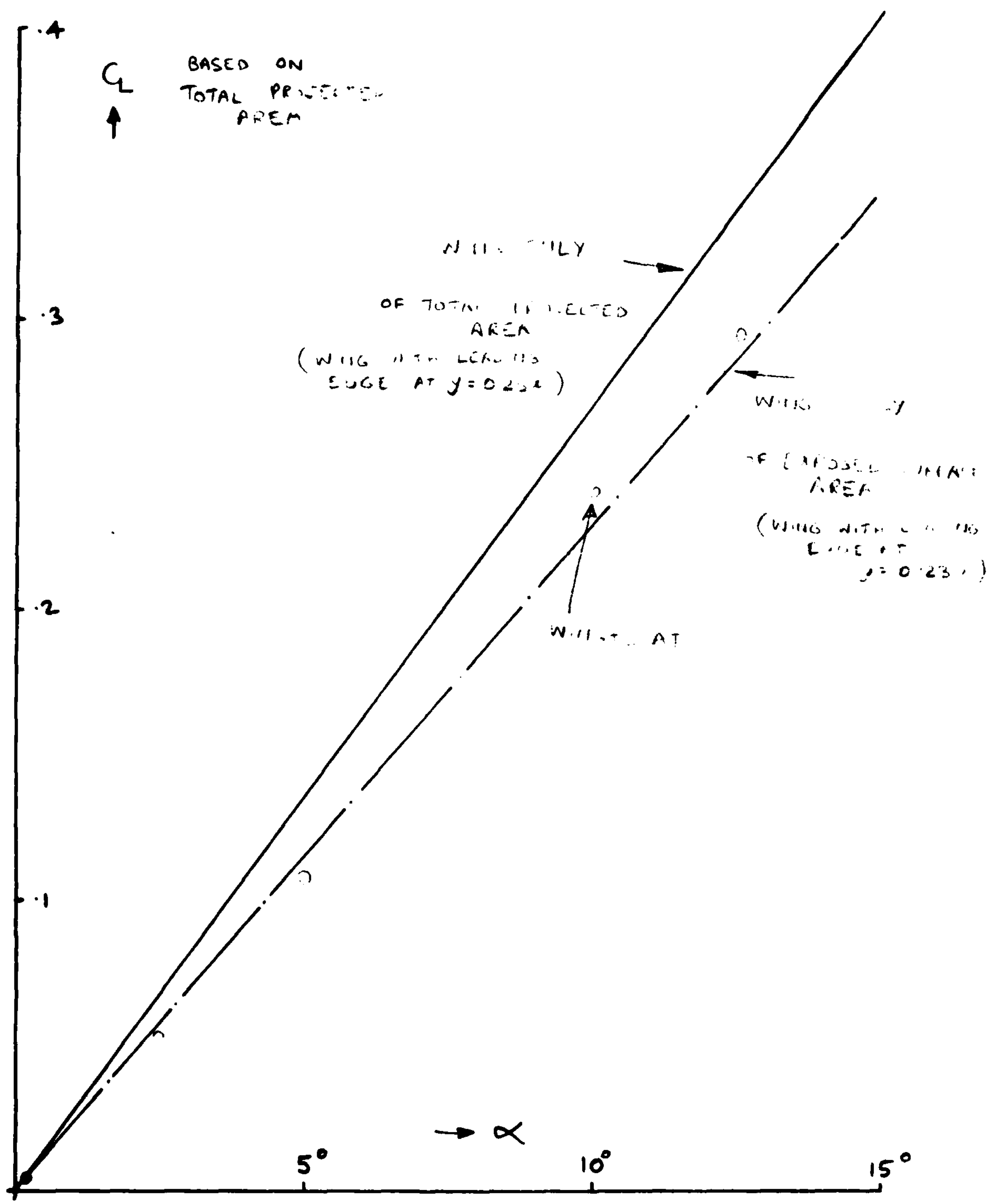

FIG. 43. WING-SLAT CONFIGURATION A-S-A

$C_L \sim \alpha$

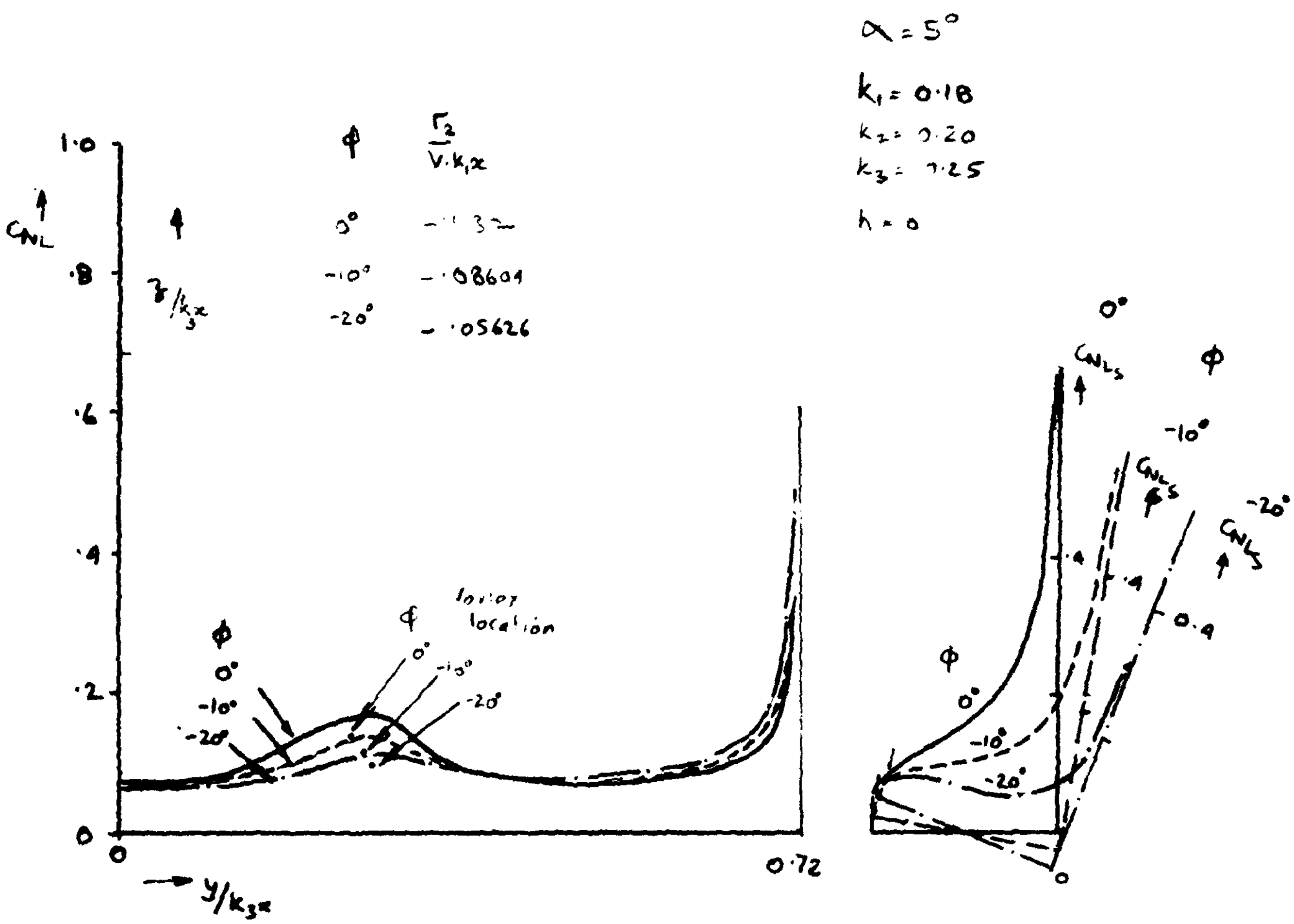

WING-SLAT CONFIGURATION A-S-A

FIG. 44. EFFECT OF SLAT DEFLECTION φ

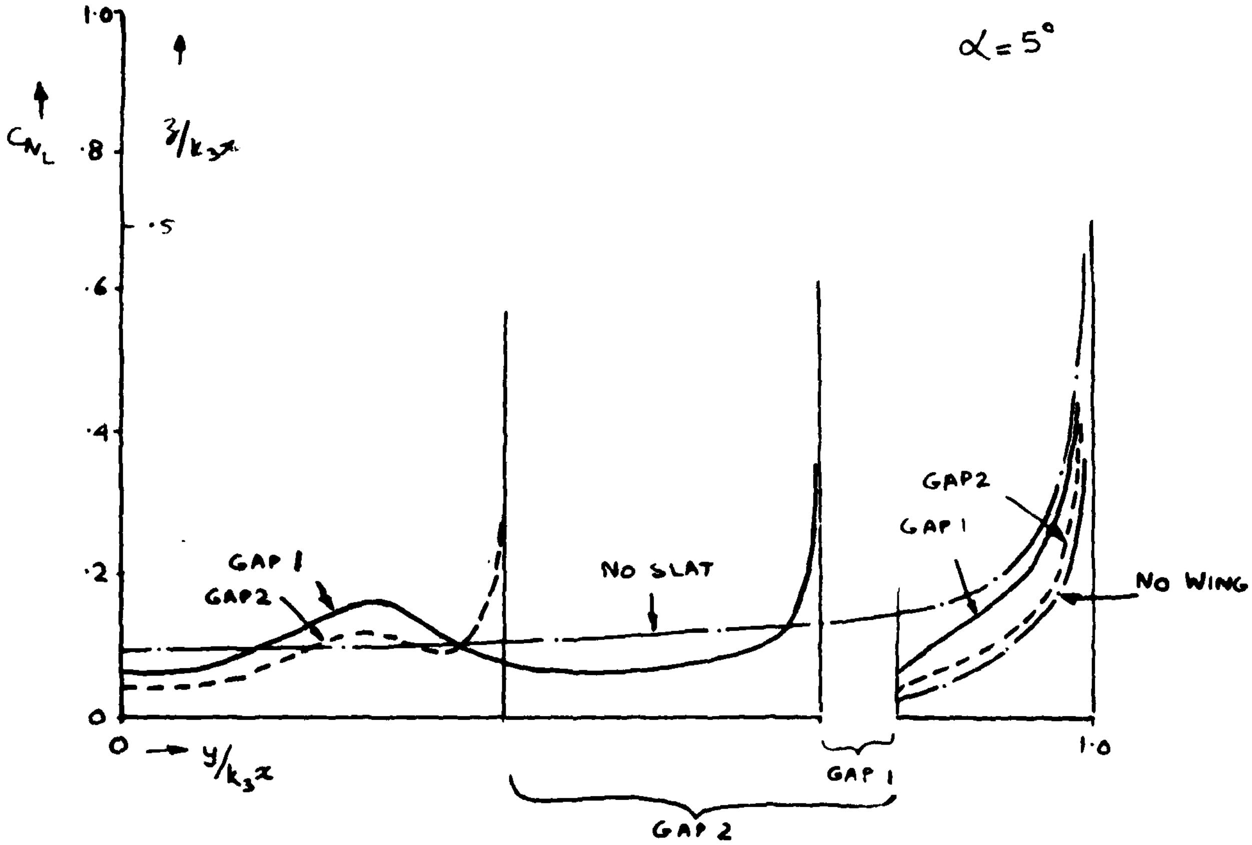

(a) $\phi = 0$

FIG 45 EFFECT OF GAP SIZE

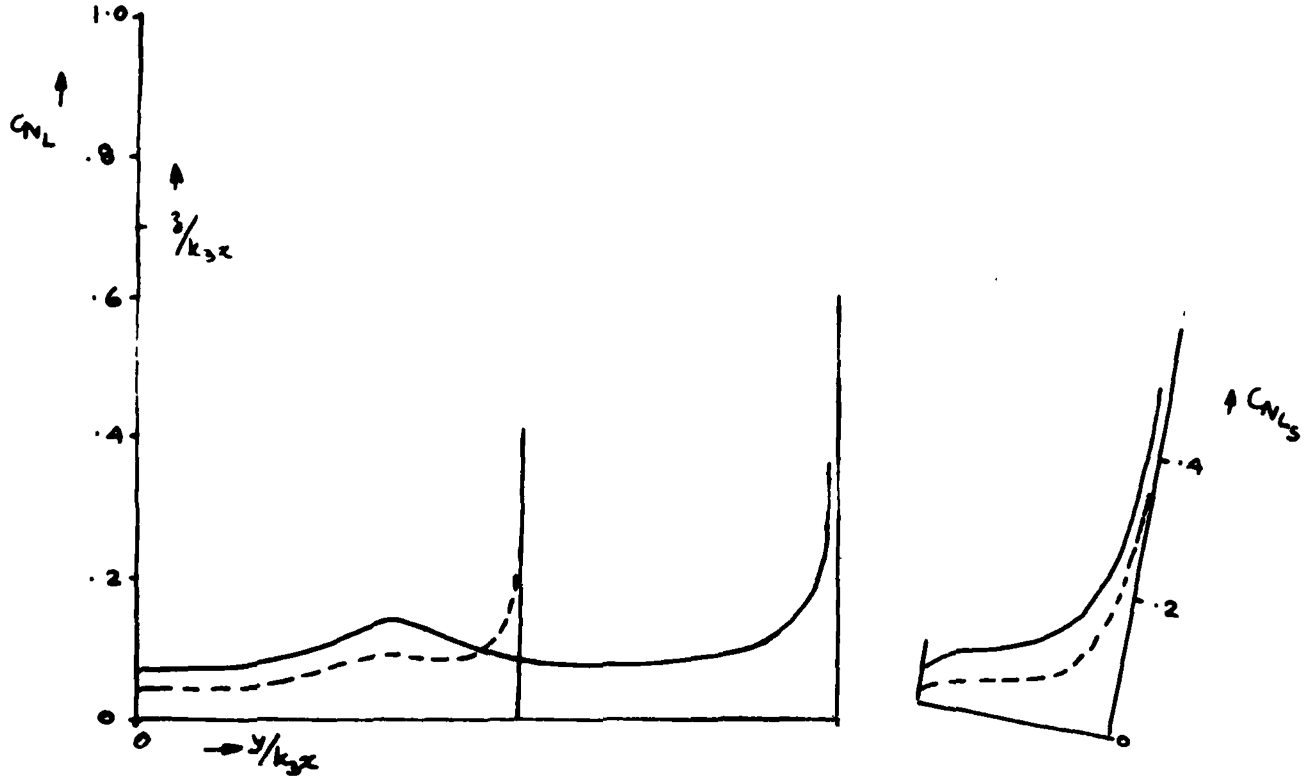

(b) $\phi = -10°$

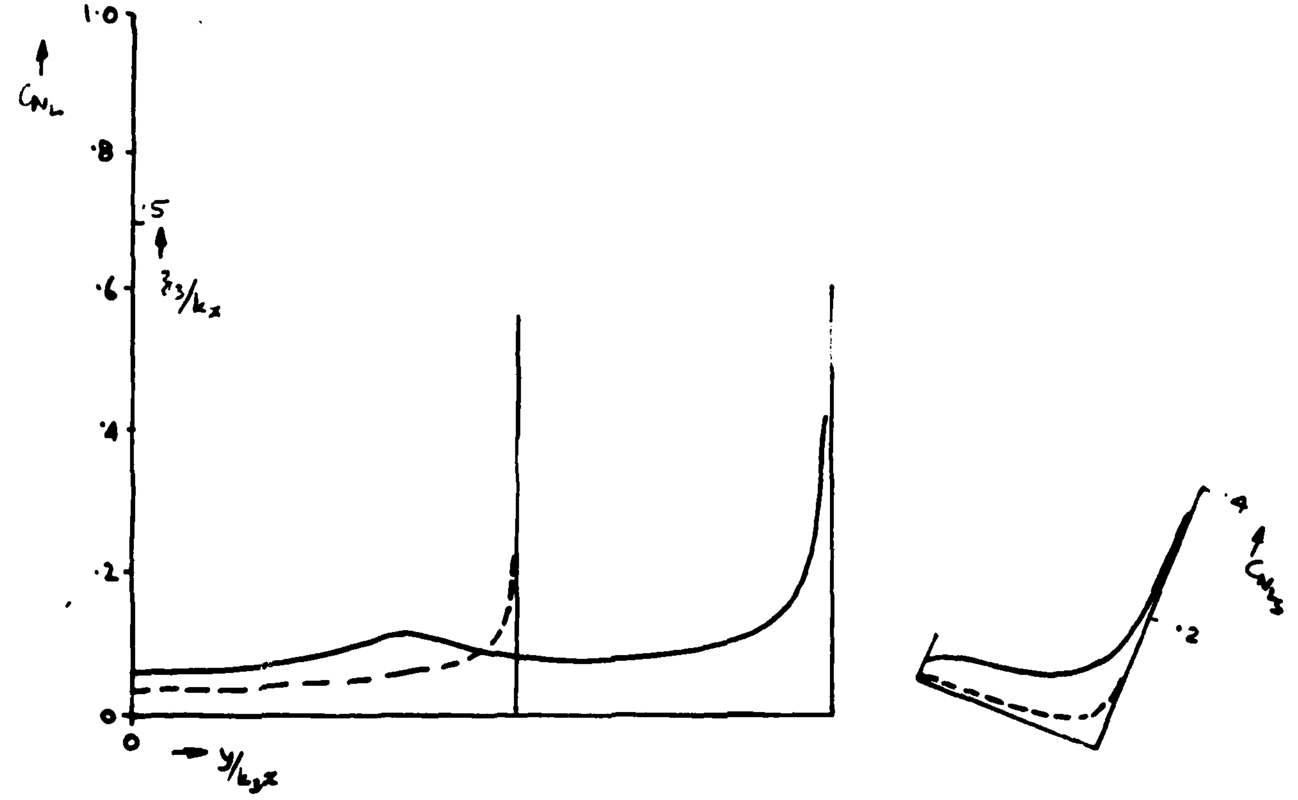

(c) $\phi = -20°$

FIG. 45 CONT'D

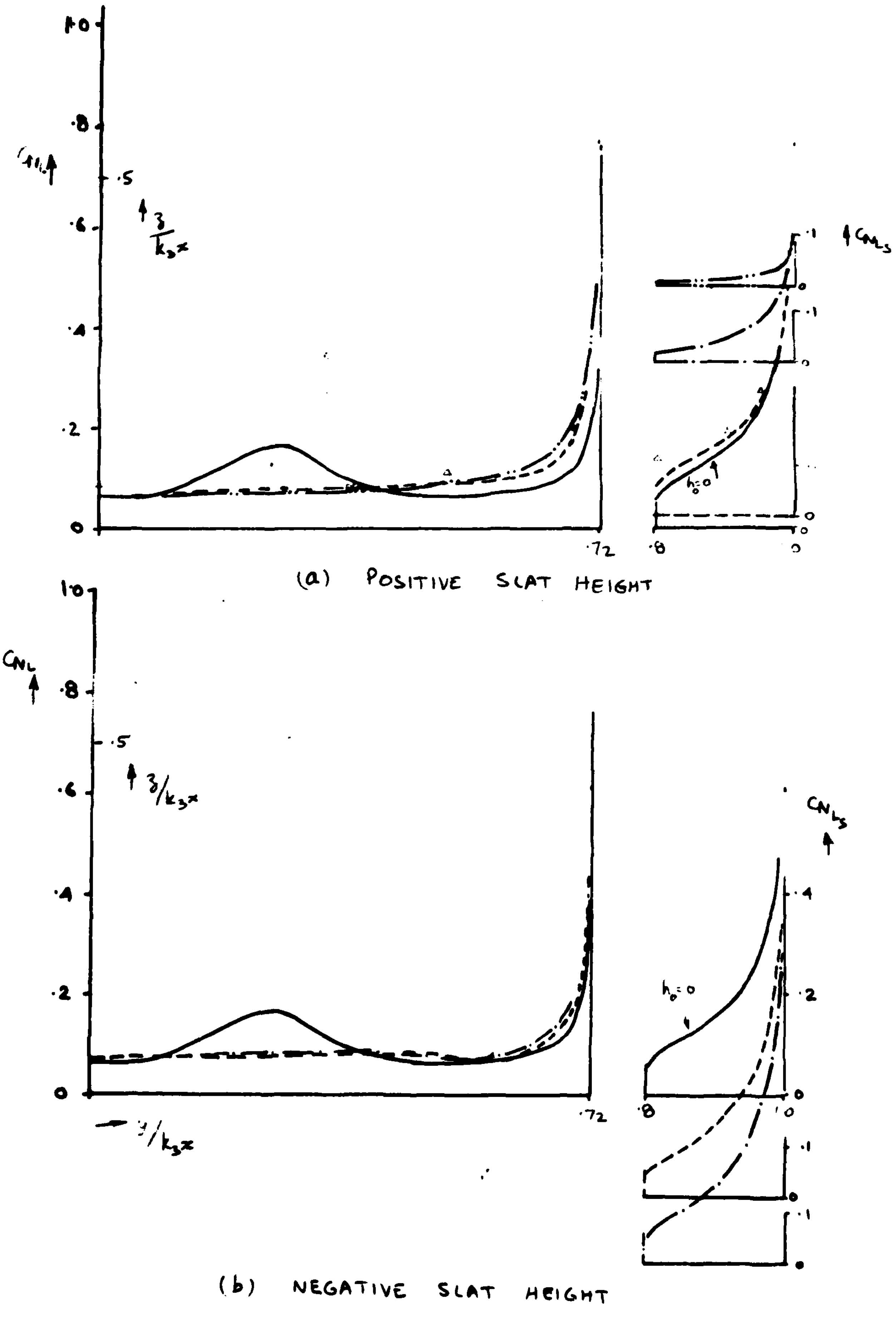

FIG. 46. WING-SLAT CONFIGURATION A-S-A

EFFECT OF SLAT HEIGHT

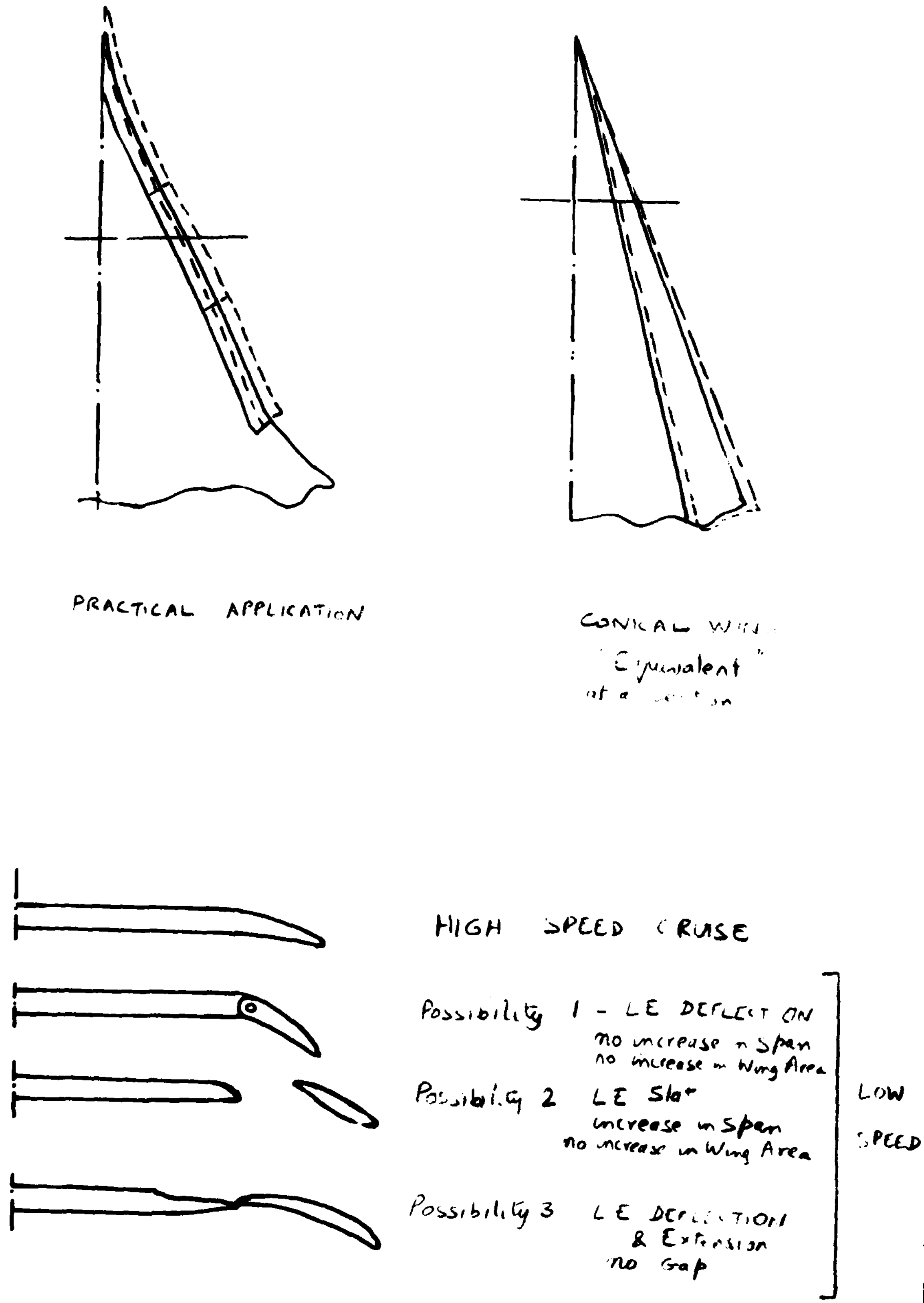

FIG. 47. LEADING EDGE DEVICE POSSIBILITIES

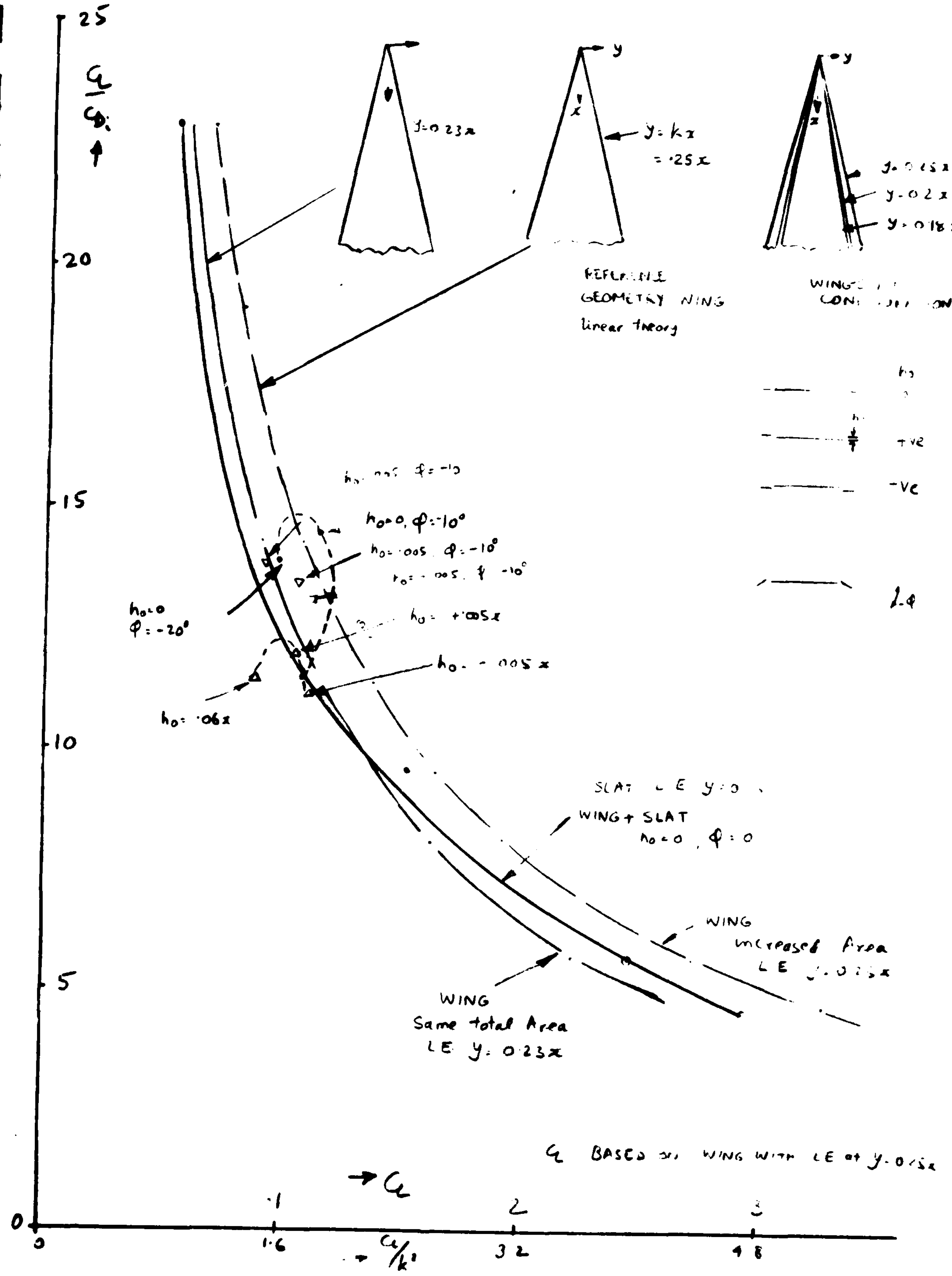

FIG 48. $C_L/C_{D_i} \sim C_L$ (No L.E. SUCTION)

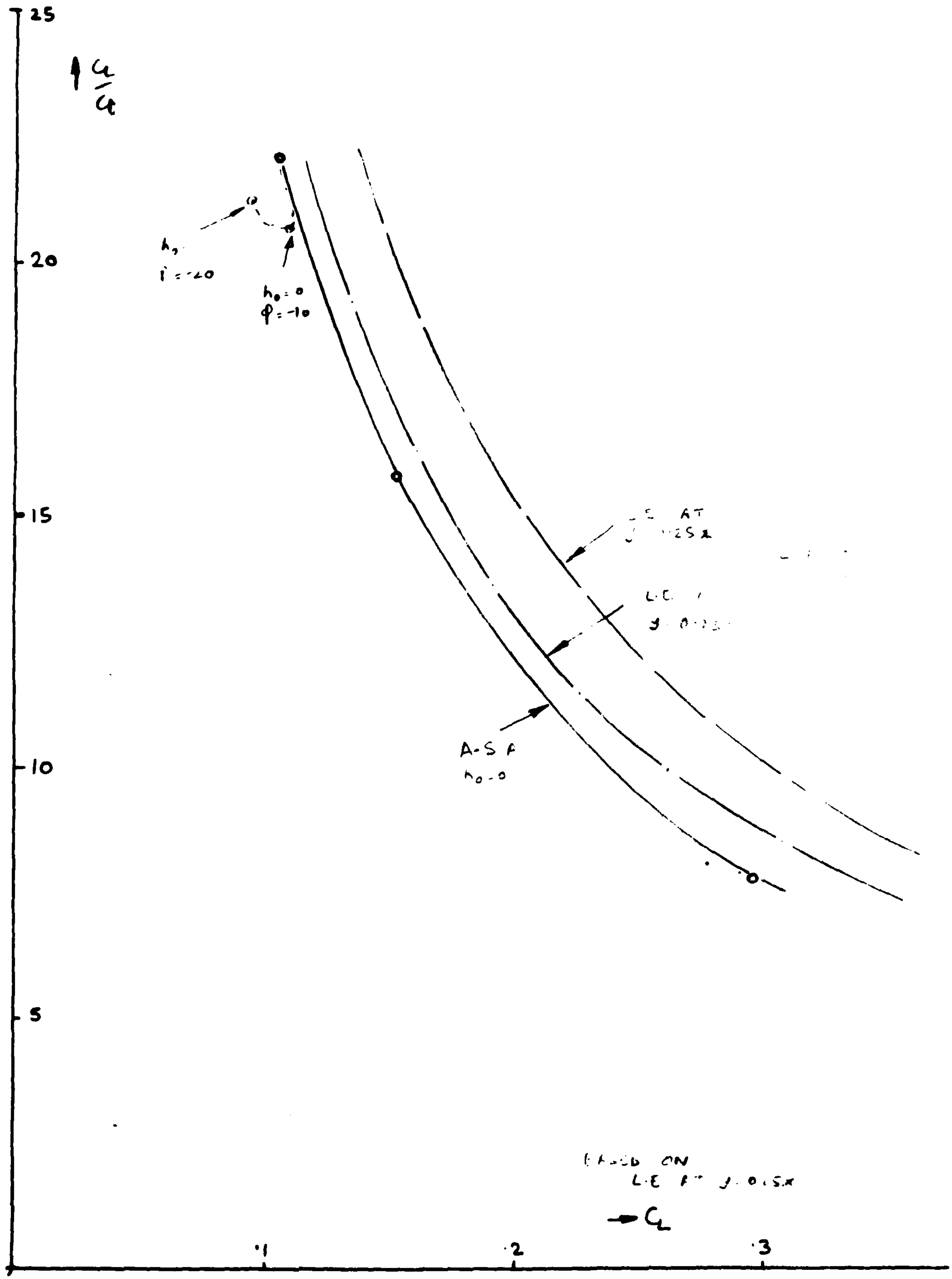

FIG. 49 WING - SLAT CONFIGURATION A-S-A

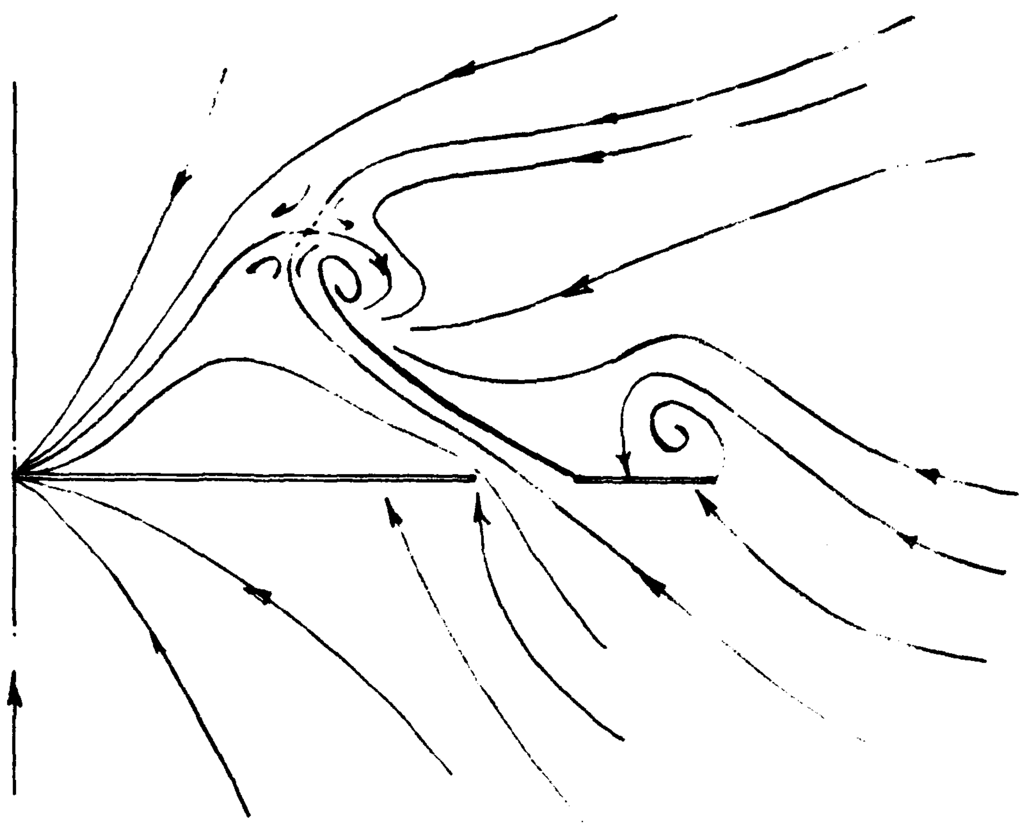

FIG. 50 WING-SLAT CONFIGURATION A-S-S

CONICAL STREAMLINES

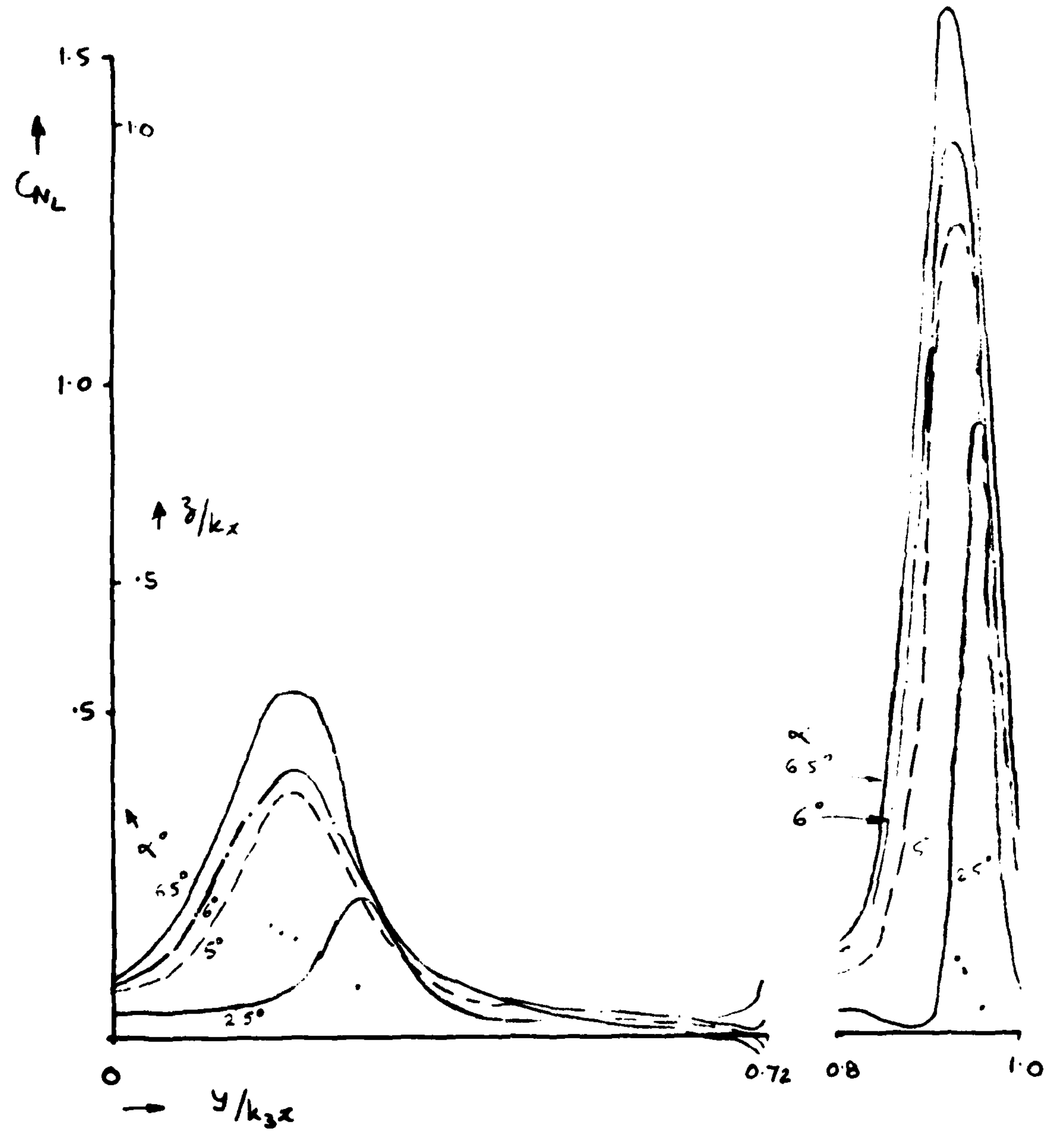

FIG. 51. WING-SLAT CONFIGURATION A-S-S

Effect of α

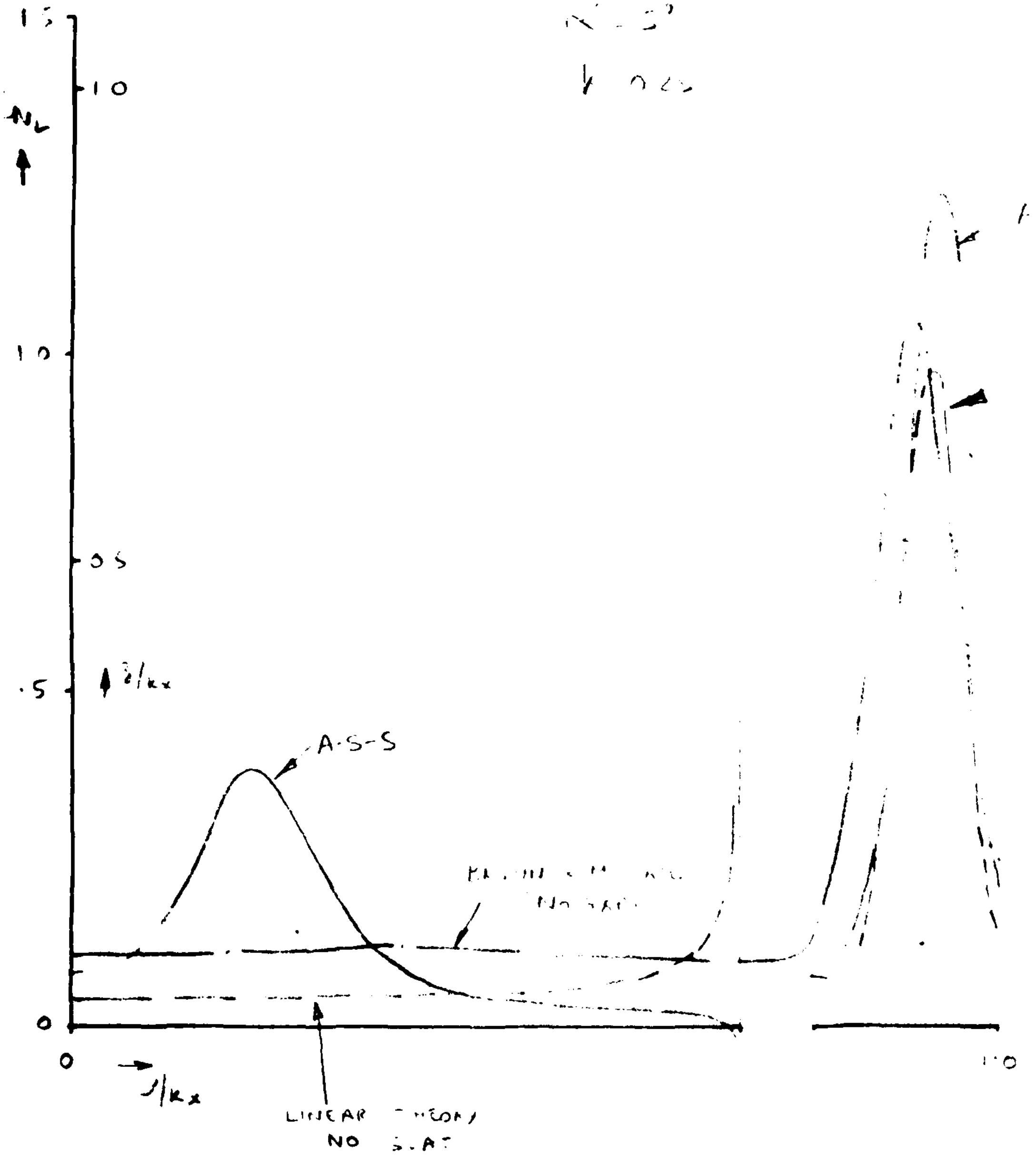

FIG. 52. WING-SLAT CONFIGURATION A-S-S

COMPARISON WITH BROWN & MICHAEL (NO GAP)

AND SLATS ONLY CONFIGURATION S-S

AND LINEAR THEORY (NO SLATS)

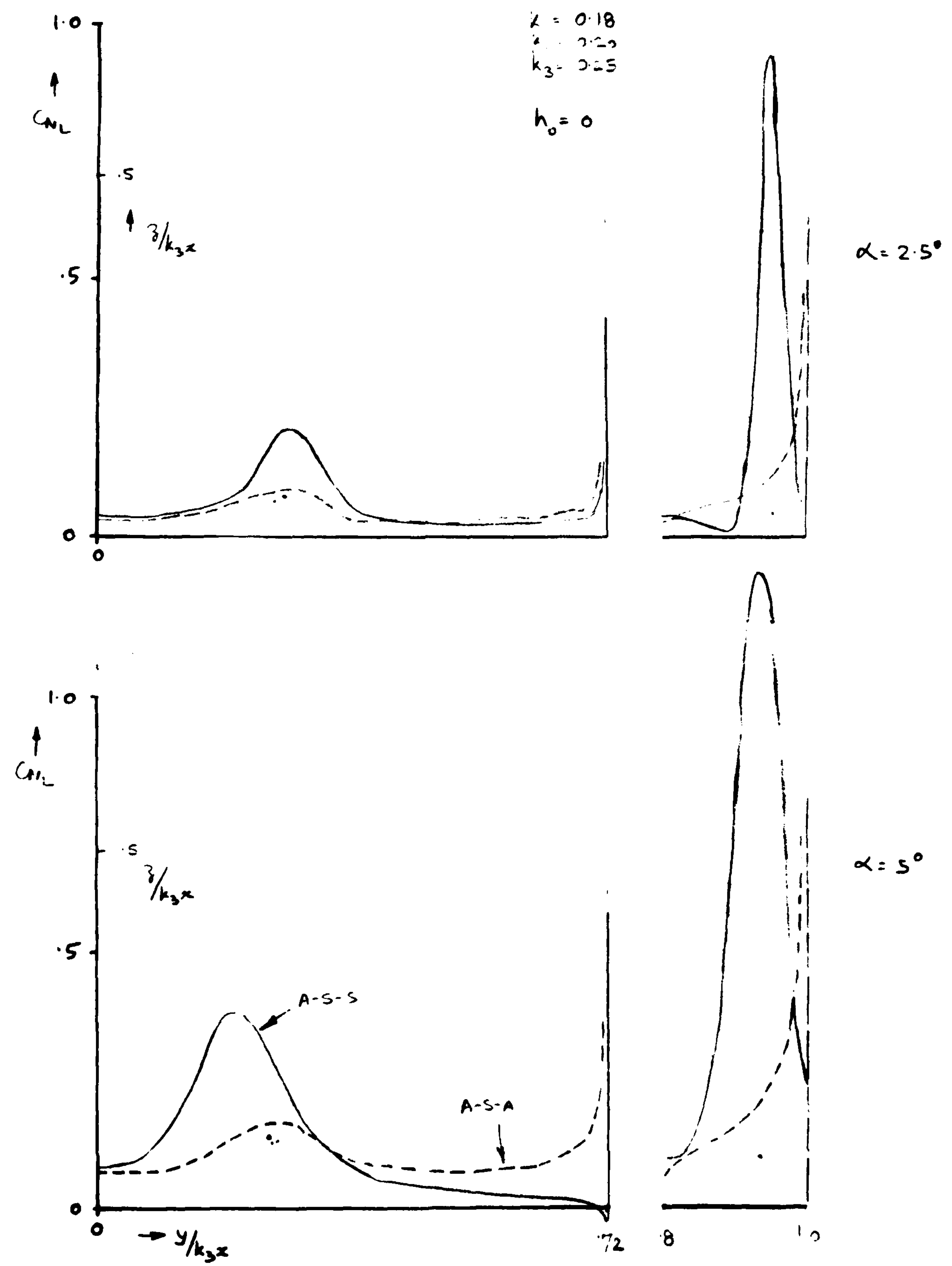

FIG. 53 WING-SLAT CONFIGURATIONS
COMPARISON OF A-S-S WITH A-S-A

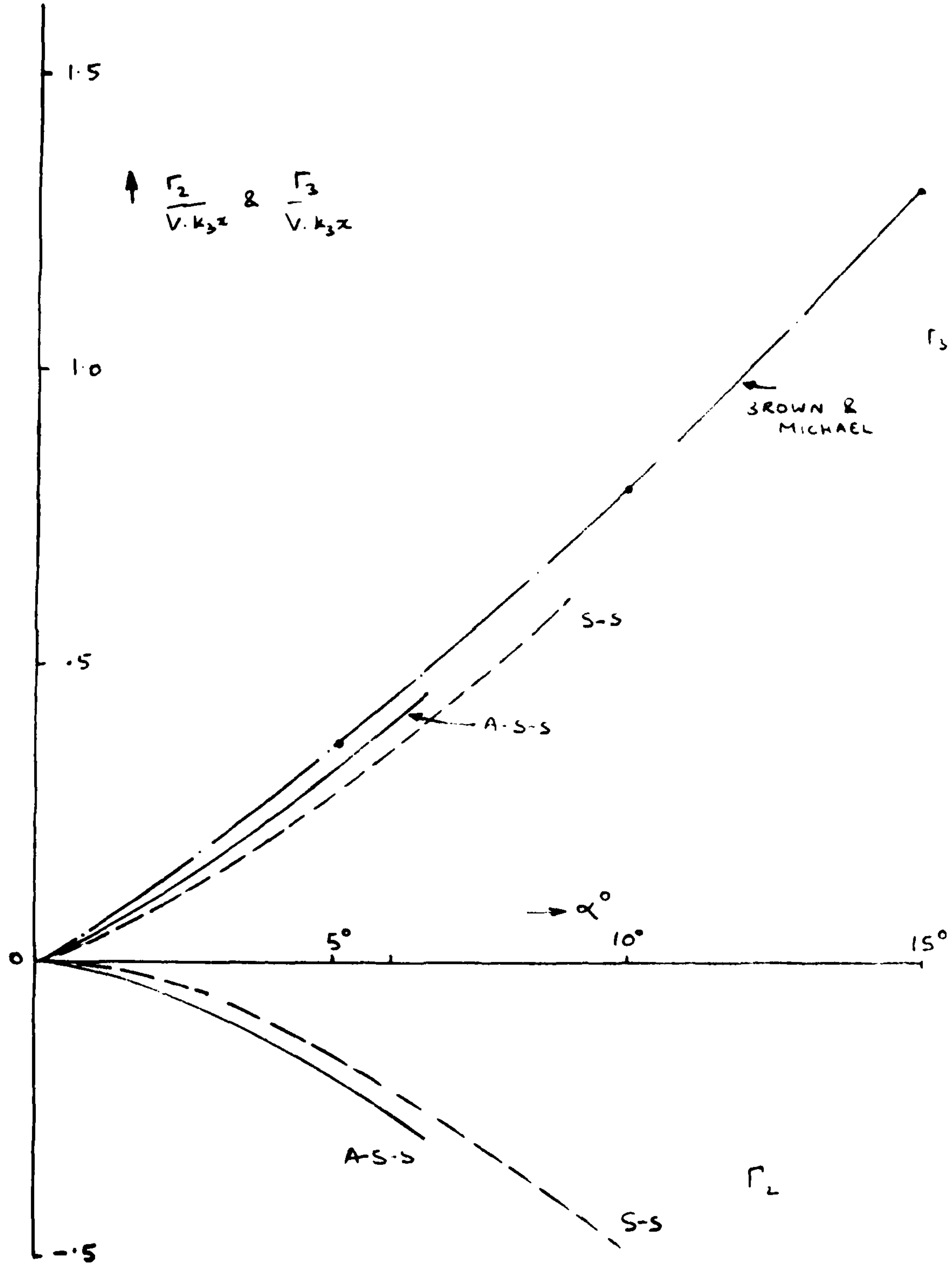

FIG 54. WING-SLAT CONFIGURATION A-S-S
COMPARISON OF VORTEX STRENGTHS WITH SLAT CONFIGURATION S-S AND BROWN & MICHAEL

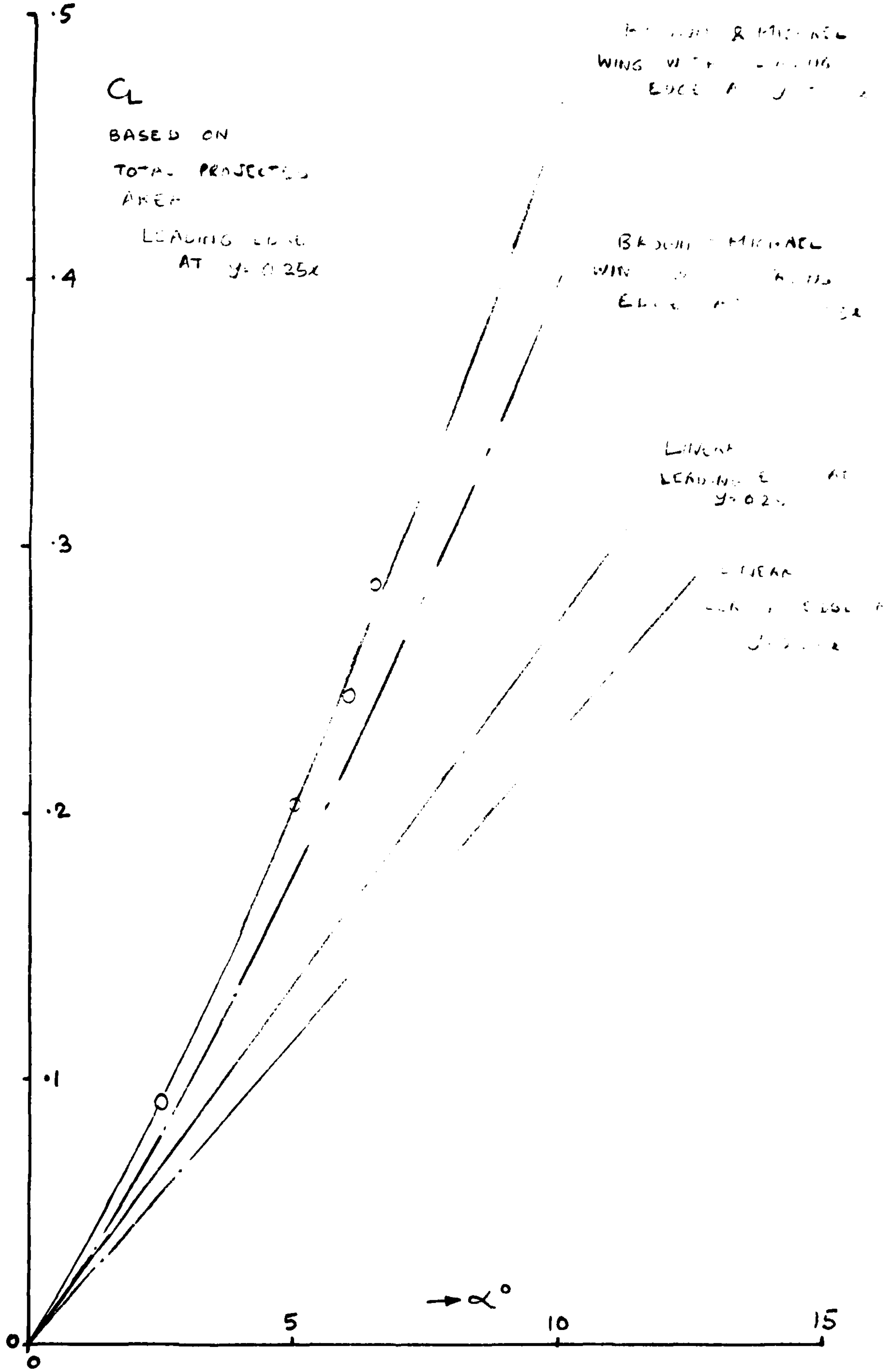

FIG. 55. WING-SLAT CONFIGURATION A-S-S
$C_L \sim \alpha$

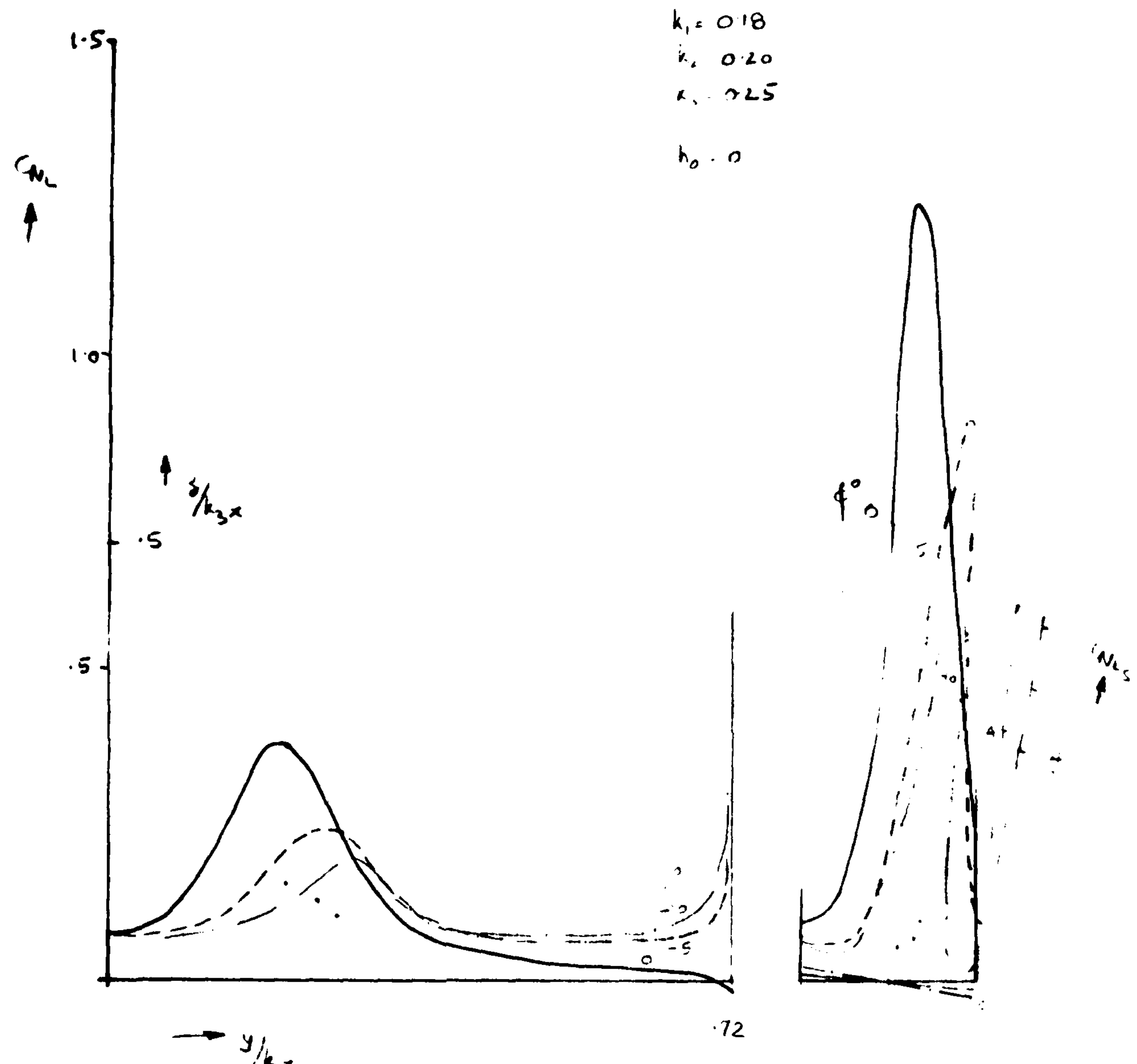

FIG. 56. WING-SLAT CONFIGURATION A S-S
EFFECT OF SLAT INCLINATION ϕ

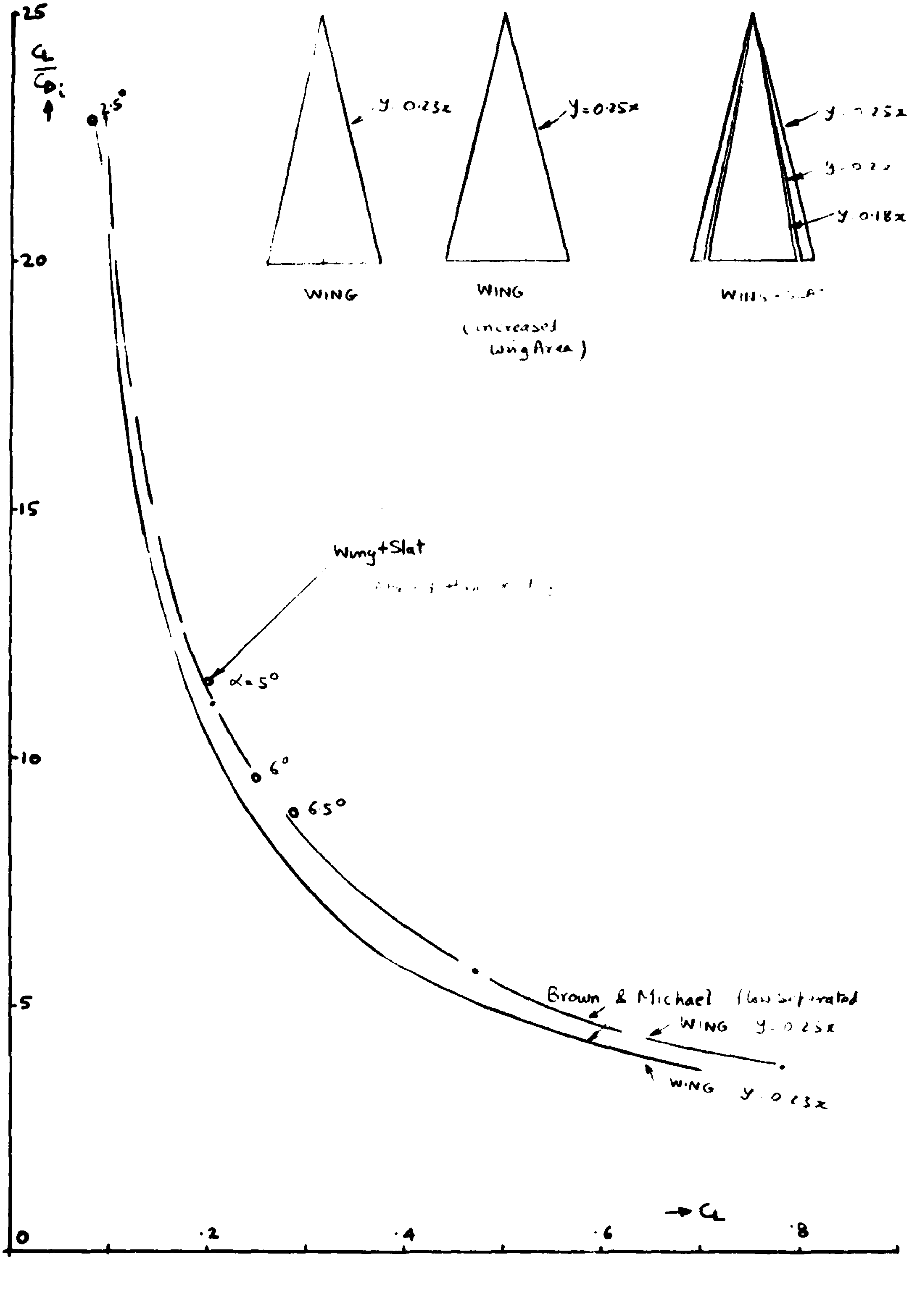

FIG. 57. WING-SLAT CONFIGURATION A-S-S

$k_1 = 0.18$
$k_2 = 0. .$
$k_3 = 0. .$
$h_0 = 0$

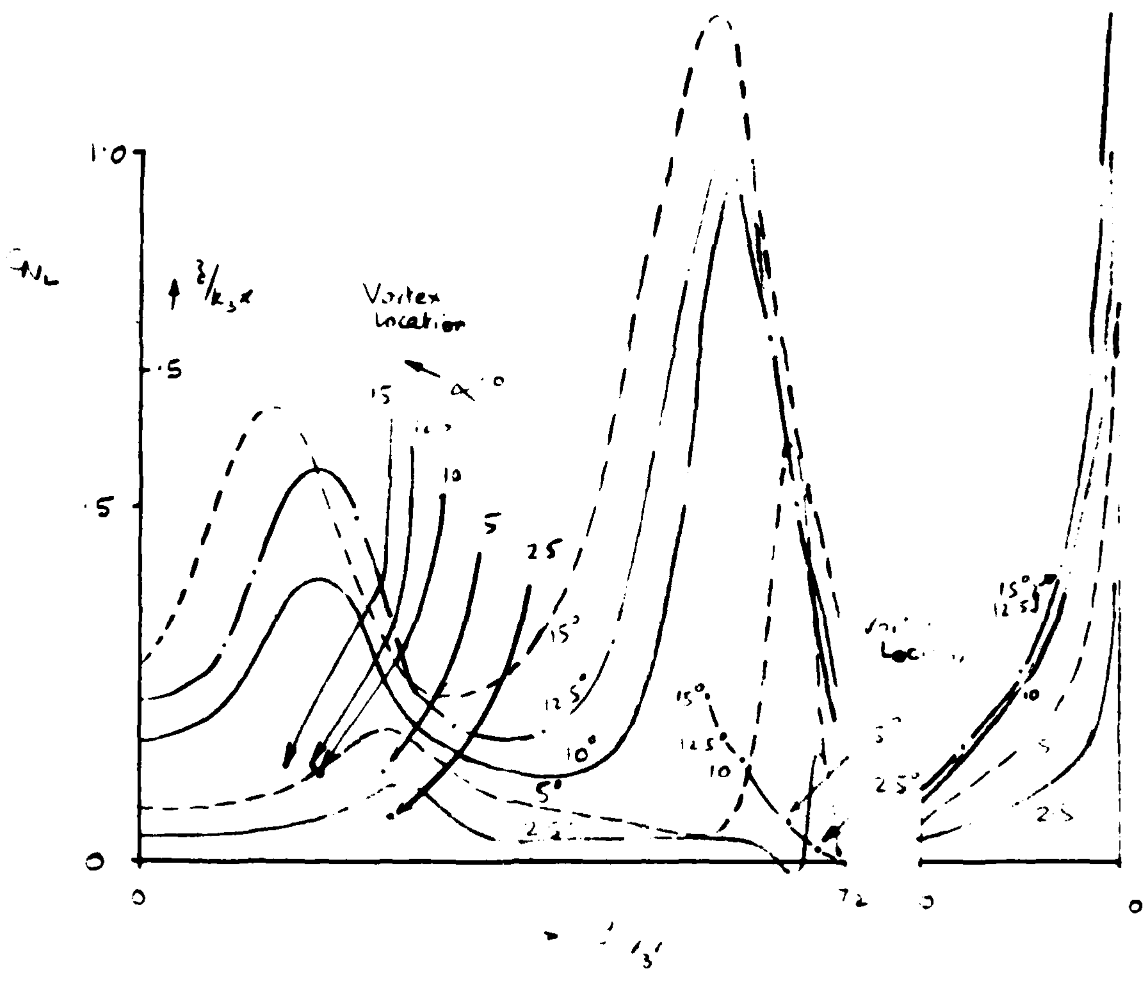

FIG. 59 WING-SLAT CONFIGURATION S-S-A

EFFECT OF α

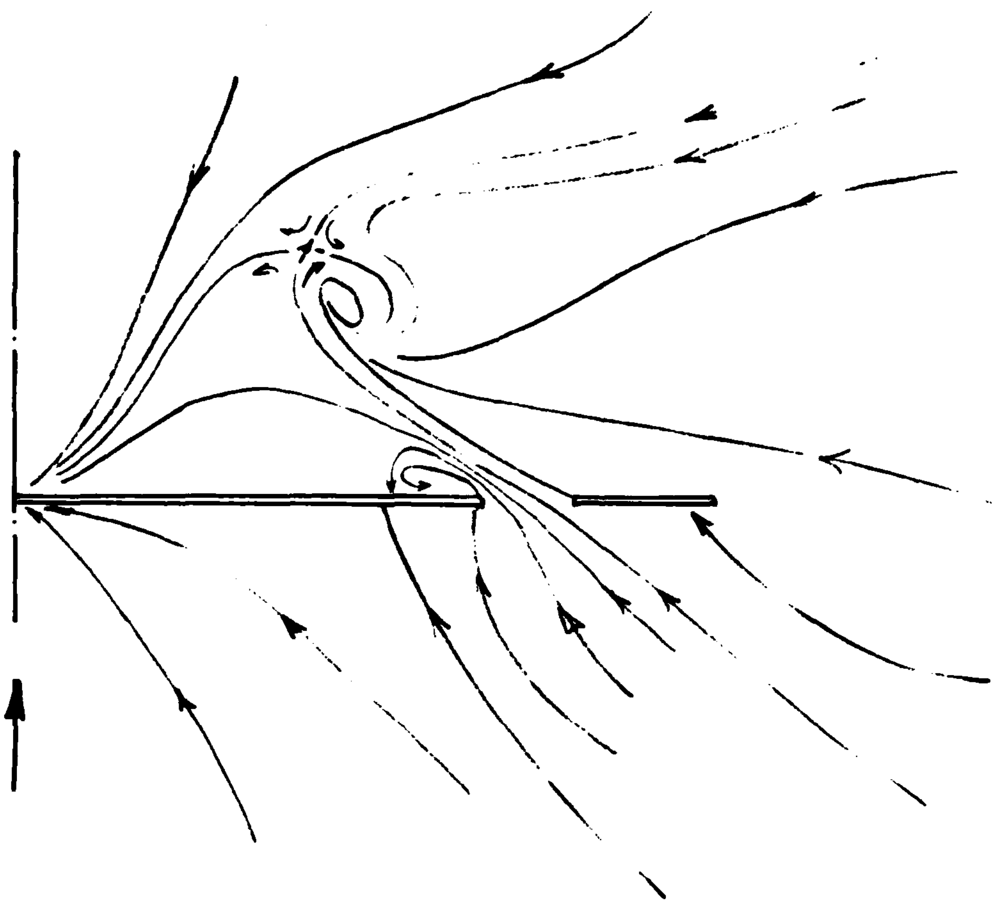

FIG. 58. WING-SLAT CONFIGURATION S-S-A CONICAL STREAMLINES

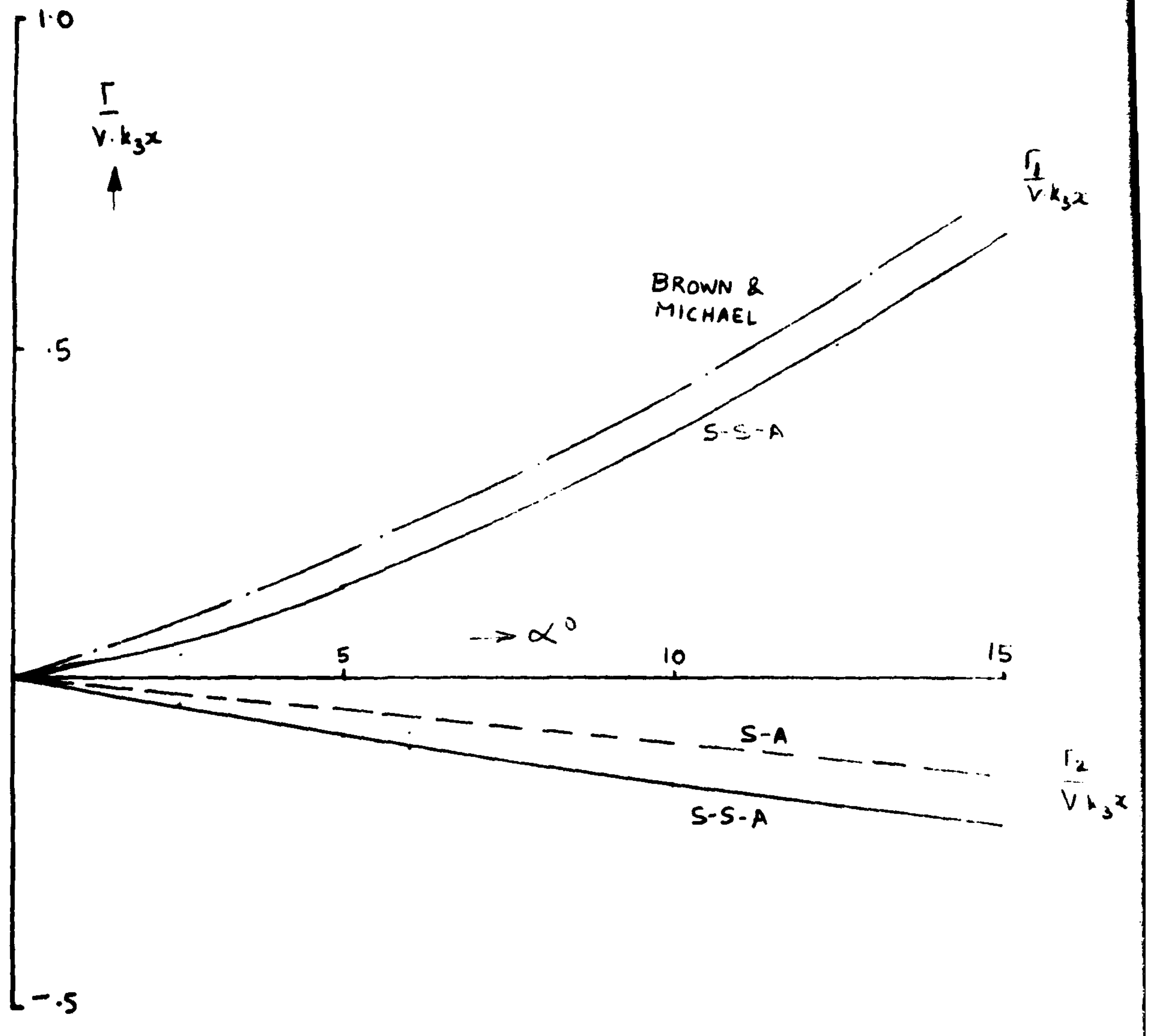

FIG. 60. WING-SLAT CONFIGURATION S-S-A

VORTEX STRENGTH ~ α

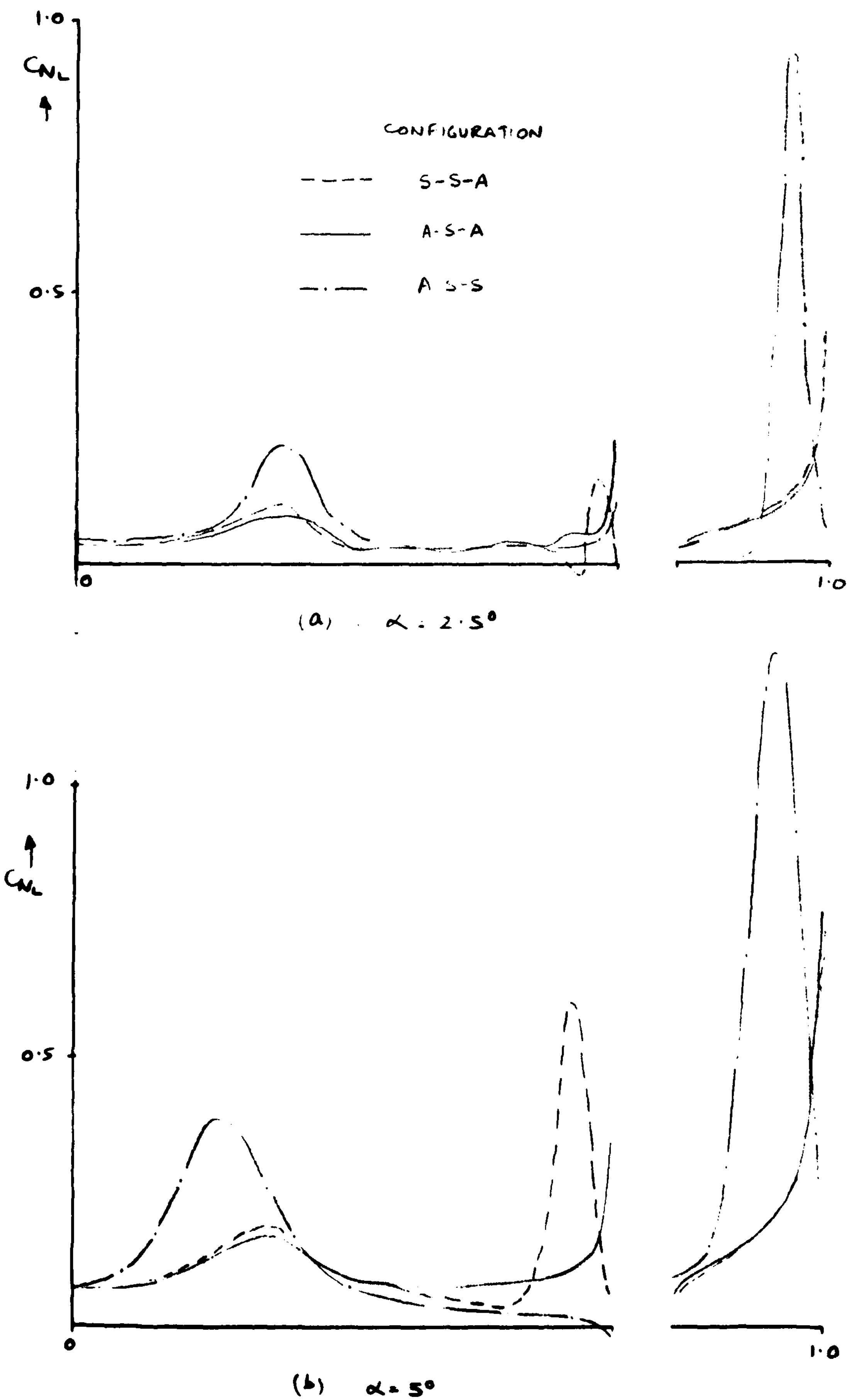

FIG. 61. WING-SLAT CONFIGURATION S-S-A
COMPARISON WITH A-S-A & A-S-S

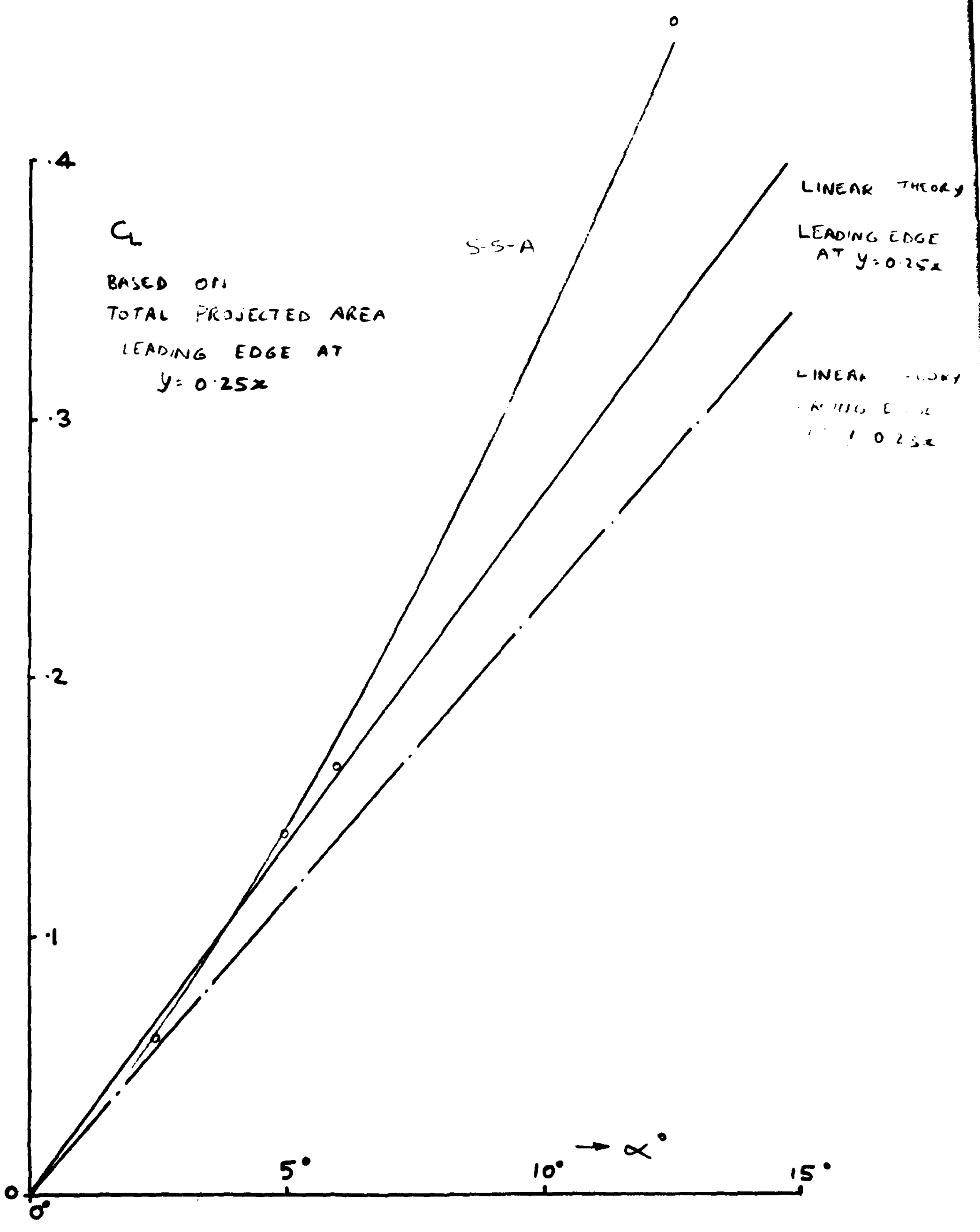

FIG. 62. WING-SLAT CONFIGURATION S-S-A

$C_L \sim \alpha$

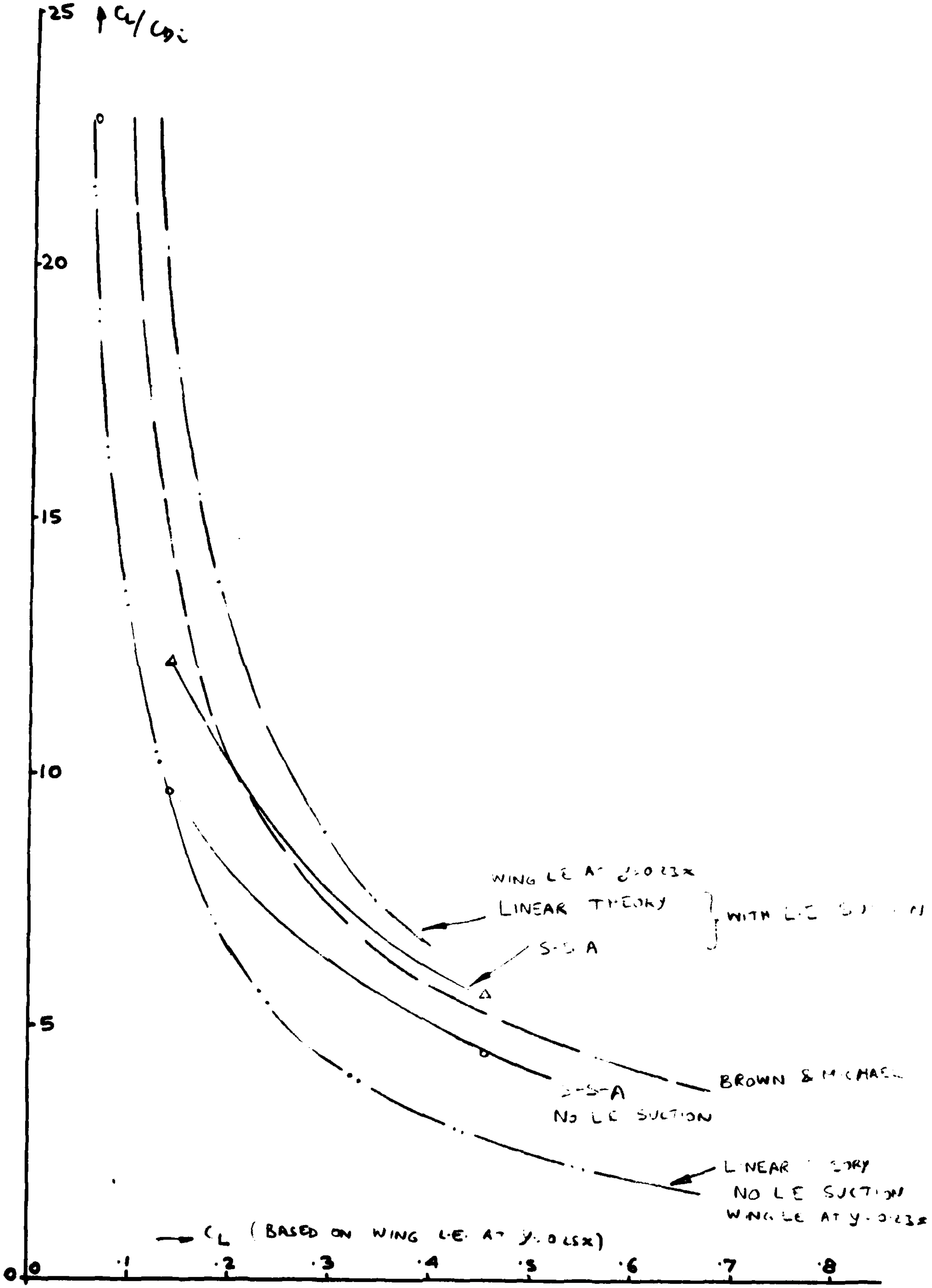

FIG. 63. WING-SLAT CONFIGURATION S-S-A

$C_L/C_{Di} \sim C_L$

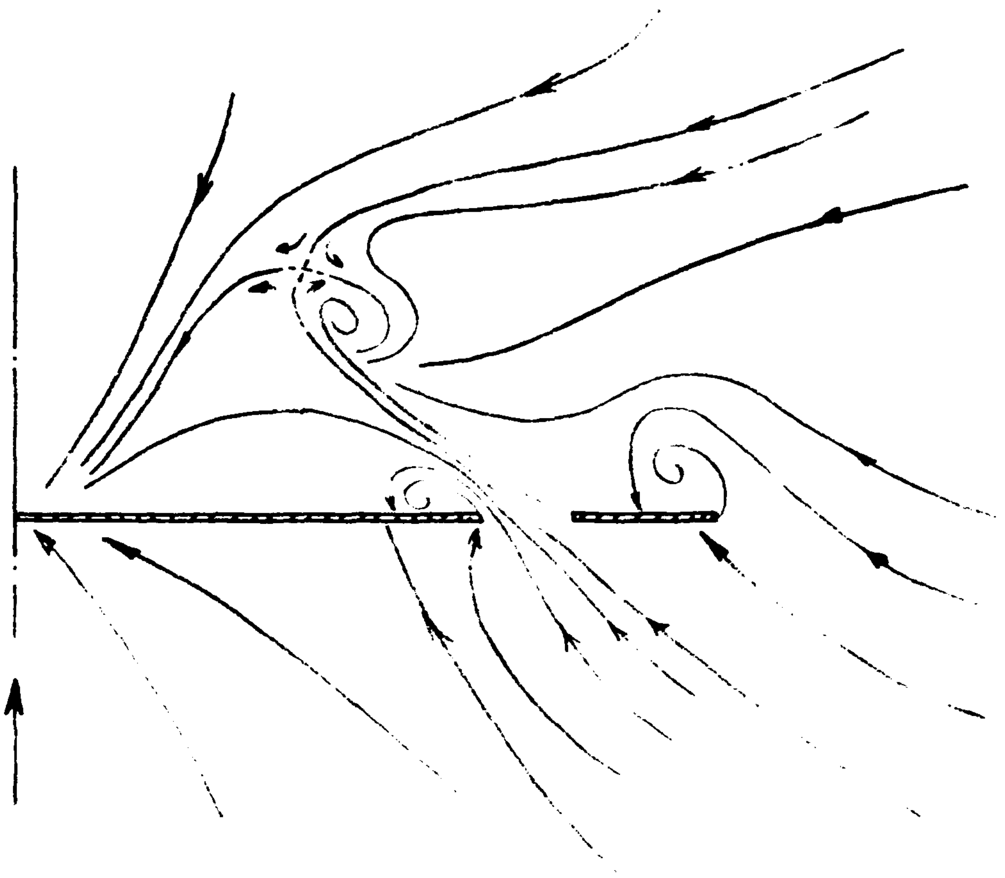

FIG. 64 WING-SLAT CONFIGURATION S-S-S
CONICAL STREAMLINES

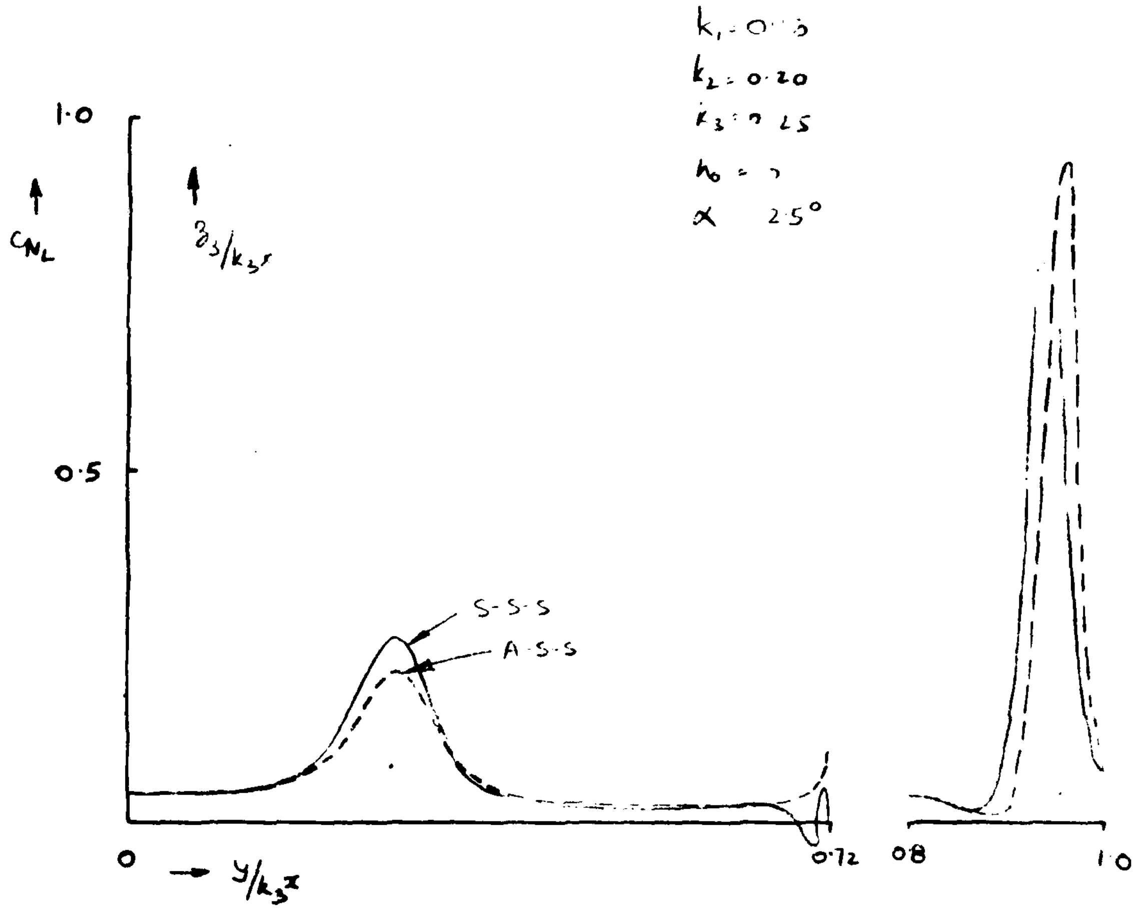

FIG. 65. CONFIGURATION S-S-S COMPARED WITH CONFIGURATION A-S-S

LOAD DISTRIBUTION & VORTEX LOCATIONS

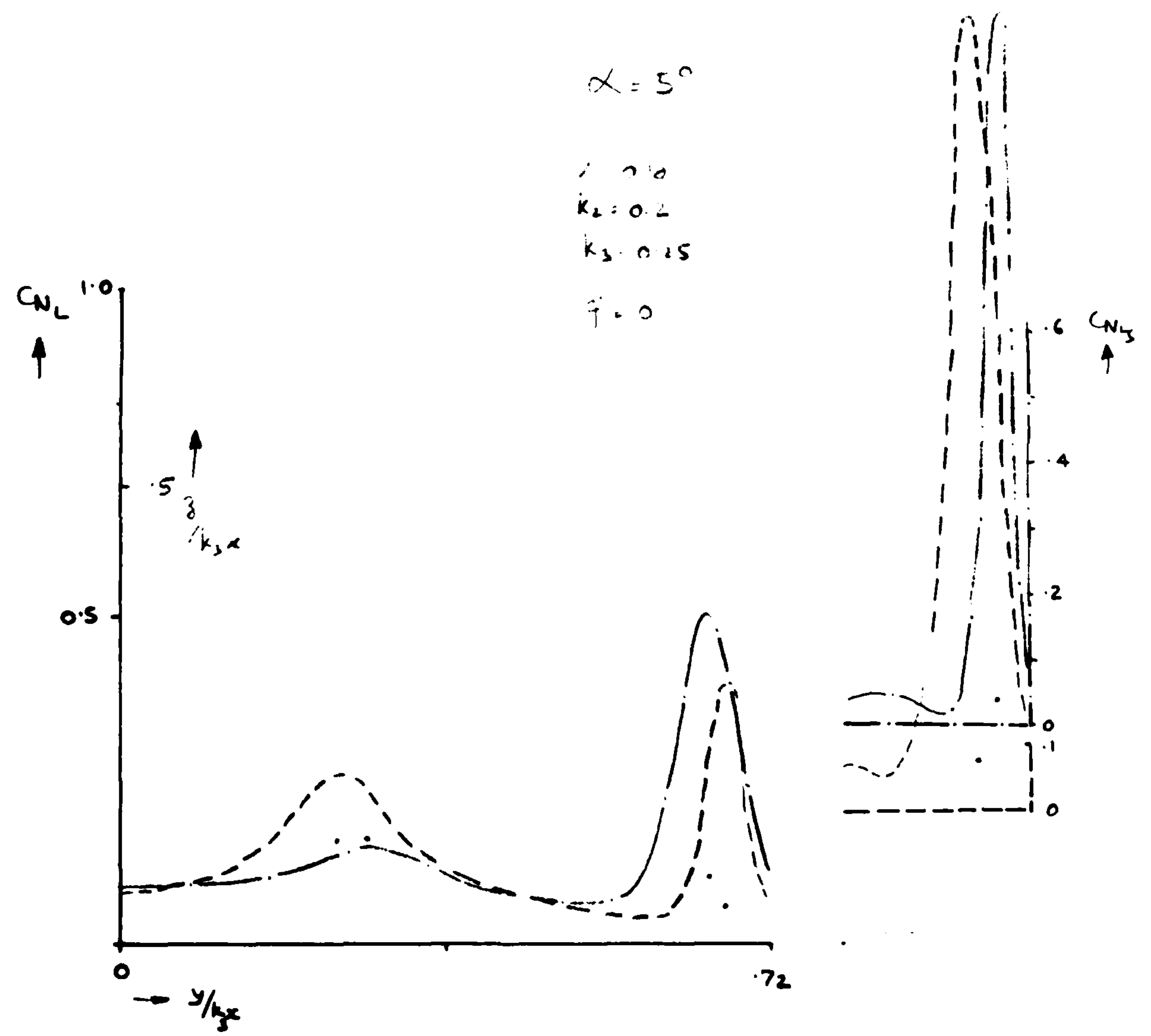

FIG. 66. WING-SLAT CONFIGURATION S-S-S

EFFECT OF SLAT HEIGHT

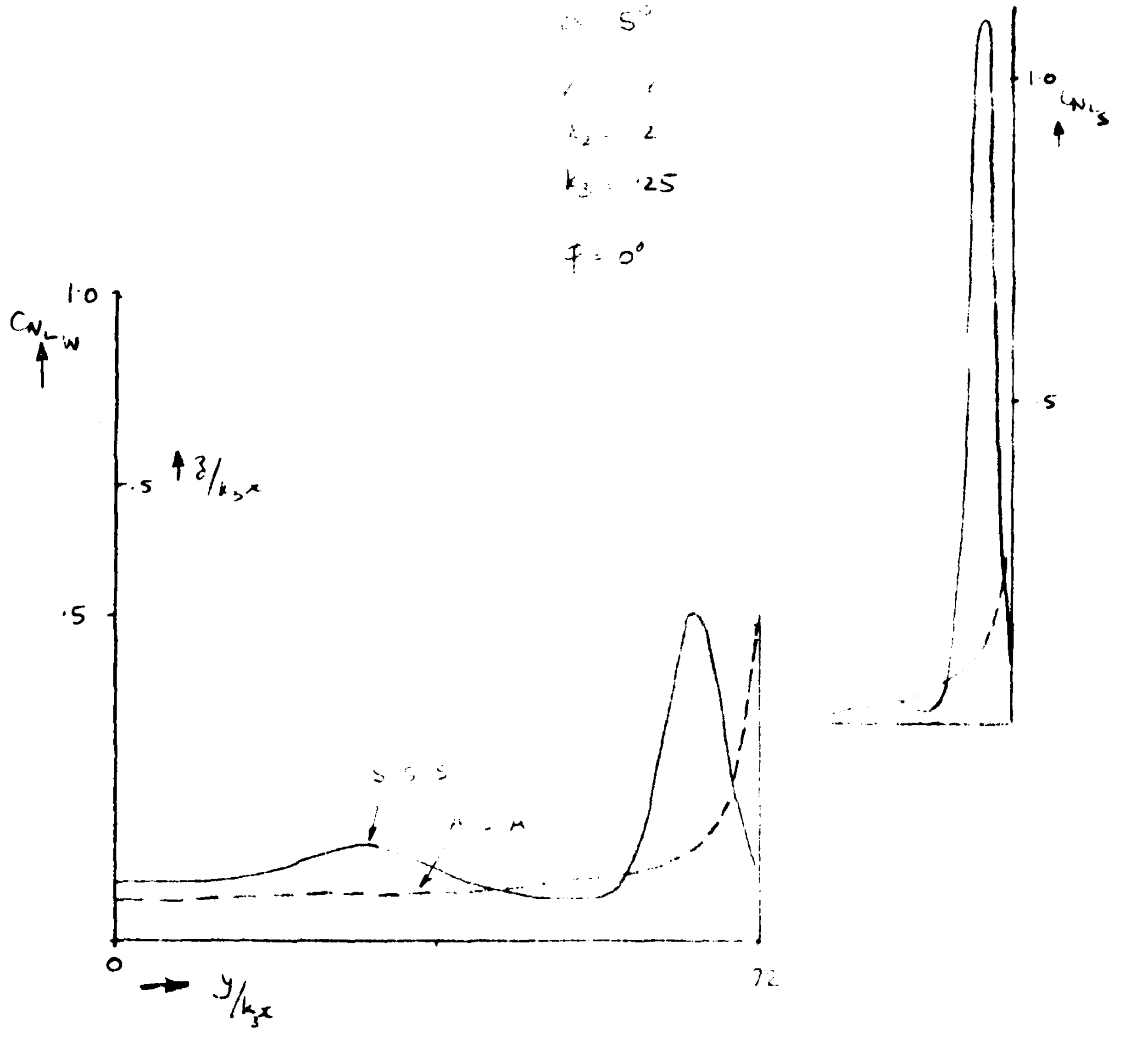

FIG. 67. WING-SLAT CONFIGURATION S-S-S
COMPARISON WITH CONFIGURATION
A-S-A

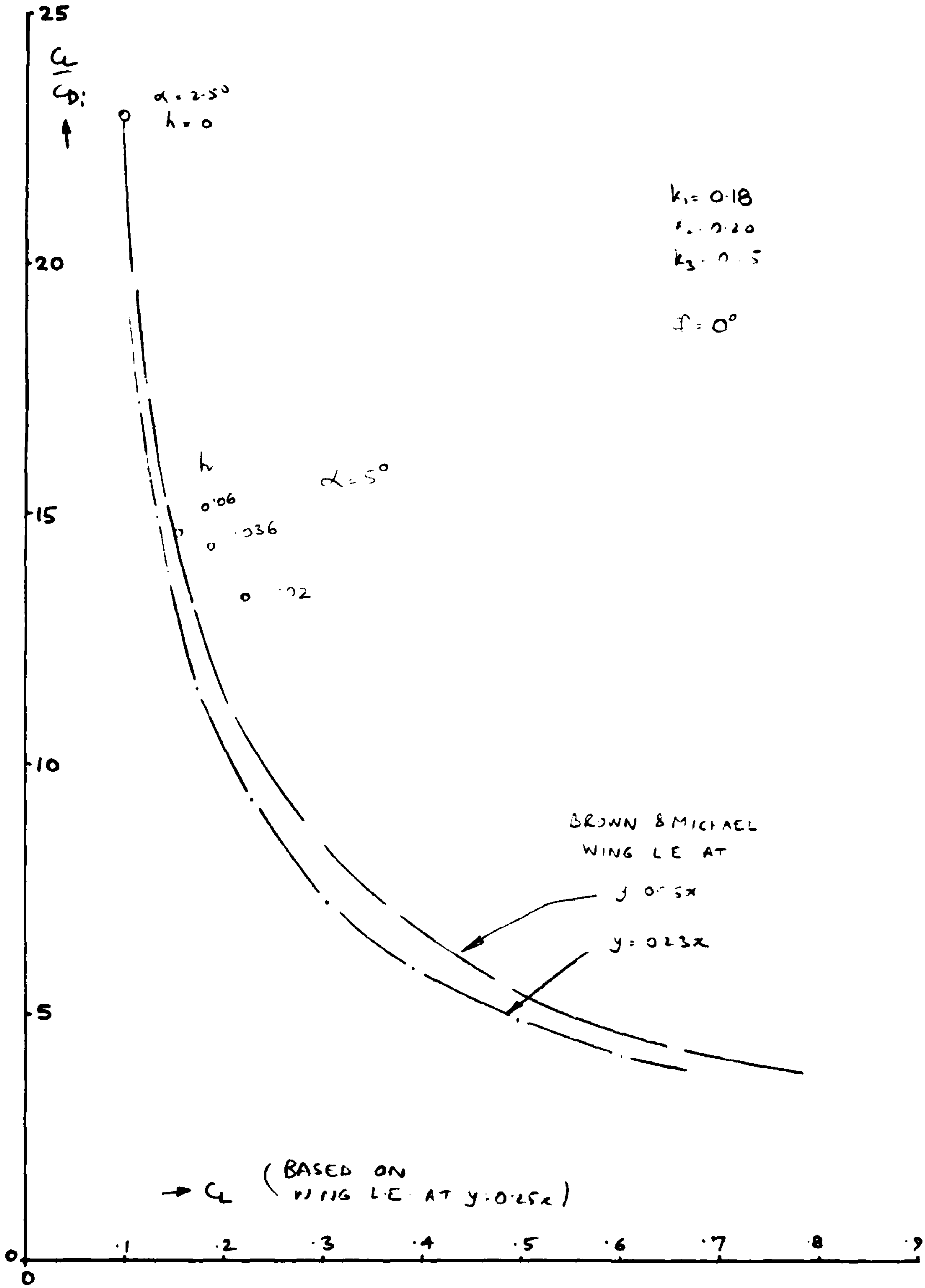

FIG. 6B WING-SLAT CONFIGURATION S-S-S

$C_L/C_D \sim C_L$

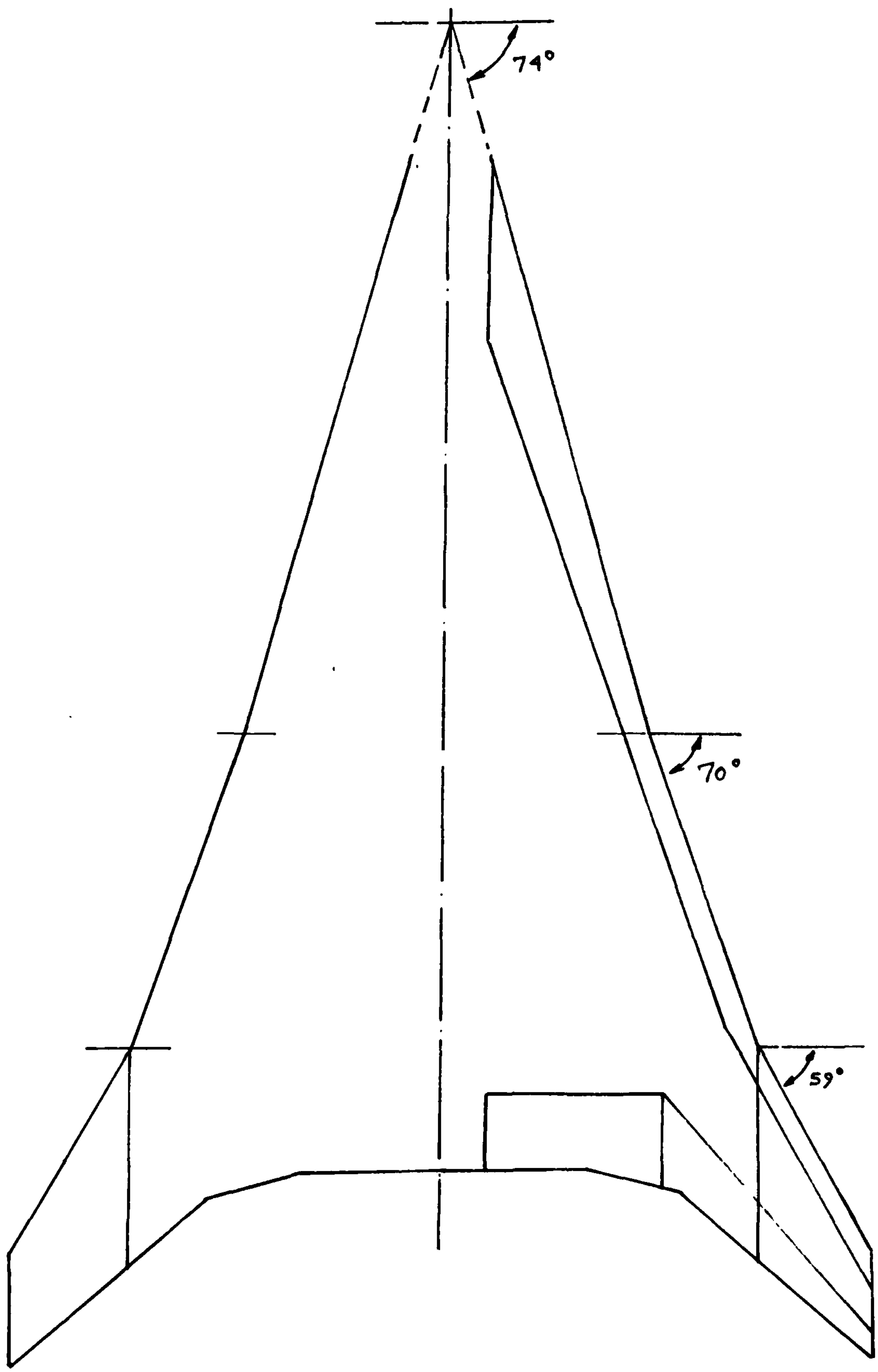

FIG. 69. 'ARROW' TYPE WINGS

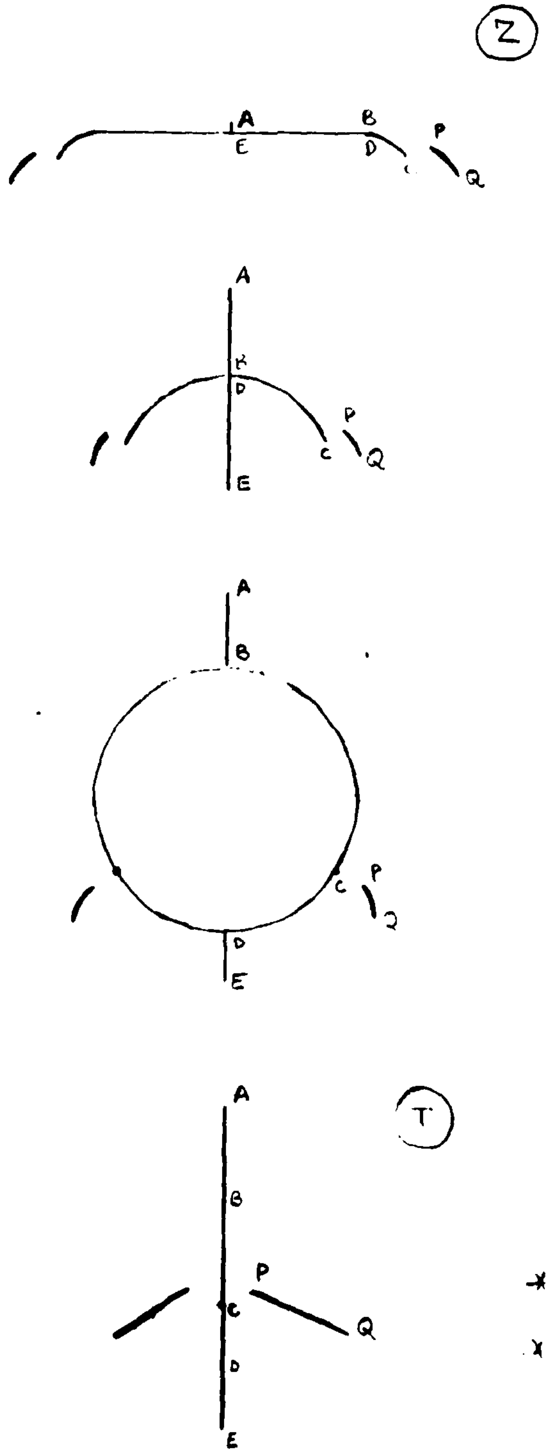

T-plane is similar to the case of
Slats only

T-plane suitable for [illegible].

* Vorticity Distributions on wing and slat

* Source Distributions on [illegible]
part of wing and the slat

FIG 70 WING-SLAT CONFIGURATION WITH CAMBER

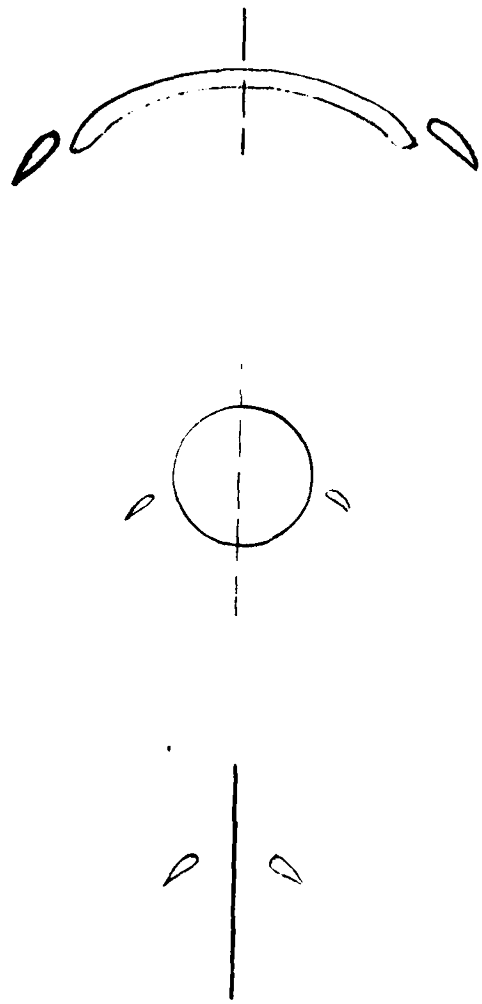

FIG. 71 WING-SLAT CONFIGURATION WITH THICKNESS & CAMBER

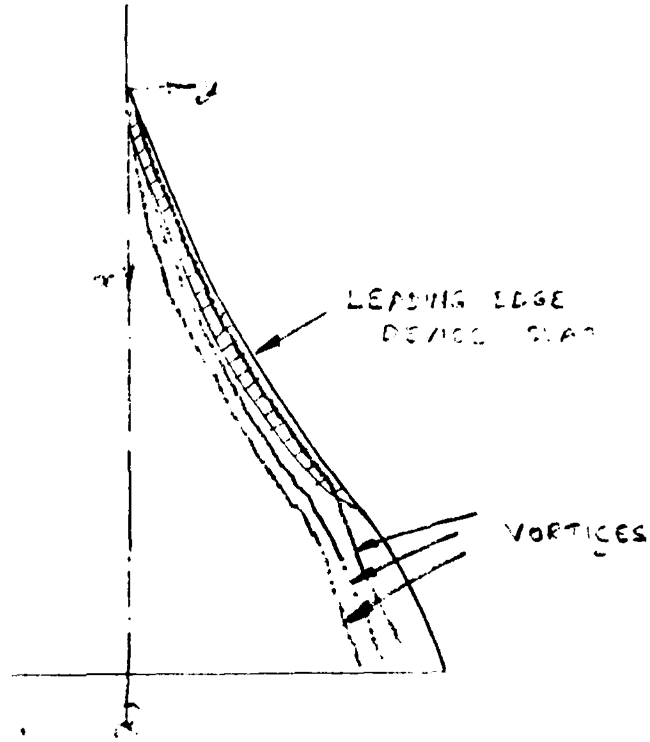

FIG. 73 PLANFORM EFFECTS

[illegible] CALCULATIONS

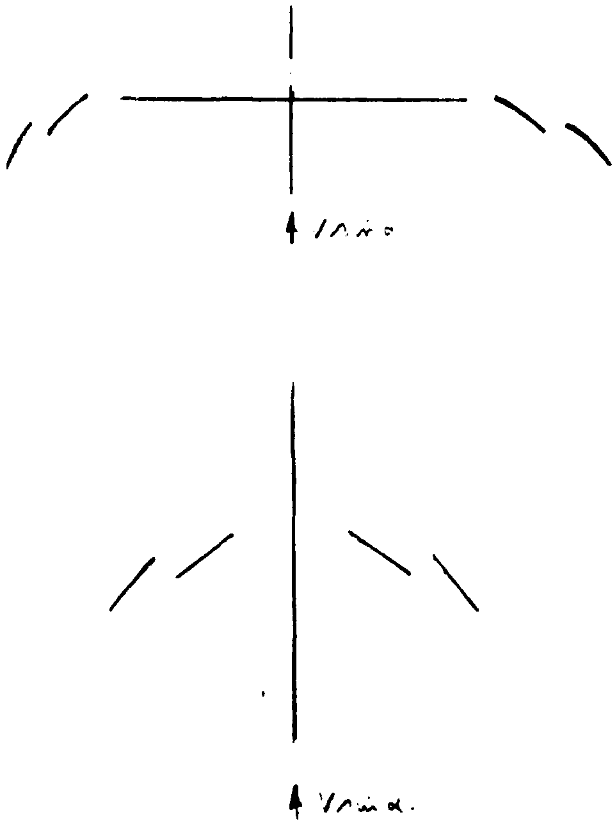

FIG 72 [illegible]

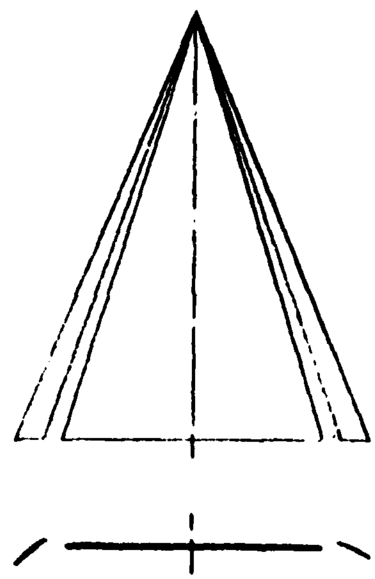

FIG. 74 CONICAL TYPE MODELS

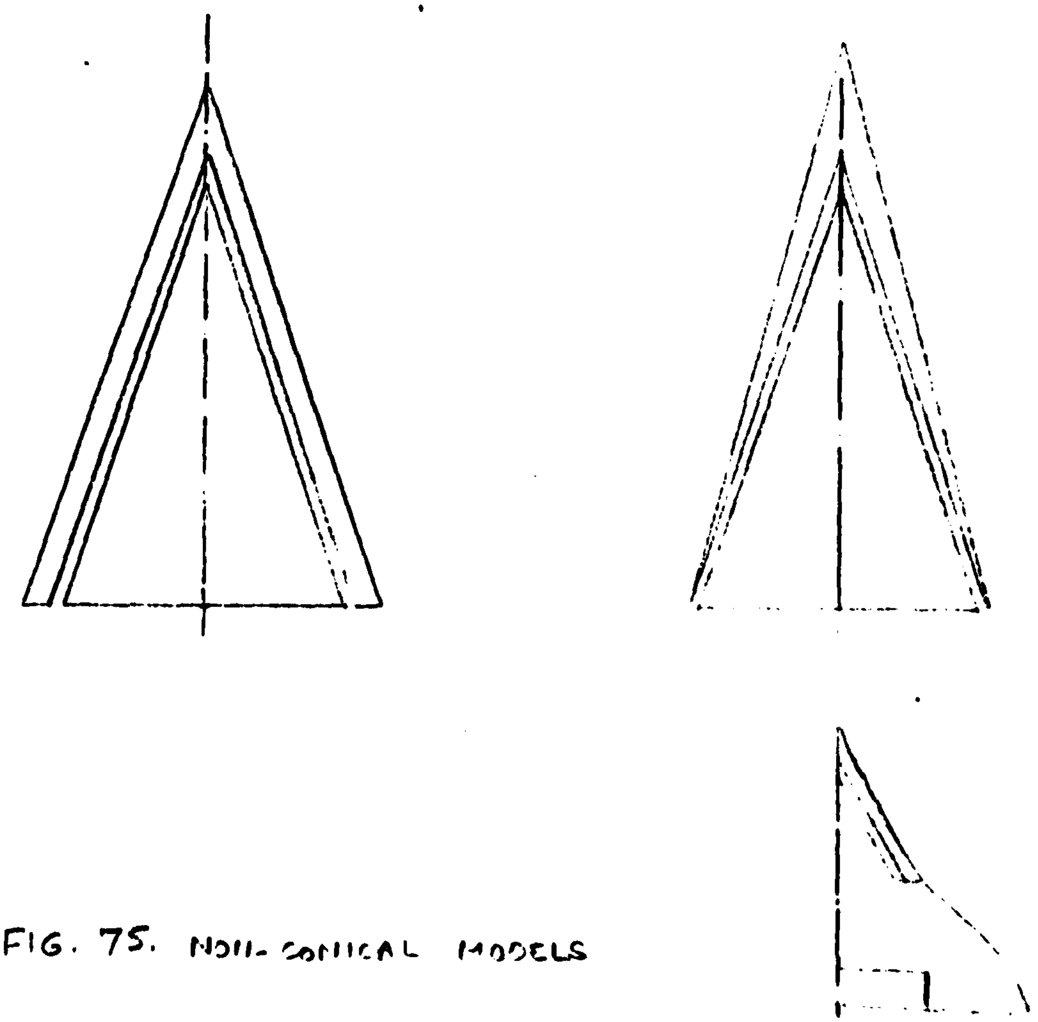

FIG. 75. NON-CONICAL MODELS

(b) α = 5°

FIG. 61. WING-SLAT CONFIGURATION S-S-A
COMPARISON WITH A-S-A & AS-S

END
DATE
FILMED
3-8
DTIC